INTERPRETATION OF SELFBORING PRESSUREMETER TESTS IN SAND

BY

RENATO PINTO DA CUNHA

B.Sc., Universidade Federal do Rio de Janeiro, 1986
M.Sc., Universidade Federal do Rio de Janeiro, 1988

A THESIS SUBMITTED IN PARTIAL FULFILLMENT OF

THE REQUIREMENTS FOR THE DEGREE OF

DOCTOR OF PHILOSOPHY

in

THE FACULTY OF GRADUATE STUDIES

Department of Civil Engineering

We accept this thesis as conforming
to the required standard

.....

THE UNIVERSITY OF BRITISH COLUMBIA

October 1994

In presenting this thesis in partial fulfillment of the requirements for an advanced degree at the University of British Columbia, I agree that the Library shall make it freely available for reference and study. I further agree that permission for extensive copying of this thesis for scholarly purposes may be granted by the head of my department or by his or her representatives. It is understood that copying or publication of this thesis for financial gain shall not be allowed without my written permission.

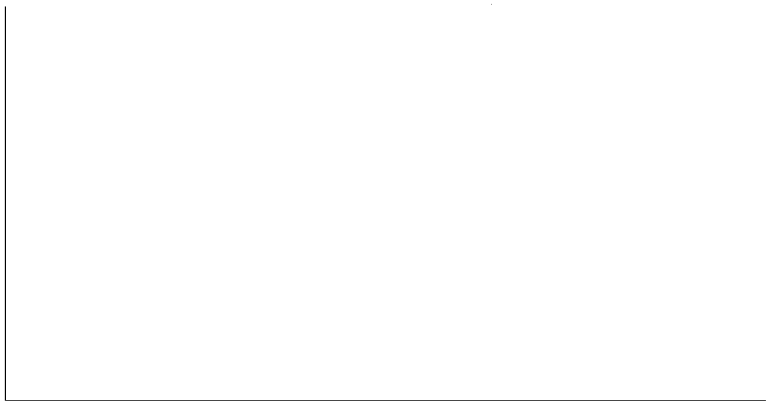

Department of CIVIL ENGINEERING

The University of British Columbia
Vancouver, Canada

Date 10-13-94

ABSTRACT

This thesis addresses the analytical interpretation of selfboring pressuremeter testing curves in sands. Emphasis is placed on the development of a new approach to analyze the data and hence to derive reliable predictions of the basic soil parameters, namely the friction angle, the lateral stress and the shear modulus.

The new methodology of interpretation relies on a "curve fitting" technique to match the experimental and idealized (model) curves, from which a set of fundamental soil parameters are derived. These parameters are linked to each other in the framework of the cavity expansion model adopted. Some of the elasto-plastic models currently available are adopted for use under the new methodology of interpretation. A new model that extends the rheological equations of Hughes et al, 1977 is also developed. Pressuremeter tests under controlled conditions are analyzed in order to verify the basic assumptions of the chosen models. Some of the best calibration chamber data from the University of Cambridge (Fahey, 1986) and from the Italian ENEL-CRIS laboratory (Bellotti et al, 1987) are used for this purpose. Once the reliability of the chosen models is established, the new methodology of interpretation is applied to field pressuremeter data. Several high quality tests carried out by the writer in a granular site in Vancouver, Canada are analyzed. The results of both field and chamber tests confirm the reliability of the new interpretation approach proposed here.

The new interpretation approach also provides the engineer with a technique to numerically quantify the disturbance of the testing curve. Using the new disturbance criterion ranges for "undisturbed", "disturbed" and "highly disturbed" testing curves are proposed. This criterion aided in the establishment of the insertion procedure of the UBC selfboring pressuremeter, allowing optimization of the insertion technique and minimization of soil disturbance during selfboring.

It is believed that the contribution given in this thesis aids pressuremeter practitioners to design more economical engineering works based on reliable soil parameters derived from the selfboring pressuremeter test. Simplicity and reliability are the essential features of the proposed methodologies of insertion, testing and interpretation described herein.

TABLE OF CONTENTS

ABSTRACT ..... **i**

TABLE OF CONTENTS ..... **iii**

LIST OF TABLES ..... **vi**

LIST OF FIGURES ..... **vii**

LIST OF SYMBOLS ..... **ix**

ACKNOWLEDGMENTS ..... **xii**

DEDICATION ..... **xiii**

CHAPTER 1.0 INTRODUCTION **1**

CHAPTER 2.0 ANALYSIS OF TESTING CURVES IN SANDS **5**

2.1 INTRODUCTION 5

2.2 CONSTITUTIVE MODELS FOR PRESSUREMETER ANALYSIS 5

2.2.1 General 5

2.2.2 Basic Considerations of an Elastic Model 9

2.2.3 Basic Considerations of an Elasto-Plastic Model without Volume Change 12

2.2.4 Unloading 15

2.2.5 Review of Elasto-Plastic Models with Volume Change 17

2.2.6 New Cavity Expansion Model 29

2.2.6.1 Introduction 29

2.2.6.2 Basis of the New Model 30

2.2.6.3 Derivation of Elastic Strains in the Plastic Zone 30

2.2.7 Comparison Between Cavity Expansion Models 40

2.3 TRADITIONAL INTERPRETATION METHODOLOGIES IN SAND 44

2.3.1 Introduction 44

2.3.2 Friction Angle 45

2.3.3 Horizontal Stress 48

2.3.4 Shear Modulus 52

2.3.4.1 Unload Reload Shear Modulus 52

2.3.4.2 Initial Shear Modulus 65

2.3.5 Conclusions of Section 2.3 69

2.4 NEW INTERPRETATION METHODOLOGY FOR PRESSUREMETERS 70

2.4.1 Basis of the Curve Fitting Technique 70

2.4.2 Link Between Gi and Gur 75

2.4.3 Modulus Reduction Curve 80

2.5 VERIFICATION OF CONSTITUTIVE MODELS WITH CHAMBER DATA 83

2.5.1 Tests with Leighton Buzzard Sand 83

2.5.2 End Effects 94

2.5.3 Tests with Ticino Sand 99

2.6 PARTICULAR ASPECTS OF THE FITTING TECHNIQUE IN SANDS 108
2.6.1 Strain Range of Curve Match 108
2.6.1.1 High Quality Testing Curves 108
2.6.1.2 Disturbed Testing Curves 120
2.6.2 Sensitivity Analysis 124
2.7 SUMMARY AND CONCLUSIONS 131

CHAPTER 3.0 INSERTION AND TESTING PROCEDURE FOR THE UBC SBPM ... 137

3.1 INTRODUCTION 137
3.2 FIELD TESTING PROGRAMME 137
3.3 UBC SBPM EQUIPMENT CHARACTERISTICS 142
3.3.1 Steel Lantern Characteristics 143
3.3.2 Effects of the Lanterns on Gur 147
3.3.3 Method of Installation 149
3.4 REVIEW OF INSERTION PROCEDURES 151
3.4.1 Key Insertion Parameters in Clays 151
3.4.2 Key Insertion Parameters in Sands 153
3.5 NUMERICAL QUANTIFICATION OF DISTURBANCE 155
3.6 INSERTION PROCEDURE FOR THE UBC SBPM 159
3.6.1 Shoe Plugging 162
3.6.2 Jetting Rod Position 165
3.6.3 Jetting System 170
3.6.4 Dimensional Differences Along Shaft 171
3.6.5 Recommended UBC SBPM Insertion Procedure 176
3.7 TESTING PROCEDURE 177
3.7.1 Rate of Inflation 177
3.7.2 Holding Time Prior to Unload Reload Loops 178
3.7.3 Recommended UBC SBPM Testing Procedure 181
3.8 SUMMARY AND CONCLUSIONS 184

CHAPTER 4.0 TEST RESULTS AT THE UBC SITE AT LAING BRIDGE 187

4.1 INTRODUCTION 187
4.2 GENERAL CHARACTERISTICS OF THE LAING BRIDGE SITE 187
4.2.1 Geology 187
4.2.2 Location and Features 189
4.2.3 Stratigraphy 191
4.2.4 Maximum Shear Modulus 194
4.2.5 Laboratory Testing Results 196
4.2.5.1 Soil Strength 196
4.2.5.2 Soil Classification 196
4.3 INTERPRETATION OF UBC SBPM DATA 197
4.3.1 Testing Curves 197
4.3.2 Curve Fitting Interpretation 201
4.3.2.1 Friction Angle 201
4.3.2.2 Coefficient of Earth Pressure at Rest 208
4.3.2.3 Shear Modulus 212
4.3.2.4 Modulus Reduction Curve 215

4.4 CONCLUSIONS 220

CHAPTER 5.0 SUMMARY AND CONCLUSIONS 222

5.1 SUMMARY 222

5.2 METHODOLOGY OF INSERTION 224

5.3 METHODOLOGY OF TESTING 226

5.4 METHODOLOGY OF INTERPRETATION 226

5.5 FINAL REMARKS 228

5.6 SUGGESTIONS FOR FUTURE RESEARCH 228

5.6.1 Equipment Development 229

5.6.2 Interpretation of SBPM Data 229

BIBLIOGRAPHY 230

APPENDIX A DESCRIPTION OF THE UBC SBPM 245

A.1 INTRODUCTION 245

A.2 PUSHING AND PUMPING UNITS 245

A.3 TESTING UNIT 247

A.3.1 Data Acquisition System and Related Sensors 247

A.3.2 UBC Selfboring Pressuremeter 250

APPENDIX B CALIBRATION OF THE UBC SBPM 254

B.1 INTRODUCTION 254

B.2 STRAIN ARMS 254

B.3 PRESSURE TRANSDUCERS 256

B.4 MEMBRANE RESISTANCE AND LANTERN COMPLIANCE 257

B.4.1 Compliance Correction of Unload Reload Loops 262

B.5 SUMMARY 265

APPENDIX C RESULTS OF THE TRIAXIAL TESTS 266

C.1 INTRODUCTION 266

C.2 TESTS WITH THE RECONSTITUTED SAMPLES 268

C.3 TESTS WITH THE "UNDISTURBED" SAMPLES 271

C.4 CONSTANT VOLUME FRICTION ANGLE 277

C.5 SUMMARY 278

LIST OF TABLES

Table 2.1: Comparison of Cavity Expansion Models for Interpretation of Pressuremeter Tests in Sands 20
Table 2.2: Comparison of Friction Angle Predicted by Different Traditional Interpretation Methodologies 46
Table 2.3: Calibration Chamber Testing Results on Leighton Buzzard Sand (Modified after Fahey, 1986) 85
Table 2.4: Fitting Results on Chamber Tests with Leighton Buzzard Sand 90
Table 2.5: Calibration Chamber Testing Results on Ticino Sand (Modified after Bellotti et al, 1987) ... 101
Table 2.6: Recommended Fitting Range of SBPM Tests in Sands 125
Table 2.7: Sensitivity of Fitting Results for Increase or Decrease in one of the Input Parameters 130
Table 2.8: Sensitivity of Fitting Results for (a) Constant Volume Friction Angle, (b) Poisson's Coefficient 132
Table 3.1: Testing Programme at the Laing Bridge Site 140
Table 3.2: Characteristic of the Pressuremeter Tests Performed at the Site 141
Table 3.3: General Characteristics of the Lanterns Used 146
Table 3.4: Successful SBPM Drilling Variables in Sand 154
Table 3.5: Establishment of the Optimum Jetting Rod and Nozzle Type 168
Table 3.6: Influence of Creep Strain on Unload Reload Modulus 182
Table 4.1: Curve Fitting Results in Laing Bridge Site 205
Table 4.2: Assessment of Coefficient of Earth Pressure by Empirical Formulae 210
Table 4.3: Strain and Stress Levels Related to Gur and Gi 214
Table B.1: General Calibration Characteristics of the UBC SBPM Sensors 255
Table C1: Results of the Triaxial Testing Programme with "Undisturbed" Samples 276

LIST OF FIGURES

Figure 2.1: Indirect Approach for Analysis of Selfboring Pressuremeter Results 6
Figure 2.2: Orientation of Stresses and Strains of a Soil Element at a Radial Distance r 8
Figure 2.3: Idealized Pressuremeter Stress Path and Elastic Plus Plastic Zones Developed Around the Cavity 13
Figure 2.4: Stress Distribution Around a Cylindrical Cavity in Sand (Modified after Howie, 1991) 16
Figure 2.5: Effect of Unloading under a Yield Surface (Modified after Hughes, 1982) 18
Figure 2.6: Stress-Strain and Volumetric Strain Shear Strain Curves for (a)Simple Shear Test Results (Stroud, 1971) and (b) Idealized by Hughes et al, 1977(after Bellotti et al, 1987) 22
Figure 2.7: Particular Stage of Cavity Expansion in Sand 32
Figure 2.8: Elastic Radial Displacement at the Cavity Wall for a Particular Stage of Expansion 35
Figure 2.9: Elastic Displacement at the Wall due to Compressive Volume Change of a Soil Element 38
Figure 2.10: Comparison of Predictions given by the Numerical and Analytical Solutions 41
Figure 2.11: Comparison of Pressuremeter Curves Predicted by Different Models 43
Figure 2.12: Comparison of Measured and Applied Lateral Stress in Calibration Chamber (after Bellotti et al, 1987) 50
Figure 2.13: Concept of Elastic Shear Stiffness as Obtained from Unload Reload Loops (Modified after Bruzzi et al, 1986) 53
Figure 2.14: Effect of Stress Level on Unload Reload Shear Modulus 55
Figure 2.15: Plastic and Elastic Zones Prior and After the Loop Stage 56
Figure 2.16: Effect of Strain Level on Unload Reload Shear Modulus 60
Figure 2.17: Variation of Shear Modulus with Shear Strain for Sands (after Idriss, 1990) 61
Figure 2.18: Determination of Initial Modulus from SBPM Curve 66
Figure 2.19: Variation of Soil Stiffness in Elastic Zone for a Particular Stage of the Cavity Expansion 68
Figure 2.20: Basis of the Curve Fitting Technique 72
Figure 2.21: Hyperbolic Soil Response at the Elastic Zone in terms of (a) Stress-Strain Curve and (b) Modulus Reduction Curve 76
Figure 2.22: Curve Matching without allowance for Finite Boundary Correction - Fahey, 1986 Tests 86
Figure 2.23: Curve Matching on Fahey, 1986 Tests: Hughes et al, 1977 Model 87
Figure 2.24: Curve Matching on Fahey, 1986 Tests: Carter et al, 1986 Model 88
Figure 2.25: Curve Matching on Fahey, 1986 Tests: New Cavity Expansion Model 89
Figure 2.26: Curve Matching on Fahey, 1986 Tests: Limits for Gi 93
Figure 2.27: (a) Curve Matching on Jewell et al, 1980 Test B5
(b) Elastic and Plastic Zones Inside the Calibration Chamber 96
Figure 2.28: Curve Matching on Bellotti et al, 1987 Test 228: Influence of Chamber to Probe Ratio 98
Figure 2.29: Curve Matching on Bellotti et al, 1987 Tests: Ideal Installation Tests 102
Figure 2.30: Curve Matching on Bellotti et al, 1987 Tests: Selfbored Tests 103
Figure 2.31: Predicted Results of the Curve Matching : Friction Angle and Lateral Stress 104
Figure 2.32: Predicted Results of the Curve Matching: Shear Modulus 105
Figure 2.33: Influence of Range of Fitting on Results: Undisturbed Test
(a) Curve Fitting at Distinct Ranges, (b) Variation of Parameters 110
Figure 2.34: Schematic of Plastic Zones Developed at Cavity Strains of 10 and 20 % 112
Figure 2.35: Idealized and Typical Experimental Stress Strain Curves of Sand During Shear 114
Figure 2.36: Effect of Continuous Shearing on Measured SBPM Response 115
Figure 2.37: Soil Elements Around the Probe Chosen for the Numerical Analysis Following Manassero, 1989 117
Figure 2.38: Results of Numerical Analysis for Test SBP09: 5.3m. (a) Volumetric Strain against Cavity Strain for Soil Elements, (b) Relation between Plastic and Critical State Zones Developed around the Probe 119

Figure 2.39: Influence of Range of Fitting on Results: Disturbed Test
(a) Curve Fitting at Distinct Ranges, (b) Variation of Parameters 121
Figure 2.40: Effect of Disturbance on Measured SBPM Response 123
Figure 2.41: Curve Fitting of Test SBP09 (5.3 m) with Carter et al, 1986 Model 127
Figure 2.42: Sensitivity Analysis of the Curve Fitting: (a) Friction Angle, (b) Shear Modulus
(c) Lateral Stress 128
Figure 3.1: Location of In Situ Tests at Laing Bridge Site 139
Figure 3.2: Steel Lanterns with Overlapping Steel Strips and Camkometer Lantern 145
Figure 3.3: Lantern Effects on Gur 150
Figure 3.4: Disturbance Evaluation of SBPM Testing Curve 157
Figure 3.5: Practical Numerical Assessment of Disturbance 160
Figure 3.6: Typical Variables Obtained with the Sounding File of the UBC SBPM 161
Figure 3.7: Typical Comparison of Curves from Tests with Different Shoe Pluggings 164
Figure 3.8: Relationship Between Disturbance and Penetration Resistance 166
Figure 3.9: Comparison of Coefficients of Disturbance for Different Testing Soundings 169
Figure 3.10: Characteristics and Effects Caused by the Oversized Lantern Retainers 173
Figure 3.11: Effects of Dimensional Differences Along Shaft 175
Figure 3.12: Influence of Rate of Inflation on Pore Pressure Development 179
Figure 3.13: Influence of Rate of Inflation on Testing Curve 180
Figure 3.14: Proposed Testing Procedure for Selfboring Pressuremeter Tests 183
Figure 4.1: (a) Laing Bridge Site Location, (b) Test Area of this Site (Modified after Sully, 1991) 188
Figure 4.2: Geological Cross Section of the Fraser Delta (after Blunden, 1975) 190
Figure 4.3: Section 1-1 of Laing Bridge Site 192
Figure 4.4: Typical Piezocone Profile in Laing Bridge Site 193
Figure 4.5: Profiles of Shear Wave Velocity and Maximum Shear Modulus 195
Figure 4.6: Typical Pressure Expansion Curves Measured by the UBC SBPM at Laing Bridge 198
Figure 4.7: Typical Displacements Measured during the Expansion Stage of the UBC SBPM 200
Figure 4.8: Final Curve Matching with Field Data: (a) Depth 5.3 m, (b) Depth 6.3 m 202
Figure 4.9: Final Curve Matching with Field Data: (a) Depth 8.3 m, (b) Depth 10.3 m 203
Figure 4.10: Final Curve Matching with Field Data: Depth 13.3 m 204
Figure 4.11: Comparison of Curve Fitting Results: Friction Angles 207
Figure 4.12: Comparison of Curve Fitting Results: Shear Modulus 213
Figure 4.13: Determination of Modulus Reduction Ratio for Different Amplitudes of Shear Strain 216
Figure 4.14: Comparison between the Predicted Gi from Curve Fitting and the Seismic Modulus G_0 217
Figure 4.15: (a) Hyperbolic Stress Strain Curve for Depth 8.3 m (SBP19)
(b) Secant Shear Modulus Ratio versus Shear Strain 219
Figure A.1: Pushing and Pumping Units of the UBC SBPM System 246
Figure A.2: Testing Unit of the UBC SBPM System 248
Figure A.3: UBC Selfboring Pressuremeter Sectional Assembly 252
Figure B.1: Membrane Resistance from Expansion in Air 258
Figure B.2: Lantern Compliance from Expansion Inside Split Cylinder 261
Figure B.3: Compliance Correction of Unload Reload Loops: (a) Compliance Test, (b) Determination
of Gsys with Basis on Power Equation 264
Figure C.1: Schematic of Triaxial Testing Apparatus 267
Figure C.2: Typical Stress Strain Response of the Reconstituted Samples: Constant C. Pressure 269
Figure C.3: Typical Stress Strain Response of the Reconstituted Samples: Constant Relative Density 270
Figure C.4: Typical Stress Strain Response in the Triaxial Test: "Undisturbed" Samples 273
Figure C.5: Determination of the Peak Friction Angle from the Triaxial Tests: "Undisturbed" Samples 274
Figure C.6: Determination of the Constant Volume Friction Angle of the Laing Bridge Sand 279

LIST OF SYMBOLS

b ..... Intermediate stress parameter
D ..... Diameter
D_r ..... Relative density
D_{10} ..... Diameter at which 10 % of soil is finer
D_{50} ..... Diameter at which 50% of soil is finer
E ..... Young modulus
f ..... Empirical factor
G ..... Shear modulus or stiffness of the sand
Gi ..... Shear modulus of the elastic sand, as obtained by the interpretation of the SBPM data
Gp ..... Shear modulus of the zone of soil encompassed by the plastic zone
Gur ..... Unload reload shear modulus
Gur^c ..... Unload reload shear modulus corrected for stress level
G_{max} ..... Maximum shear modulus predicted with the pressuremeter Gur
$Gmeasured$ Measured (not corrected) shear modulus from the unload reload loop
$Gsys$ ..... System shear modulus, defined by Fahey and Jewell, 1990 to correct the Gur
G_0 ..... Maximum shear modulus of the sand
g ..... Green strain
g_r ..... Radial green strain
g_θ ..... Circumferential green strain
H ..... Height
K ..... Coefficient of lateral pressure
K_{cv} ..... Upper bound of the constant K from Rowe's stress dilatancy equation
K_0 ..... Coefficient of earth pressure at rest
K_a ..... Coefficient of active earth pressure
K_p ..... Coefficient of passive earth pressure
K_g ..... Modulus number
L ..... Length
N ..... Principal stress ratio
n ..... Constant from Rowe's stress dilatancy equation
P' ..... Stress component of diagram of Lambe and Whitman, 1979
P_{cu} ..... Effective internal pressure at the start of unload reload loop
P_a ..... Atmospheric pressure
P ..... Effective pressure at the cavity wall of expanding cavity
Q ..... Stress component of diagram of Lambe and Whitman, 1979
Q_t ..... Cone bearing resistance corrected for pore pressure
r ..... radius
r_w ..... radius of the cavity wall
r_u ..... radius of the cavity wall at a deformed position
r_0 ..... initial radius of the cavity wall or the pressuremeter
u_r ..... Radial displacement
u_θ ..... Circumferential displacement
u_w ..... Displacement at the cavity wall
u_{rw} ..... Radial displacement at the cavity wall
u_{rew} ..... Elastic radial displacement at the cavity wall
u_{rpw} ..... Plastic radial displacement at the cavity wall
u_{rp} ..... Displacement at the elasto-plastic boundary
u^*_e ..... Displacement at the inner soil ring caused by the external ring

u_{re} ..... Elastic radial displacement at the soil ring
U_0 ..... Hydrostatic ground water pressure
U_1 ..... Dynamic pore pressure measured at the face of the piezocone
U_2 ..... Dynamic pore pressure measured behind the tip of the piezocone
U_3 ..... Dynamic pore pressure measured behind the friction sleeve of the piezocone
V ..... Volume
V_s ..... Shear wave velocity
w_n ..... Water content
σ ..... Stress
σ_h ..... Effective lateral stress of the soil
σ_r ..... Effective radial stress
σ_θ ..... Effective circumferential stress
σ_v or σ_z..... Effective vertical stress
σ_m ..... Average normal effective stress in the horizontal plane
σ_{av} ..... Average normal stress within the plastic zone that existed prior to the loop stage
σ_{rw} ..... Effective radial stress at the cavity wall or cavity pressure
σ_R ..... Limit effective radial stress to start yielding of the sand
σ_f ..... Limit effective radial stress to start yielding of the sand at the cavity wall
σ_d ..... Deviator stress of triaxial test
σ'_c ..... Effective confining pressure of triaxial tests
σ'_1 ..... Major principal effective stress of triaxial test
σ'_2 ..... Intermediate principal effective stress of triaxial test
σ'_3 ..... Minor principal effective stress of triaxial test
σ_b ..... Effective boundary stress of calibration chamber tests
ε ..... Strain
ε_r ..... Radial strain
ε_θ ..... Circumferential strain
ε_z ..... Vertical strain
$\varepsilon_{\theta w}$ ..... Circumferential strain at the cavity wall or cavity strain
$\varepsilon_{\theta R}$ ..... Limit circumferential strain to start yielding of the sand
$\varepsilon_{\theta h}$ ..... Circumferential strain at the start of the holding phase
α ..... Almansi strain
α_r ..... Almansi radial strain
α_θ ..... Almansi circumferential strain
$\alpha_{\theta w}$ ..... Almansi circumferential strain at the cavity wall
δ ..... Dilation angle
δ_{an} ..... Direction of plane of anisotropy from Oda, 1981 tests
β ..... Empirical parameter
ν ..... Coefficient of Poisson
γ ..... Shear strain
γ_f ..... Limit shear strain to start yielding of the sand
γ_{av} ..... Average shear strain amplitude imposed by the loop in the surrounding soil
ρ ..... Deformed radius or soil density
τ ..... Shear stress
τ_m ..... Average shear stress in the horizontal plane
τ_f ..... Limit shear stress to start yielding of the sand
τ_{max} ..... Maximum shear stress of the sand in the horizontal plane
ϕ ..... Friction angle
ϕ_{cv} ..... Constant volume friction angle

ϕ_{TRX} ..... Axially symmetric friction angle
ϕ_{TRX}^{PS} ..... Plane strain (converted) friction angle
$\Delta\gamma_c$ ..... Amplitude of shear strain at the cavity wall
ΔV ..... Increment in volume
$\Delta\sigma_h$ ..... Increment in effective horizontal stress
$\Delta\sigma_v$ ..... Increment in effective vertical stress
dP ..... Increment of effective internal pressure above σ_h
dP_u ..... Increment of effective internal pressure during unload stage
dr ..... Increment of radius
$d\theta$ ..... Increment of angle
dl_0 ..... Initial length of a small liner element
dl ..... Length of this element in the deformed state
$d\sigma_r$ ..... Increment of effective radial stress
$d\sigma_\theta$ ..... Increment of effective circumferential stress
$d\sigma_z$ ..... Increment of effective vertical stress
$d\sigma_{rw}$ ..... Increment of effective radial stress at the cavity wall
$d\varepsilon_v$ ..... Increment of volumetric strain
$d\varepsilon_a$ ..... Increment of axial strain
$d\varepsilon_\theta$ ..... Increment of circumferential strain at the cavity wall during unload stage
$d\varepsilon_{rw}$ ..... Increment of radial strain at the cavity wall
$d\varepsilon_{\theta w}$ ..... Increment of circumferential strain at the cavity wall
$d\gamma$ ..... Increment of shear strain

ACRONYMS:

CD .....Coefficient of disturbance
CJ .....Central jetting system
CPTU.....Piezocone
CVL.....Civil
ENEL-CRIS.....Italian National Electricity Board-Hydraulic and Structural Research Center
FDP sounding...Testing sounding in which FDPM tests were carried out
FDPM.....Full displacement pressuremeter
LL .....Liquidity limit
OCR.....Overconsolidation ratio
OLR.....Oversized lantern retainer
PI .....Plastic index
Pl .....Limit Pressure
PL .....Plastic Limit
SBP sounding...Testing sounding in which SBPM tests were carried out
SBPM .....Selfboring pressuremeter
SC tests.....Calibration chamber tests with smooth boundaries and constant boundary pressure
SCPT .....Seismic cone
SH .....Shower Head system
SPT .....Standard penetration test
ST1 .....Stationary piston sampler from Rocktest Inc.
TOLR .....Tapered oversized lantern retainer
UBC.....University of British Columbia

ACKNOWLEDGMENTS

To the Lord, for the guidance of my life and destiny

To my parents Aldo da Cunha Rosa and Acilea Pinto da Cunha, for their love and support throughout my life

To my wife Daniela Abrahami Pinto da Cunha and daughter Bianca Abrahami Pinto da Cunha, for their support and strong encouragement

To the Brazilian Council of Research and Development (CNPq) for their generous 4 years scholarship

To my advisor Dr. R.G.C. Campanella, for his valuable assistance and guidance

To Dr. J.M.O. Hughes, for his enthusiastic assistance, encouragement and numerous discussions of both theoretical and practical aspects of the pressuremeter testing

To Drs. Byrne, Vaid and Fannin for their valuable discussions throughout my years at UBC and critical review of the contents of this thesis

To Dr. J.A.R. Ortigão for his encouragement in the initial stages of the research and valuable technical discussions

To Dr. Pat Stewart for the critical review, friendship and English correction of my thesis

To the colleges Matt Kokan, Thandara Murthy, John Sully, Mike Davies, Tim Boyd and Jody Everard for their field help as well numerous technical discussions

To the technical (and talented) staff of the Department of Civil Engineering for their support and patient, with special attention to Art Brookes, Jim Greig, Thomas, Scott Jackson, Harald Schremp, Pat Sheenan and Flora Lew

To Dr. De Souza Coutinho, for the permission of use of the cavity expansion model "Anabela"

To all those people who directly or indirectly contributed and helped me in the development of this thesis

DEDICATION

This thesis is dedicated to my wife Daniela Abrahami Pinto da Cunha, for her emotional support, understanding and patient throughout this endeavor

CHAPTER 1.0 INTRODUCTION

Site investigation and the assessment of the characteristics of the soil are important aspects of the geotechnical design process. In situ testing has become increasingly important in geotechnical engineering as a complement as well as a substitute for laboratory tests. The demand for in situ testing has developed with a growing awareness that field sampling and laboratory testing may have problems of disturbance. This can be principally the case in granular soils, where the absence of cohesion demands an extremely high (and costly) technology to retrieve truly representative samples from the site.

On the other hand, in situ tests have a much more complex boundary condition than those imposed by laboratory test devices. This considerably complicates the interpretation of in situ data as the stress and strain conditions of the soil surrounding any of the in situ probes are difficult (if not impossible) to define. This major difficulty leads to the large array of empirical relationships that are applied to derive basic soil parameters from in situ measured values. Since the empirical relationships mainly rely on correlations with laboratory tests, sample disturbance effects from to these tests will be inherently imposed on the empirically derived in situ soil predictions. Moreover, the empirical relationships are valid for a particular type of soil and testing conditions, that do not universally apply for all the existing natural deposits.

In situ methods are basically divided into two general groups, namely logging and specific methods (Campanella and Robertson, 1982). The logging methods were primarily developed for stratigraphic profiling determinations. They are fast and relatively economical in comparison to the specific in situ methods. The best example is the piezocone test. The specific in situ methods were developed in order to extend the particular knowledge of some soil property at specific locations defined by the logging tools. In general these methods are much more specialized and often slower to execute than the logging methods. Although the specific methods can also rely on empirical relationships to define the soil parameters, they have the potential to define the soil properties in terms of a specific stress-strain model.

It was in the context of the specific in situ methods that the pressuremeter was developed. Similarly, like all other specific in situ tools, the pressuremeter does not directly measure any soil parameter, but rather the pressure and the change in volume or radius of an expanding cylindrical membrane. However, the major attraction of the pressuremeter test is the fact that it constitutes a simple boundary value problem

in soil mechanics. It can be theoretically modeled by the expansion of an infinitely long cylindrical cavity, where boundary conditions are well defined and controlled. This offers the possibility of the simultaneous derivation of both in situ deformation and strength parameters when applying any of the several available cavity expansion theories.

The original concept of lowering a balloon like device down a borehole and inflating it to measure deformation properties dates from 1930 or 1931 (Baguelin et al, 1978). The first reference to such device was given by Kögler, 1933 who developed a simple probe with length of 125 cm and diameter of 10 cm. This first device consisted of a long sausage shaped bladder which stretched between two metal discs. The discs were held apart at a fixed distance by a steel rod which formed the backbone of the device. It was lowered into a predrilled hole and gas inflated. The impact of Kögler's invention in the geotechnical area was insignificant, even though he was able to use the equipment to record pressure volume change curves that are similar to those obtained nowadays with more sophisticated equipments.

It was only in the 50's that the pressuremeter was developed and started to be used in real engineering terms. Without knowledge of Kögler's work, a civil engineering student at the Univ. of Illinois called Menard developed a pressuremeter in 1955 (Menard, 1955). In less than 3 years the Menard pressuremeter started to be produced by Menard's own firm and used as a consulting tool in France. At that time Menard was able to benefit from technological and analytical interpretation advance that was not available in Kögler's time. Like Kögler's original probe, the Menard pressuremeter was designed to be inserted in prebored holes. Due to the high disturbance generated at the cavity wall by the preboring process, results of Menard pressuremeter tests are generally interpreted by empirical rather than analytical methods. Rules for the design of piles under vertical and horizontal load were developed by Menard and his co-workers in the early sixties. Experience grew until nowadays in France (see Briaud, 1986, Baguelin et al, 1978 and Baguelin, 1982), and there exists a large database of experimentation and observation.

Since Menard's pioneering work there have been major developments in the pressuremeter, especially in the 70's and 80's. These developments can be subdivided into areas of pressure and strain measurement, probe insertion, analytical and numerical interpretation, and new types of pressuremeters (Wroth, 1982). The selfboring pressuremeter (SBPM) was devised to eliminate the disturbance problems caused by the soil preboring adopted by the Menard pressuremeter. The first SBPM was developed and used at the Saint

Brieuc Laboratoire des Ponts et Chaussées in 1967 (Baguelin et al, 1978), and also called the Pressiomètre Autoforeur, or PAF. The French work about this pressuremeter was only published in 1972 by Baguelin et al. At about the same time the development of the British SBPM was taking place at the University of Cambridge. The first publication about the British research was by Hughes, 1973. The initial English name chosen was Camkometer (Cambridge K_0 meter), although it is nowadays called selfboring pressuremeter.

The advantage of the selfboring pressuremeter is the fact that this probe can ideally be inserted into the soil without disturbance, thus avoiding any stress and density changes on the original ground conditions. With this characteristic the test results can be properly analyzed in the light of cavity expansion theories, where the initial conditions are well established. However, Hughes in 1973 demonstrated in the laboratory with the X-ray technique that even under "perfect" selfboring conditions a disturbance of at least 0.5 % of the pressuremeter radius can be induced in sands. In real selfboring cases an even higher disturbance percentage can be expected. This disturbance undoubtedly hampers the major premise and potential advantage of the use of selfboring pressuremeters, at least in sands.

Since its original development the selfboring pressuremeter test has been subjected to close scrutiny by a number of researchers. It has been found that the results of this test are extremely sensitive to installation techniques, test procedures and methodologies of interpretation, which is not surprising in view of the sophisticated nature of the pressuremeter probe (Mair and Wood, 1987). The degree of success in obtaining reliable predictions of soil parameters from the selfboring pressuremeter is critically dependent on the combined influence of the methodology of interpretation and the disturbance built in the testing curve. An urgent need for the establishment of less sensitive interpretation methodologies is required.

The emphasis of this thesis is placed on the methodology of interpretation of the selfboring pressuremeter testing data in sands. The current methodology of analysis of the pressuremeter testing curves is reviewed and a new and less sensitive interpretation approach is proposed. The reliability of the derived soil parameters, and the sensitivity of this new approach, are respectively addressed and based on pressuremeter tests in controlled environments and parametric studies. The discussion of the most advanced existing cavity expansion models that can be applied in this new approach are also presented, together with the development of a proposed new cavity expansion model.

The complementary information that is obtained with the new interpretation methodology is the numerical quantification of the disturbance present in the testing curve. With the aid of this new methodology of disturbance assessment it is also possible to show the quantitative effects caused by the variables that influence the testing curve of the UBC SBPM. This discussion considers the large database of field testing trials, in which equipment, insertion and site related variables were changed. With these specific findings the UBC SBPM insertion procedure was established. As will be demonstrated, the suggested procedure not only aid in the standardization of the use of this complex in situ tool, but also leads to "optimum" conditions of insertion where the likelihood of disturbance is considerably reduced.

With the adoption of the suggested insertion procedure it was possible to obtain high quality testing curves. The interpretation of these curves using the new interpretation methodology led to predictions of the basic soil parameters of the sand (friction angle, shear modulus and lateral stress). The discussion on the reliability of such predictions is also explored herein.

CHAPTER 2.0 INTERPRETATION OF PRESSUREMETER DATA IN SANDS

2.1 INTRODUCTION

The objective of this chapter is to examine the methods and models used to determine soil parameters from selfboring (SBPM) pressuremeter data in sands. It describes the assumptions of the existing cavity expansion models developed for the analytical and numerical interpretation of the testing curve of the SBPM test, and introduces a new cavity expansion model. The chapter also introduces the new analytical interpretation methodology proposed in this thesis to derive meaningful soil parameters from the SBPM. In order to assess the need of a new interpretation methodology the reliability of the soil parameters derived with the traditional interpretation methodologies is initially reviewed. These parameters are the friction angle ϕ, the horizontal stress σ_h, and the shear modulus G of the sand.

2.2 CONSTITUTIVE MODELS FOR PRESSUREMETER ANALYSIS

Pressuremeter testing results can be used in geotechnical design by two distinct approaches, the indirect and the direct one. The direct approach, adopted in the empirical relationships of Menard, uses the pressuremeter data to empirically derive the bearing capacity, settlement, etc. of engineering works. The indirect approach, depicted in Figure 2.1, uses interpretation methods that allow the evaluation of the parameters that describe the basic material characteristics of the sand. This approach requires a model to describe the expansion process in the sand. This thesis will adopt only the indirect approach to predict soil parameters from pressuremeter testing results.

This section introduces the cavity expansion models developed to solve the complex boundary value problem of a pressuremeter test in sand.

2.2.1 General

The pressuremeter can be simply modeled as the expansion of an infinitely long cylinder. The soil is assumed to be homogeneous and isotropic. The radial (r) and circumferential (θ) directions are considered, respectively, the major and minor principal directions of stress and strain. The initial stress condition is assumed to be isotropic in the horizontal plane, i.e., the lateral stress (σ_h) is initially equal to the radial (σ_r) and circumferential (σ_θ) stresses.

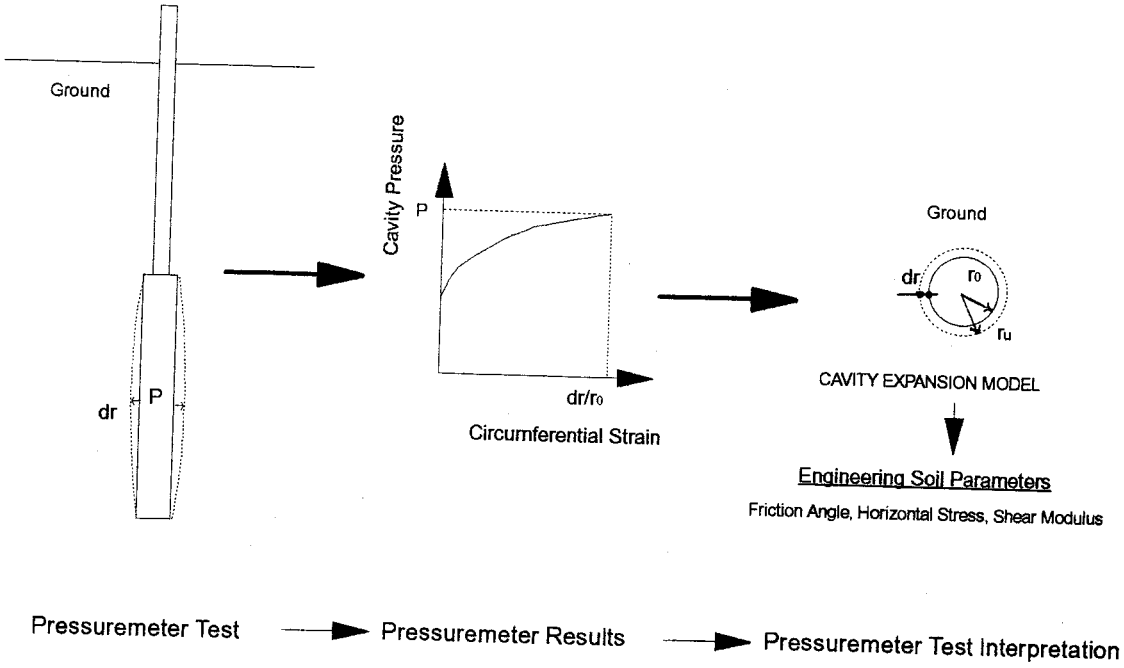

Figure 2.1: Indirect Approach for Analysis of Selfboring Pressuremeter Results

Measurements during a test are made of cavity (internal) pressure and cavity volume or strain. The system is at the rest condition when the internal cavity pressure P equals the horizontal stress σ_h, and lift off of the arms occurs. A pressure increase dP above this horizontal stress causes expansion of the cavity in the radial direction. Under this condition, a particle located initially at a distance r to the center of the cavity will displace to a new deformed radius ρ so that:

$$\rho = r + u_r \tag{2.1}$$

where u_r is the radial displacement.

The surrounding soil will be subjected to plane strain deformation if the length of the pressuremeter is much greater than its radius. In this case no deformation will occur in the vertical direction. Figure 2.2 shows the orientations of stresses and strains considered here. Elongation is considered positive, whereas contraction negative, as assumed by Baguelin et al, 1978 for the following mathematical equations.

The strain acting in the radial and circumferential directions can be determined from the displacement field. For small deformations Cauchy (ε) definition of strain can be used, since Cauchy's definition involves just the first derivatives of the displacement vector with respect to the Cartesian coordinates.

Using the orientation of strains given by Figure 2.2 the following compatibility equations can be derived:

$$\varepsilon_\theta = \frac{(r + u_r)\theta - r\theta}{r\theta} = \frac{u_r}{r} \tag{2.2}$$

$$\varepsilon_r = \frac{u_r + \frac{du_r}{dr}dr - u_r}{dr} = \frac{du_r}{dr} \tag{2.3}$$

where ε_θ is the circumferential strain and ε_r the radial strain.

For large strains, Green (g) or Almansi (α) definitions of strain are used. In this case:

$$g = \frac{1}{2}\frac{dl^2 - dl_0^{\,2}}{dl_0^{\,2}} = \frac{1}{2}((1+\varepsilon)^2 - 1) \tag{2.4}$$

$$\alpha = \frac{1}{2}\frac{dl^2 - dl_0^{\,2}}{dl^2} = \frac{1}{2}\left(1 - \frac{1}{(1+\varepsilon)^2}\right) \tag{2.5}$$

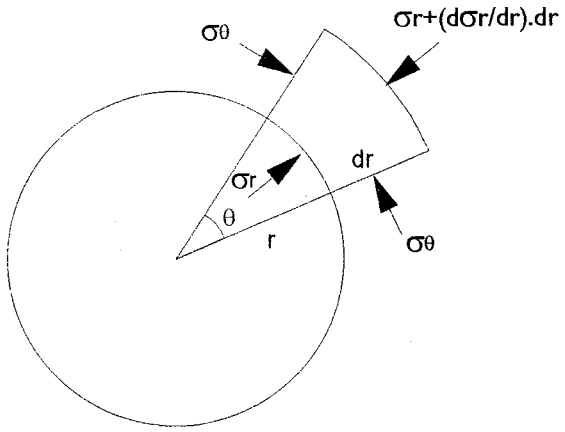

Radial and Tangential Stresses

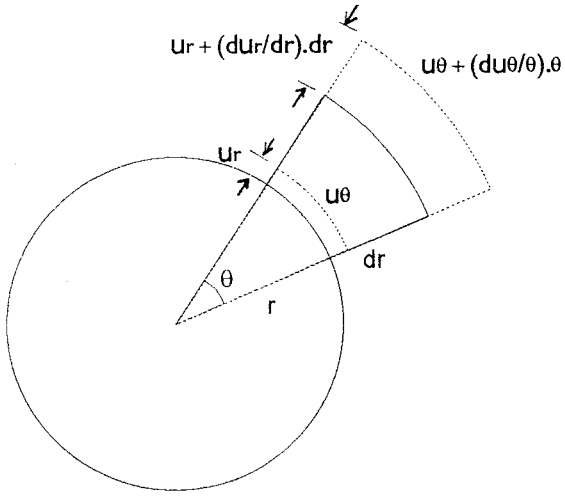

Radial and Tangential displacements

Figure 2.2: Orientation of Stresses and Strains of a Soil Element at a Radial Distance r

where: dl_0 = initial length of a small linear element

dl = length of this element in the deformed state

and ε is the Cauchy strain (=$(dl-dl_0)/dl_0$)

The relationship given by Equations 2.4 and 2.5 allows the determination of circumferential strains (g_θ and α_θ) based on the Cauchy circumferential strain ε_θ, as well as radial strains (g_r and α_r) based on the Cauchy radial strain ε_r.

2.2.2 Basic Considerations of an Elastic Model

For the initial deformation stage of the cavity the soil is assumed to behave elastically. From the theory of elasticity the principal stress changes $d\sigma_r$ (radial), $d\sigma_\theta$ (circumferential) and $d\sigma_z$ (vertical) can be found from Hooke's law (rheological equations), as presented in Baguelin et al, 1978:

$$-E.\varepsilon_r = d\sigma_r - \upsilon(d\sigma_\theta + d\sigma_z) \tag{2.6}$$

$$-E.\varepsilon_\theta = d\sigma_\theta - \upsilon(d\sigma_z + d\sigma_r) \tag{2.7}$$

$$-E.\varepsilon_z = d\sigma_z - \upsilon(d\sigma_r + d\sigma_\theta) \tag{2.8}$$

where: E is the Young modulus

ν the Poisson's coefficient. Assuming plane strain conditions

$$\varepsilon_Z = 0 \tag{2.9}$$

therefore $$d\sigma_z = \upsilon(d\sigma_r + d\sigma_\theta) \tag{2.10}$$

Substituting (2.10) into (2.6) to (2.8) and combining with (2.2) and (2.3):

$$\frac{-E}{(1-\upsilon)(1+\upsilon)}\frac{du_r}{dr} = d\sigma_r - \frac{\upsilon}{1-\upsilon}d\sigma_\theta \tag{2.11}$$

$$\frac{-E}{(1-\upsilon)(1+\upsilon)}\frac{u_r}{r} = d\sigma_\theta - \frac{\upsilon}{1-\upsilon}d\sigma_r \tag{2.12}$$

Solving for $d\sigma_r$ and $d\sigma_\theta$ we obtain:

$$d\sigma_r = \frac{-E(1-\upsilon)}{(1-2\upsilon)(1+\upsilon)}\left(\frac{du_r}{dr} + \frac{\upsilon}{1-\upsilon}\frac{u_r}{r}\right) \tag{2.13}$$

$$d\sigma_\theta = \frac{-E(1-\upsilon)}{(1-2\upsilon)(1+\upsilon)}\left(\frac{u_r}{r} + \frac{\upsilon}{1-\upsilon}\frac{du_r}{r}\right) \tag{2.14}$$

To determine the state of stress an equation of equilibrium is required to relate radial and tangential stresses. This equation must satisfy the boundary conditions of the problem. The equilibrium equation for the cylindrical expanding cavity is obtained by considering the equilibrium in the radial direction. Considering a small element in the radial plane (Figure 2.2) we obtain:

$$\sigma_r . r . \theta + 2 . \sigma_\theta . dr \frac{\theta}{2} = \theta . (r + dr)(\sigma_r + \frac{d\sigma_r}{dr} . dr), \text{ or } \quad \frac{d\sigma_r}{dr} + \frac{\sigma_r - \sigma_\theta}{r} = 0 \qquad (2.15)$$

Compressive stresses are taken as positive by Baguelin et al, 1978. Substituting (2.13) and (2.14) into (2.15) results in the following differential equation:

$$r^2 \frac{d^2 u_r}{d r^2} + r \frac{du_r}{dr} - u_r = 0 \qquad (2.16)$$

which has solution in the form of $u_r = A.r + B/r$. For a large r, $u_r \rightarrow 0$, therefore A= 0.

At the cavity wall $u_w = u_r = B/r_w$, therefore $B = u_w . r_w$ and

$$u_r = \frac{u_w . r_w}{r} = \varepsilon_{\theta w} \frac{r_w^2}{r} \qquad (2.17)$$

where: $\varepsilon_{\theta w}$ is the circumferential strain at the wall.

Combining (2.2) and (2.3) with (2.13) and (2.14) we obtain:

$$\varepsilon_\theta = \frac{\varepsilon_{\theta w} . r_w^2}{r^2} \qquad (2.18), \qquad \varepsilon_r = -\frac{\varepsilon_{\theta w} . r_w^2}{r^2} \qquad (2.19)$$

and:

$$\sigma_r = \sigma_h + d\sigma_r = \sigma_h + \frac{E}{(1+\upsilon)} \frac{\varepsilon_{\theta w} . r_w^2}{r^2} \qquad (2.20)$$

$$\sigma_\theta = \sigma_h + d\sigma_\theta = \sigma_h - \frac{E}{(1+\upsilon)} \frac{\varepsilon_{\theta w} . r_w^2}{r^2} \qquad (2.21)$$

Based on Equations 2.20 and 2.21 it is observed that all (elastic) soil elements around the cavity will follow a unique stress path during the cavity expansion. Moreover, every increase of radial stress produces an equal decrease of tangential stress ($d\sigma_r = -d\sigma_\theta$, Lamé, 1852). Similarly, the circumferential strain will be

equal and opposite in sign to the tangential strain, i.e. $\varepsilon_\theta = -\varepsilon_r$ and no volume change takes place during expansion.

Noting that the shear modulus (G) of the soil is given by E/2 (1+ν) it follows that Equations 2.20 and 2.21 can be changed to:

$$\sigma_r = \sigma_h + d\sigma_r = \sigma_h + 2G\frac{\varepsilon_{\theta w} . r_w^{\,2}}{r^2} \tag{2.22}$$

$$\sigma_\theta = \sigma_h + d\sigma_\theta = \sigma_h - 2G\frac{\varepsilon_{\theta w} . r_w^{\,2}}{r^2} \tag{2.23}$$

These equations will control the stress distribution in the elastic soil for pre yielding conditions. At the cavity wall $r_w = r$, and the boundary stress-strain relation becomes:

$$\sigma_r = \sigma_h + 2G.\varepsilon_{\theta w} \tag{2.24}$$

$$\sigma_\theta = \sigma_h - 2G.\varepsilon_{\theta w} \tag{2.25}$$

As commented before, plane strain conditions are assumed. Since $\sigma_r + \sigma_\theta = 2\sigma_h$ = constant (i.e. radial and circumferential stresses change by equal and opposite amounts from the in situ lateral stress), the average normal stress σ_m (or $(\sigma_r+\sigma_\theta)/2$) in the horizontal plane remains constant. Only the shear stress τ_m (equal to $(\sigma_r-\sigma_\theta)/2$) in the horizontal plane will vary from element to element. Therefore, the expansion of the cavity in the elastic medium is a pure shearing process at constant σ_m.

Rearranging Equation 2.24 it is possible to obtain the following expression for the shear modulus of the elastic sand:

$$G = \frac{1}{2}\frac{\sigma_r - \sigma_h}{(\varepsilon_{\theta w})} = \frac{1}{2}\frac{dP}{d\varepsilon} \tag{2.26}$$

where:

dP is the increment of cavity pressure above σ_h and
dε the corresponding cavity strain amplitude.

Therefore the shear modulus is obtained by measuring the initial slope of the SBPM testing curve. If the soil responds (linearly) elastically, as assumed, this slope will be a straight line.

The elastic model is, however, restricted to small deformations. Once the applied shear stress in the sand equals the available shearing strength, failure (or yield) occurs. As soon as yielding starts to be generated at the cavity wall the elastic model no longer applies.

2.2.3 Basic Considerations of an Elasto-Plastic Model without Volume Change

As the pressure is further increased the soil starts to yield at the cavity wall. An annulus of failed soil commences to develop, extending from the deformed cavity radius r_u to an elasto-plastic boundary with radius r_p, as schematically shown in Figure 2.3(a). This boundary will expand as the pressure in the cavity increases. In the zone beyond this boundary the shear stress has not reached the failure value, hence the soil responds elastically. The elasto-plastic boundary, therefore, divides the soil into two distinct zones, the "plastic" and the "elastic" zones.

The Mohr Coulomb failure criterion is assumed to rule the onset of yielding. This failure criterion is given by the following equation:

$$\frac{\sigma_\theta}{\sigma_r} = N = \frac{1-\sin\phi}{1+\sin\phi} \tag{2.27}$$

At the elasto plastic boundary both elastic and plastic conditions apply. Therefore:

$$\frac{\sigma_\theta}{\sigma_r} = \frac{\sigma_h - d\sigma_r}{\sigma_h + d\sigma_r} = \frac{1-\sin\phi}{1+\sin\phi} \tag{2.28}$$

and hence

$$d\sigma_r = \sigma_h \sin\phi \tag{2.29}$$

The limiting cavity pressure at wall at which yielding commences is given by:

$$\sigma_f = \sigma_h + d\sigma_r = \sigma_h (1+\sin\phi) \tag{2.30}$$

where: σ_f is the limiting effective radial stress to start yielding of the soil.

The shear stress of any element of soil at the onset of yielding (as element B of Figure 2.3(a)) is:

$$\tau_f = \sigma_h \sin\phi \tag{2.31}$$

where: τ_f is the limiting shear stress to start yielding of the soil.

Since

$$\gamma = \tau/G \tag{2.32}$$

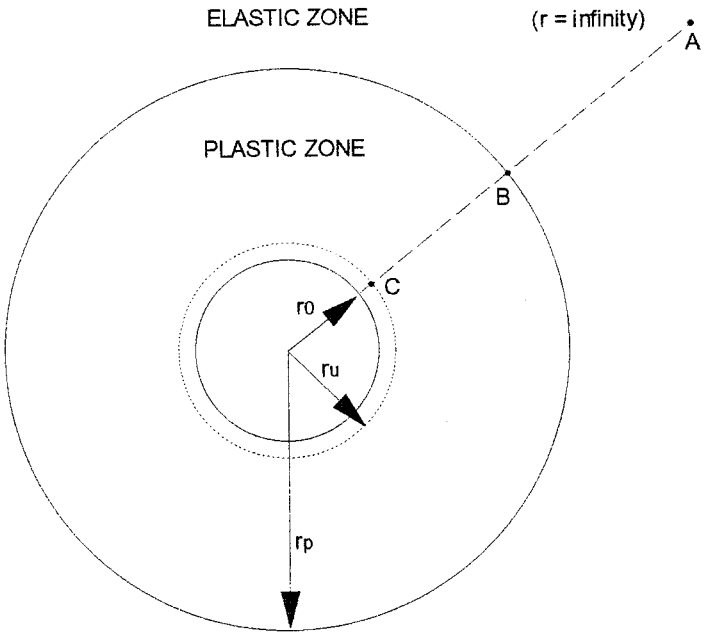

(A) ELASTIC AND PLASTIC ZONES DEVELOPED AROUND THE CAVITY

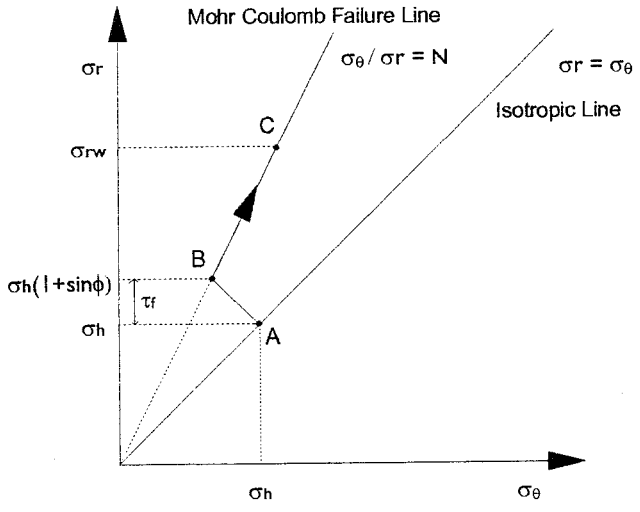

(B) STRESS PATH FOR DRAINED LOADING

Figure 2.3: Idealized Pressuremeter Stress Path and Elastic Plus Plastic Zones Developed Around the Cavity

the shear strain amplitude of any element at the limiting (yield) conditions is:

$$\gamma_f = \frac{\tau_f}{G} = \frac{\sigma_h \sin\phi}{G} \tag{2.33}$$

where: γ_f is the limit shear strain to start yielding of the soil.

Since the elasto plastic boundary represents the limiting (yield) condition of the soil surrounding the probe as expansion proceeds, the elements of soil at this interface (like element B of Figure 2.3(a)) will always be under levels of shear strain amplitude γ_f.

As the internal pressure of the cavity increases the elements of soil inside the plastic zone are subjected to levels of shear stress above τ_f. The stress path of the soil elements inside this zone will follow the Mohr Coulomb failure line. Figure 2.3(b) presents the idealized stress path of elements of soil around the probe for a particular expansion stage. As failure is mobilized at the cavity wall the stress path moves upwards with a constant stress ratio N (as the path shown from points B to C). At this time, different elements of soil will be at different positions along this unique path.

Within the annulus of soil under the plastic regime the equilibrium equation must be satisfied, therefore substitution of Equation 2.27 into 2.15 leads to the following result:

$$\frac{d\sigma_r}{dr} + \frac{\sigma_r(1-N)}{r} = 0 \tag{2.34}$$

Using the boundary conditions at a generic expansion stage after the development of the plastic zone, we can adopt $\sigma_r = \sigma_{rw}$ at $r = r_w$ (cavity wall). Substituting into Equation 2.34 and integrating from the cavity radius to a generic radius r it is obtained:

$$\ln\frac{\sigma_r}{\sigma_{rw}} = -(1-N)\ln\frac{r}{r_w} \tag{2.35}$$

or within the plastic zone (for $r < r_p$, where r_p is the radius of the elasto-plastic boundary):

$$\sigma_r = \sigma_{rw}\left(\frac{r_w}{r}\right)^{(1-N)} \tag{2.36}$$

Similarly, the circumferential stress is given by:

$$\sigma_\theta = N.\sigma_{rw}\left(\frac{r_w}{r}\right)^{(1-N)} \tag{2.37}$$

This solution demonstrates that the rate of decrease of stress with distance within the plastic zone depends on the slope of the Mohr's envelope (or the friction angle of the sand).

The variation of radial and circumferential stress along the radius for a particular stage of the plastic radius r_p (or the effective internal pressure of the cavity σ_{rw}) is schematically shown in Figure 2.4. The same soil elements considered in Figure 2.3(a) are represented in the former figure. It is noticed that the distributions of stresses inside the plastic zone follows a different path than those given inside the elastic zone, since the equations that rule each case are different. It is also noticed inside the plastic zone that the difference between the two stress distributions (σ_r and σ_θ), in other words the shear stress, is variable.

Using the Equations 2.36 and 2.37 it is possible to obtain the value of the average normal stress σ_m at any soil element in the plastic zone, for a particular stage of the cavity expansion. Therefore:

$$\sigma_m = \frac{\sigma_r + \sigma_\theta}{2} = \frac{1}{2}(1+N)\sigma_{rw}\left(\frac{r_w}{r}\right)^{(1-N)} \tag{2.38}$$

Hence the average normal stress increases in the plastic zone as expansion proceeds.

In summary, based on elasto-plastic considerations, the initial rise of the pressuremeter testing curve follows a straight line with slope 2G. Once yielding starts at the cavity wall, and propagates further with the development of a plastic zone, the testing curve becomes non linear. Within the elastic zone the average stress remains constant and only shearing takes place. Elements of soil at the elasto-plastic boundary will be under a unique condition of shear stress and shear strain level. Within the plastic zone both the average normal stress and the shear stress increase during the expansion process.

2.2.4 Unloading

If the cavity pressure is reduced in the course of a pressuremeter test, then the soil around the cavity will initially behave elastically. An immediate transformation of the whole plastic zone into elastic occurs in the start of unloading, as the stress paths of the soil elements will fall below the yield surface of the sand. This simple concept was put forward by Hughes, 1982 and Wroth, 1982 based on the ideal behavior of soils introduced by Roscoe et al, 1958.

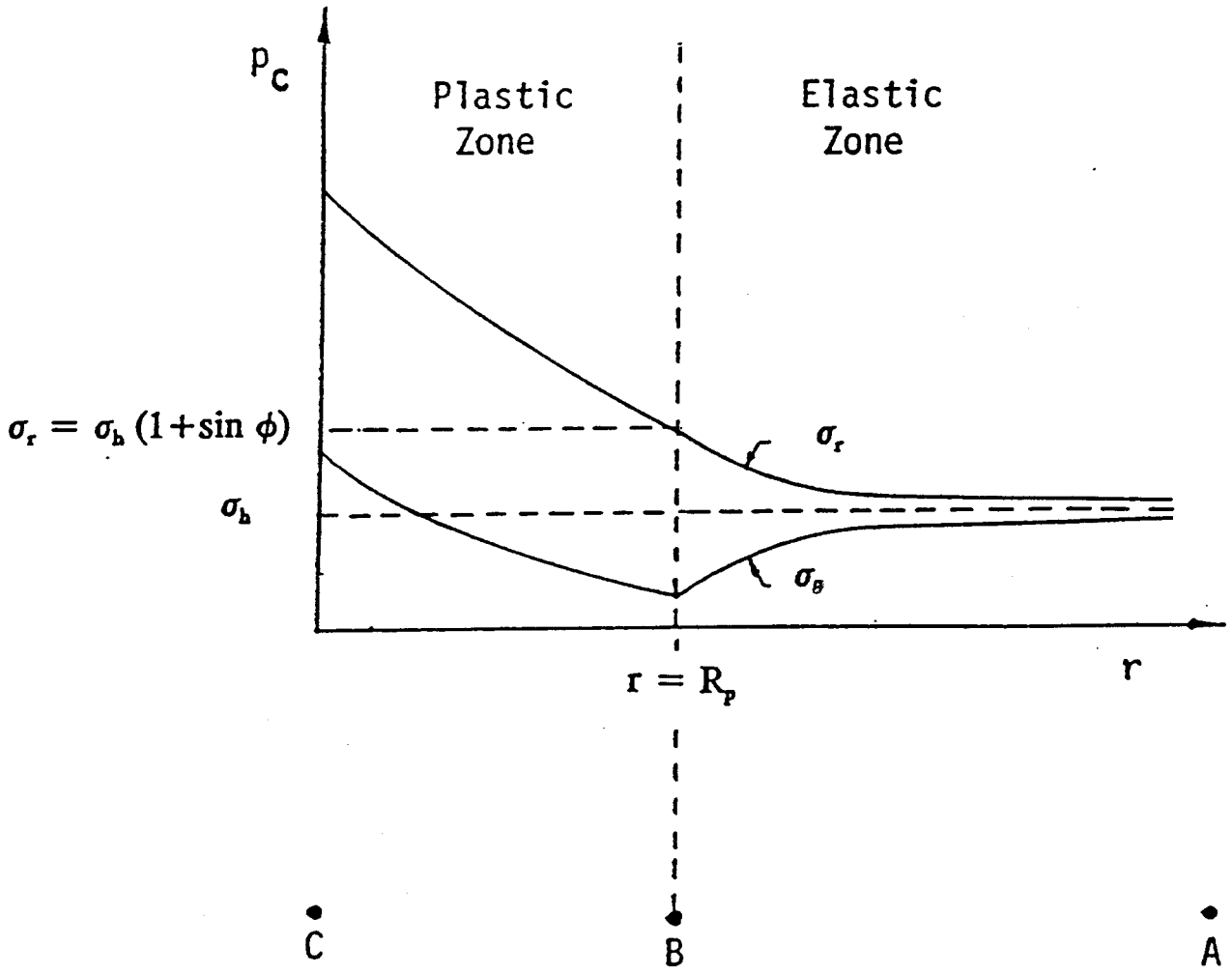

Figure 2.4: Stress Distribution Around a Cylindrical Cavity in Sand (Modified after Howie, 1991)

Figure 2.5 presents a typical response during the loading and unloading stages of the pressuremeter, and the corresponding stress path of an element of soil at the cavity wall. The initial stresses at the probe and at all the soil surrounding the cavity are given by the effective horizontal stress σ_h. As the pressure in the cavity wall is increased beyond σ_h lift off occurs, and the pressuremeter produces a linear testing response. Once the cavity stress reaches the limiting value (given by Equation 2.30) yield starts at the wall, and the stress path moves out at a constant stress ratio (path 1-2). The stress path of soil elements at distinct radii r from the cavity wall will lag behind that shown in Figure 2.5, as the level of stresses will decay with radius (see Figure 2.4). As the stress path of the soil element at the wall moves along the failure line, so does the current yield surface of this element. At point 2 of Figure 2.5 the current yield surface is shown by a dotted line. At this stage both the current yield surface and the stress state will coincide. The same will happen for other soil elements around the cavity. As the cavity pressure is reduced the stress state of all the soil elements around the probe will fail below the (respective) current yield surfaces. Therefore, these elements will behave elastically if the unloading is sufficiently small to avoid plastic strains. On the basis of the above concept, the behavior during an unload reload loop of the pressuremeter test can be expected to be elastic.

Wroth, 1982 pointed out that on the continuation of the unloading process reverse failure may occur, with the circumferential stress as the major principal stress. Assuming that the elastic response is only mobilized for stress paths between the Mohr Coulomb "passive" and "active" failure lines, he derived an equation to predict the maximum decrease of effective cavity pressure for the elastic response of the surrounding sand. This maximum pressure decrease shall be observed when performing unload reload loops to measure the shear modulus (Gur) of the sand.

2.2.5 Review of Elasto-Plastic Models with Volume Change

Analytical models for the simulation of cavity expansion in sands are based on the compatibility conditions between strains and displacements and on the equilibrium equation of the medium that envelopes the cavity. These basic conditions are the same for all models.

In the previous subsection the cavity expansion solution for a purely elastic frictional medium was given. It was also demonstrated that on the onset of yielding a plastic zone develops. Within this zone high levels of shear stress are imposed in the sand.

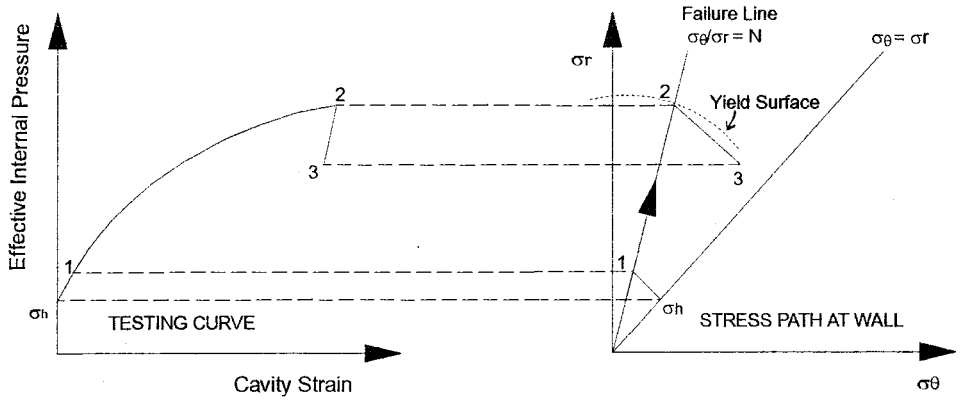

Figure 2.5: Effect of Unloading under a Yield Surface (Modified after Hughes, 1982)

Sands may dilate or increase in volume during shear. The phenomenon known as dilatancy has already been illustrated by many laboratory tests on sand (Rowe, 1962, Stroud, 1971, Vaid et al, 1980) and has been shown to have an important influence on the behavior of medium dense to dense granular materials during pressuremeter expansion (Baguelin et al, 1978). Hence, in order to derive the displacement field within the plastic zone an assumption regarding the volume change of the sand during shear must be made. Table 2.1 shows all the models developed so far for the analysis of pressuremeter tests in sands, in which the dilatancy behavior of this material is considered.

The first solution that incorporated volume changes for cavity expansion in sands was the solution derived by Ladanyi, 1963. His model assumed the soil as an elasto-plastic material with a constant rate of volume change during the Mohr Coulomb failure condition. The relationship between volume change and shear strain was given by a simple and unique relationship. The general solution, however, required a step by step procedure and the volumetric strain at failure had to be interactively chosen to give a straight line in a log-log graph of cavity pressure versus strain. Although more complex, this model did not lead to a significant improvement over the previous Gibson and Anderson, 1961 model, which was the first model exclusively developed for sands. Gibson and Anderson's model did not consider volume changes during shear, and historically their main contribution was the drawing of the log-log graph of cavity pressure versus strain to predict the friction angle.

Vesíc, 1972 developed solutions for the spherical and cylindrical expansion in sand. A linear elastic plastic behavior with volume change was considered. His theory was based on laboratory tests (plane strain or triaxial compression) to determine the volume change relationship in the plastic zone. The basic approach was to estimate the volume change in such a way that, together with the limit pressure, it would allow the derivation of the peak friction angle. The major drawback of this model was the necessity of laboratory tests to define the shear induced volume change of the soil.

In 1975 Wroth and Windle expanded the finite difference method of Baguelin et al, 1972 (for clays, called the "subtangent" method) to account for volume changes in the soil, and hence was used in the evaluation of tests in sands. The complete stress path, stress-strain and strength for an element of soil at the cavity wall could be obtained, if the constant rate between ε_θ and volume change was known.

MODEL	STRESS-STRAIN	APPROACH	ADVANTAGES	DISADVANTAGES	USEFULNESS IN SANDS
Ladanyi, 1963	Linear elastic perfectly plastic. Volume change by fixed flow rule	Step by step numerical procedure	Simple relationship between volume change and shear strain	Cumbersome to use. Flow rule may be unrealistic	C
Vesic, 1972	Linear elastic perfectly plastic. Volume change from laboratory tests	Limit pressure of field curve	Solutions for spherical and cylindrical expansion in sand	Needs laboratory tests and in situ density	C
Wroth and Windle, 1975	Not assumed. Volume change by linear flow rule	Numerical solution by finite difference technique	Allows the knowledge of the stress-strain behavior of the sand	Needs flow rule constant. Numerical instability	C
Hughes et al, 1977	Linear elastic perfectly plastic. Volume change by stress dilatancy	Log-log plot of pressure expansion curve	Easy to solve manually or via computer. Incorporates Rowe's stress dilatancy	No compression during shear. Constant ϕ during failure	A
Robertson and Hughes, 1986	Linear elastic perfectly plastic. Volume change by stress dilatancy	Log-log of pressure expansion curve and nomogram	Accounts for initial compressive behavior of loose sands	Empirical correction is applied. Valid for loose sands	B
Carter et al, 1986	Linear elastic perfectly plastic. Volume change by stress dilatancy	Not exclusively developed for pressuremeter analysis, but to derive limit pressure in pile problems	Incorporates elastic strains in plastic zone. Easy to solve via computer.	Not possible to use into a log-log approach. Small strain solution	A
Houlsby et al, 1986	Linear elastic perfectly plastic. Volume change by stress dilatancy . Contraction model	Optimization routine using model and field curves	Disturbance is minimized in the contraction stage of the test	Contraction of pressuremeter may not follow the assumptions of the model	C
Manassero, 1989	Not assumed Volume change by stress dilatancy	Numerical solution by finite difference technique	Allows the knowledge of the stress-strain behavior of the sand	Numerical instability	B
De Souza Coutinho, 1990	Rigid not perfectly plastic. Volume change by stress dilatancy	Numerical solution by finite difference technique	Allows the knowledge of the stress-strain behavior of the sand	Numerical instability	B
Juran and Mahmoodzadegan, 1989	Not assumed. Volume change by stress dilatancy	Numerical solution with the testing curve	Flow rule incorporates most of the characteristic behavior of sands during shear	Needs laboratory tests and in situ density	C
Ferreira, 1992	Hyperbolic. Volume Change by stress dilatancy	Optimization routine using model and field curves	Stress-strain idealization is more realistic for strain hardening sands	Preliminary assessment gave unreliable results for chamber data	A

A = HIGH B = MODERATE C = LOW

Table 2.1: Comparison of Cavity Expansion Models for Interpretation of Pressuremeter Tests in Sands

Hughes et al, 1977 proposed the first model that incorporated all the main features of sand behavior during shear without the need of extensive laboratory input data. The model idealizes the material as behaving in an elasto-plastic manner, where only volumetric plastic and shear strains due to dilation would be in effect in the plastic zone. The soil behaves elastically until the peak stress ratio at the wall is reached. At the onset of yielding the Mohr Coulomb failure criteria is followed with only plastic dilative strains in the emerging plastic zone. The volume changes occur throughout expansion at a constant dilation rate, leading to a constant mobilized friction angle. Hughes et al, 1977 based this sand behavior on simple shear tests of Stroud, 1971, as demonstrated in Figure 2.6, as well as on the stress dilatancy theory of Rowe, 1971. Stroud, 1971 demonstrated that for dense sands at low to moderate confining pressures dilation starts from the beginning of the test (with a small contractive section) progressing in a close to constant rate.

The cylindrical cavity expansion model of Hughes et al, 1977 does not consider this initial contractive section[1], and relies on the stress dilatancy equation put forward by Rowe, 1971 to link the peak stress ratio (or friction angle) to the dilation rate of the material. This equation has been found to be valid to describe the sand behavior at large stress ratios (Barden and Khayatt, 1966, Rowe, 1971), and shown to be path independent (Tatsuoka, 1976). Rowe's stress dilatancy equation is given by:

$$\frac{\sigma_r}{\sigma_\theta} = K_{cv}\,\frac{1+\sin\delta}{1-\sin\delta} \tag{2.39}$$

where:

δ is the dilation angle (Hansen, 1958)

$K_{cv} = (1+\sin\phi_{cv})/(1-\sin\phi_{cv})$

The term K_{cv} depends on the constant volume friction angle (ϕ_{cv}) of the sand. This constitutes the only laboratory data input of this model. The stress dilatancy equation is used together with the equations that govern both the radial distribution of stresses and displacements within the plastic zone to predict the pressure expansion relationship at the cavity wall.

[1] Actually the theory incorporates a constant "c" representative of the initial contractive section. But, based on the theoretical analysis with pressuremeter data in sands, these authors state that c is sufficiently small to be neglected.

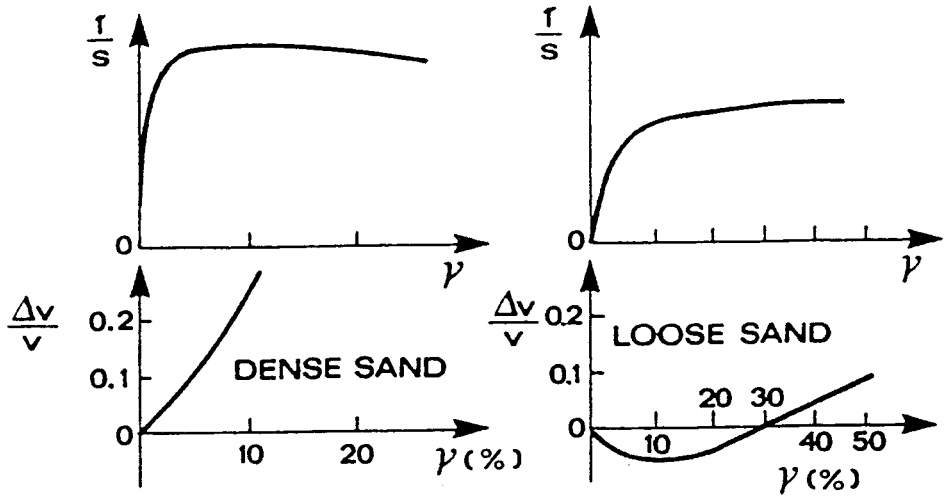

a) RESULTS OF SIMPLE SHEAR TEST

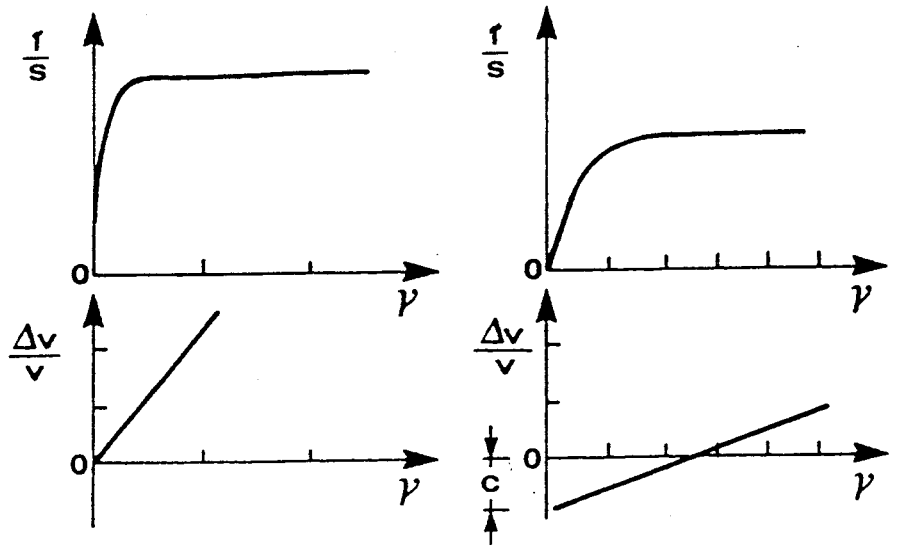

b) SIMPLIFIED MODEL

Figure 2.6: Stress-Strain and Volumetric Strain Shear Strain Curves for (a) Simple Shear Test Results (Stroud, 1971) and (b) Idealized by Hughes et al, 1977 (after Bellotti et al, 1987)

$t = (\sigma_r - \sigma_\theta)/2$, $s = (\sigma_r + \sigma_\theta)/2$

This relationship is given by:

$$\left(\varepsilon_{\theta w} + \frac{c}{2}\right) = \left(\varepsilon_{\theta r} + \frac{c}{2}\right)\left(\frac{\sigma_r}{\sigma_R}\right)^{\frac{(n+1)}{(1-N)}} \tag{2.40}$$

setting c = 0 (suggested by authors) and rearranging, we find:

$$\sigma_r = \sigma_R \left(\frac{\varepsilon_{\theta w}}{\varepsilon_{\theta R}}\right)^{\frac{(1-N)}{(n+1)}} \tag{2.41}$$

where:

$\varepsilon_{\theta w}$ = Circumferential plastic strain at the cavity wall.

c = Intercept of the idealized relation between volumetric and shear strain of Figure 2.6.

$\varepsilon_{\theta R}$= Limit circumferential strain at elasto-plastic boundary = $\gamma_f/2$, as given by Equation 2.33.

$\sigma_r = \sigma_{rw}$ = Effective internal pressure at cavity wall.

σ_R = Limit effective radial pressure to start yielding of the sand = radial pressure at elasto-plastic boundary, or $\sigma_h (1 + \sin\phi)$ as given by Equation 2.30.

$$N = (1 - \sin\phi)/(1 + \sin\phi) \tag{2.42}$$

$$n = (1 - \sin\delta)/(1 + \sin\delta) \tag{2.43}$$

Taking logarithms of both sides of Equation 2.40 and solving with the stress dilatancy equation of Rowe, 1971 (Equation 2.39), it is possible to derive 2 equations that respectively relate ϕ and δ to the slope of the pressuremeter testing curve in a log-log (cavity pressure x strain) graph (see for instance Figure 10 of Hughes et al, 1977). This constitutes the common interpretation procedure used to derive ϕ or δ from the pressuremeter testing curve in sand.

Robertson and Hughes, 1986 argued that in loose sand the expansion of the pressuremeter up to 10 % will not strain the soil sufficiently for it to reach the maximum dilation rate, and hence "c" (Figure 2.6) would be of significant importance. Therefore, they constructed nomograms based on the drained simple shear behavior of Ottawa sand to empirically correct Hughes et al, 1977 model for its usage in loose granular materials. The empiricism built in this correction, however, may erase any eventual gain of accuracy for the derived ϕ.

Carter et al, 1986 extended the Hughes et al, 1977 model to incorporate elastic strains in the plastic zone. The same basic input variables of Hughes et al, 1977 were adopted, with the additional requirement for Poisson's coefficient of the sand. Carter et al, 1986 assumes that the total volumetric strains in the plastic zone are a combination of plastic dilational strains related to the shear strain and elastic compression strains related to changes in the average normal stress in the horizontal plane. The model does not differentiate between shear moduli used in either plastic or elastic zones, ignoring the fact that the soil stiffness will increase in the former zone due to increase in σ_m.

Similarly as in Hughes et al, 1977, the Carter et al, 1986 model is developed on the basis of Cauchy strains (small strain definition). The particular solution for the pressure versus expansion at the cavity wall is given by:

$$\varepsilon_{\theta w} = \varepsilon_{\theta R}\left[A\left(\frac{\sigma_r}{\sigma_R}\right)^X + B\left(\frac{\sigma_r}{\sigma_R}\right) + C\right] \qquad (2.44)$$

where:

$$A = \frac{T}{1+n}, \quad B = \frac{-Z}{1-\eta}, \quad X = \frac{1+n}{1-\eta}, \quad T = 2\left(1+\frac{\Omega}{n+\eta}\right), \quad Z = \frac{2\Omega}{n+\eta}$$

$$\eta = 1 - N, \quad \Omega = (1-\upsilon)(N.n+1) - \upsilon(N+n)$$

with the same σ_R and $\varepsilon_{\theta R}$ as those of the Hughes et al, 1977 model.

Carter et al, 1986 pointed out that the predicted pressure expansion curve of their model does not differ significantly from the prediction given by the Hughes et al, 1977 model, whenever high values of relative elastic stiffness (Gi/σ_h) are used and the expansion $\varepsilon_{\theta w}$ is limited to 10 %. This is because the use of a high elastic stiffness reduces the contribution of the elastic components of strain in the plastic zone. This model can not be used under the same log-log interpretation methodology given by Hughes et al, 1977 to derive friction and dilation angles.

In 1989 Manassero presented an analysis similar to the one developed by Wroth and Windle, 1975. A finite difference technique was adopted to numerically derive the curve of mobilized stress ratio versus shear strain of an element of soil in the cavity wall, as well as the stress path in the P' vs. Q diagram of Lambe and Whitman, 1979 (where $P' = (\sigma_r+\sigma_\theta)/2$ and $Q = (\sigma_r-\sigma_\theta)/2$) for this same element. The volumetric strain-shear strain relationship is also obtained. This numerical technique simultaneously solves, at each step, the stress dilatancy equation of Rowe, 1971 and the differential equations of the equilibrium of

stresses and compatibility of strains around the cavity. It considers the non-linear nature of the volume change during shear, so that tests in both loose and dense sands can be analyzed. The only input parameters are the complete σ_r versus $\varepsilon_{\theta w}$ (testing curve) and ϕ_{cv}, as the model does not consider the initial pre yield linear elastic idealization, i.e. only volumetric dilational plastic strains are considered.

The numerical solution presented by this author consisted of:

$$\varepsilon_{rw}(i) = A - B + C + D \tag{2.45}$$

where:

$$A = \frac{\sigma_r(i)[\varepsilon_{\theta w}(i-1) + K_{acv}.\varepsilon_r(i-1)]}{2[\sigma_r(i)(1+K_{acv}) - \sigma_r(i-1)]}, B = \frac{\sigma_r(i-1)\varepsilon_{\theta w}(i)}{2[\sigma_r(i)(1+K_{acv}) - \sigma_r(i-1)]}$$

$$C = \frac{\sigma_r(i)[\varepsilon_{\theta w}(i-1) - \varepsilon_r(i-1)]}{2[K_{acv}.\sigma_r(i-1)]}, C = \frac{\sigma_r(i-1)[\varepsilon_r(i-1) + (1+K_{acv}) - \varepsilon_{\theta w}(i)]}{2[K_{acv}.\sigma_r(i-1)]}$$

with $K_{acv} = 1/K_{cv}$. The circumferential stress at the cavity wall is obtained by:

$$\sigma_\theta(i) = \left(\frac{\sigma_r(i)}{K_{cv}}\right)\left(\frac{d\varepsilon_{rw}}{d\varepsilon_{\theta w}}\right) \tag{2.46}$$

where: $d\varepsilon_{rw} = 1 + \frac{d\varepsilon_v}{d\gamma}$ and $d\varepsilon_{\theta w} = 1 - \frac{d\varepsilon_v}{d\gamma}$.

the symbols $d\varepsilon_v$ and $d\gamma$ are the increment of volumetric and shear strain components at the cavity wall.

They are found in the step by step numerical solution by:

$d\varepsilon_v = \varepsilon_v(i) - \varepsilon_v(i-1), d\gamma = \gamma(i) - \gamma(i-1)$, with $\varepsilon_v(i) = \varepsilon_{rw}(i) + \varepsilon_{\theta w}(i)$, and

$\gamma = \varepsilon_{\theta w}(i) - \varepsilon_{rw}(i)$

Using the results from "ideal installation" pressuremeter tests in calibration chambers, Manassero, 1989 was able to show that under optimum conditions it is possible to derive more acceptable values of ϕ from his model than from Hughes et al, 1977, with or without Robertson and Hughes, 1986 correction. He basically compared the predicted SBPM ϕ's (corrected to axially symmetric conditions) to the results of ϕ from drained triaxial tests with the calibration chamber sand. With the "selfboring installation" testing curves similar results were obtained in relation to the other traditional methods, most probable due to disturbance effects.

Howie, 1991 in a preliminary analysis of this numerical approach noted instability problems and a high sensitivity to the noise and shape of the testing curve. This finding corroborates the experience of other researchers when dealing with finite difference techniques to solve the cavity expansion problem (see comments of Denby, 1978 and Benoit, 1983 in regard to the "subtangent" method), and appears to be a drawback of these techniques in general.

Following the same approach as Manassero, De Souza Coutinho, 1990 proposed another very similar finite difference technique to derive the soil parameters with a pressuremeter test. His model constituted an improvement of Manassero's work in the sense that large strains (Almansi) and an additional rheological hypothesis (e.g. equation) regarding the variation of volumetric strain at cavity wall are considered.

This latter author demonstrated in 2 high quality field testing examples that similar (but slightly above) ϕ's as those predicted by the Hughes et al, 1977 log-log approach could be obtained, with the added advantage that the stress path and the volumetric behavior of the sand could also be determined. This finite difference methodology of analysis, however, incorporates the same instability and sensitivity features commented on before for Manassero, 1989 when applied to slightly disturbed testing curves.

Using the concepts put forward by many of the above mentioned models, Juran and Mahmoodzadegan, 1989 developed a complex model to simulate the cavity expansion in sands. An elasto-plastic stress strain idealization with both contraction and dilation during shear was assumed. The soil was also considered as a homogeneous, isotropic and strain hardening material with a non associated flow rule. These authors conducted laboratory "pressuremeter type" expansion tests (in a hollow cylinder cell) on Fontainbleau sand specimens, aiming at both the simulation of the ideal SBPM test and evaluation of the capabilities of their model. A reasonably good agreement between experimental and idealized pressure expansion curves was noticed, with higher values of the plane strain ϕ's in comparison to the axially symmetric values of the triaxial tests. The drawback of this model is the requirement of extensive laboratory triaxial tests to furnish parameters for the flow rule of the model. Moreover, a step by step determination of the slope of the loading pressuremeter curve is required in order to incrementally obtain the shear stress-strain curve at the cavity wall. Therefore, the same instability problems noticed for the method of Manassero, 1989 may exist in this case.

The most recent analytical model for the interpretation of drained selfboring pressuremeter results was put forward by Ferreira, 1992. An hyperbolic constitutive law between the stress ratio (Q/P') and the circumferential cavity strain with a linear relationship between dilative volume change and shear strain, was adopted to simulate the loading stage of the pressuremeter test. An additional relationship between the cavity strain and the radial coordinate r was included in the solution, following the equation proposed by Wroth and Windle, 1975. The Mohr Coulomb failure criterion was assumed to define the relationship between the ultimate shear and the normal stresses of the hyperbolic curve, and Rowe's stress dilatancy equation was applied to establish a link between both the dilation and the ultimate hyperbolic friction angle.

Although the hyperbolic model is able to closely capture the nonlinear nature of the stress strain behavior of sheared sands, the preliminary assessment of this model using results from selfboring pressuremeter tests performed on a calibration chamber with Ticino sand (Bellotti et al, 1987) was not satisfactory. The predicted plane strain friction angles and lateral stresses of the hyperbolic model were underestimated in relation to the reference values related by Bellotti et al, 1987 (plane strain ϕ by laboratory tests and σ_h from the chamber boundary stresses). The predicted shear moduli were considerably overestimated, being on average 4 times the low strain modulus of the tested sand (assessed by resonant column tests).

Cavity contraction theory was also proposed to predict parameters from the sand. The basis of the contraction theory is the fact that there is a consistency on the shape of the unload curve of SBPM tests in sands. This consistency is evident when comparing tests by different pressuremeters in the same sand. Although the loading stages of the testing curves are different, the shape of the unload stages are similar. It appears, therefore, that the unloading stage of the pressuremeter test is much less sensitive to any initial disturbance caused by the installation of this probe.

Houlsby et al, 1986 were the first authors to introduce the cavity contraction theory to analyze the unloading stage of SBPM tests in sands. Plane strain, cylindrical coordinates and an elasto-plastic behavior with volume change ruled by Rowe's stress dilatancy theory was adopted in a similar fashion as Hughes et al, 1977. Despite the high potential of this model, preliminary interpretation of SBPM tests in United Kingdom revealed inconsistencies for the derived loading friction angle. In fact the results demonstrated that conservative estimates of this variable are obtained by setting the unloading friction

angle to ϕ_{cv}. This led Houlsby et al, 1986 to comment on the necessity of a large strain formulation to improve their model. Withers, et al, 1989 after the analysis of several pressuremeter tests in sand concluded that simple cavity contraction models are not suitable to derive strength parameters from either full displacement pressuremeter (FDPM) or SBPM tests. This is due to the extremely complicated behavior of the cavity during unloading.

In summary, several different cavity expansion models exist and can be applied to the interpretation of tests in sands. Table 2.1 shows the basic features and problems of all the aforementioned models. Models that encompass the shear volume strain coupling characteristic of the granular material under shear have to be considered in the SBPM interpretation. All the models require some input from laboratory tests, but some of them (like Ladanyi, 1963, Vesíc, 1972 and Juran and Mahmoodzadegan, 1989) require complex laboratory variables to define the stress-strain-volume change behavior adopted in the rheological equations. This latter necessity constitutes a drawback since the problems inherent to the in situ density estimation and sample disturbance may be present with granular materials.

Some of the above models can be solved by an analytical manner (Hughes et al, 1977, Carter et al, 1986, Ferreira, 1992) where closed form solutions are used. Others are applied in a numerical finite difference technique (Wroth and Windle, 1975, Manassero, 1989, De Souza Coutinho, 1990) that directly uses the testing data points to obtain the shearing characteristics of the sand. This latter interpretation approach gives more information regarding the stress-strain-volume change behavior of the sand than the interpretation approach associated with the closed form solutions. The experience gathered so far to validate the finite difference approach is mainly derived from "ideal installation" SBPM tests in calibration chambers. Little experience exists with the finite difference interpretation method, but preliminary analyses indicated that both numerical instability and high sensitivity to even small disturbance in the pressuremeter curve may constitute an impeding factor for its usage in practice.

The model of Hughes et al, 1977 is most commonly used to interpret SBPM results in sands. It is a simple and easy to use model that incorporates the main (simplified) features of sand behavior in simple shear. The Carter et al, 1986 model is a refined version of the Hughes et al, 1977 model, but is not currently used in the interpretation of pressuremeter results in sands. This is probably due to the fact that it can not be incorporated into the traditional log-log approach to derive ϕ. Both models assume a constant

dilation rate on the onset of yielding, thus not taking into consideration the possible strain softening of the sand during the expansion process.

The models that have the best potential for use in the new interpretation methodology are those which simulate the soil behavior in a simple but reasonably accurate manner, do not depend on extensive laboratory input data, and ideally have closed form solutions that are easy to apply. At present, these models are those put forward by Hughes et al, 1977 and Carter et al, 1986.

2.2.6 New Cavity Expansion Model

2.2.6.1 Introduction

Using the Hughes et al, 1977 or any other model it is possible to predict the whole idealized testing curve of the pressuremeter test (at the cavity wall). This is accomplished by combining Equations 2.24 and 2.41(in the case of the Hughes et al, 1977 model), respectively valid for the elastic and plastic zones. By varying the input cavity strain $\varepsilon_{\theta w}$ in these equations it is possible to obtain the cavity pressure σ_{rw} at any stage of the expansion. It shall be observed, however, that:

- For a given mobilized strain $\varepsilon_{\theta w}$ (or γ) below $\varepsilon_{\theta R}$ (or γ_f) the curve is only ruled by Equation 2.24. In this case the medium is entirely in the elastic range and a linear relation between σ_{rw} and $\varepsilon_{\theta w}$ is obtained.

- For a $\varepsilon_{\theta w}$ (or γ) above $\varepsilon_{\theta R}$ (or γ_f) the curve is given by Equation 2.41, as an annulus of yielding soil (plastic zone) will start to expand at the cavity boundary, in accordance with the assumptions of this model.

This approach was not followed by Hughes et al in 1977 to simulate pressuremeter testing curves, due to the extensive mechanical calculations needed and lack of personal computers at that time. Instead, the "log-log approach" was adopted to predict ϕ and δ. Only in 1989, with the use of fast personal computers, Dr. J.M.O. Hughes (personal communication) was able to write the first computer program that simulates pressure expansion curves with the equation of the model that he developed 12 years before. The purpose of the 1989 aforementioned computer program was to use the Hughes et al, 1977 model under a new concept of pressuremeter data interpretation, to be described in section 2.4 of this thesis.

Using the aforementioned program it was possible for the writer to directly compare the predictions given by Hughes et al, 1977 and the Carter et al, 1986 models, with the same input parameters. A new cavity expansion model was developed after it was found that different pressure expansion curves were obtained for the Hughes et al, 1977 and Carter et al, 1986 models, when a Poisson's coefficient of 0.5 was

used in the Carter's model. This finding may indicate some inconsistency in Carter's model, in the sense that elastic strains in the plastic zone are not fully erased in the limiting condition[2] of ν.

The new cavity expansion model was originally suggested by Dr. J.M.O. Hughes in 1993 (personal communication) for use in the interpretation of pressuremeter curves in sands. With his assistance it was possible for the writer to further develop and implement this model into a computer program. This program predicts the pressure expansion response at the cavity wall (testing curve) for a given set of input parameters.

2.2.6.2 Basis of the New Model

The new model relies on both the basic principles advanced in 2.2.1 and 2.2.2 and the rheological equations of Hughes et al, 1977. This model focused the implementation of the traditional Hughes et al, 1977 model with the concept of elastic strains in the plastic zone put forward by Carter et al, 1986. The new model, however, allows the adoption of different shear moduli in both elastic and plastic zones around the probe.

The basic assumptions of the new model are the same as those presented by Hughes et al, 1977, with the incorporation of elastic strains in the plastic zone. In this zone the total volumetric strains are defined by the combination of dilative plastic strains, caused by plastic shear, and compressive elastic strains caused by the increase in the average normal stress.

The elastic strains are defined with the aid of the elasticity theory presented before, and can be estimated by either a numerical (interactive) or analytical approach.

2.2.6.3 Derivation of Elastic Strains in the Plastic Zone

Approximate Numerical Solution

In subsection 2.2.3 it was shown that a plastic zone develops once yielding starts at the cavity wall. This zone increases as the cavity pressure increases, leading to a simultaneous increase of both normal and shear stress in the horizontal plane. This was shown in Figures 2.3 and 2.4. The high values of average normal stress σ_m can compress the sand inside the plastic zone imposing a compressive "elastic" volumetric strain, in opposition to the dilative "plastic" volumetric strain induced by the increase in shear stress τ_m in this same zone.

---

[2] This limit corresponds to the case where no compressive volume changes take place, hence the compressive elastic strains given by the increase in the stress level should be null.

Carter et al, 1986 developed a closed form solution to deal with this particular condition of the cavity expansion process in sands, but as commented above some inconsistency appears to exist with this model. The following solution overcomes the apparent deficiency of Carter's model, and allows for a variation of elastic parameters in the plastic zone different from the elastic zone. In the following approach the elastic strains are determined by an approximate numeric (interactive) method.

Consider a particular stage of the cavity expansion process, where the initial cavity radius r_0 is expanded to a deformed radius r_u and a plastic zone of radius r_p (say = 3 r_0) is developed around the cavity. At this stage, depicted in Figure 2.7(a), the expansion takes place under an increment of effective internal cavity pressure $d\sigma_{rw}$ (or σ_{rw}-σ_h) above the initial horizontal stress of the sand. The radial displacement measured at the cavity wall, defined by u_{rw} in Figure 2.7(b), will be the sum of all the plastic and elastic radial displacements that are induced within the plastic zone plus the elastic deformation of the surrounding elastic zone. The total plastic radial displacement at the cavity wall (u_{rpw}) is derived by the direct application of Hughes et al, 1977 Equation 2.41 in the whole plastic zone, and represents the plastic dilation of this zone. This variable also includes the elastic deformation of the elastic zone. The total elastic radial displacement measured at the wall due to elastic compression of the plastic zone (u_{rew}) can be approximately assessed by assuming that the zone of soil encompassed between r_0 and r_p compresses elastically. The stresses inside the plastic zone are defined by the Mohr Coulomb failure condition.

In the subsection 2.2.2 the elastic solution was presented for the expansion of the cavity in an infinite medium. It was shown that the differential equation that rules the elastic distribution of displacements in the medium surrounding the cavity (Equation 2.16) has a solution in the form of $u_r = Ar + B/r$.

The total elastic radial displacement at the cavity wall, for the particular stage of cavity expansion of Figure 2.7(a), is given by the substitution of the constants A and B into the above equation of u_r. At this stage of expansion the boundary conditions are given by the conditions existing in both cavity ($r = r_0$) and elasto-plastic ($r = r_p$) boundaries. This latter boundary, on the other hand, is assumed to be rigid at this particular moment, such that the elastic radial displacement distribution varies from a high value at wall to zero at r_p.

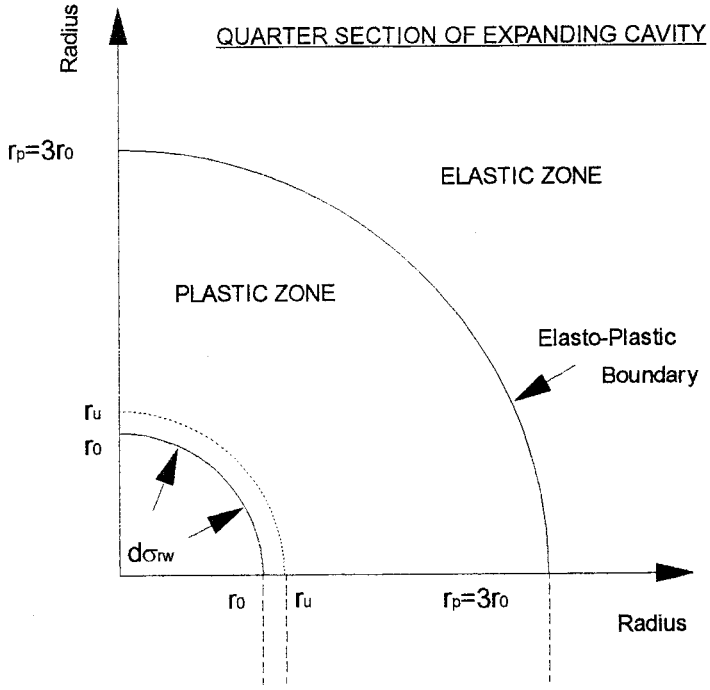

(A) ELASTIC AND PLASTIC ZONES AROUND THE CAVITY

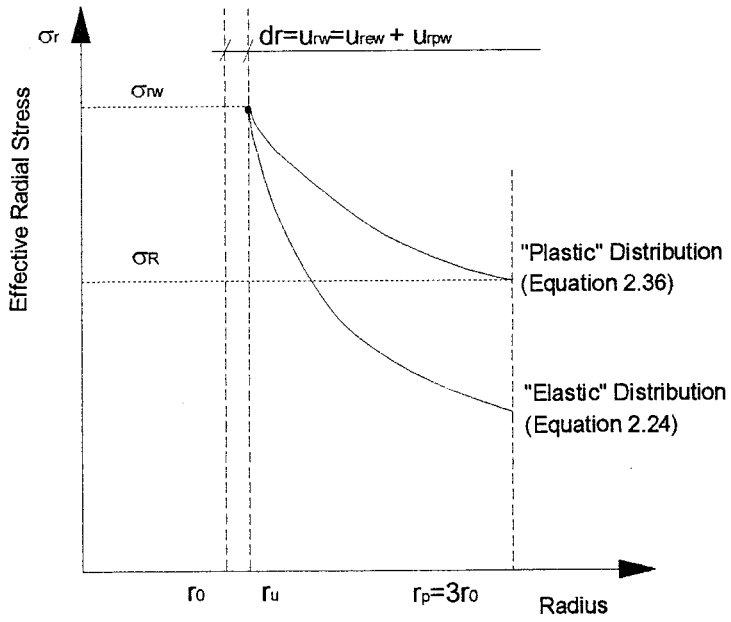

(B) IDEALIZED RADIAL STRESS DISTRIBUTION INSIDE PLASTIC ZONE

Figure 2.7: Particular Stage of Cavity Expansion in Sand

This assumption leads to the following equation:

$$u_{rp} = Ar_p + B/r_p = 0, \text{ hence } Ar_p = -B/r_p \tag{2.47}$$

at the cavity wall $r = r_0 = r_w \approx r_u$ and the following equation is obtained:

$$u_{rw} = Ar_w + B/r_w = A.r_u + B/r_u \tag{2.48}$$

and hence $du_{rw}/dr_w = A - B/r_w^2 = A - B/r_u^2$ (2.49)

Equations 2.48 and 2.49 can be substituted into the (linear) elastic rheological equation (Equation 2.13) that combines σ_r, u_r and du_r/dr of the expanding cavity. Therefore:

$$d\sigma_{rw} = \frac{-(1-\upsilon)}{(1-2\upsilon)(1+\upsilon)} E\left(A - \frac{B}{r_u^{\,2}}\right) - \frac{\upsilon}{(1-2\upsilon)(1+\upsilon)} E\left(A + \frac{B}{r_u^{\,2}}\right) \tag{2.50}$$

rearranging terms and substituting E/(2(1+ν)) for G yields:

$$d\sigma_{rw} = \frac{-2G}{(1-2\upsilon)}\left(A - \frac{B}{r_u^{\,2}} + \frac{2.\upsilon.B}{r_u^{\,2}}\right) \tag{2.51}$$

substituting now Equation 2.47 into 2.51 and rearranging again the terms it follows that:

$$d\sigma_{rw} = \frac{-2G}{(1-2\upsilon)} A\left[1 + (1-2\upsilon)\left(\frac{r_p}{r_u}\right)^2\right] \tag{2.52}$$

hence $$A = -\frac{d\sigma_{rw}}{2G}(1-2\upsilon)\frac{r_u^{\,2}}{r_u^{\,2} + (1-2\upsilon)\,r_p^{\,2}} \tag{2.53}$$

$$B = +\frac{d\sigma_{rw}}{2G}(1-2\upsilon)\frac{r_u^{\,2}.r_p^{\,2}}{r_u^{\,2} + (1-2\upsilon)\,r_p^{\,2}} \tag{2.54}$$

Substituting A and B of Equations 2.53 and 2.54 into the equation of u_r leads to the derivation of the equation that predicts the total (from the plastic zone) elastic radial displacement at the cavity wall for this expansion stage. Therefore:

$$u_{rew} = \frac{d\sigma_{rw}}{2G}(1-2\upsilon)\left[\frac{r_u\,(r_p^{\,2} - r_u^{\,2})}{r_u^{\,2} + (1-2\upsilon)\,r_p^{\,2}}\right] \tag{2.55}$$

By assuming that the soil encompassed between r_0 and r_p behaves elastically, it is implicit that the distribution of radial and circumferential stresses in this zone follow the elastic equations given in

section 2.2.2, i.e. Equations 2.24 and 2.25. As schematically shown in Figure 2.7(b) the "plastic" and "elastic" radial stress distributions are different between r_u and r_p, with exception of the inner boundary of the cavity (where $r = r_u$). Thus, in order to "force" the derivation of a cavity u_{rew} with a stress distribution that closely resembles the plastic distribution depicted in Figure 2.7(b), the division of the zone of soil between r_u and r_p into a series of concentric rings shall be considered. Generalizing Equation 2.55 for several concentric rings between r_u and r_p, it follows that:

$$u_{re(n)} = \frac{d\sigma_{R(n)}}{2G}(1-2\upsilon)\left[\frac{r_{(n)}\left(\left(r_{(n-1)}\right)^2-\left(r_{(n)}\right)^2\right)}{\left(r_{(n)}\right)^2+(1-2\upsilon)\left(r_{(n-1)}\right)^2}\right] \tag{2.56}$$

where: $u_{re(n)}$ is the elastic radial displacement at a concentric ring with inner boundary at a radius $r_{(n)}$ and outer boundary at a radius $r_{(n-1)}$.

The variable $d\sigma_{R(n)}$ (or $\sigma_{R(n)} - \sigma_h$) is the "plastic" increment of radial stress (above σ_h) in the inner boundary of the concentric rings. The general equation for $\sigma_{R(n)}$ comes from Equation 2.36, as follows:

$$\sigma_{R(n)} = \left[\frac{r_{(n-1)}}{r_{(n)}}\right]^{(1-N)} \sigma_{R(n-1)} \tag{2.57}$$

For the purpose of determining the approximate (total) elastic radial displacement at the cavity wall, the outer boundary of each of the concentric rings is considered fixed. The elastic radial displacement of the inner boundary of each of the rings is calculated with both Equations 2.56 and 2.57 above. The (total) elastic displacement at the wall is the sum up of the elastic radial displacements induced in each of the concentric rings.

In order to illustrate the above procedure let's consider that, in the particular stage of the cavity expansion of Figure 2.7(a), the zone of soil between r_u ($\approx r_0$) and r_p is divided in only 2 concentric rings. This is schematically shown in Figure 2.8(a). The outer boundary of the external ring 1 (at the elasto-plastic boundary) does not displace. Equation 2.56 is applied by using the "plastic" distribution of stress depicted for both rings in Figure 2.8(b), with the value of $\sigma_{R(1)}$ from Equation 2.57. The value of the radial elastic displacement at the inner boundary of ring 1 ($u_{re(1)}$) is then determined, as presented in

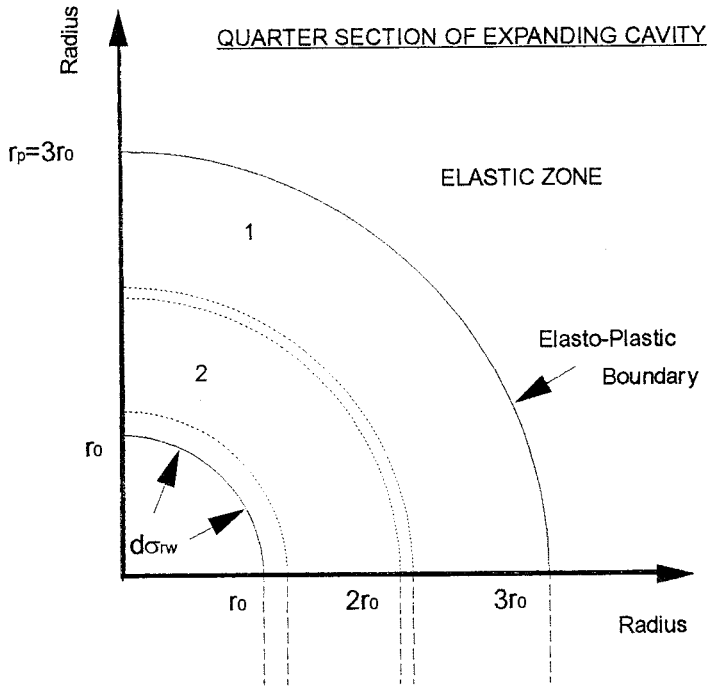

(A) DIVISION OF PLASTIC ZONE

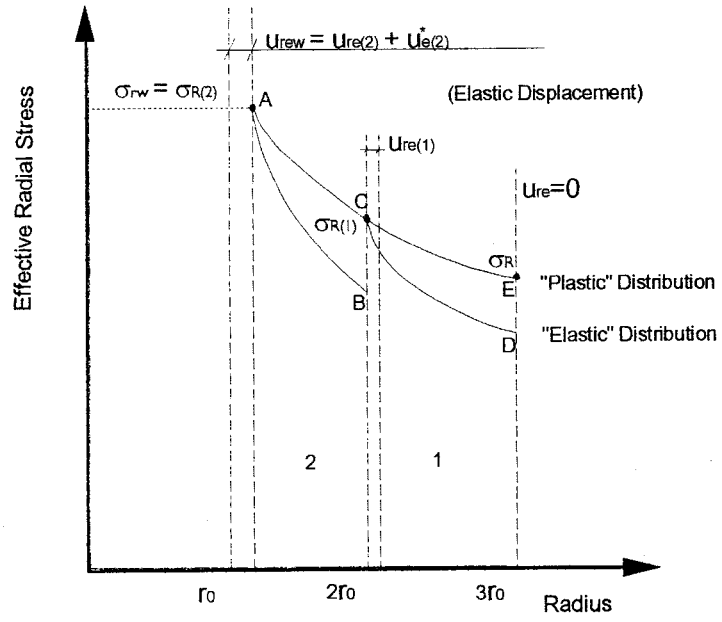

(B) DERIVATION OF RADIAL STRESS AND DISPLACEMENT AT EACH RING

Figure 2.8: Calculation of Elastic Radial Displacement at the Cavity Wall for a Particular Stage of Expansion

Figure 2.8(b). The same procedure is adopted for the ring 2. The outer boundary of ring 2 (at a radius $r = 2\ r_0$) does not displace for the purpose of calculation of the radial elastic displacement ($u_{re(2)}$) induced at the inner boundary of this same ring. Equation 2.56 is again applied with the value of $\sigma_{R(2)}$ defined by Equation 2.57. The total elastic radial displacement at the cavity wall will be the value of $u_{re(2)}$ added to an additional displacement $u^*_{e(2)}$, as shown in Figure 2.8(b).

For strain compatibility reasons an additional displacement $u^*_{e(2)}$ has to be considered at the cavity wall, due to the movement of the outside boundary (ring 1). To determine this additional displacement it is assumed, at this expansion stage, that the concentric (inner) rings move at constant volume. Therefore, for the example of Figure 2.8 the displacement caused at the cavity wall by the movement of the external ring 1 is given by:

$$2.\pi.r_1.u_{re(1)} = 2.\pi.r_2.u^*_{e(2)}, \text{ where } r_1 = 2r_0 \text{ and } r_2 = r_0$$

$$u^*_{e(2)} = \frac{r_1}{r_2} u_{re(1)} = \frac{2r_0}{r_0} = 2\ u_{re(1)} \qquad (2.58)$$

The final displacement at the cavity wall (at this stage of expansion) will be the value of u_{rew} ($u_{re(2)} + u^*_{e(2)}$) added to the value of u_{rpw}, which is derived by the application of Hughes et al, 1977 Equation 2.41. For the example of Figure 2.8 this latter displacement is calculated in a single step by:

$$u_{rpw} = \varepsilon_{\theta R} \left(\frac{\sigma_{R(2)}}{\sigma_R} \right)^{\frac{(n+1)}{(1-N)}} \qquad (2.59)$$

where: $\sigma_{R(2)}$ is the effective radial stress at the cavity wall.

The values of $\varepsilon_{\theta R}$ and σ_R are respectively calculated by Equations 2.33 and 2.30.

Once the value of u_{rw} ($= u_{rew} + u_{rpw}$) is obtained, the circumferential strain $\varepsilon_{\theta w}$ at the cavity wall is computed by the use of Equation 2.2. This allows the derivation of a pair of testing coordinates ($\varepsilon_{\theta w}$, σ_{rw}) that represents the idealized pressure expansion response at the cavity wall when the plastic zone has a radius $r_p = 3\ r_0$.

In Figure 2.8(b) it can be noticed that, with the incorporation of 2 rings between r_0 and r_p, the idealized "elastic" radial stress distribution within the rings (points A-B, C-D) becomes indeed closer to the "plastic" radial stress distribution (points A-C-E). The higher the number of concentric rings between r_0 and r_p, the closer the elastic stress distribution will be to a smooth function, approximating to the "plastic" stress

distribution. The division of the plastic zone into 30 concentric rings was used herein. The division of the plastic zone into 30 concentric rings is sufficient to get results within 2 % of the values obtained with 400 (or more) concentric rings.

As the cavity pressure increases, so does the size of the plastic zone. Therefore, the elastic component of strain (as well as the total) at the cavity wall is recalculated for each increment of r_p/r_0. The computer program developed for the simulation of the cavity expansion with this numerical approach varies r_p to a maximum extension of 15 times r_0, at which stage the cavity strains are usually greater than 10 %. For each r_p/r_0 stage both the $\varepsilon_{\theta w}$ and σ_{rw} are calculated, allowing the determination of the complete (idealized) testing curve of the SBPM for a given set of input parameters. This set is given by ϕ, σ_h, G, ϕ_{cv} and ν (as in the Carter et al, 1986 model) plus the shear modulus of the plastic zone. This latter modulus can be higher than the modulus of the elastic zone, due to stress level differences.

Closed Form Solution

The prediction of the elastic strains within the plastic zone can be also done with the aid of an analytical solution.

Figure 2.9 presents the stress and strain conditions at a particular stage of the cavity expansion. For a particular soil element inside the plastic zone it is considered that the imposed (radial and tangential) stresses are given by Equations 2.36 and 2.37. These equations rule the distribution of the failure stresses within the plastic zone, with basis on the Mohr Coulomb failure condition.

The imposed stress regime will cause an increase in the mean normal stress of the considered soil element, leading to an overall decrease of volume. The (elastic) unit volume contraction of this element is given by:

$$\varepsilon_v = \varepsilon_r + \varepsilon_\theta + \varepsilon_z \tag{2.60}$$

where:

$\varepsilon_z = 0$, assuming plane strain conditions.

Combining Equations 2.6, 2.7 and 2.10 in the Equation 2.60 above it is possible to obtain:

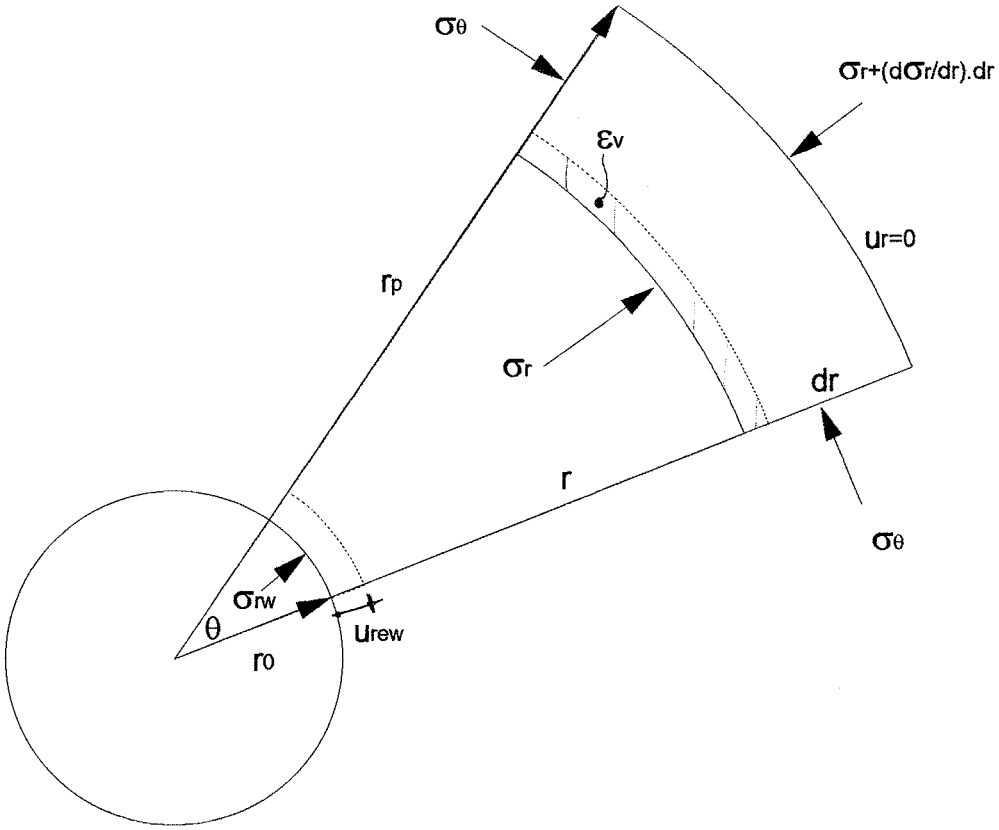

Figure 2.9: Elastic Displacement at the Wall due to Compressive Volume Change of a Soil Element

$$\varepsilon_v = \frac{1}{E}\left[d\sigma_r(1-\upsilon^2) - d\sigma_\theta(\upsilon+\upsilon^2)\right] + \frac{1}{E}\left[d\sigma_\theta(1-\upsilon^2) - d\sigma_r(\upsilon+\upsilon^2)\right] \quad (2.61)$$

where: $d\sigma_r$ is the increment of effective radial stress imposed in the soil element above σ_h

$d\sigma_\theta$ is the increment of effective tangential stress imposed in the element above σ_h

Using Equations 2.36 and 2.37 in Equation 2.61 gives:

$$\varepsilon_v = \frac{1}{E} d\sigma_{rw}\,(1-2\upsilon^2-\upsilon)(N+1)\left(\frac{r_0}{r}\right)^{1-N} \quad (2.62)$$

where: $E = 2G\,(1+\nu)$ (2.63)

$d\sigma_{rw}$ is the increment of effective radial stress at the cavity wall above σ_h

In order to find the contribution of all the elements of soil encompassed between r_0 and r_p, hence the total elastic volume change within the plastic zone, it is necessary to integrate Equation 2.62 over the area of this zone. Therefore:

$$\text{Total } \varepsilon_v = \frac{d\sigma_{rw}}{2G}\frac{(1-2\upsilon^2-\upsilon)}{(1+\upsilon)}(N+1)\int_0^{2\pi}\int_{r_0}^{r_p}\left(\frac{r}{r_0}\right)^{N-1} r.dr.d\theta \quad (2.64)$$

or

$$\text{Total } \varepsilon_v = \frac{d\sigma_{rw}}{2G}(1-2\upsilon).2\pi.\frac{r_p^{\,N+1} - r_0^{\,N+1}}{r_0^{\,N-1}} \quad (2.65)$$

but the total volume change within this zone will be equivalent to:

$$\text{Total } \varepsilon_v = 2.\pi.r_0.u_{rew} \quad (2.66)$$

where: u_{rew} is the total elastic displacement at the cavity wall

hence

$$u_{rew} = \frac{d\sigma_{rw}}{2G}(1-2\upsilon)\left[\frac{r_p^{\,N+1} - r_0^{\,N+1}}{r_0^{\,N}}\right] \quad (2.67)$$

Comparison of Solutions

As commented before, the new cavity expansion model adds the elastic component of cavity displacement to the plastic component, which is derived with the use of the Hughes et al, 1977 model.

The total elastic radial displacement at the cavity wall, at a given position of the elasto-plastic boundary (r_p/r_0), can be predicted by a numerical (interactive) or an analytical solution. In order to compare the predictions by both solutions a numerical example was carried out. Figure 2.10 presents the predicted testing curve obtained by each of the solutions outlined before. The same set of (elastic) input parameters was used to generate the elastic radial displacements at the cavity wall. These parameters were estimated as G = 40 MPa and $\nu = 0.2$.

The effective internal pressure at the wall $d\sigma_{rw}$ was computed with Equation 2.36 for each position of the elasto-plastic boundary. The horizontal stress was assumed to be 100 kPa and the plastic radial displacements at the wall were computed with the Hughes et al, 1977 model. This latter model adopted a friction angle ϕ of 45°, a constant volume friction angle ϕ_{cv} of 35° and a shear modulus of the elastic zone of 20 MPa.

The results presented in Figure 2.10 suggest that the numerical interactive solution matches the closed form solution with an acceptable accuracy. The agreement of the predicted testing curves would be even better, if a higher number of concentric rings were used with the numerical solution (this solution adopted 30 rings between r_0 and r_p). Nevertheless, for a practical purpose, any of the above approaches to compute the elastic strains in the plastic zone can be used.

It is recognized that there are alternate methods of calculating the radial displacement at the cavity wall that may not agree with the methods described herein. This arises because a consistent elastic-plastic approach was not used to calculate the displacements. However it is felt that the approach used suitably accounts for the elastic and plastic volume changes.

In the following sections of this thesis the new cavity expansion model is defined as the model that adopts the numerical (interactive) solution to compute the elastic strains in the plastic zone.

2.2.7 Comparison Between Cavity Expansion Models

Using the computer program developed for the new cavity expansion model it was possible to compare the idealized predictions of cavity pressure versus expansion of this model with the predictions given by

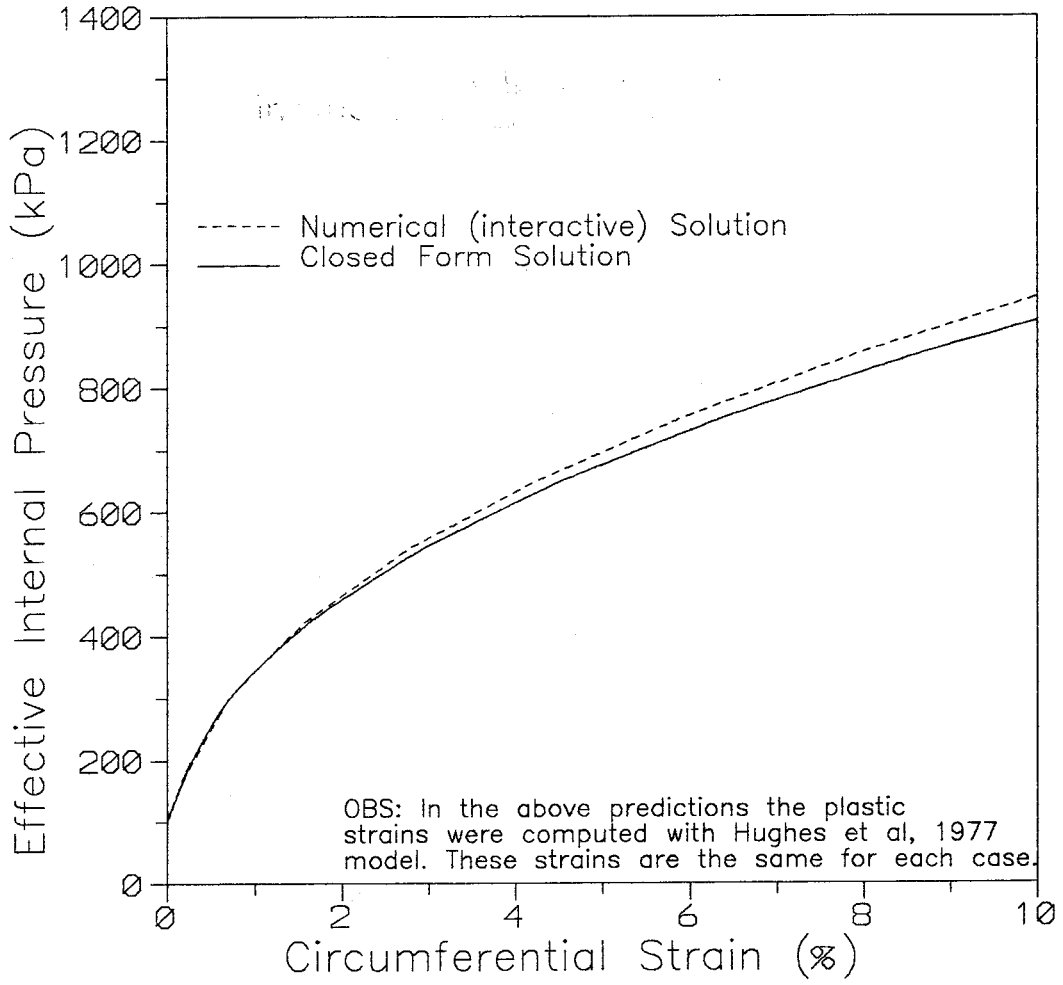

Figure 2.10: Comparison of Predictions given by the Numerical and Analytical Solutions to Compute Elastic Strains in the Plastic Zone

distinct rheological models. The same set of input parameters was chosen for the comparison between the new, Hughes et al, 1977 and Carter et al, 1986 models. These parameters are given by the strength, the lateral stress and the stiffness of the sand.

These cavity expansion models consider a stiffness "G" which governs the soil response in the "elastic" zone (see Figure 2.3). This stiffness is defined by Equation 2.26, and for ideal elastic soils will represent the slope of the initial stage of the testing curve. This stiffness is defined herein as "Gi", or the initial elastic shear modulus of the sand. Both the new and the Carter et al, 1986 models take on consideration the stiffness "G" in order to predict the soil response in the "plastic" zone (see Figure 2.3). This latter stiffness is used in both models to compute the elastic strains within this zone. For Carter et al, 1986 model a unique value of "G" is defined for both elastic and plastic zones, whereas in the new model a distinction between shear moduli can be done. The shear modulus in the plastic zone is defined herein as "Gp".

The input soil parameters adopted for the comparison of the models are the same as those used to generate the plots of Figure 2.10, i.e.: $\phi = 45°$, $\phi_{cv} = 35°$, $\sigma_h = 100$ kPa, Gi = 20 MPa, Gp $\approx$ 2Gi = 40 MPa and $\nu = 0.2$ as well as 0.5. The Hughes et al, 1977 model does not consider elastic strains in the plastic zone. This model adopted Gi only to compute the initial elastic displacement of the cavity wall caused by the pure shearing process that takes place in the elastic zone. In the Carter et al, 1986 model the same value of Gi was adopted in both elastic and plastic zones. The new model simulated the cavity expansion by considering (a) same G (= Gi) in both plastic and elastic zones, and (b) Gi in the elastic zone with Gp in the plastic zone. A Poisson's coefficient ν varying from 0.5 to 0.2 was adopted in both the new and Carter et al, 1986 models, in order to see its influence over the final testing curve.

The relationship between Gi and Gp is based on the average results obtained by the writer with the interpretation of field SBPM data, assuming Gp $\approx$ Gur (unload reload shear modulus from the testing loop). These results will be presented in Chapter 4.

The comparison of the pressure expansion curves for all the models with the aforementioned parameters is presented in Figure 2.11. The following observations apply:

1. With the incorporation of elastic strains in the plastic zone ($\nu < 0.5$) there is a softening effect over the predicted testing curve. Compare curves A-B with A-E or A-F.

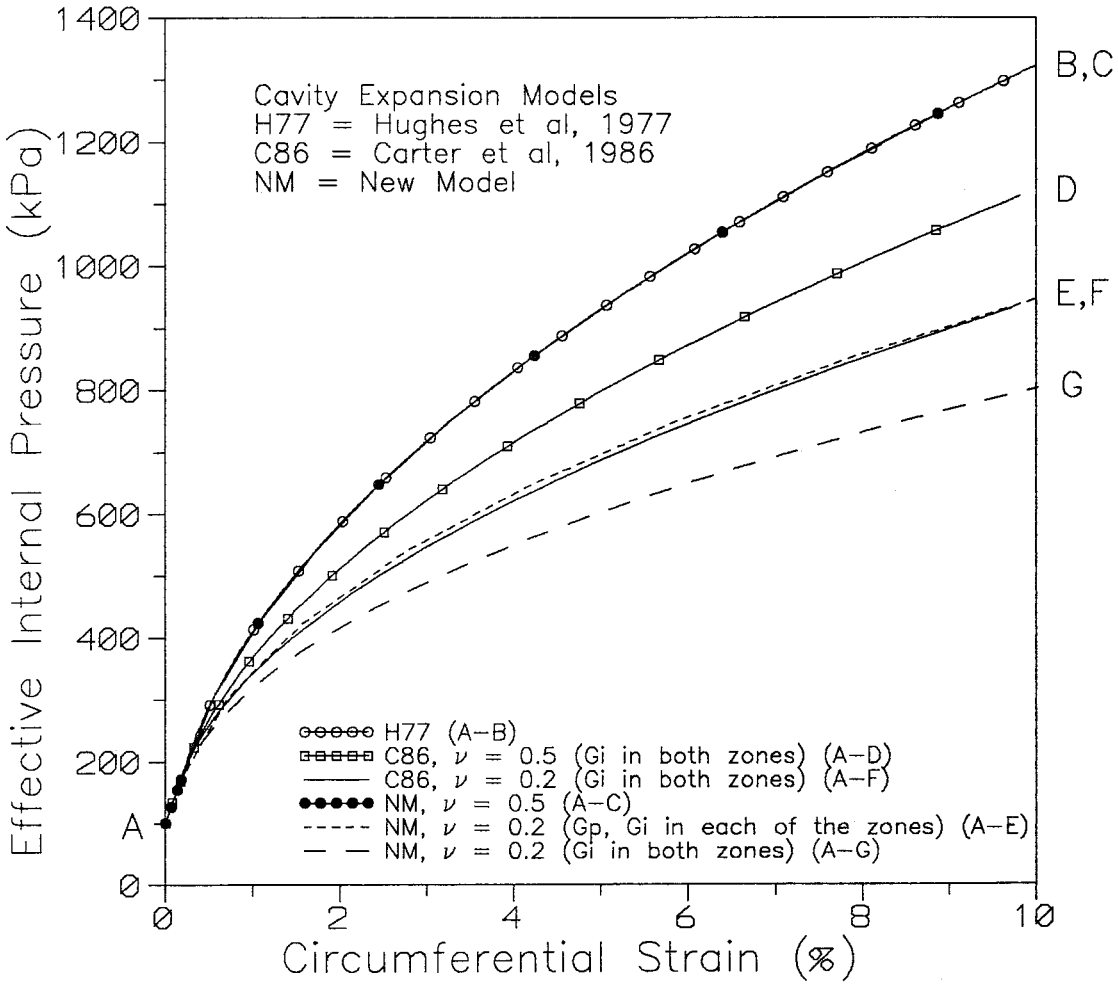

Figure 2.11: Comparison of Pressuremeter Curves Predicted by Different Models

2. The new and Hughes et al, 1977 models lead to similar results when the Poisson's coefficient is equal to 0.5 (compare curves A-B and A-C). This is not observed for the model of Carter et al, 1986 (compare curves A-B and A-D), and perhaps indicates that this model incorporates some other elastic (strain) variable in the plastic zone.

3. With the new model the incorporation of the same shear modulus (Gi) in both elastic and plastic zones leads to a very soft pressure expansion curve (curve A-G). Considering a higher stiffness in the plastic zone (G = Gp), it is possible to obtain a stiffer pressure expansion response at the cavity wall (curve A-E). Indeed, since in the plastic zone the level of stresses are higher than in the elastic zone, it is more appropriate to use a higher stiffness (than Gi) to compute the elastic strains in this former zone. This is so given the recognized stress level dependency of the shear modulus (to be addressed in the subsection 2.3.4). The stiffness in the plastic zone can be approximately measured when performing an unload reload loop during the test, since the testing loop is generally carried out at a stage where an expanded plastic zone exists around the cavity. The determination of the unload reload shear modulus Gur from the testing curve is discussed in subsection 2.3.4.1.

4. Surprisingly, Carter et al, 1986 and the new model gave identical testing curves when a Poisson's coefficient equal to 0.2 was adopted, and a stiffness Gp was adopted in the new model.

In summary, the incorporation of elastic strains in the plastic zone leads to softer (idealized) testing curves. Both the new and Hughes et al, 1977 models converge when a Poisson's coefficient of 0.5 is adopted in the former model. On the other hand, this is not observed for the Carter et al, 1986 model. The new model has the capability to incorporate a larger sand stiffness in the plastic zone to predict the elastic strains. This stiffness can be approximately assessed by performing an unload reload loop during the test.

2.3 TRADITIONAL INTERPRETATION METHODOLOGIES IN SAND

2.3.1 Introduction

With the available theoretical models described in the previous section it is possible to derive the friction angle, the shear modulus and the lateral stress of the tested sand. The traditional interpretation methodologies use the SBPM testing curve for this purpose.

It is the objective of this section to briefly review these interpretation methodologies, addressing their limitations and the possible need of better alternative interpretation approaches.

2.3.2 Friction Angle

As commented in subsection 2.2.5 the most common interpretation approach in sands for deriving the friction angle is the use of Hughes et al, 1977 model with the log-log plot of the testing curve. Robertson and Hughes, 1986 nomogram can be additionally applied in loose granular materials. Finite difference techniques were recently proposed for a more refined interpretation analysis of the SBPM testing curve.

In order to assess the capability of the above interpretation methodologies, Bellotti et al, 1987 conducted 47 SBPM tests in the Italian ENEL-CRIS calibration chamber using both Ticino and Hokksund sands. Pressuremeter tests were performed with the probe cast in place (ideal installation) as well as by selfboring into the sand. The English Camkometer with an L/D = 6 was used. The samples were subjected to 1D consolidation under K_0 conditions and then unloaded, where K_0 is the coefficient of earth pressure at rest. Both normally consolidated (NC) and overconsolidated (OC) sand specimens were tested. Triaxial compression tests with the same sand under similar density and confinement conditions as those used in the chamber were performed in order to define baselines of ϕ. The triaxial ϕ's were further corrected to both stress level at failure (by the curved strength envelope equation of Baligh, 1976) and to plane strain conditions (by the empirical equation of Lade and Lee, 1976). Ring shear tests were used to derive the constant volume friction angle ϕ_{cv} required by the interpretation methodologies. The summary of the results obtained by these authors is shown in Table 2.2, where the following observations apply:

1. In general all the interpretation methodologies lead to average values of ϕ that are close to each other, with some scatter (average $\pm 3.9°$) in the predicted ϕ's. The scatter of the ideal installation tests is considerably lower than the scatter found in the selfbored tests, suggesting that for the ideal installation tests the accuracy of the predicted ϕ's by the log-log or the other interpretation methodologies is higher than the accuracy found with the selfbored tests. Indeed, Jewell et al, 1980 showed that Hughes et al, 1977 model can predict friction angles by the log-log approach that are extremely comparable to baseline values from laboratory simple shear apparatus. This is only the case if high quality (ideal installation) testing curves are used. Eldridge, 1982 also demonstrated that in the absence of any disturbance the ϕ predicted by the log-log approach of Hughes et al, 1977 is extremely reliable. He used a plane strain finite element mesh, with a model that incorporates the shear volume coupling of the sand with a non linear incremental

CONDITION	REFERENCE ϕ (Deg)	SBPM INTERPRETATION METHODOLOGIES (Deg)			REFERENCE
		(A)	(B)	(C)	
Ideal Installation, OCR = 1	43.5 ± 1.5	40.1 ± 2.4	43.1 ± 2.2	41.6 ± 3.2	Bellotti et al, 1987
Ideal Installation, OCR > 1	44.7 ± 2.4	37.2 ± 3.7	40.9 ± 2.6	37.5 ± 4.1	Calibration Chamber Tests - Camkometer
					Ticino Sand - Dr = 40 to 71 %
Selfbored, OCR = 1	41.9 ± 0.6	39.9 ± 3.6	42.8 ± 3.0	NA	
Selfbored, OCR > 1	43.5 ± 3.4	43.7 ± 9.6	46.1 ± 7.7	42.8 ± 8.5	
					CALIBRATION CHAMBER
Borehole 4003	39.1 ± 1.1	39.8 ± 7.0	43.1 ± 5.1	NA	Bruzzi et al, 1986
Borehole 4017	37.8 ± 1.3	30.3 ± 3.4	36.4 ± 2.2	NA	Field Tests - Camkometer
Borehole 5050	37.7 ± 1.6	46.7 ± 9.8	48.9 ± 7.7	NA	Po River Sand - Loose to Medium Dense Sand
					Depths 6.2 to 23 m
					FIELD TESTS

(A) Hughes et al, 1977 model with the log-log interpretation approach
(B) Robertson and Hughes, 1986 empirical correction of (A) using a nomogram
(C) Manassero, 1989 model with finite difference interpretation approach

OBSERVATIONS:
Data ± 1 standard deviation.
Reference (plane strain) ϕ of Bellotti et al, 1987 from Lade and Lee, 1976 correlation, using conventional Triaxial compression testing results.
Reference (axially symmetric) ϕ of Bruzzi et al, 1986 from Durgunoglu and Mitchell, 1975 theory, using data from piezocone tests.
NA = Not Available.

Table 2.2: Comparison of Friction Angle Predicted by Different Traditional Interpretation Methodologies

dependency of stiffness to confining pressure, to simulate the cavity expansion in sands. Finite element simulated pressure expansion curves were analyzed by the Hughes et al, 1977 log-log approach, predicting ϕ's that were closer (within $\pm$ 10 %) to the input ϕ's of the finite element program.

2. The scatter of ϕ's observed in the selfbored tests was mainly due to disturbance. For instance, the major effect of disturbance on the traditional log-log approach of Hughes et al, 1977 is in regard to the non linearity of the log-log curve. Disturbance makes it difficult to define a unique slope in the log-log plot, hence a unique and reliable ϕ. The highly scattered results of Bellotti et al, 1987 for the selfbored tests suggest that field pressuremeter curves, that invariably have some disturbance built in, are not suitable for the prediction of ϕ by any of the above traditional interpretation methodologies. On the other hand, if the field curve is of extremely high quality, then the prediction of ϕ will be accurate. According to Bellotti et al, 1987 none of the methods above provide a reliable estimate of ϕ for sands from the SBPM, although the method of Robertson and Hughes, 1986 produces the lesser amount of scatter.

The results of Bruzzi et al, 1986 can be used to check the suitability of field SBPM curves for the determination of the friction angle. These authors carried out a similar program of SBPM tests to assess the above interpretation methodologies. 53 SBPM tests were performed with the English Camkometer in the aged granular deposit of Po River sand. The reference ϕ values were derived from empirical correlations with piezocone soundings (Durgunoglu and Mitchell, 1975 theory) which, according to the authors, are only 1 to 2° lower than the ϕ's of triaxial tests. The ring shear ϕ_{cv} was used in the SBPM interpretation methodologies. The results of these authors are also shown on Table 2.2 and, similarly as in the previous case, highly scattered values were obtained in all the boreholes tested. It is noticed in this table that the scatter of the field results is of the same order of magnitude as the scatter obtained by Bellotti et al, 1987 with the OC selfbored chamber tests.

According to Bruzzi et al, 1986 the Hughes et al, 1977 log-log interpretation approach leads to highly scattered values of ϕ that are generally too low but sometimes too high. The correction proposed by Robertson and Hughes, 1986 works in the right direction, but still does not yield consistent values of ϕ. Bruzzi et al, 1986 speculate that the major difficulties in predicting ϕ from the SBPM are linked to factors like the inadequacy of the constitutive relationships, the curvilinear strength envelope of sands and possibly the finite length of the probe. On the contrary, they feel that the scattered ϕ results are not caused by

disturbance effects, since their SBPM tests did not show signs of "large initial disturbance", as, for example, in Hughes et al, 1977 and Robertson and Hughes, 1986.

Based on the review of this subsection it is concluded that the ϕ predicted by the current SBPM interpretation methodologies is far from a reliable parameter if disturbed testing curves are interpreted. On the other hand, reasonably accurate results of ϕ are obtained with high quality testing curves.

For the disturbed curves, the difference of the results for different constitutive relationships was not observed to be appreciably high, which suggests that the simplified assumptions of the traditional rheological models are not the major factor responsible for the failure of the analysis to properly estimate a repeatable and reliable ϕ. Disturbance, numerical instability of the finite difference interpretation approach and the subjectivity built in the derivation of slopes from the log-log method are, without question, the major variables that influence the current predictions of ϕ from SBPM tests.

There have been, however, improvements on the log-log approach of Hughes et al, 1977 to take account of the interpretation of disturbed curves. Mair and Wood, 1987 suggested a trial and error procedure to chose a correct reference strain (related to σ_h) to be used as datum in the log-log plot of pressure versus strain, such that this plot would become a straight line over a larger strain range of the test. Fahey and Randolph, 1984 suggested a similar approach, but proposed as a first basis of datum strain the use of the strain at which the cavity pressure is equal to the total vertical stress at the test position.

Nevertheless, those corrective approaches are cumbersome to use and may not lead to a substantial increase in the reliability of the interpretation of disturbed SBPM data.

2.3.3 Horizontal Stress

The lateral stress is a parameter of primary importance in soil mechanics and its evaluation has always been a matter of concern. The lateral stress is commonly used with the vertical stress to derive the in situ coefficient of earth pressure at rest (K_0) of the deposit.

The current approach followed by the SBPM test in sands is the direct measurement of the original horizontal stress of the deposit. For that, the only method available consists on the visual determination of the lift off pressure at each of the strain arms of the SBPM probe (Mair and Wood, 1987). The lift off pressure (P_0) is defined by the pressure at which a "break" or substantial change of slope occurs in the early stages of the testing curve. The lateral stress of the sand is commonly assigned to the average value

of the lift off pressures defined in each of the strain arms of the SBPM. The selfboring lateral stress ratio ($K = \sigma_h/\sigma_v$) is commonly quoted as the value closest to K_0. Therefore this value is currently used as a reference basis for all other in situ estimations of lateral stress.

Empirical relationships can be used as a basis to form opinions regarding the reliability of the SBPM σ_h measurements. However, these empirical relationships do not always account for all the intrinsic variables that affect the lateral stress in a natural environment. An alternative approach to evaluate SBPM σ_h results is the interpretation of tests performed in a controlled environment, such as inside a calibration chamber. Although the chamber environment can not fully simulate the soil conditions in situ, the boundary stresses are very well known.

Therefore, the results of the chamber tests performed by Bellotti et al, 1987 were also used here to assess the capability of the SBPM to predict σ_h with lift off measurements. For that purpose, the average P_0 measured by the 3 strain arms of the Camkometer was compared to the boundary stress σ_b of the chamber. For the ideal installation tests the lift off stresses were significantly different than the applied chamber boundary stresses. The reasons cited by these authors were the stress concentration around the rigid SBPM, the mechanical compliance of the strain arms and arching effects caused by the presence of an annulus of looser sand around the pressuremeter. The possibility of stress concentration was investigated with a unique ideal installation test where a rigid selfboring K_0 cell was used. Apparently little or no stress concentration was noticed. This led to a redesign of the strain arms of the Camkometer used by these authors. A new series of tests were then carried out with the new design, as indicated by the results of the top plot of Figure 2.12. In this plot it is noted that a small difference of $\pm$ 10 to 15 % between P_0 and the boundary stresses was found. It appears, therefore, that for high quality testing curves it is possible to define accurate predictions of lateral stress with lift off measurements.

The lower plot of Figure 2.12 shows the results for the selfbored tests of this same authors. As can be seen by this plot the measured average lift off pressures were lower than the applied chamber stresses. According to Bellotti et al, 1987 the lift offs were often close to the water pressure of the chamber, indicating that significant disturbance occurred during the probe installation, especially in the loose and medium dense sands. The average ratio P_0/σ_h of the selfbored tests was 0.47 ± 0.28, indicating that even

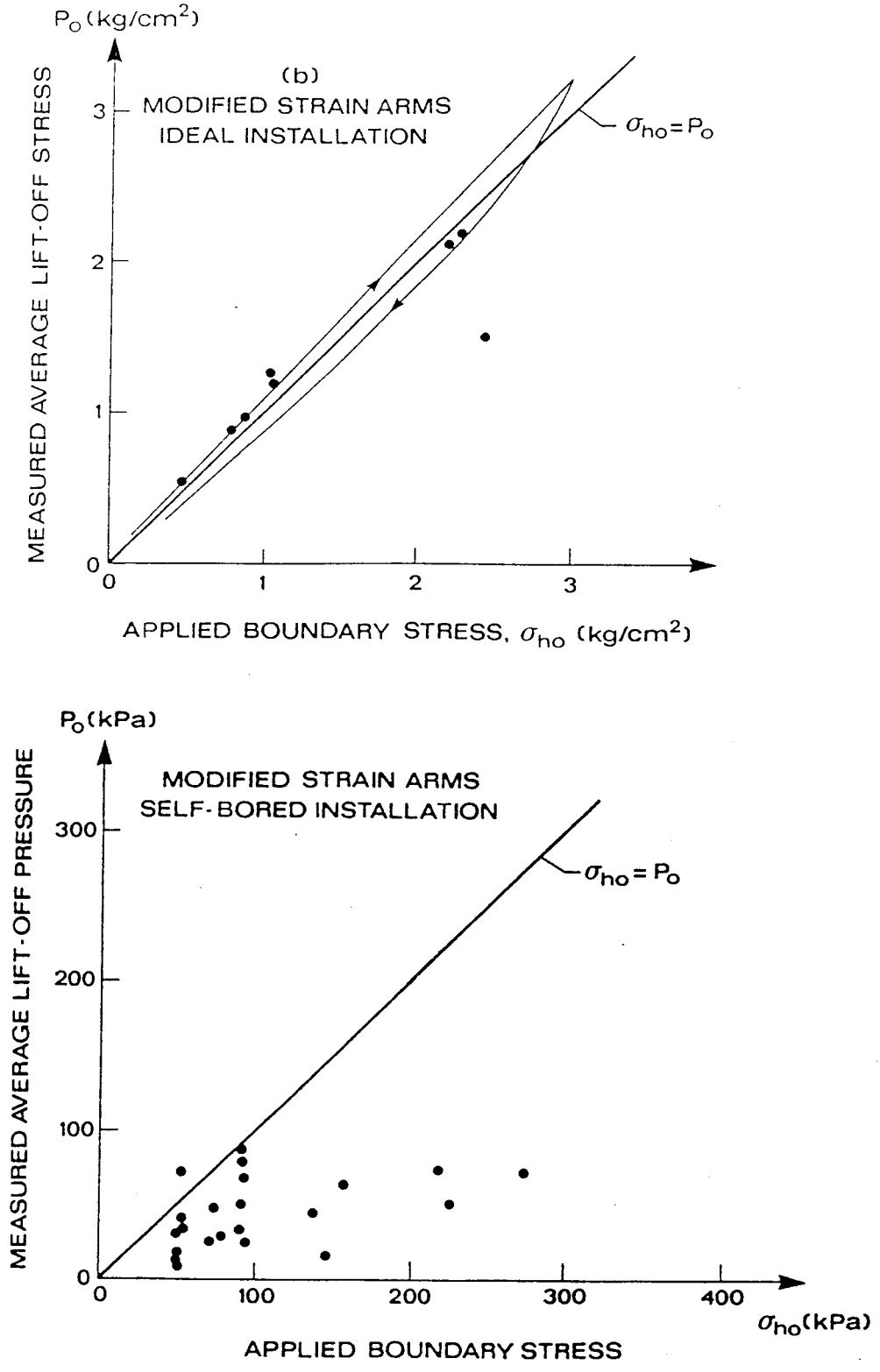

Figure 2.12: Comparison of Measured and Applied Lateral Stress in Calibration Chamber (after Bellotti et al, 1987)

under controlled conditions selfbored SBPM tests render lateral stress predictions that are highly scattered and generally unreliable. This appears to be the case when lift off measurements are used.

In natural sand deposits, however, more reliable predictions of σ_h may be obtained. According to Bellotti et al, 1987 the sand tested in the Italian chamber (i.e. freshly deposited, unaged, uncemented, clean sand) may create particularly unfavorable conditions with respect to the reliable assessment of the in situ stress. Clarke and Wroth, 1985, stated that the level of knowledge of the selfboring process with the traditional system in sands has evolved considerably in the last years, making it possible to obtain valid values of lateral stress by improved drilling techniques in the field. Thus, the field results of Bruzzi et al, 1986 can also be discussed here to check the suitability of SBPM curves for the σ_h determination in granular deposits.

Bruzzi et al, 1986 were able to optimize the cutter setting by sequential selfboring trials, such that "reasonable" values of in situ horizontal stress were obtained (Lacasse et al, 1990). The "reasonable" estimates of the Camkometer were considerably scattered and 20 to 50 % higher than the author's best estimate of the in situ σ_h with basis on the empirical formulas that relates K_0 with OCR (OCR estimated from oedometer tests on embedded silt layers of the deposit). The results obtained from tests using the French PAF-76 SBPM in the same Po River sand deposit yielded lower values than the best estimates of σ_h. Most of the scatter observed by Bruzzi et al, 1986 came from the same reason as the one found in the chamber tests of Bellotti et al, 1987: the disturbance of the test. The above results suggest that a small amount of disturbance in the pressuremeter curve is enough to cause a large scatter of lateral stresses predicted by the visual inspection technique. This is valid for selfboring pressuremeter tests in either controlled (chamber) or natural (field) environments.

In summary, the lateral stress determined by the visual inspection method (lift off) is unreliable if disturbed data is analyzed. Scatter in the results is prone to occur even if slightly disturbed SBPM testing curves are analyzed. Lift off pressures can be accurately used only with undisturbed curves. It is claimed that by a proper optimization of the selfboring insertion technique undisturbed curves and reliable values of σ_h can be obtained. The experience gathered by Bellotti et al, 1987 in the calibration chamber and Bruzzi et al, 1986 in the field dismiss that, suggesting that the sensitiveness of P_0 to any disturbance generated during insertion is so high that the visual inspection technique can not be efficiently used in selfbored tests.

Therefore, in view of the limited experience for the evaluation of the in situ stress in sands by the visual inspection technique (Lacasse et al, 1990), the ability of the SBPM probe to accurately determine σ_h has not been fully proven yet.

2.3.4 Shear Modulus

The SBPM is one of the most promising in situ tools that can be used to directly measure the stiffness of the sand. The shear modulus of the pressuremeter can be currently evaluated by a interpretation procedure that uses different parts of the testing curve, as is described next.

2.3.4.1 Unload Reload Shear Modulus

Hughes, 1982 and Wroth, 1982 noted that the elastic modulus could be directly obtained by performing loops during the expansion phase of the test, with the advantage that the modulus derived in this manner would be much less influenced by disturbance (Mair and Wood, 1987). As discussed in subsection 2.2.4, within the framework of the theory of elasto-plasticity any unload of the expanding cavity wall brings the surrounding soil below the currently expanded yield surface. This is illustrated in the top plot of Figure 2.13, which shows a typical section of the testing curve with an unload-reload loop BCD. It is noticed on the stress path (bottom plot) of this same figure that the elastic soil during the unload stage is only subjected to variation in the shear stress level, provided that the maximum unload criteria of Wroth, 1982 is followed.

The slope of the previously executed loop BCD corresponds to the shear modulus of the elastic surrounding medium, as derived in Equation 2.26. Therefore the unload reload modulus is given by:

$$Gur = \frac{1}{2}\frac{dP_u}{d\varepsilon_\theta} \tag{2.68}$$

where: dP_u is the effective cavity stress difference applied during unloading

$d\varepsilon_\theta$ the circumferential strain amplitude at the cavity wall

However, the deformation parameter can not be considered to be a constant and inherent property of the soil, but rather a complex function of several variables (Hardin and Drnevich, 1972) that act simultaneously during the penetration of the in situ probe. This is so because in real sands:

1. The deformation parameter is a function of the level of mean stress that exists surrounding the in situ device, as well as stress history imposed prior to and during penetration.

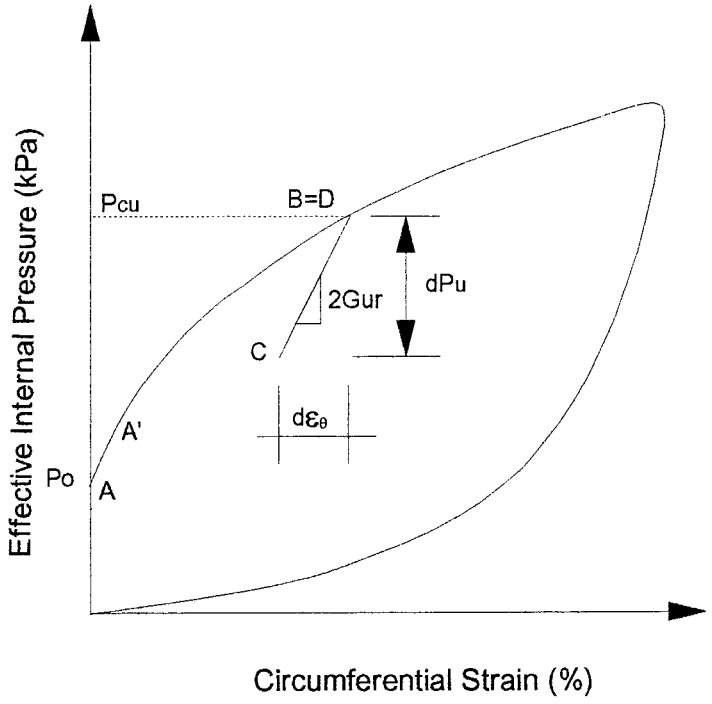

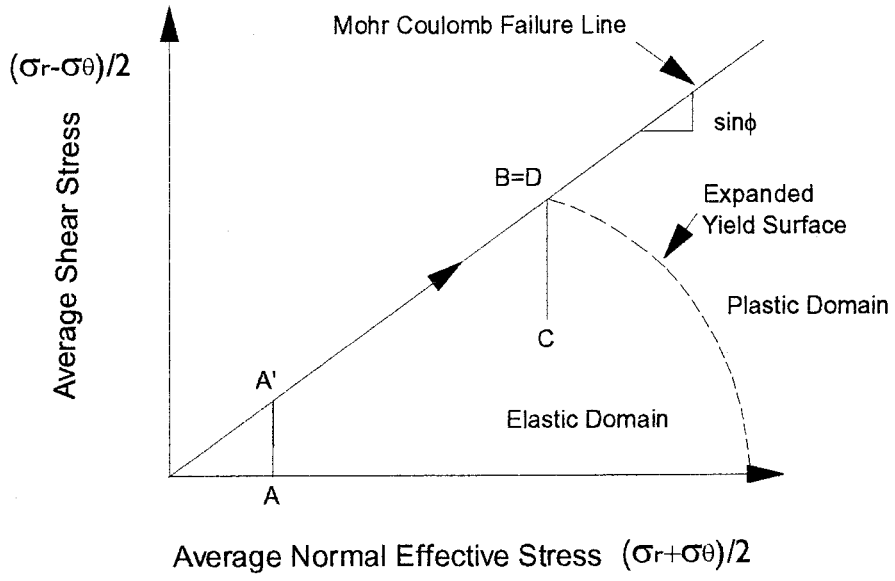

Figure 2.13: Concept of Elastic Shear Stiffness as Obtained from Unload Reload Loops (Modified after Bruzzi et al, 1986)

2. The deformation parameter behaves in a non linear manner in regard to the level of in situ shear stress and strain imposed during probe penetration.

Effect of Stress Level:

In order to illustrate the stress level effects in Gur let's assume that the only distinction between the element of soils surrounding the cavity prior and during unloading relates to normal effective stress (σ_m) differences. Figure 2.14(a) shows a hypothetical testing curve in which two unload reload loops were performed. Two distinct shear moduli (Gur_1 and Gur_2) were measured, with Gur_2 greater than Gur_1. Figure 2.14(b) shows the stress path of the soil (at the cavity wall) during the loading and unloading stages. For the loop carried out in BCD the soil has been loaded elastically along the line A-A' and then plastically along A'-B. It is noticed that at each different position of the testing curve (Figure 2.14(a)), a different level of average normal (σ_m) and shear (τ_m) stress is mobilized at the wall (Figure 2.14(b)).

Figure 2.15(a) shows the elastic and plastic zones developed prior (and after) the unload stage of the loop BCD. It is noticed in this figure that, prior to the loop BCD, the elasto-plastic boundary will be under a level of (shear and normal) stress similar to those of the point A' of the testing curve (see Figure 2.14). One element of soil at an infinite radius will be under a level of stress similar to those of point A of the testing curve. The cavity wall will be under a level of stress similar to those of point B of the testing curve.

Upon unloading all the zone of soil surrounding the probe responds elastically, and the previously plastic zone is encompassed by the elastic zone (see Figure 2.15(a)). During unloading, the stress paths of all the elements of soil between A and B will follow a similar path as the one presented in Figure 2.14(b) for the cavity wall (path B-C). In this latter figure it can be seen that after unload the cavity wall will be under the same level of normal stress as before (equal to σ_{m1}) but the level of shear stress will decay from τ_{m1} to τ_{m2}.

Each element of soil between A' and B in Figure 2.15(a) will have a different level of normal stress σ_m prior to the unload stage, for instance element A' will be under σ_{m0} whereas B will be under σ_{m1} (see Figure 2.14(b)). This implies that each element of soil will have a different modulus G that differs from element to element as a function of σ_m. This modulus will be constant for each of the elements, as the soil is idealized to respond in a linear elastic manner with a unique modulus. Since the level of normal stress

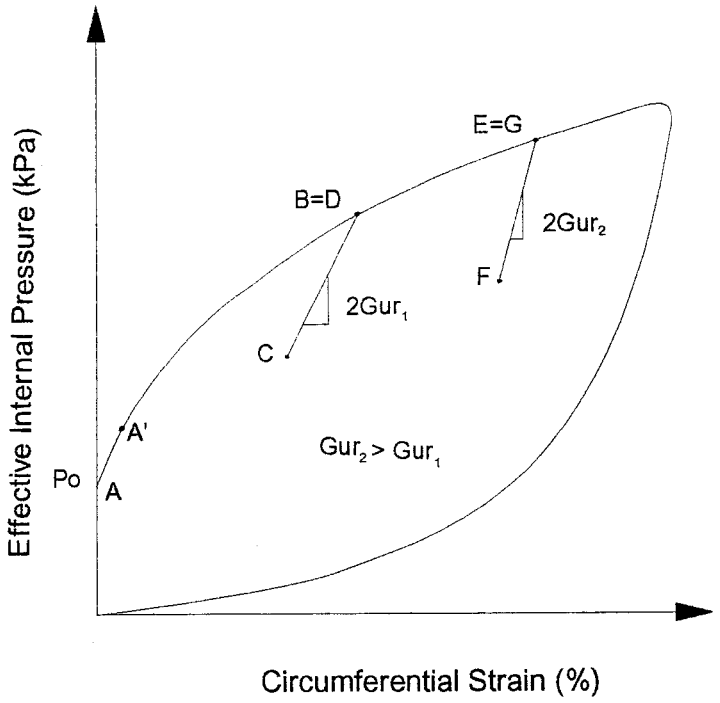

(A) Hypothetical Testing Curve

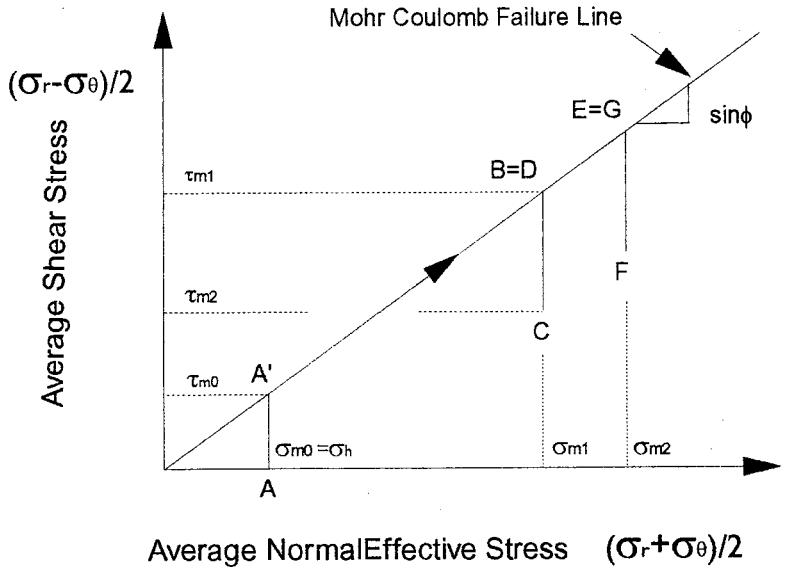

(B) Stress State for Different Points of the Testing Curve

Figure 2.14: Effect of Stress Level on Unload Reload Shear Modulus

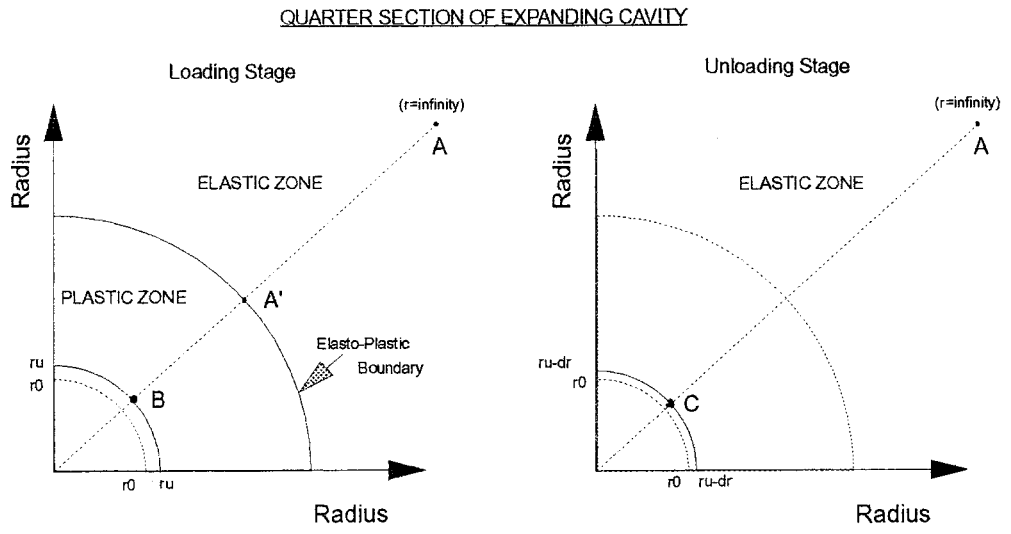

(A) ELASTIC AND PLASTIC ZONES FOR THE UNLOAD-RELOAD LOOP BCD

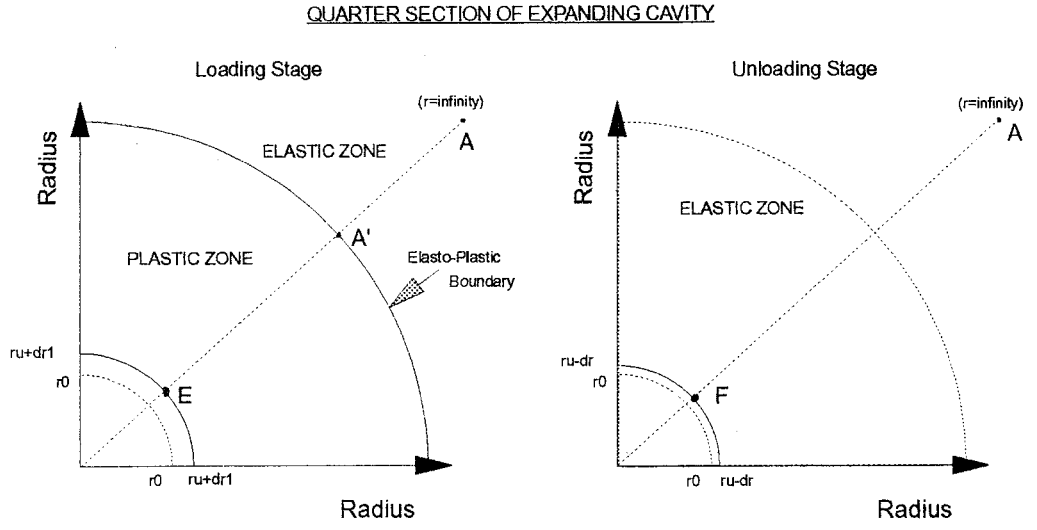

(A) ELASTIC AND PLASTIC ZONES FOR THE UNLOAD-RELOAD LOOP EFG

Figure 2.15: Plastic and Elastic Zones Prior and After the Loop Stage

decreases from the cavity wall (element B of Figure 2.15(a)) to soil elements located at a greater radius than r_u, the shear modulus will also decrease throughout the soil surrounding the probe. Thus the slope of the loop (i.e. Gur_1) will reflect an "average" stiffness of the whole material surrounding the probe during the unloading stage, and shall be assessed with the knowledge of the average level of normal stress that exists within the plastic zone prior to this stage.

If the expansion of the cavity continues, the plastic zone increases to a radius greater than the radius observed prior to the first unload-reload stage (BCD). Figure 2.15(b) shows the plastic and elastic zones developed prior to (and after) the unload stage of the loop EFG. As shown in Figure 2.14(b), the cavity wall element E will be under a much higher level of normal stress than before, as σ_{m2} is greater than σ_{m1}. This implies that each element of soil between A' and E (in Figure 2.15(b)) will also be under a higher σ_m level than the level that each element had prior to the first unloading stage. Consequently, prior to the second loop the average level of normal stress within the plastic zone is higher than the level that existed (in the plastic zone) prior to the first loop. Given again the stress level dependency of the modulus, it is to be expected that the measured Gur for the second loop (Gur_2) will be higher than the modulus of the first loop (Gur_1). This implies that Gur will increase in the course of a expansion test, i.e. the relative position of the unload reload loop. This effect is substantiated by Clarke and Wroth, 1985, which noticed that by plotting Gur against mean effective stress, rather than depth, the scatter of results decreases considerably.

The above influence of the stress level in Gur led Robertson, 1982 and Bellotti et al, 1989 to propose expressions to derive the average stress level σ_{av} surrounding the probe (in the plastic zone) that exists prior to the loop stage, and hence obtain a corrected for stress level modulus (Gur^c) with the Janbu, 1963 equation. Robertson, 1982 proposed the first approximation of the average mean octahedral effective stress that acts in the plastic zone, assuming that:

$$\sigma_{av} = 0.5\, P_{cu} \tag{2.69}$$

where P_{cu} is the effective cavity pressure at the start of unloading, as defined in Figure 2.13.

Bellotti et al, 1989 developed an analytical equation, based on the cavity expansion in an elasto perfectly plastic sand, to derive the average normal stress of the plastic zone. Their equation was developed based on the integration of the normal effective stress of each element of soil encompassed by the plastic zone.

Their final equation is:

$$\sigma_{av} = \frac{\int_{r_u}^{r_p} \sigma_m \cdot \frac{dr}{r}}{\int_{r_u}^{r_p} \frac{dr}{r}} = \chi . P_{cu} \text{ , where } \chi = \left(\frac{1}{1-\sin\phi}\right)\left(\frac{\left(\frac{r_p}{r_u}\right)^N - 1}{\left(\frac{r_p}{r_u}\right) - 1}\right) \qquad (2.70)$$

where r_p is the radius of the plastic zone prior to unloading stage, and r_u the respective cavity radius.

In order to simplify the above equation these authors have scrutinized the chamber results of Bellotti et al, 1987. Since all the variables, including the plane strain ϕ of the tested sand is known for Bellotti's 1987 tests, a modified equation for σ_{av} was suggested:

$$\sigma_{av} = \sigma_h + \alpha(P_{cu} - \sigma_h) \qquad (2.71)$$

where α is an empirical reduction factor equal to 0.2.

The deficiency of this method is that by integrating along a radius the expression fails to incorporate the larger volume of soil subjected to increase in stress as the test progresses. Besides, the incorporation of an empirical parameter α leads to an approximate (not accurate) determination of the average stress in the plastic zone. Nevertheless, Howie, 1991 argues that given the unknown effects of disturbance, anisotropy, etc. over Gur no justification can be found to refine even more the above corrections.

Once a reference stress is obtained it is possible to normalize Gur to Gur^c, where Gur^c is the modulus at the in situ normal stress (horizontal stress σ_h). For granular materials the relationship between elastic modulus and stress level can be expressed in a similar way to that suggested by Janbu, 1963:

$$\frac{G}{Pa} = K_g \left(\frac{\sigma_{av}}{Pa}\right)^n \qquad (2.72)$$

where: K_g is the modulus number,

n the modulus exponent

Pa the atmospheric pressure.

The value of n is typically in the range of 0.4 to 0.8 (Bruzzi et al, 1986 and Bellotti et al, 1989) and is dependent on the strain amplitude over which the modulus is measured (Wroth et al, 1984). For all

purposes, it will be assumed as 0.5 in this thesis. Using the Equation 2.72 above, and noting that Gur is an average modulus which is a function of σ_{av} and the normalized Gur^c is referent σ_h, it is possible to derive:

$$Gur^{c} = Gur\left(\frac{\sigma_h}{\sigma_{av}}\right)^{0.5} \tag{2.73}$$

The above discussion indicates that Gur reflects an average stiffness that shall be related to some measure of the relevant stress level around the cavity for its proper use in design. Empirical and semi-empirical methodologies to assess this stress level do exist in the literature.

Effect of Strain Level:

In order to illustrate the effects of the strain level on Gur let's now assume that the only distinction between the elements of soil surrounding the cavity prior and during unloading relates to the levels of induced shear strain. Figure 2.16 presents the same testing curve as discussed before, with two hypothetical unload reload loops. The second loop is carried out to a degree of cavity strain unload higher than the degree of the first loop and, in a opposite fashion as before, the shear modulus of the second loop Gur_2 is lower than the modulus of the first loop Gur_1. The loops have a non linear shape, suggesting that more than one shear modulus can be defined. In this case, Gur is defined with the slope of the upper (B, E) and lower (C, F) "cross over" points of the loop.

The non-linear behavior of the loop occurs because real cohesionless soils have an elastic threshold shear strain above which the behavior is non-linear. Research carried out by Dobri et al, 1980 with sands demonstrated that the maximum modulus G_0 is mobilized for shear strains below 10^{-3} % to $6x10^{-3}$ %. At this level of induced shear strain the soil behaves in a linear elastic manner, as hypothesized by the linear equations of subsection 2.2.2. For higher strain amplitudes, like those mobilized during the unload reload loops, the behavior is non linear and the modulus varies according to the applied cavity strain $d\varepsilon_\theta$, i.e. the induced shear strain at the cavity wall and surrounding soil. Figure 2.17 shows the experimental modulus reduction curve of granular materials presented by Idriss, 1990, based on the range proposed by Seed and Idriss, 1970 defined after the compilation of several laboratory investigations of shear moduli for sandy soils. The higher the induced strain the lower is the shear modulus of the material in the non linear range of

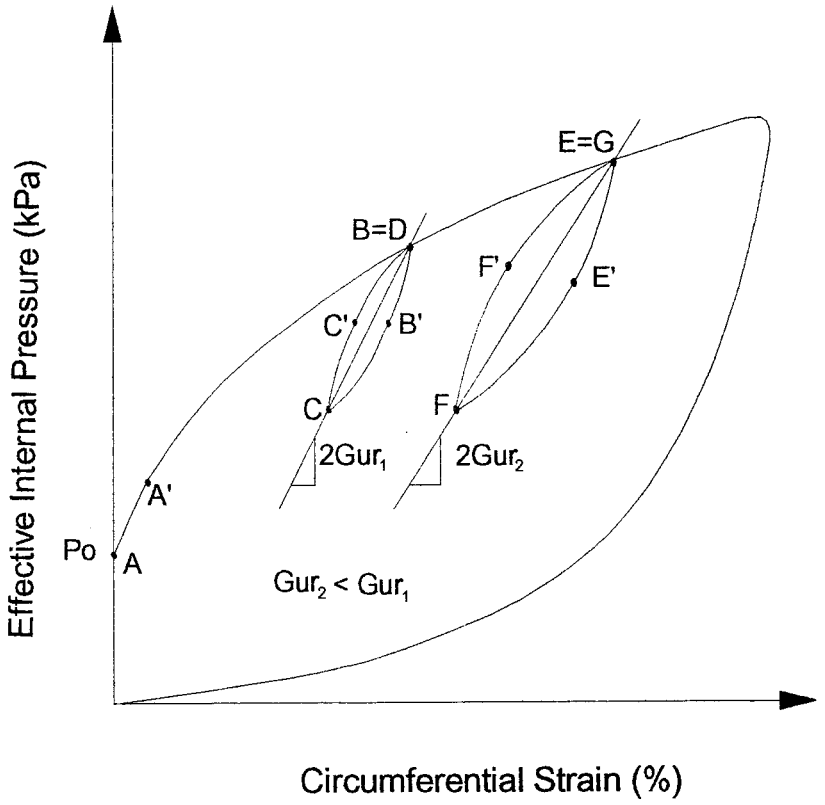

Figure 2.16: Effect of Strain Level on Unload Reload Shear Modulus

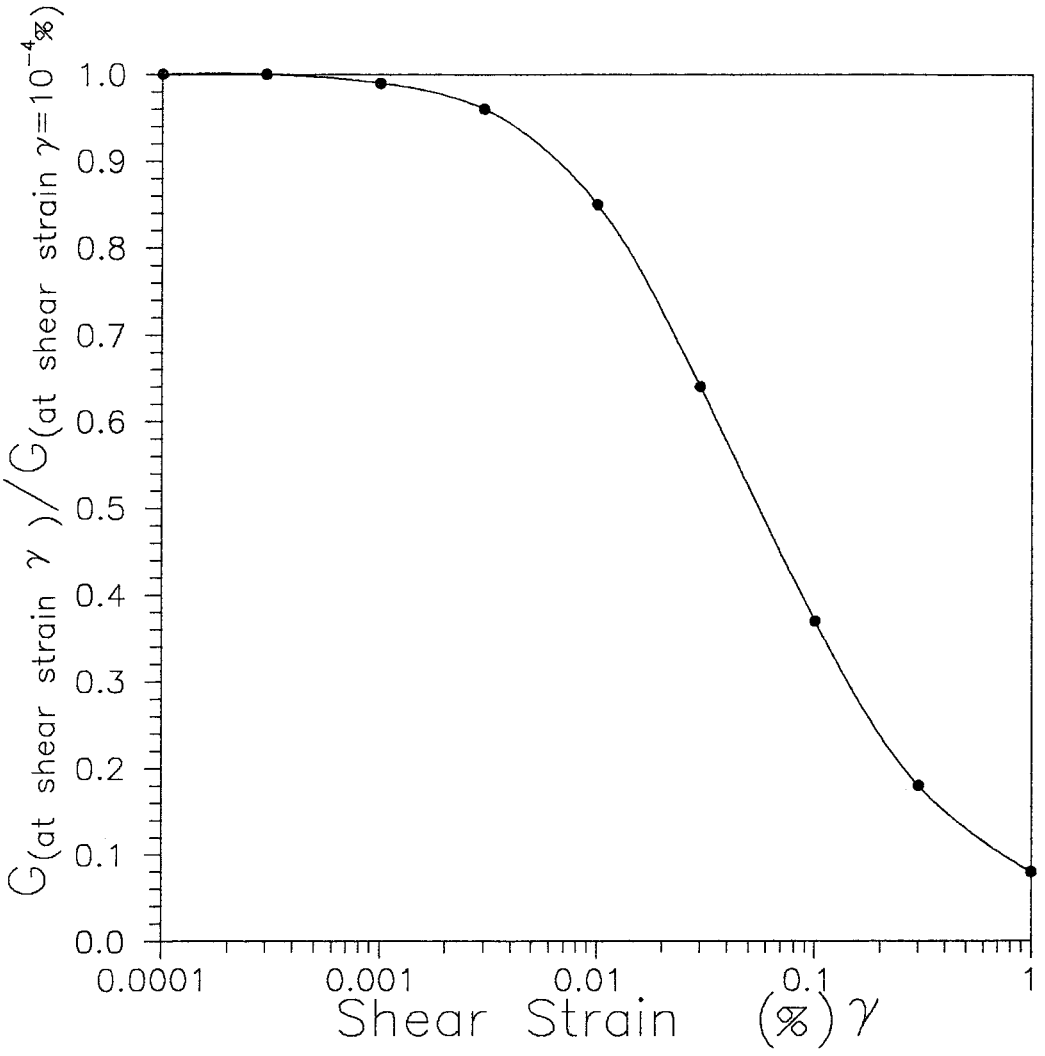

Figure 2.17: Variation of Shear Modulus with Shear Strain for Sands (after Idriss, 1990)

stress-strain behavior, and vice-versa. During the unload stage (B-B'-C) of the first loop BCD all the soil elements between A and B in Figure 2.15(a) will be strained by a different amount, hence leading to a differential decrease of the modulus along the soil. As noted by Whittle et al, 1992 (and Equation 2.18) for a linear elastic isotropic soil the distribution of strain around the cavity varies inversely with the square of the radius, meaning that elements of soil at the cavity wall will be much more strained than elements located at a higher distance from the wall. This implies that the modulus decay at the cavity wall will be much higher than the decay at the adjacent outer elements, leading to a much softer soil response at the cavity wall. The soil response will gradually become stiffer as the position of the soil elements increase in relation to the cavity radius. This is the opposite effect to that observed in the case of the stress level, but similarly as before the modulus measured at the cavity wall will reflect an "average" stiffness of the whole material surrounding the probe.

Since during the unload process the loaded soil becomes softer as a whole, given the overall increase of shear strain, the measured modulus at the wall will constantly decrease. This leads to the non-linear rounded shape of the unload stages of the loops BCD (B-B'-C) and EFG (E-E'-F). Upon reloading the same straining effect that happened before occurs, but at the opposite direction. This leads to the non-linear rounded shape of the reload stages of the loops BCD (C-C'-B) and EFG (F-F'-E), where the secant cavity modulus G constantly decreases.

Moreover, given the strain level dependency of the shear modulus of the sand, the higher the degree of unload at the cavity wall the higher will be the straining induced at each of the elements of soil surrounding the cavity. Consequently, the softer will be the general response of the medium and the lower is the measured modulus. Figure 2.16 schematically shows that the modulus of the second loop Gur_2 is lower than the modulus of the first loop Gur_1. This effect was also observed by Whittle et al, 1992 with SBPM tests in London clay. These authors noticed that by increasing the loop amplitude there is a decrease in the measured shear modulus.

Thus in order to make use of the pressuremeter unload reload shear modulus Gur the assessment of the average level of shear strain which corresponds to this modulus is also required. The assignment of an average shear strain γ_{av} for a particular testing loop is a function of the behavior of the soil elements around

the probe prior and during unloading. Empirical or analytical expressions can be used with this objective, as those respectively proposed by Robertson, 1982 and Bellotti et al, 1989.

Robertson, 1982 proposed that an average shear strain amplitude γ_{av} equal to $0.5.\Delta\gamma_c$, where $\Delta\gamma_c$ is the shear strain amplitude of the loop cycle in the cavity wall (= $2d\varepsilon_{\theta w}$), shall be assigned as the strain increment relevant to Gur. Bellotti et al, 1989 defined the relevant strain increment of Gur as the average elastic shear strain induced in the surrounding zone of soil during the unload stage of the loop. The zone of soil considered is the zone that was previously occupied by the plastic zone prior to loop stage. Idealizing the sand as an elasto-plastic medium they were able to obtain this average induced strain with an analytical equation. This equation is dependent on the P_{cu}, the plastic radius r_p, the ϕ and σ_h of the sand and on the degree of cavity unload. However, similar to the case of stress level, with the use of the calibration chamber data of Bellotti et al, 1987 they were able to simplify their equation to:

$$\gamma_{av} = 0.5.\beta.\Delta\gamma_c \tag{2.74}$$

where: 0.5 is a factor to produce the single amplitude of shear strain

β is an empirical reduction factor equal to 0.5.

Howie, 1991 suggested that an average strain level equal to $0.15.\Delta\gamma_c$ could be assigned to Gur. He based this suggestion on the same chamber results of Bellotti et al, 1987, since by plotting Bellotti's data with this strain definition a very reasonable agreement could be obtained with the Seed and Idriss, 1970 general envelope for sands.

Therefore, as discussed above, the Gur also reflects the integrated effect of the soil deformation along the expanding cavity, and shall be related to some relevant measure of the average induced strain level for its use. Empirical and semi-empirical methodologies to assess the relevant strain level also exist in literature. This strain is in general of the order of 10^{-1} %, with basis on the extensive data gathered in the calibration chamber by Bellotti et al, 1987 and in the field by Bruzzi et al, 1986.

Combined Effect of Stress and Strain Level:

The combined effect of both stress and strain levels induced around the probe prior and during the unload reload stage shall be considered for the rational use of the pressuremeter Gur.

Bellotti et al, 1989 attempted to develop a methodology that corrected Gur for stress as well as strain level, in order to link the high strain modulus of the pressuremeter to the low strain modulus of the soil.

With the stress level correction of Equations 2.71 and 2.73 it is possible to convert Gur to the modulus Gur^c, valid for a particular average normal stress level. Using the hyperbolic stress strain relation of Kondner, 1963 these authors were able to link Gur^c to the low strain G_o, or as defined in this thesis[3] by G_{max}. Their hyperbolic equation is given by:

$$\frac{Gur^c}{G_{max}} = \frac{1}{1 + \frac{G_{max}\,\gamma_{av}}{\tau_{max}}} \tag{2.75}$$

Using the approach suggested by these authors it is also possible to link the Gur to the stiffness relevant to the design problem, where the average level of induced strain will differ from the average values imposed by the pressuremeter in the soil.

Byrne et al, 1990 followed a more elegant direction for the problem of assigning stress and strain levels to Gur in order to link this variable to G_{max}. These authors carried out a plane strain axisymmetric finite element analysis in which both the stress and void ratio changes in the plastic zone were considered, as well as the non linear stress strain response of the sand during unloading. Stress ratio effects on G_{max} were included with the expression of Yu and Richart, 1984 and the unloading stress strain response was modeled with the hyperbolic equation of Kondner, 1963.

The finite element analysis of these authors considered stress and strain changes in all the soil elements surrounding the probe during unloading. The unloading was simulated in a number of small steps with the cumulative displacement at cavity wall being used at each stage to compute the cavity strain increment. The analysis output was presented in a chart format, such that for a given dP_u/P_{cu} and P_{cu} of the loop it is possible to correct the measured Gur for both stress and strain amplitude, and hence predict the low strain modulus G_{max} at the in situ normal stress level.

The finite element analysis of Byrne et al, 1990 demonstrated that, as the expansion testing proceeds, it is possible to obtain a reasonably constant Gur if the size of the loops (dP_u) also increases. This is so because the opposite effects caused by the increase of strain amplitude and increase of stress level over Gur tend to cancel each other.

---

[3] Both G_{max} and G_0 are defined for the same strain level. G_{max} refers to pressuremeter predictions via Gur, whereas G_0 refers to the actual in situ maximum modulus measured by highly accurate techniques, such as geophysics tests.

Recently Fahey and Carter, 1993 expanded the pressuremeter capability of stiffness derivation, by using the pressuremeter unload reload loop into finite element simulations. A finite element analysis that considers void ratio, stress ratio and stress level over G_{max} in the plastic zone, and assumes a non linear hyperbolic variation of stiffness in the elastic zone, was developed to simulate the expansion and unload reload testing stages. By matching numerical predictions with field data these authors were able to simulate the degradation of the stiffness ratio with the increase in strain amplitude for the tested sand. Thus, this methodology allows the derivation of the in situ modulus for any strain level, rather than the assessment of a unique Gur^c modulus at some average strain level.

The above discussion indicates that the unload reload modulus of the pressuremeter represents an index to the average stiffness of the whole soil surrounding the cavity, in which each soil element is under a particular stress and strain level.

2.3.4.2 Initial Shear Modulus

The elastic shear modulus of the sand can be also obtained by the measurement of the initial slope of the testing curve. This modulus, previously defined as "Gi", governs the soil response at the "elastic" zone where the sand is assumed to deform in a linear elastic manner.

The top plot of Figure 2.18 demonstrates how this modulus is obtained in a typical testing curve. The modulus Gi is defined with the use of Equation 2.26, which assumes the initial stress strain response of the sand as linear.

However, given the previously discussed strain level dependency of the shear modulus, the initial stress strain response of the sand (as measured by the SBPM) should not be expected to be linear. Similarly as the reload stage of the loop, during the initial (elastic) loading of the sand there will be an overall increase of shear strain in the surrounding material, leading to a gradual decay of the soil response measured at the cavity wall. Therefore, the stiffness measured at the cavity wall shall vary non-linearly from a very high value, ideally equal to G_0, to a low value equivalent to the stiffness at the limit (yielding) condition of the sand. The blow up of the initial section of the testing curve of Figure 2.18 indicates that the "actual" response of the sand does not follow the "idealized" response of the linear elastic theory. However, the current SBPM versions do not have the high accuracy required to measure the sand stiffness

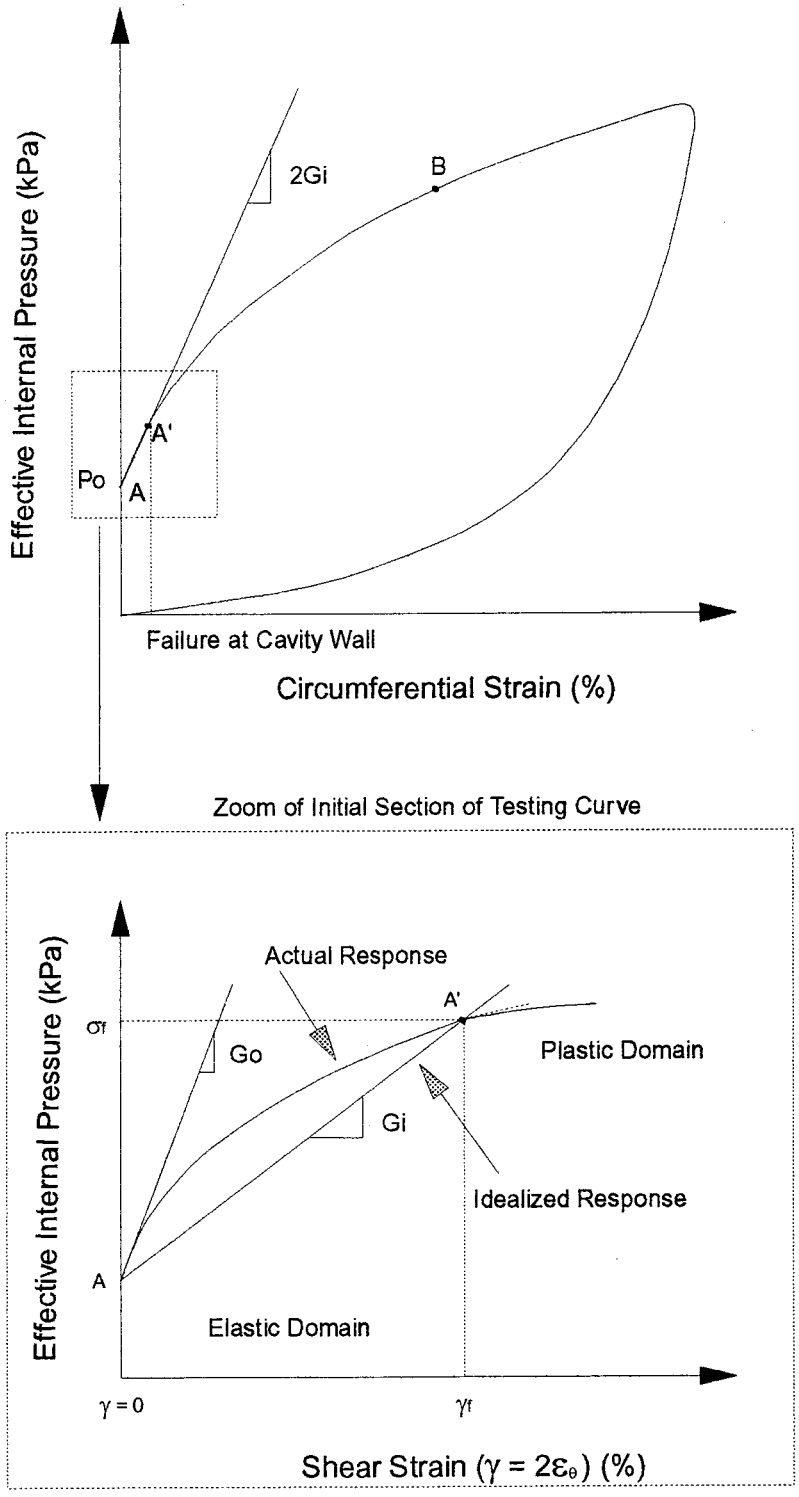

Figure 2.18: Determination of Initial Modulus from SBPM Curve

variation at the very low levels of strain mobilization (Hughes, 1993 personal communication). In other words, they can not precisely define the non-linear stress strain behavior of the sand showed in Figure 2.18 for cavity shear strains below the failure (γ_f, which in general is in the order of 10^{-1} %). Therefore, in the current SBPM versions the initial slope approximates to a straight line, leading to an easy measurement of Gi if the testing curve is not disturbed.

Given the non linear response of each of the soil elements around the probe, it is concluded that the assumption of a unique modulus for the whole elastic zone is an over simplification of the cavity expansion process. During the expansion process, say at point B of Figure 2.18, the induced strain amplitude in the (idealized) elastic zone will vary from a very high value at the elasto-plastic boundary, to a value close to zero at an infinity distance from the cavity. The shear modulus will consequently vary from a low value at this boundary to a high value at infinity, equal to the maximum modulus G_0. This variation is schematically shown in Figure 2.19. This same figure shows the idealized variation of soil stiffness (Gi) assumed by all the cavity expansion theories discussed in section 2.2. It is concluded that Gi does not represent the true stiffness of the sand, but reflects some index stiffness that relates to the average (γ_{av}) behavior of the soil elements at a variety of strain levels within this zone. Similarly as Gur, some relevant strain level shall be assigned to Gi. In this thesis the index modulus Gi is assigned to the failure strain level induced at the elasto-plastic boundary (γ_f). This limiting strain can be easily computed with Equation 2.33 once the soil parameters are known, and is in general in the order of 10^{-1} %. It is believed that γ_f is in the same order of magnitude as the average (unknown) strain level γ_{av} induced in the elastic zone.

In summary the present review indicates that the shear modulus of the sand can be predicted, via SBPM, with the use of the unload reload loops as well as the initial slope of the testing curve. The estimation of the sand stiffness by the initial slope of the testing curve is not commonly done, due to the high sensitiveness of this section of the testing curve to disturbance. At present the only modulus derived from the SBPM testing curves is the unload reload modulus Gur. Both moduli reflect some simplified weighted "average" stiffness of the sand elements around the probe, and are determined based on the "elastic" idealization of the medium. The advantage of Gi over Gur is the fact that the former modulus is already measured at the in situ normal stress σ_h, thus not requiring any sort of correction for stress level. However, similarly as Gur, some relevant strain amplitude has to be assigned to Gi.

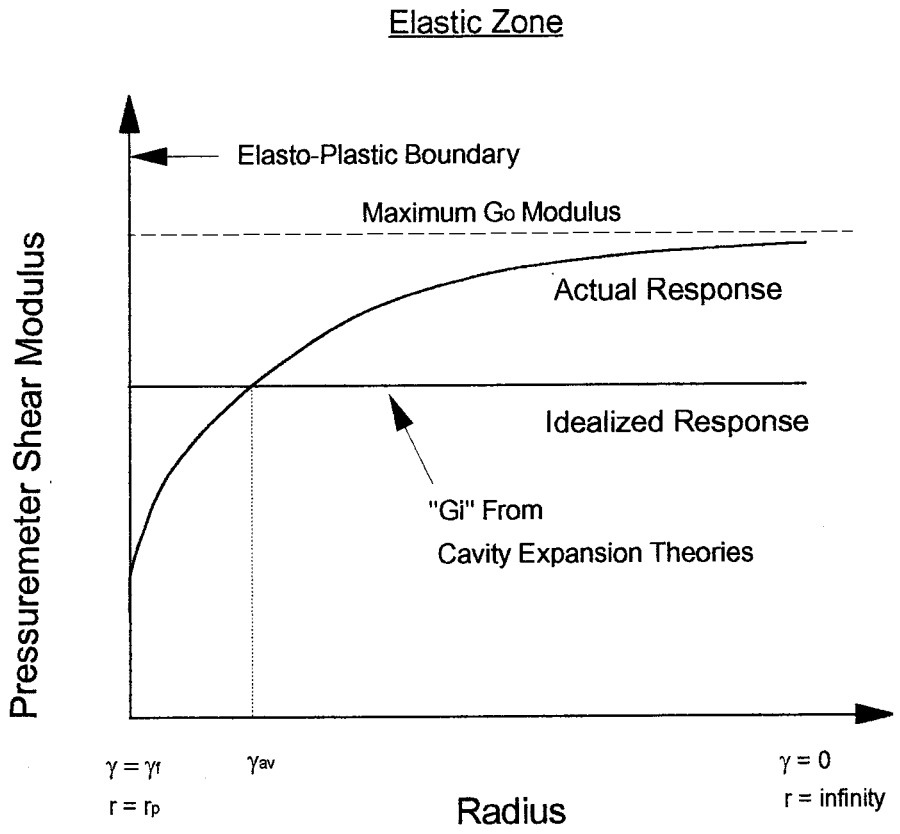

Figure 2.19: Variation of Soil Stiffness in Elastic Zone for a Particular Stage of the Cavity Expansion

2.3.5 Conclusions of Section 2.3

All the points of this section indicate that there are difficulties with the interpretation approaches currently in use with SBPM testing curves in sand. The general conclusions can be given by:

- The best current interpretation approaches adopted with the existing cavity expansion models, namely log-log, nomogram or numerical solution, lead to highly scattered ϕ results in disturbed curves. Disturbance during selfboring tends to considerably increase ϕ predictions, and even in controlled environments a spread of results can be noticed. Although ϕ is the least sensitive parameter in relation to the disturbance of the curve (Robertson and Hughes, 1986), the current approaches are not reliable for disturbed (selfbored) testing curves. This would be the case even if the constitutive relationships were highly realistic to simulate the complex sand behavior around the cavity. Reliable predictions of ϕ are only possible in high quality testing curves.

- Lateral stress predictions by the SBPM (using the lift off stress) proved to be totally unreliable even under controlled conditions in the laboratory or under "optimum" insertion conditions in the field. A broad range of lateral stress is in general the only information currently obtained from the interpretation of selfbored testing results. Reliable results of σ_h are only obtained with ideal installation SBPM tests.

- The shear modulus derived from the pressuremeter reflect an average weighted stiffness of the soil around the probe, given the complex stress and strain gradients mobilized during the loading and unloading stages of the field test. For instance the combined (and opposite) effects of increase in stress level and strain amplitude prior and during the loop stage, lead to Gur values that are in the same order of magnitude of the G_0 measured by shear wave velocity techniques at equivalent depths. As will be commented in Chapter 3, the ratio of G_{ur}/G_0 is close to 1 based on the data of Bellotti et al, 1987, Hughes and Robertson, 1984 and Bruzzi et al, 1986. However, average strain levels assigned to the pressuremeter moduli (Gur or Gi) are 2 to 3 times higher than the strain amplitude of G_0. The pressuremeter moduli also reflect the deformation of the material in the horizontal direction.

- All the basic soil parameters are determined in a "decoupled" manner, without any link between them. ϕ, σ_h and Gi are related to different interpretation methodologies that respond differentially to the disturbance of the test.

From the above conclusions it is evident that research emphasis shall be placed on the reduction of the sensitivity of the predicted SBPM sand parameters to the disturbance generated prior to the test. Improvement of the predictions of this tool can be accomplished by the adoption of a new less (disturbance) sensitive interpretation methodology. The new interpretation methodology shall ideally derive all the desired soil parameters in a "coupled" manner. The next section introduces this methodology.

Another manner to improve the reliability of the predicted SBPM parameters is accomplished by reducing the disturbance generated during the insertion of this probe. Chapter 3 addresses this problem using the results of the field testing programme carried out with the UBC SBPM probe.

2.4 NEW INTERPRETATION METHODOLOGY FOR PRESSUREMETERS

2.4.1 Basis of the Curve Fitting Technique

The prime objective of an in situ tool is to measure one or more parameters in situ, which can be related to some material property. Most of the in situ tools rely on some sort of empirical correlation to relate what is measured to what is desired. This is so because the measured (in situ) parameter is simultaneously dependent on all the desired soil properties. Pressuremeter tests, on the other hand, represent an inverse boundary value problem in soil mechanics. From the pressuremeter test no direct particular soil parameter is measured, rather the pressure versus expansion data on the boundary of the cavity is obtained. Nevertheless, from these measurements of pressure and displacement there is a potential to determine the basic soil parameters of the sand.

This concept was initially put forward by Hughes, 1986 in a very simple manner. Suppose, for example, that we wish to find the properties of a material which can be described by three independent parameters, A, B and C. To do this, we could have an in situ tool that would measure three values a, b and c that would be dependent on the original parameters A, B and C. If these measurements are independent of each other, then a = F (A, B, C), b = G (A, B, C) and c = H (A, B, C) and the original soil parameters could be found. Most of the in situ tools, however, can not provide independent values of a, b and c, but rather a unique variable z at the same depth. In contrast with any other tool, the pressuremeter is able to provide an abundance of data a, b, c, ... n at each testing depth that can be independently connected to the material properties A, B and C.

Suppose, for instance, that an idealized set of soil measurements a, b, c, ... , n can be predicted at each depth based on a given set of original soil parameters A, B and C and some sort of constitutive relationship. In this case:

$a = P_1 = F(A, B, C, \text{ and } D_1)$, $b = P_2 = F(A, B, C \text{ and } D_2)$ .... $n = P_n = F(A, B, C \text{ and } D_n)$

Where P and D are respectively pressure and displacement at the boundary, and the function F is given by the equations of the cavity expansion model adopted.

It will be possible, therefore, to compare the idealized prediction a, b, c ... n to the measured a, b, c ... n of the field test and derive some conclusions regarding the assumed A, B and C parameters of the constitutive model. The better the rheological equations and assumptions of the model in relation to the real shearing phenomena, the closer will be the agreement of the idealized pressure expansion curve with respect to the field curve.

As presented in the section 2.2 several cavity models can serve for this purpose. For undisturbed as well as slightly disturbed testing data one has to rely on a interactive "curve fitting" analysis, to obtain full convergence of the idealized and field testing curves. The set of parameters A, B and C that leads to the closer simulation of the measured testing curve represents the basic characteristics of the material. The better the simulation of the testing curve, the higher is the reliability that one can place on the obtained parameters. The fitting analysis has also the potential to be applied on disturbed testing data. In the case of disturbed curves the loading stage of the test shall be preferentially analyzed over its last part, which is in general less influenced by the disturbance generated during selfboring. This latter aspect is further explored in section 2.6.

The interactive analysis described above is here referred to as the "curve fitting technique". The fitting technique is easily employed in any personal computer with fast processing as well as graphical capabilities, and basically consists of adjusting interactively the input parameters of the constitutive model until a "match" is achieved between both field and model curves. By varying each of the possible sets of data, as schematically presented in Figure 2.20, it is possible to change the whole shape of the model curve. It can be noted that independent parameters A, B and C, represented in this figure as σ_h, Gi and ϕ are simultaneously derived once the match is achieved.

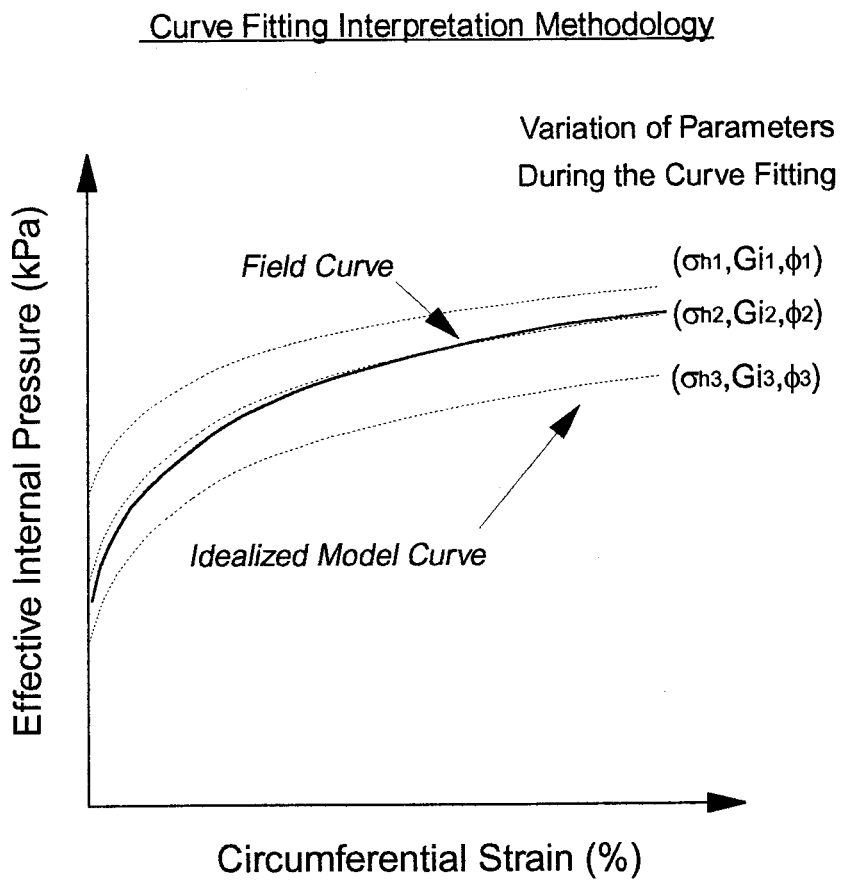

Figure 2.20: Basis of the Curve Fitting Technique

The fitting technique concept is not new in the pressuremeter technology, although it is almost ignored nowadays to derive soil parameters in clays or sands. In the case of clays the first mention to a technique like that was given by Arnold, 1981. He proposed the fit of the test data with an analytical relationship based on Kondner's hyperbolic equation. Jefferies, 1988 was the first author to suggest an image-matching procedure to derive the soil parameters, due to advance in terms of data acquisition and processing systems for the pressuremeter in the 80's. This author used this technique in the interpretation of SBPM results in the Beaufort Shelf clay, and concluded that "once the model curve is fitted the numerical values are unarguable, at least within the validity of the model". In sands Hughes, 1989 was the first author to adopt the fitting technique with constitutive models for granular materials. This author showed with examples in lightly cemented sand and dense cobbly till that the fitting technique leads to reasonable results in materials which are almost impossible to sample and where the test data shows strong indications of disturbance.

The success of the technique is based on the fact that the soil parameters are related to each other in the context of the theoretical framework. This aspect represents the essence for a good quality of the geotechnical parameters obtained by the pressuremeter. Previously the parameters were obtained without coupling between them, leading to "loose" relationships between the variables and possible misleading predictions if one would attempt to use these parameters simultaneously in any classical elastic or plastic theory for soil mechanics. With the fitting technique there is a strong bond between the parameters, and therefore the set of parameters, rather than each individual value, can be used in a more effective way to simulate the soil in further design analyses. No one parameter has necessarily greater importance over another, but it is the coupled set that must be used to describe the soil behavior. The theoretical cavity expansion models to be used in this new interpretation methodology shall rely on few variables such that the match can be easily handled in practical cases. As demonstrated in section 2.2, the cylindrical cavity expansion models that were chosen for that purpose rely on 4 or a maximum of 5 input variables. These are the basic four parameters of the sand (σ_h, Gi, ϕ and ϕ_{cv}) plus ν (for some models).

Matching between the idealized model curve and the pressuremeter testing curve was accomplished in this thesis with the computer aided modeling programs (briefly described in section 2.2) written to simulate the testing curve for different rheological models and input parameters. These programs allowed any of the field testing curves to be plotted together with the idealized curves from any of the chosen cavity expansion

models. One simple method to match the curves involves the visual comparison between field and idealized curves, i.e. the set of input parameters is manually varied to accomplish the fit. Mathematically it is also possible to use standard statistical tools to accomplish the fit between field and idealized model curves. Programs like the Sigmaplot™ (Jandel Scientific, V.4.1) or the Kaleidagraph™ incorporate a nonlinear automatic curve fitter (Marquardt-Levenberg algorithm in the case of Sigmaplot™), that uses a least square procedure to minimize the sum of the squares of the differences between the idealized and field curves. These programs interactively guess and find out the required input parameters for the fit, but they are not able to predict reliable parameters on disturbed data. This is so because other factors have to be considered for the curve fit with the disturbed testing curves (as will be discussed in subsection 2.6.1), and the fitting can not be blindly accomplished without some input based on personal experience. For high quality testing curves either the visual or the statistical fitting approach lead to similar results. The difference between each of these approaches is the fact that with the use of the curve fitter software the interaction process is done in a rather more efficient manner. In this thesis, however, only the visual fit between field testing and idealized model curves was adopted to predict the basic soil parameters of the sand.

In order to establish the curve fit it is necessary, but not mandatory, to know the possible order of magnitude of the basic parameters adopted by the cavity expansion model, regardless if curve fitter software is used or not. The initial estimate of ϕ is done with any soil mechanics table once the general characteristics of the tested sand are evaluated. Whenever possible, washed samples from the selfboring process shall be retrieved at particular depths for use in laboratory characterization tests. In addition to that, piezocone sounding results can be used to infer the density characteristics of the studied granular profile. The initial estimate of σ_h is done using the average value of the lift off stress measured by all the strain arms of the pressuremeter. The estimate of the constant volume friction angle can be done with the table proposed by Robertson and Hughes, 1986. The initial estimate of the pressuremeter modulus Gi can be done with the measurement of the initial slope of the testing curve in the strain range below 10^{-1} %.

However, for slightly disturbed or disturbed data it may be extremely difficult to define the initial estimates of Gi and σ_h, given the high sensitivity of these variables to the disturbance generated during selfboring. A possible alternative to aid in the estimation of the initial magnitude of these variables, and

hence optimize the process of curve fitting, is the establishment of some sort of link between the input variables and some other pressuremeter variable that is less disturbance sensitive.

In the last section it was stated that the initial slope currently measured in the pressuremeter testing curve is equivalent to the secant shear modulus at a level of shear strain in the order of 10^{-1} %. This secant modulus can be theoretically linked to the low strain modulus of the soil, related to the soil response at very low levels of strain mobilization. In the absence of seismic shear wave measurements to define G_0 the unload reload loop can be adopted. As commented in subsections 2.3.4 and 2.3.5 this modulus is readily obtained in any standard pressuremeter testing curve, and in general appears to have a magnitude close to the (low strain) modulus G_0. Moreover, the methodologies proposed by Bellotti et al, 1989 or Byrne, et al 1990, to correct the measured Gur for both stress and strain levels can be additionally used for a refined estimation of the maximum shear modulus of the sand (G_{max}).

Therefore, in order to optimize the process of curve fitting a link between Gi and the unload reload modulus was devised. An approximate theoretical development of such a link took in consideration the hyperbolic model put forward by Kondner, 1963, and was originally advanced by Dr. Hughes in 1992.

2.4.2 Link Between Gi and Gur

The shear stress strain behavior of the sand is recognized to be highly non linear with the stiffness depending on stress and strain levels, as discussed in the previous section. The strain level influence over the shear modulus was schematically depicted in Figure 2.19, where the stiffness variation was presented in the elastic zone at a particular stage of the expansion process. It is noticed in this figure that at the cavity wall close to failure moduli will exist, whereas at a large radius the soil modulus approach the low strain modulus G_0. The establishment of a link between this latter modulus and Gi leads to the knowledge of the modulus variation in the elastic zone, i.e. the determination of the non linear curve of this same figure.

A better way to visualize the modulus variation of Figure 2.19 is presented in Figure 2.21(a). It is assumed here that the stress strain curve that rules the stiffness variation in the elastic zone follows the hyperbolic shape. This hyperbolic variation is a good approximation of the real shear behavior of granular materials over a variety of strain ranges, as successively demonstrated by Hardin and Drnevich, 1972, Ishihara, 1982, Bellotti et al, 1989, Fahey, 1992, and others. The hyperbolic model was originally

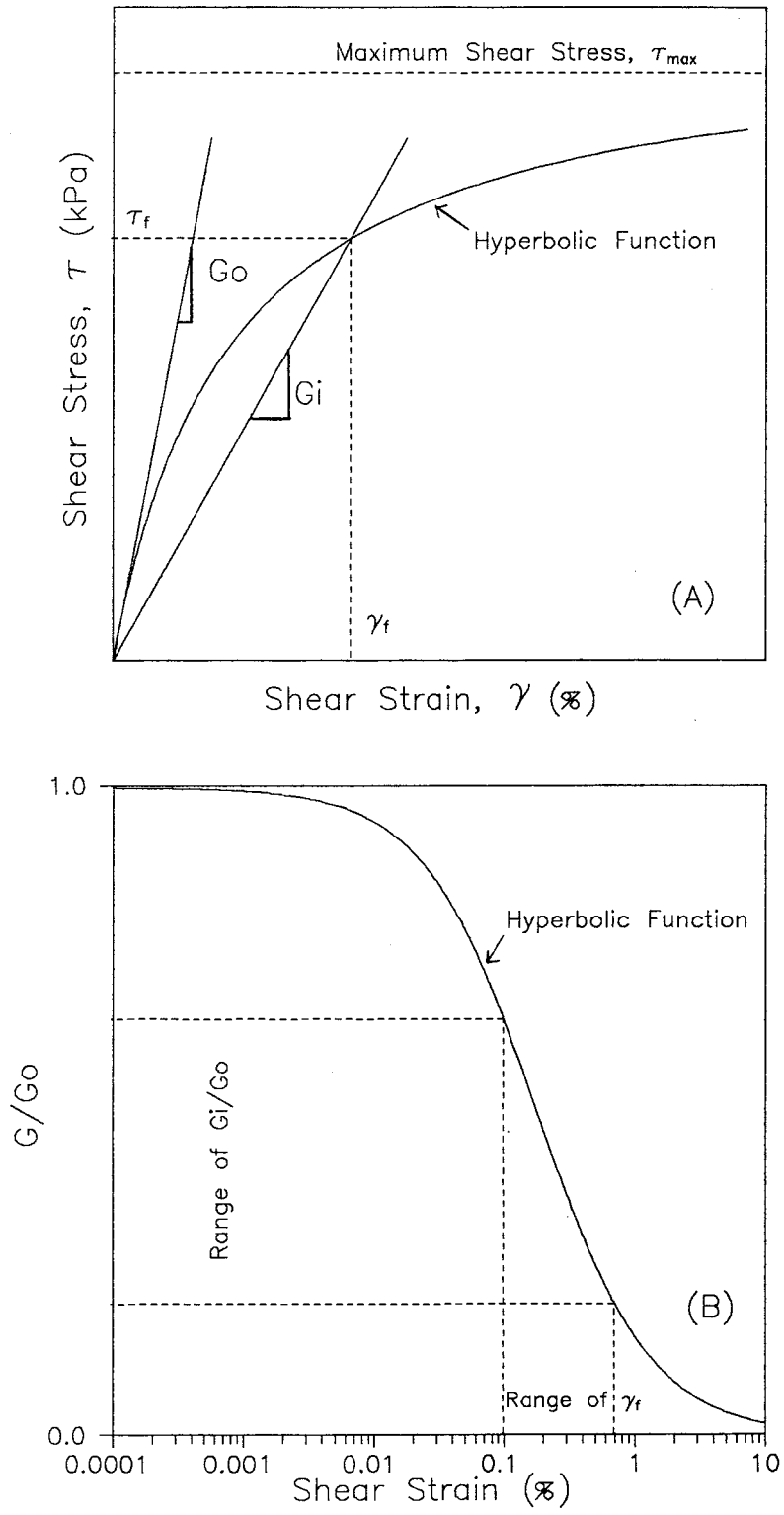

Figure 2.21: Hyperbolic Soil Response at the Elastic Zone in terms of (a) Stress-Strain Curve and (b) Modulus Reduction Curve

presented by Kondner, 1963 and used by Hardin and Drnevich, 1972 to show that the peak points of cyclic stress strain loops at successively higher stress amplitudes laid on an approximately hyperbolic "backbone" curve. In the hyperbolic model the parameters that are required to specify the structure of the whole stress strain curve are the (low strain) maximum modulus G_0 and the maximum shear stress τ_{max}. These variables have to be defined with tests that take consider the in situ density and stress level conditions of the sand analyzed.

The hyperbolic curve of Kondner, 1963 is given by:

$$\frac{\tau}{\gamma} = \frac{1}{\frac{1}{G_0} + \frac{\gamma}{\tau_{max}}} \tag{2.76}$$

rearranging Equation 2.76 and noting that $\tau = G.\gamma$ it is possible to derive:

$$\frac{G}{G_0} = 1 - \frac{\tau}{\tau_{max}} \tag{2.77}$$

The maximum shear stress that can be applied to an element of soil adjacent to the pressuremeter is derived by assuming pure elastic behavior prior to yield (no variation in the average normal stress up to failure) and failure ruled by the Mohr Coulomb failure criteria (failure stress ratio ruled by the friction angle of the sand). The maximum shear stress is given by:

$$\tau_{max} = \sigma_h \tan \phi \tag{2.78}$$

Substituting into Equation 2.77 it is possible to obtain:

$$\frac{G}{G_0} = 1 - \frac{\tau}{\sigma_h \tan \phi} \tag{2.79}$$

This latter equation was also obtained by Fahey, 1990 in order to derive the secant shear moduli over any range of shear stress.

In the elastic zone pure shear conditions will prevail. A unique and constant secant modulus Gi is defined for this zone by the cavity expansion theories. As presented in Figure 2.21 (a) Gi is referenced to a known strain amplitude γ_f, which is induced at the elasto-plastic boundary with a yield shear stress τ_f. This

limiting yield stress, previously derived in section 2.2 (Equation 2.31) can be substituted together with Gi into Equation 2.79. This leads to the following equation:

$$\frac{Gi}{G_0} = \frac{\sigma_h \sin \phi}{\sigma_h \tan \phi} \qquad (2.80)$$

or $$Gi = G_0 (1-\cos \phi) \qquad (2.81)$$

As noted before, the value of Gur obtained in standard pressuremeter tests can be used as a first approximation of the (low strain) maximum modulus G_0. Therefore, assuming $G_0 \approx$ Gur we obtain:

$$Gi = Gur (1-\cos \phi) \qquad (2.82)$$

Therefore, in slightly disturbed or disturbed data the fitting process can be optimized with the use of Equations 2.81 or 2.82 above. These equations help in the establishment of the initial magnitude of Gi, based on a less disturbance sensitive parameter.

The curve fitting process has to be carried out until full convergence of both curves is accomplished for most of the strain range of the field test. The initially guessed soil parameters will undoubtedly lead to an idealized curve that differs from the field curve. Therefore, these initial parameters have to be gradually changed one by one (ϕ_{cv} and ν are generally kept constant) until convergence takes place. With high quality testing curves the possible set of parameters is in fact very narrow, as the testing curve can be fitted by an ideal model curve in an almost unique manner. This is mainly valid for cavity expansion models that rely on few parameters, as those discussed in section 2.2. In contrast to that, with models that contain many variables it is likely that a large array of combinations of the input variables suffice to provide full convergence of both idealized and field curves. Thus, with these models it may be difficult to define a narrow, or unique, combination of soil parameters that represents the response of the tested sand.

Subjectiveness is often required on the part of the engineer during the curve fitting process, in which each of the input parameters has to be varied within physically acceptable boundaries. The higher the quality of the testing curve, the easier is the final derivation of the model parameters. In the case of slightly disturbed or disturbed data it is useful to have some constraint between the input parameters in order to guide the engineer with respect to their variation during the fitting stage, and hence optimize the fitting process. Therefore the constraint imposed by Equations 2.81 or 2.82 can be also used to aid in the establishment of the value of Gi at each step of the fitting stage, when the set of input parameters is chosen.

Basically Gi has to be varied simultaneously with ϕ, in order to keep its proportionality to G_0 or Gur as expressed by these equations.

All the SBPM testing curves interpreted by the writer in Chapters 3 and 4 adopted the constraint of Equation 2.81 during the curve match, regardless of the individual quality of each of the curves. The values of G_0 from downhole seismic shear wave measurements were used in the interpretation process, rather than the values of Gur, since they were already known.

Some final general observations have to be made in regard to the proposed interpretation technique:

1. The use of Equations 2.81 and 2.82 for undisturbed or slightly disturbed data complements the fitting technique, establishing an additional constraint between the input soil variables. These equations aid in the establishment, of the initial value of Gi, as well as the establishment of its possible variation in the course of a fitting analysis. Basically, these equations reflect an approximation of what is experimentally expected in a granular material when sheared. This means that loose sands (with lower ϕ's) are expected to have a lower stiffness Gi than dense sands (with higher ϕ's) if all other variables (G_0, confining stress, etc.) are kept the same. Thus, it is logical that by setting a higher value of ϕ during the curve fit a higher value of Gi (as predicted by these equations) shall be also required, and vice-versa. Nevertheless, some care shall be taken when using Equations 2.81 or 2.82 as they may not be universally applicable for all the exiting granular deposits.

2. The subjectiveness built in the fitting technique is an inherent characteristic of this methodology of interpretation. It will also exist when adopting highly refined finite element models to generate the idealized pressuremeter curve, or when using the curve fitter algorithm of the commercially available softwares written for this specific purpose.

3. Some of the soil parameters impose a higher variation in the idealized testing curve than the others. This is due to the differential sensitivity of the cavity expansion model to each of the input variables. A better insight in this aspect is given later in order to evaluate the accuracy of the final results.

Lastly, one must address questions relating to the consistency and simplicity desired for the suggested interpretation methodology. When dealing with the solution of an inverse boundary value problem such as the pressuremeter, consistent and physically meaningful soil parameters shall be derived. According to Jefferies, 1988, when basic soil parameters are sought the solution via curve fitting technique

is in the great majority of the cases well conditioned and consistent. Mathematically many sets of coupled parameters can lead to an analytical equation that represents the experimental response. However, physically, just a small variation of the coupled set of parameters is acceptable because the analytical response will considerably deviate from the experimental measurements. The larger the range of testing curve available for match, and the higher the quality of this curve, the lower is the variation of the set of parameters that allows the curve match. Simplicity of the methodology of analysis is a characteristic of the proposed approach. A simple interpretation technique is usually desired when the final objective is the use by engineering practitioners.

In summary the proposed interpretation methodology leads to a coupled set of parameters that are related to each other by the framework of some constitutive theory. No parameter has a higher significance in relation to the others, but it is the coupled set that can be simultaneously used to predict the soil response to the external action of any engineering work. The higher the capability of the model to simulate the testing curve, the higher is the reliability of the parameters. With high quality testing data it is possible to obtain an almost unique set of input variables that allows the curve match. This is valid for the models discussed in section 2.2, since they rely on few parameters. With slightly disturbed or disturbed data it is also possible to obtain meaningful soil parameters if a constraint is imposed between the parameters. This constraint helps in the initial establishment, and subsequent variation, of the parameter Gi in the course of the fitting process. Thus, the constraint optimizes the curve fit as well as reduces the variability of the final set of input parameters that allows the curve match.

2.4.3 Modulus Reduction Curve

Once the fitted soil parameters for the tested depth are known it is possible to mathematically generate the shear stress-shear strain monotonic "elastic" curve of the sand. This is the curve schematically shown in Figure 2.21(a). The importance of determining the non linear elastic response of the sand is related to the assessment of relevant secant moduli at the appropriate working strain levels of the design problem. For instance, as demonstrated by Fahey et al, 1993, the knowledge of the in situ stress strain curve is extremely useful in deformation problems.

As commented in subsection 2.3.4.1 Fahey and Carter, 1993 introduced a finite element methodology to extend the information that is usually obtained from the unload reload loops of the pressuremeter, i.e. to

allow the derivation of the pressuremeter modulus at any strain level. This methodology, however, still suffers from some problems related to the finite element modeling of the pressuremeter expansion, as outlined by this same authors. A possible approach to derive the modulus reduction curve of the sand is the use of the hyperbolic equation of Kondner, 1963 with the fitting parameters.

Using the information obtained by the curve fitting technique with any of the previously described cavity expansion models, and Equations 2.76, 2.78 and 2.81 or 2.82, it is possible to derive:

$$\frac{\tau}{\gamma} = \frac{1}{\frac{1}{Gi}(1 - \cos\phi) + \frac{\gamma}{\sigma_h \tan\phi}} \tag{2.83}$$

This equation allows the generation of the approximate spectrum of soil stiffness ratio (G/G_0) variation with the induced level of shear strain, as schematically shown in Figure 2.21(b). This curve can be derived for each testing depth, based on the predicted parameters of the fitting technique.

The modulus reduction curve derived from Equation 2.83 is already assigned to the average normal stress level that operates at the depth of the tested sand. This is so because the interpreted (coupled) soil parameters of the fitting technique are related to the in situ density and normal stress levels. This is also the case for the maximum shear stress (τ_{max}). This is an important aspect of Equation 2.83 since, as experimentally shown by Hardin and Drnevich, 1972 and Iwasaki et al, 1978, the modulus reduction curve of granular materials varies in accordance with the level of confining stress.

The derivation of Equation 2.83 assumed that the behavior of the soil can be adequately represented by a hyperbolic curve. However, as observed by Hardin and Drnevich, 1972, the stress strain curves of the soil are not truly hyperbolic. Nevertheless, these authors suggested that a hyperbolic form could still be obtained by imposing a distorted normalized strain scale. The distorted strain, called the hyperbolic shear strain, is a function of empirical constants a and b. These empirical parameters determine the deviation of the stress strain relation of the soil from the hyperbolic shape, and are given by these authors in accordance with the soil type (sands or clays) and presence of water (dry or saturated sand).

Another approach was followed by Fahey and Carter, 1993 to allow the simple hyperbolic model to fit the observed shearing behavior of the sand.

These authors proposed a modified form of the hyperbolic Equation 2.77, as follows:

$$\frac{G}{G_0} = 1 - f\left(\frac{\tau}{\tau_{max}}\right)^g \tag{2.84}$$

where: f and g are empirical parameters, introduced in an analogous manner to the parameters a and b of Hardin and Drnevich, 1972.

Using the data of Teachavorasinskun et al, 1991 from drained simple shear tests on hollow cylindrical specimens of Toyora sand, Fahey and Carter, 1993 were able to estimate f and g as being respectively 0.98 and 0.25.

In this thesis only the original hyperbolic equation was adopted to predict the modulus reduction curve of the sand, at particular testing depths of the SBPM field programme carried out by the writer. This was done to simplify the prediction of this curve, by avoiding the incorporation of empirical variables a, b, f or g of difficult estimation. The example of usage of Equation 2.83 is presented in Chapter 4.

In summary the hyperbolic model used to establish a constraint between G_0 (or Gur) and Gi also allows the establishment of the modulus reduction curve of the sand, if the remaining fitting parameters are known at the testing depth. This curve is already related to the in situ normal stress and will serve to estimate the sand stiffness at a variety of strain levels. The most important aspect of the predicted modulus reduction curve is the fact that it is obtained based on a reference index modulus (Gi) in the strain range of 10^{-1} %. This range is close to relevant strain levels of civil engineering works, which in accordance to several case histories presented by Burland, 1989 lies in the range of 10^{-2} to 10^{-1} %.

The curve fitting technique can be adopted with any of the cavity expansion models discussed before. In order to validate the assumptions built in each of these models, and hence impose a great amount of certainty on the predicted soil parameters, pressuremeter tests in controlled conditions have to be analyzed. This is so because under such conditions it is possible to establish baselines in terms of soil parameters for the further comparison with the model predictions. With this objective calibration chamber testing results were analyzed with the new interpretation methodology, using the models discussed in subsection 2.2.7. This is shown next.

2.5 VERIFICATION OF CONSTITUTIVE MODELS WITH CHAMBER DATA

2.5.1 Tests with Leighton Buzzard Sand

Fahey, 1986 described a series of 13 calibration chamber tests to investigate the interpretation with the Hughes et al, 1977 theory. Given the high quality of Fahey's testing results, and the particular conditions of the tests, they are extremely useful here.

The tests of Fahey, 1986 were performed with dry pluvially deposited Leighton Buzzard sand of the type 14/25. All the tests were carried out with a small pressuremeter of L/D of 5, ideally installed (cast) in the sample. For all the cases the constant volume friction angle was determined with the ring shear tests of Budhu, 1979 and Cole, 1967 using the same sand. Reference peak friction angles were estimated based on the simple shear tests of Stroud, 1971, also on Leighton Buzzard sand at similar density and mean normal stress conditions as those employed by Fahey, 1986. Unload reload loops were not performed by Fahey, 1986 in his pressuremeter tests, and only the modulus Gi obtained by the measurement of the initial pressure expansion slope is related by this author. For additional details on the tests, sand parameters and characteristics of the chamber the reader is referred to Fahey, 1986.

Tests with both frictionless top and bottom sections were used to simulate a perfect plane strain expansion, without any of the possible end effects previously noticed by Jewell et al, 1980 in the University of Cambridge. A pressure controlled boundary with a constant boundary pressure during the testing stage was also adopted in some of the chamber tests. According to Fahey, 1986 allowance for the influence of the finite dimension of the chamber (hence influence of the constant boundary pressure on the observed results) had to be made, since the chamber radius was only 10 times the initial radius of the pressuremeter used. Using the basic principles of elasticity and the Mohr Coulomb failure criteria, Fahey 1986 was able to demonstrate the influence of this finite boundary over the cavity pressure, and to derive theoretical equations to adjust the cavity expansion models for this effect.

In order to assess the capabilities of the selected cavity expansion models two of the high quality SC chamber testing series, with smooth end plates and constant boundary pressure, were adopted here. These tests are the ones denoted as SC7 and SC8. Both tests have similar void ratios and are normally consolidated. They differ solely with respect to the level of mean normal stress applied to the chamber prior

to the probe expansion. Table 2.3 presents a summary of the general conditions of the chosen tests after the sample consolidation as well as the reference soil parameters at each case.

Tests SC7 and SC8 did not present three dimensional end effects, given the fact that the pressuremeter was constrained by upper and lower smooth plates. Nevertheless these tests have to be analyzed in the light of the analytical correction proposed by Fahey, 1986 for the finite boundary. Figure 2.22 presents the possible curve fit with any cavity expansion model (in this example the Hughes et al, 1977 model) that is not adjusted for the finite boundary of the chamber. It is noticed that both curves begin to diverge significantly beyond a cavity strain of ≈ 1 %. For the infinite diameter (idealized) curve the pressure continues to increase, while for the finite diameter (experimental) curve the cavity pressure eventually reaches a maximum when the plastic zone approaches the outer boundary of the chamber. Therefore, the models selected to be analyzed here were adjusted to include the finite boundary effect.

Tests SC7 and SC8 were interpreted using the proposed methodology presented in the last section. Throughout the fitting analysis the lateral stress was set to a constant value equal to the lateral (boundary) stress of the chamber, presented in Table 2.3. The models adopted the constant volume friction angle experimentally measured for this sand. For both the new and the Carter et al, 1986 models a value for the Poisson's coefficient was required. Fahey, 1986 estimated this value as 0.25 in his analyses with the same data. The same value for ν was adopted here. For any of the selected models the simulation of the cavity pressure versus cavity strain curve was carried out up to the limit condition imposed by the chamber, i.e. up to the development of a plastic zone with the same size of the calibration chamber. This limit condition is given by r_p/r_0 equal to 10, where r_p is the radius of the plastic zone and r_0 the initial pressuremeter radius.

The plots showing the comparison between the experimental loading curves and the idealized model curves are presented through Figures 2.23 to 2.25. In Figure 2.23 the curve fit with the Hughes et al, 1977 model is shown for each of the adopted chamber tests. Figure 2.24 presents the fit with the Carter et al, 1986 model, whereas in Figure 2.25 the results with the new model are shown. The numbered points in each of the plots represent the position of the elasto-plastic boundary in the course of the expansion test, as idealized by each of the models. It is noticed that in all the cases the expansion is carried out up to the limiting condition of r_p/r_0 of 10, as commented above. The soil parameters predicted for each case are presented in Table 2.4.

TEST	SAND TYPE	VOID RATIO	OCR	σ_v (kPa)	σ_h (kPa)	ϕ_{cv} [1] (Deg)	Gi [2] (MPa)	ϕ [3] (Deg)
SC7	LB 14/25	0.5115± 0.016	1	90	90	35	20.6	48 - 50
SC8	LB 14/25	0.5115± 0.016	1	45	90	35	25	48 - 50

Tests SC7 and SC8 are tests in which the pressuremeter was ideally installed

1-Constant volume angle from Ring Shear tests of Budhu, 1979 and Cole, 1967
2-Defined with the initial slope of the testing curve, for $\varepsilon_\theta < 0.5$ %
3-Plane strain friction angle from simple shear tests of Stroud, 1971, with Leighton Buzzard sand at a void ratio of 0.53 ± 0.005 and $\sigma_m = 90$ kPa

Table 2.3: Calibration Chamber Testing Results on Leighton Buzzard Sand (Modified after Fahey, 1986)

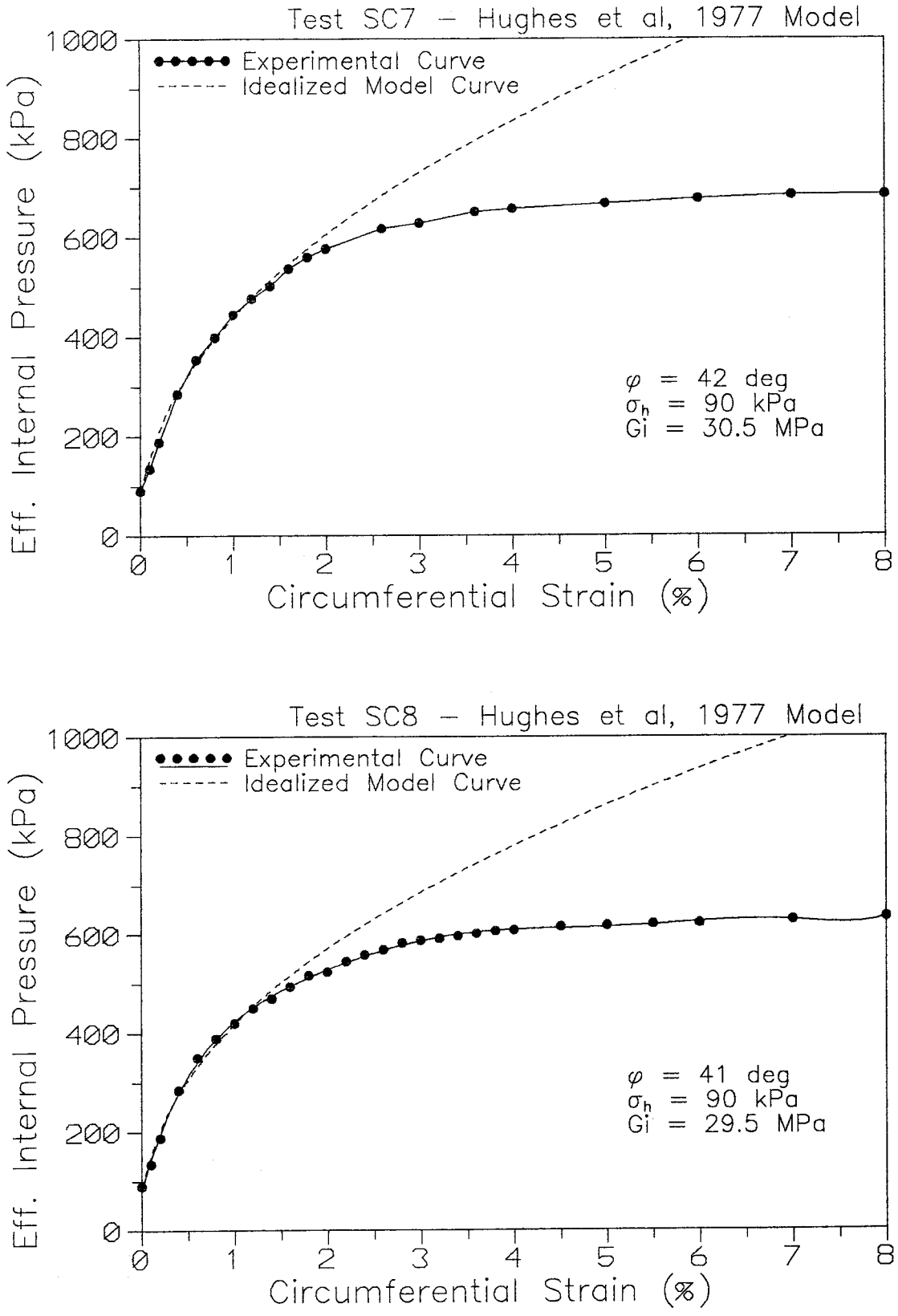

Figure 2.22: Curve Matching without allowance for Finite Boundary Correction - Fahey, 1986 Tests

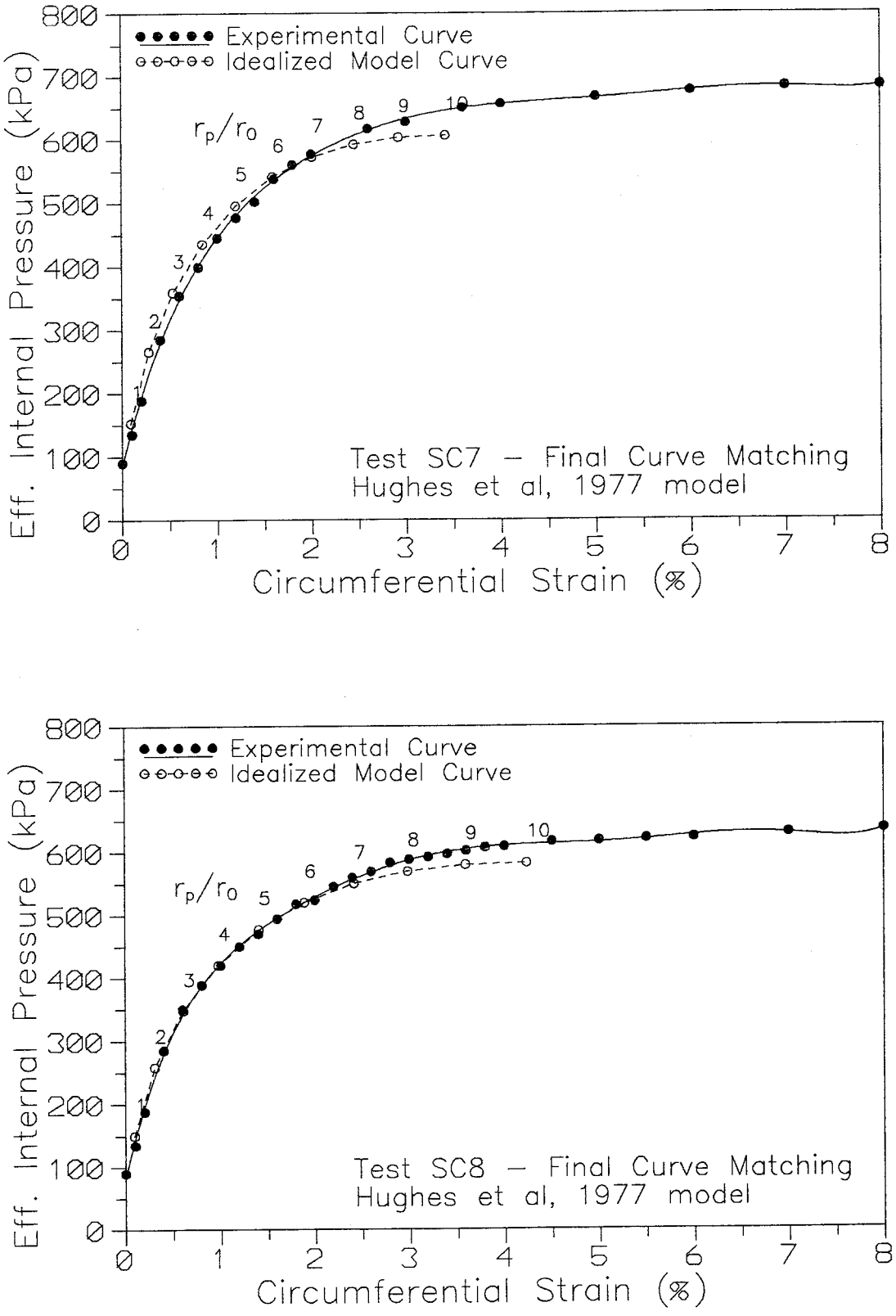

Figure 2.23: Curve Matching on Fahey, 1986 Tests: Hughes et al, 1977 Model

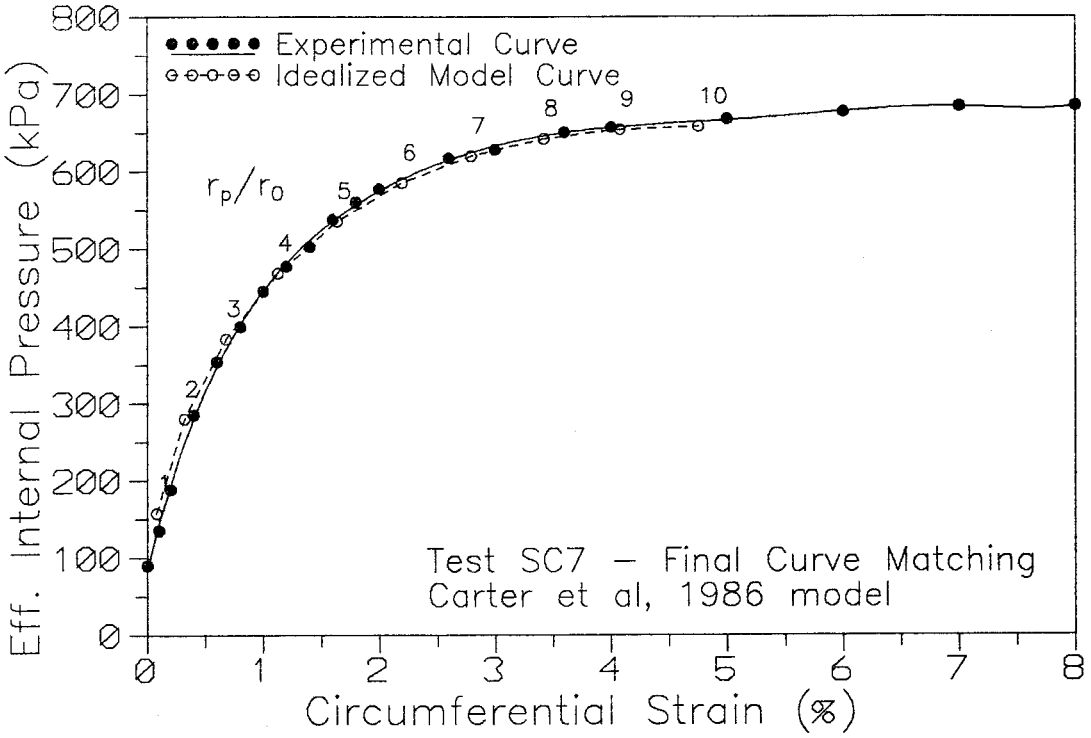

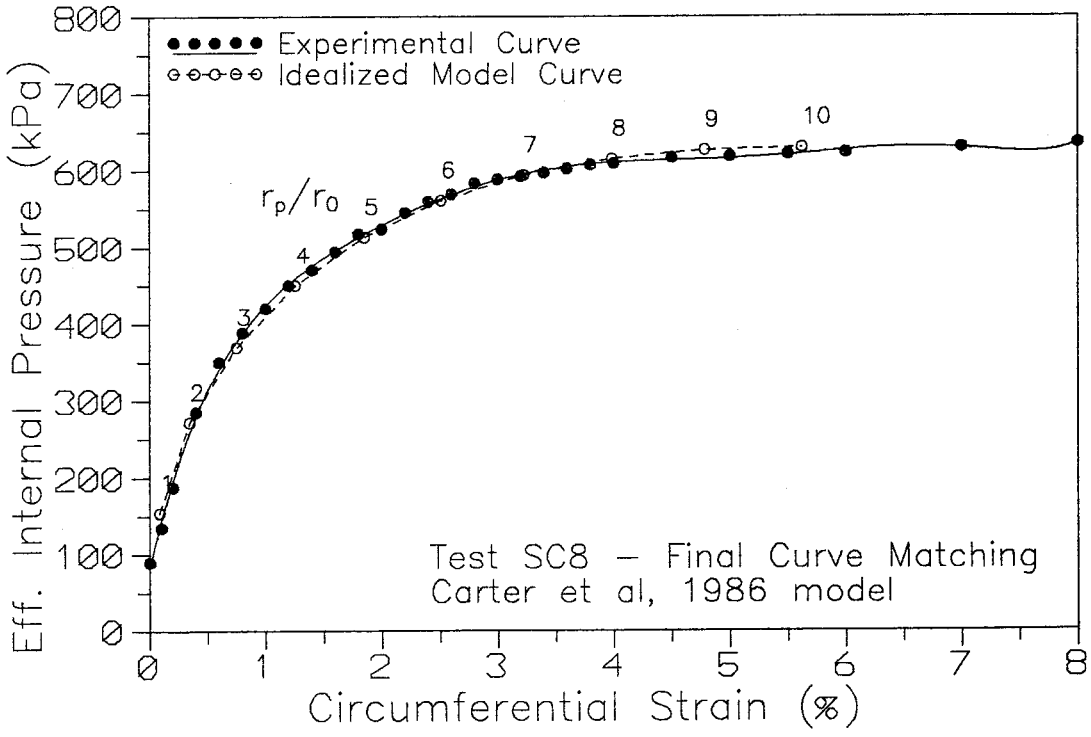

Figure 2.24: Curve Matching on Fahey, 1986 Tests: Carter et al, 1986 Model

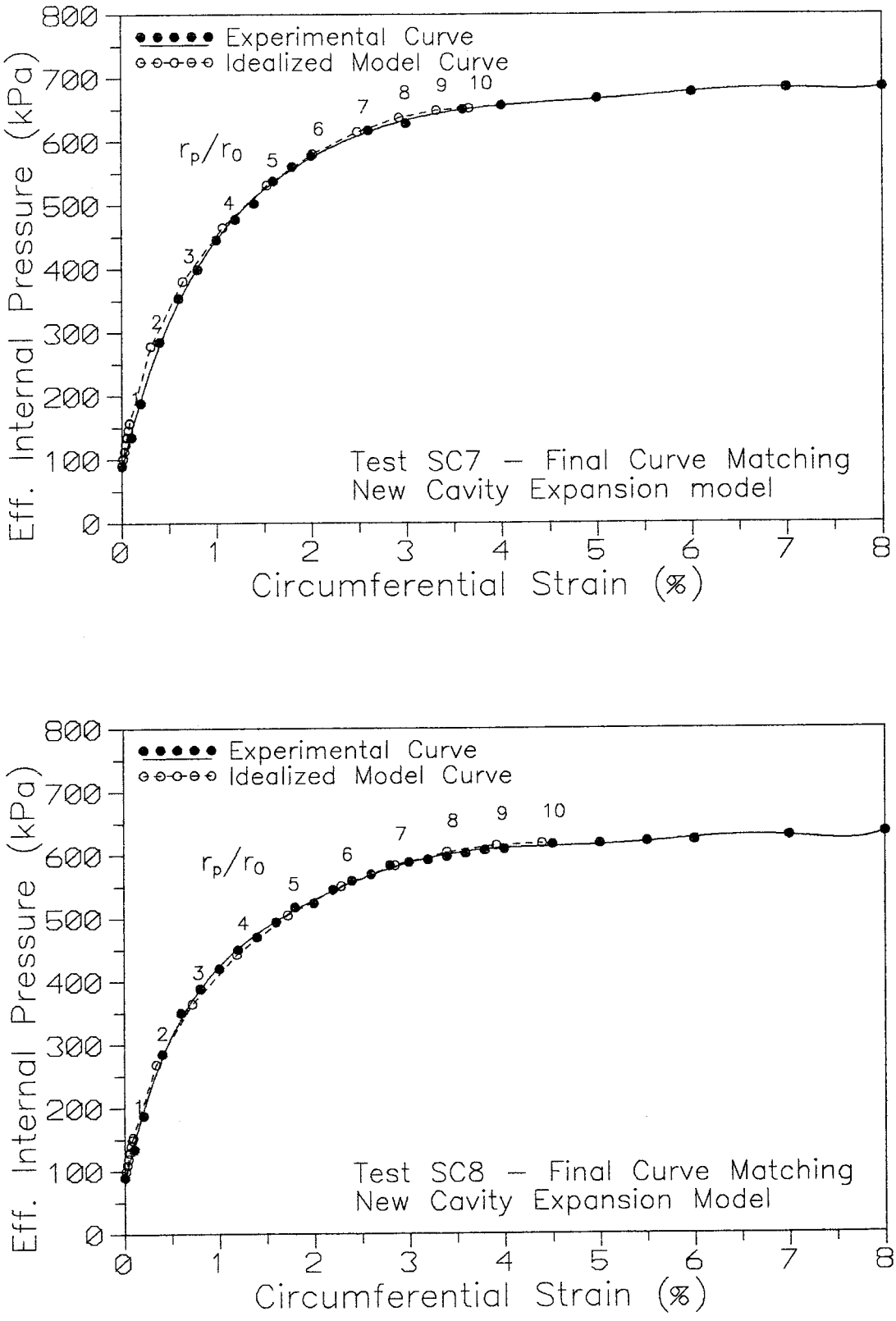

Figure 2.25: Curve Matching on Fahey, 1986 Tests: New Cavity Expansion Model

MODEL	PARAMETERS	CALIBRATION CHAMBER TESTS		QUALITY OF CURVE FITTING
		SC7	SC8	
Hughes et al, 1977	ϕ (Deg) Gi (MPa) σ_h (kPa)	45 35.1 90	43 32.2 90	Good to Very Good
Carter et al, 1986	ϕ (Deg) Gi (MPa) σ_h (kPa) ν	49.5 42 90 0.25	47 38.1 90 0.25	Very Good to Excellent
New Cavity Expansion Model	ϕ (Deg) Gi (MPa) σ_h (kPa) Gur (Mpa) ν	49 41.3 90 71 0.25	46 36.6 90 71 0.25	Very Good to Excellent

$\phi_{cv} = 35°$ for all the cavity expansion models

Table 2.4: Fitting Results on Chamber Tests with Leighton Buzzard Sand

The following observations can be drawn from all the results shown:

1. In general the quality of matching between the curves is reasonably good for Hughes et al, 1977 model with some discrepancy in both the early and latter stages of the loading points. With the consideration of elastic strains in the plastic zone, as done by the new as well the Carter et al, 1986 models, the quality of the curve match increases. Similarly as in the example of subsection 2.2.7 close results in terms of the shape of the idealized curve were obtained for these two models, besides of the different approaches adopted to derive the elastic strains in the plastic zone. This suggests again that similar results are achieved by either the new or the Carter et al, 1986 models when a Poisson's coefficient in the range of 0.2 is used.

2. The friction angle derived by Hughes et al, 1977 model in both testing cases is smaller than respective values obtained by the other models. This is so due to the fact that the lack of elastic strains in the plastic zone leads to a "more rigid" pressure expansion curve (see Figure 2.11) with the Hughes et al, 1977 model in comparison to the other models. Consequently Hughes et al, 1977 equations require a lower ϕ input to bring the analytical curve up to the experimental curve or a higher ϕ decrease to bring this same curve down to the experimental one. As expected, similar numerical results were obtained by both Carter et al, 1986 and the new model. The plane strain ϕ's predicted by these latter models agree with the range defined by Stroud, 1971 for Leighton Buzzard sand under the chamber density and confining conditions.

3. For all the cases the predicted Gi's were above the moduli defined by the measurement of the initial slope of the experimental curve. A possible reason for that may be related to the density of the sand adjacent to the pressuremeter shaft. According to Jewell et al, 1980 during the raining process it is likely that the suspended pressuremeter (ideal installation) has a local influence on the sand, thus producing around its shaft a thin annulus of sand with random density variations. This variation biases the shear modulus of the sample predicted by the initial slope of the testing curve. This is so given the high sensitivity of this initial section of the curve to the disturbance of the sample. According to Ferreira, 1992 for ideal installation SBPM tests the initial slope of the experimental curve is unrealistically low.

In order to obtain a definitive conclusion in regard to the accuracy of the magnitude of the predicted Gi's a parametric analysis with the test SC7 and the new cavity expansion model was carried out. The

optimum parameters for this case (presented in Table 2.4) were adopted, and Gi was allowed to vary from 30 to 50 MPa. Figure 2.26 presents the predicted idealized curves as well as the experimental curve. It is noticed that for shear moduli outside the specified range it is not possible to obtain an analytical curve close enough to the experimental curve for a proper match. This suggests that the Gi's of the elasto-plastic models used here indeed shall have a magnitude that differs from the magnitude of the moduli obtained with the initial slope of the testing curve.

Using Equation 2.81 it is possible to estimate the (low strain) maximum shear modulus of the sand at the chamber density and confining conditions based on the predicted value of Gi and ϕ. Using the parameters obtained by the new cavity expansion model in the chamber test SC7, a value of G_0 in the range of 120 MPa was obtained. As commented before the tests of Fahey, 1986 did not incorporate unload reload loop stages. However, a rough estimate of the possible Gur as well as G_{max} for this chamber test can be obtained through the chamber test C2 of Jewell et al, 1980, since in both cases the same sand and similar testing conditions were employed[4] . In Jewell's case one unload reload loop stage was carried out during the test ($dP_u = 155$ kPa, $d\varepsilon_\theta = 0.11$ %), leading to a Gur of 71 MPa. Using the methodology proposed by Byrne et al, 1990 with the loop variables of Jewell's C2 test it is possible to estimate the (low strain) modulus of the sand tested in Fahey's SC7 test. A value of G_{max} in the range of 130 MPa is obtained, which is remarkably close to the value estimated with the use of Gi and Equation 2.81. This again validates the proposed interpretation approach to derive the stiffness of the sand, as well as the other coupled variables.

In conclusion the above results place a high degree of confidence on the assumptions of the simple elasto-plastic models compared in this thesis, as well as on the interpretation approach suggested in the last section. Based on two high quality chamber tests it appears that Hughes et al, 1977 model gives a conservative estimate of the strength and stiffness of the sand. Carter et al, 1986 and the new cavity expansion model lead to more accurate predictions of the plane strain ϕ and Gi. Therefore, the incorporation of elastic strains in the plastic zone improves the quality of the analytical simulation of the pressuremeter test in sands. From a practical point of view the predictions of both the new and Carter et al, 1986 models are identical, suggesting that both of them can be used.

---

[4] Jewell's C2 test was carried out with a sample with $\sigma_m = 90$ kPa and void ratio = 0.527.

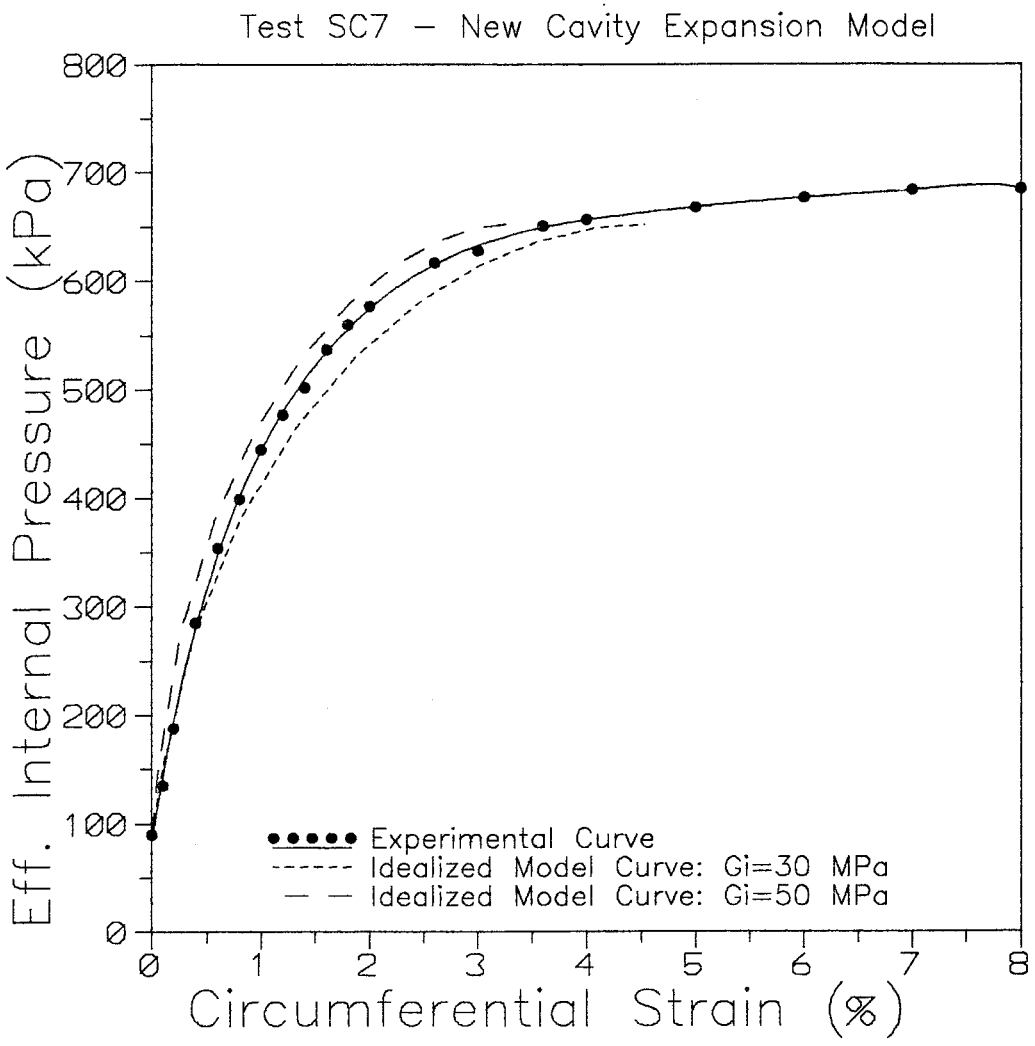

Figure 2.26: Curve Matching on Fahey, 1986 Tests: Limits for Gi

The calibration chamber tests adopted above are particularly useful to assess the suitability of plane strain solutions because they represent "special" tests in which the L/D (end) effect of the pressuremeter is intentionally suppressed. In real cases, however, end effects may be of importance for the final results. According to Fahey and Carter, 1993, the incorporation of end effects on the testing results can lead to improper soil predictions with the use of 1D cavity expansion models. 2D models solved via finite element technique would be then recommended in this case. In order to assess the capability of the new cavity expansion model for practical use additional chamber data is analyzed and presented next, together with a brief literature review of this topic.

2.5.2 End Effects

The influence of the length to diameter (L/D) ratio of the probe is a subject of controversy.

Suyama et al, 1983 used X ray radiography techniques in model experiments to investigate the pattern of expansion in monocell (L/D = 10) and tricell (L/D = 8.3) Menard type pressuremeters. The displacement patterns showed a tendency to cylindrical expansion for both cases, which corroborates the use of cylindrical cavity expansion models to interpret the testing curve. Yan, 1988 by modification of the finite element program CONOIL of the University of British Columbia analyzed the cavity expansion problem of the pressuremeter with both a 2D axisymmetric and a plane strain finite element mesh. He found that, in comparison to the plane strain predictions, the expansion of a pressuremeter with an L/D = 4 and 12 leads to an overestimation of ϕ respectively equal to 10 and 2 %. However, by carrying out a similar analysis using as reference a field SBPM curve of Hughes and Robertson, 1985, for a granular deposit of Vancouver, he concluded that "pressuremeters with L/D = 6 can provide the field pressure expansion curve that is close enough to the axisymmetrical plane strain condition". More recently Yu and Houlsby, 1992 presented a finite element numerical analysis similar to the one described by Yan, 1988. These authors used an elastic perfectly plastic model following the Matsuoka, 1976 flow rule to account for dilatancy during cavity expansion. As in Yan's case the Hughes et al, 1977 log-log approach was used, and an overestimation of 11 to 17 % of the plane strain ϕ could be predicted from a pressuremeter with L/D = 6 and soil stiffness ratio (G_i/σ_h) respectively of 5.2 to 7.0.

In order to understand in this subject, Salgado and Byrne, 1990 used the calibration chamber tests of Jewell et al, 1980 as a basis for comparison with their finite element predictions. They used an

elasto-plastic stress strain model coupled to the Matsuoka's flow rule with a 2D axisymmetric finite element mesh, hence simulating the geometry of the probe (L/D = 6.2) as well as the chamber boundary conditions. Analyses were also carried out using a plane strain axisymmetric domain, with finite or infinite boundaries. The soil parameters for the model came from the simple shear tests of Stroud, 1971 and the predicted finite element response at the cavity wall was directly compared to tests B3 and B5 of Jewell et al, 1980. Salgado and Byrne, 1990 results suggest that some error may be introduced by applying a plane strain model in the analysis of a finite length pressuremeter since, as observed by the (finite element) simulated displacement patterns inside the chamber, vertical movements will exist in the soil surrounding the probe at the latter stages of expansion.

In order to check the findings of these latter authors, the same reference chamber test of Jewell et al, 1980 was interpreted here with the (plane strain) new cavity expansion model. The analysis was carried out with the same methodology presented before up to a stage where the plastic zone radius, predicted by the model, started to touch the outer boundary of the chamber (i.e. $r_p/r_0 = 11$). Allowance was again made for the finite boundary of the chamber via the Fahey, 1986 equations.

Figure 2.27(a) presents the comparison between the experimental and the model curves. It is observed that the quality of matching is reasonably good for values of r_p/r_0 below 7. At r_p/r_0 greater than 7 the idealized curve stays below and deviates from the experimental curve. The same trend was obtained by Salgado and Byrne, 1990 using the plane strain mesh (with finite boundary), but with a much larger deviation. Nevertheless, the parameters obtained are representative of the Leighton Buzzard sand at the chamber density and confining conditions ($\phi = 48°$, Gi = 36.4 MPa, σ_h = boundary stress = 90 kPa).

The discrepancy observed for r_p/r_0 below 7 is partially caused by the disturbance of the soil around the probe due to the raining process, as previously noted. The deviation of the curves after a r_p/r_0 of 7 may be explained with the help of the Figure 2.27(b). This figure presents (in scale) the elastic and plastic zones developed for the limiting condition of $r_p/r_0 = 7$, at a mobilized cavity strain of $\cong$ 3 %. During the test as the pressure increases in the pressuremeter a plastic zone of yielding material extends rapidly outward from the cavity wall, decreasing substantially the proportion of material outside this zone. It is this outside material, or elastic zone, which supports the plastic zone. When the cavity strain has reached $\cong$ 3 % the

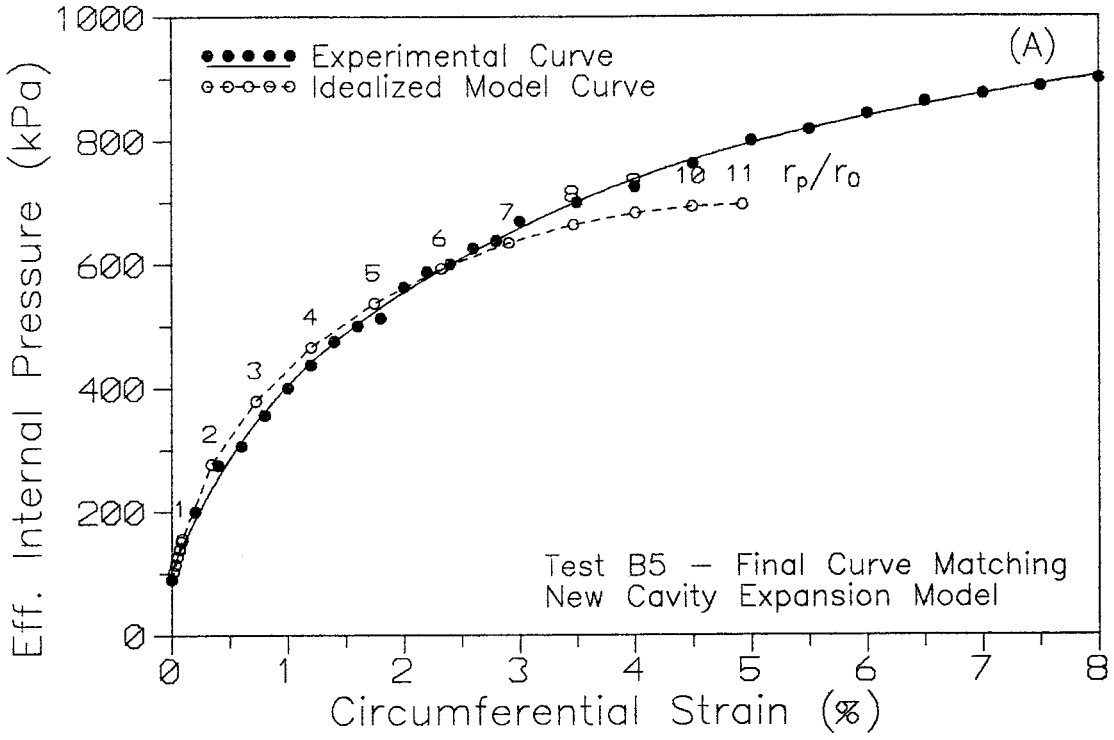

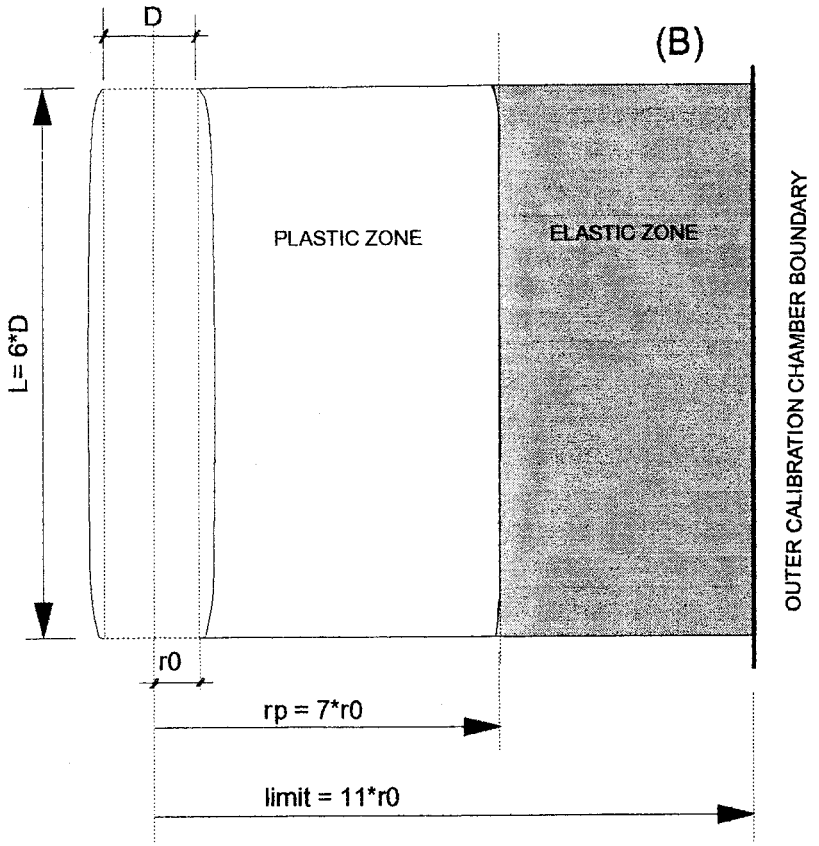

Figure 2.27: (a) Curve Matching on Jewell et al, 1980 Test B5
(b) Elastic and Plastic Zones Inside the Calibration Chamber

plastic zone is considerably large in relation to the size of the chamber, 11 radius wide. Nevertheless even allowing for the influence of the outer boundary via Fahey, 1986 equations, the difference between the curves increased after this cavity strain. It is suspected that end or L/D effects, not considered by Fahey, 1986 correction, start to dominate after this stage due to the reduction of the elastic zone.

It appears, therefore, that end effects are solely evident when the effects of the finite outer boundary also start to influence the expansion process, at least for pressuremeters with L/D above 6. This same observation was given by Fahey, 1986 based on the rough ended series of calibration chamber tests. As stated by Fahey, 1986, end effects could not be noticed at the early stages of the chamber tests, but they became obvious when the effects of the finite outer boundary were also present.

By carrying out tests in which the chamber to probe radius ratio is increased it may be possible to decrease the influence of the boundary as well as the influence of the finite length of the pressuremeter over the results. In order to illustrate this statement the interpretation of another calibration chamber data is presented. The Italian ENEL-CRIS chamber reported by Bellotti et al, 1987 for tests with Ticino sand is larger than the one used by Jewell et al, 1980 at Cambridge. The Italian chamber has a radius 14.6 times that of the probe. Similar to the Leighton Buzzard case, the tests were carried out with a pressuremeter of L/D equal to 6. Figure 2.28(a) and (b) present the final curve matching using the chamber test 228. The new cavity expansion model was adopted in the interpretation, with (Figure 2.28(a)) and without (Figure 2.28(b)) the correction for finite boundary proposed by Fahey, 1986. The same set of input parameters was used in both cases.

For this particular analysis the larger size of the chamber, together with the characteristics of the tested sand, allowed the cavity strain to build up to over 10 % before the radius of the plastic zone has expanded to 7-8 times that of the pressuremeter. This means that throughout the expansion process the plastic zone did not occupy more than 50 % of the whole volume of soil inside the chamber, and hence the boundary effects will be lower than those existing in Jewell's tests. Indeed, if no allowance is made for the outer boundary then the new cavity expansion model can be used to predict the chamber test data with remarkable accuracy, as illustrated in Figure 2.28(b). This suggests that for Bellotti et al, 1987 data neither end nor boundary effects are high enough to hamper the analysis with plane strain models. The

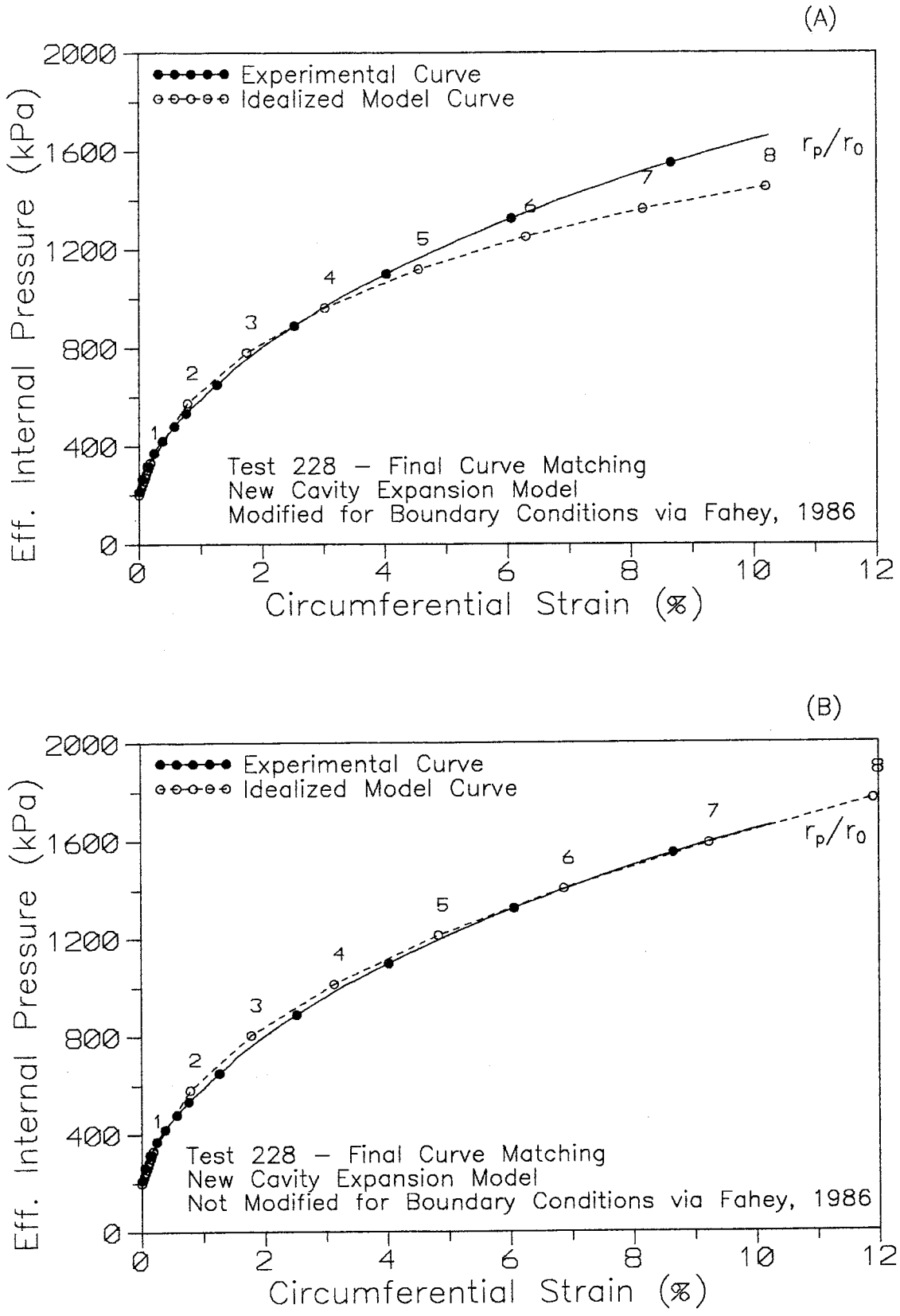

Figure 2.28: Curve Matching on Bellotti et al, 1987 Test 228: Influence of Chamber to Probe Ratio

same opinion is shared by Manassero, 1989. As will be presented in the next subsection, the parameters obtained in the analysis of the test 228 are also representative for Ticino sand.

Extending the findings of Figure 2.28 to a hypothetical field test, where boundary effects do not exist, it may be concluded that the selfboring pressuremeter can be analyzed by using simple plane strain models. This is so provided that the cavity strains are limited to the usual testing values (< 10 %) and a probe with slenderness ratio of at least 6 is used.

To further validate the capabilities of the new cavity expansion model more SBPM data from the calibration chamber tests with Ticino sand is analyzed next. Given the findings of this subsection, the 3 ideal installation and 2 selfbored tests chosen for interpretation are analyzed without any allowance for boundary effects.

2.5.3 Tests with Ticino Sand

Bellotti et al, 1987 carried out 47 SBPM tests in the Italian calibration chamber of ENEL-CRIS. The tests were performed in both dry pluvially deposited Ticino and Hokksund sands, and are grouped in accordance to the stress history of the samples as well as the mode of pressuremeter installation. Similar to Fahey's tests a pressure controlled boundary type chamber was used.

The tests chosen to be interpreted using the proposed methodology are the tests 228 (presented before), 222 and 234, representative of an ideal installation case, and tests 246 and 252, representative of the selfbored installation case. These tests were chosen since they cover a large range of relative density varying from 43 to 77 %, were performed with different types of Ticino sand (TS-4 to 6) and with effective horizontal boundary stresses ranging from 53 to 215 kPa. The overconsolidation of the samples also varied considerably, from 1 to 5.5. For additional details on the tests the reader is referred to Bellotti et al, 1987.

For all the tests the maximum dynamic shear modulus G_0 was determined by Lo Presti, 1987 via resonant column tests on Ticino sand under similar conditions as those found in the chamber tests. Unload reload loop stages were carried out for each of the tests and the values of Gur and Gur^c are also given by Bellotti et al, 1987. The constant volume friction angle of this sand is 34°, as defined by the latter authors with ring shear tests. The reference peak friction angles were measured for each sample by conventional triaxial tests. The axisymmetric angles were further converted to plane strain values with the empirical

relationship put forward by Lade and Lee, 1976. Table 2.5 presents a summary of the general conditions of the chosen tests after the sample consolidation as well as the reference soil parameters in each case.

The chosen tests were interpreted with the proposed interpretation methodology and the new cavity expansion model. A value of Poisson's ratio of 0.20 was adopted based on the estimate given by Bellotti et al, 1989 for this same sand. The constant volume friction angle adopted is the value obtained experimentally by Bellotti et al, 1987. As for the previous analyses, the simulation of the testing curve was carried out up to the limit condition of the chamber, in this case up to a r_p/r_0 of 14. All the basic soil parameters of the model (ϕ, σ_h and Gi) were allowed to vary during the fitting process. Both the Gur and G_0, related by Bellotti et al, 1987 for each of the chamber tests, were used during the curve fitting. The Gur was used with the new model to allow the incorporation of elastic strains in the plastic zone. The G_0 was used with Equation 2.81 to establish the value of Gi at each step of the fitting process.

The plots showing the comparison between experimental and idealized model curves are presented in Figures 2.29 and 2.30, respectively for the ideal and selfbored tests. The results of test 228 were already presented in Figure 2.28. In general terms the curve matching is very good for the entire range of cavity strains, although with a quality slightly inferior as observed before for the "perfect plane strain" tests of Fahey, 1986. It may be the case, therefore, that some small influence given by the finite boundary is still present for the experimental results of Bellotti et al, 1987. Nevertheless, for practical purposes the fit is reasonably acceptable.

It appears, however, that disturbance is present in some of the chamber tests, irrespective of the mode of pressuremeter installation. This particularly seems to be the case of tests 222 and 252, although to a very limited and small extent. No perceptible difference in the quality of the match is found with respect to the different initial conditions existing in each sample. This perhaps suggests that the model can be universally applied within the range of density, stress level and stress history observed for these particular chamber tests. Indeed, provided that the sand has a dilatant response during shear, the basic assumptions of the model are met. For Bellotti et al, 1987 tests dilatant behavior during shear was the rule rather than the exception given the high density and low confining stress levels of most of the samples.

Figures 2.31 and 2.32 present a comparison between the predicted soil parameters and the reference values reported by Bellotti et al, 1987 for the chamber tests.

TEST	SAND TYPE	D_r (%)	OCR	σ_v (kPa)	σ_h (kPa)	ϕ_{cv} [1] (Deg)	Gur [2] (MPa)	Gur^C [3] (MPa)	Gi [4] (MPa)	G_0 [5] (MPa)	ϕ [6] (Deg)	OBSERVATIONS
222	TS-4	46.2	5.5	111.8	95.16	34	53.8	46.9	17.4	80.3	42.7	Ideal Installation
228	TS-4	77	1	518	215.82	34	67.3	64.6	33.4	139.7	48.2	Ideal Installation
234	TS-4	76.1	5.3	115.8	103.99	34	53.5	47.7	24.7	102.8	48.9	Ideal Installation
246	TS-5	43	1	102	52.97	34	18.6	17.1	12.7	59.6	42.7	Selfboring Installation
252	TS-6	75	1	101	52.97	34	34.6	28.8	18.1	74.9	50.3	Selfboring Installation

1-Constant volume angle from Ring Shear tests of Bellotti et al, 1987
2-First series of unload reload loops: Degree of pressure unload = 20 %, $d\varepsilon_\theta = 0.06$ %
3-Corrected for stress level via Bellotti et al, 1987 or 1989 equations
4-Defined with the initial slope of the testing curve, for $\varepsilon_\theta < 0.5$ %
5-Low strain modulus from Resonant Column tests of Lo Presti, 1987
6-Plane strain angle from Lade and Lee, 1976 correlation, using conventional Triaxial compression testing results of Bellotti et al, 1987

Table 2.3: Calibration Chamber Testing Results on Ticino Sand (Modified after Bellotti et al, 1987)

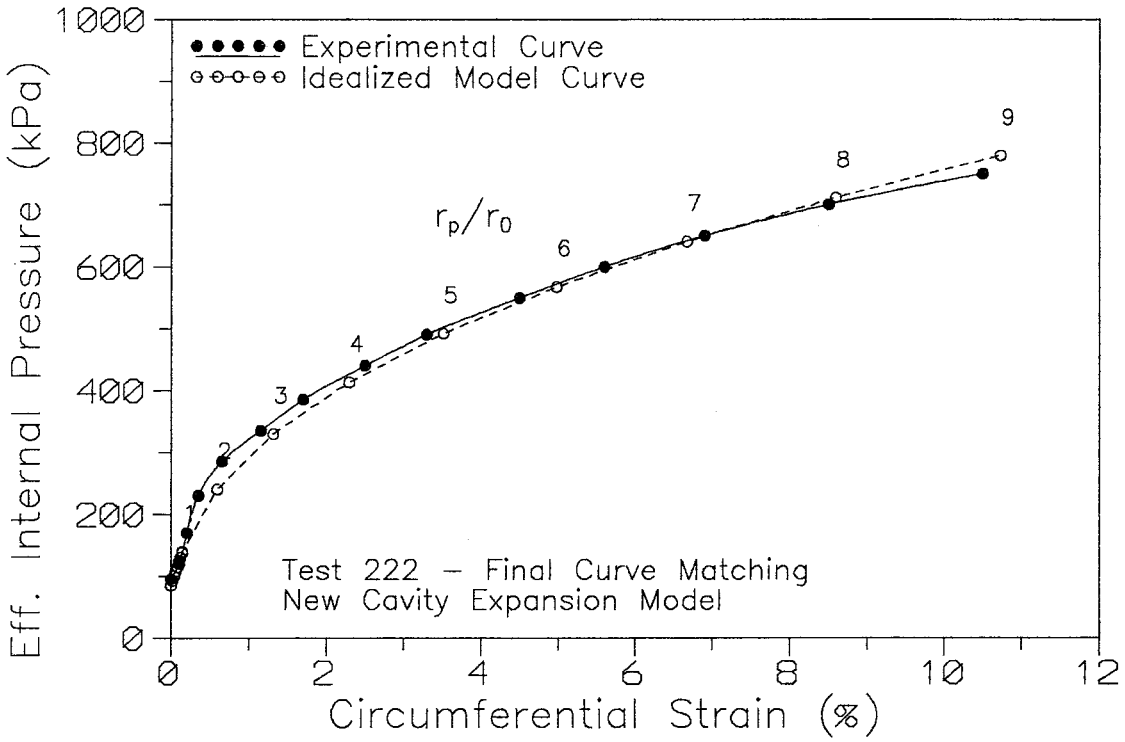

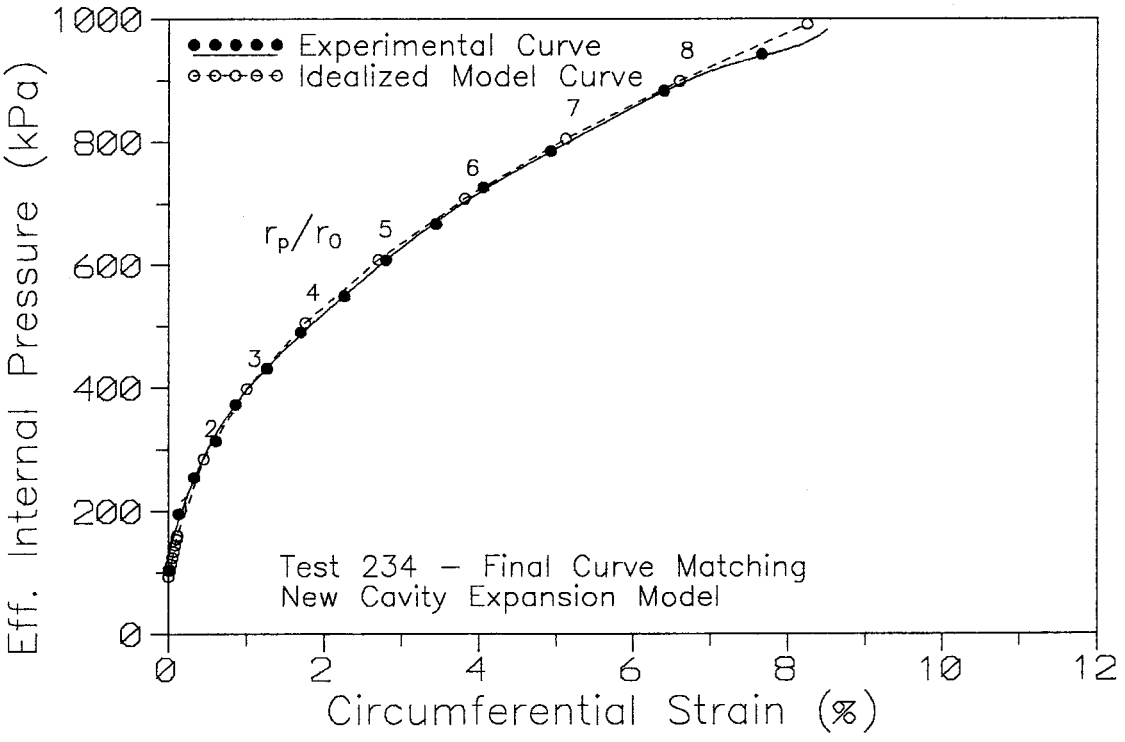

Figure 2.29: Curve Matching on Bellotti et al, 1987 Tests: Ideal Installation Tests

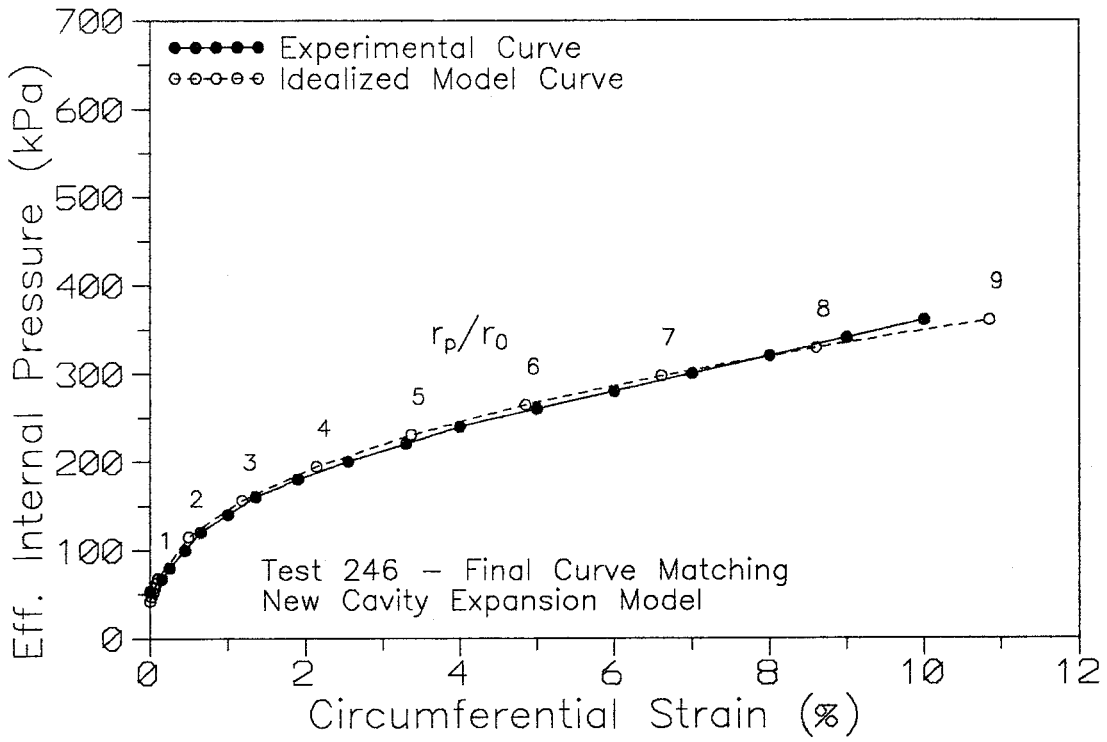

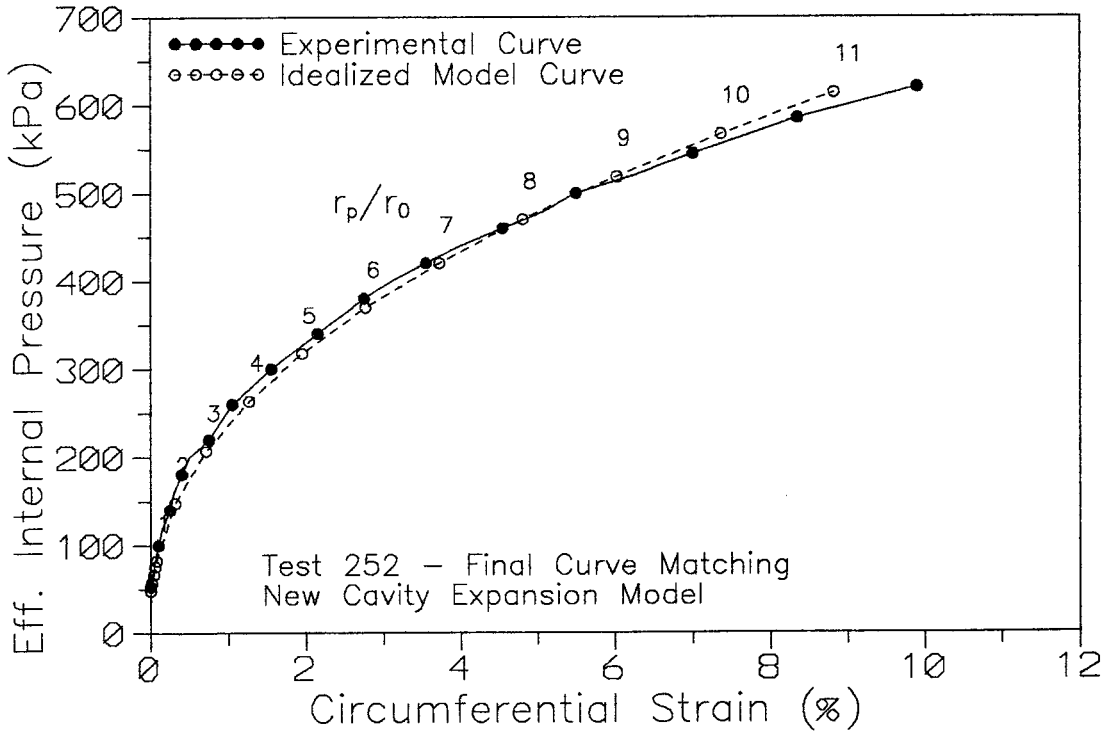

Figure 2.30: Curve Matching on Bellotti et al, 1987 Tests: Selfbored Tests

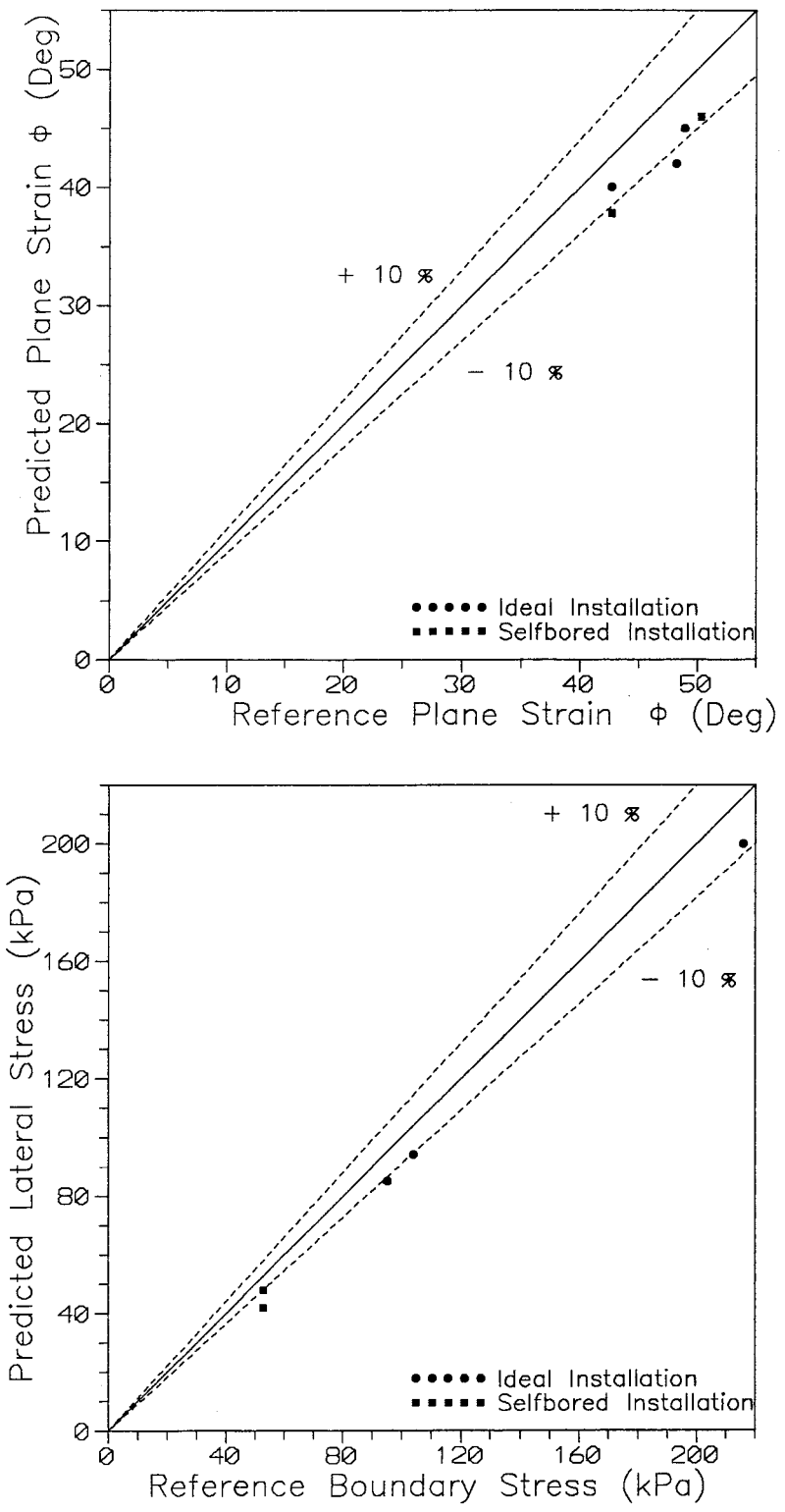

Figure 2.31: Predicted Results of the Curve Matching : Friction Angle and Lateral Stress

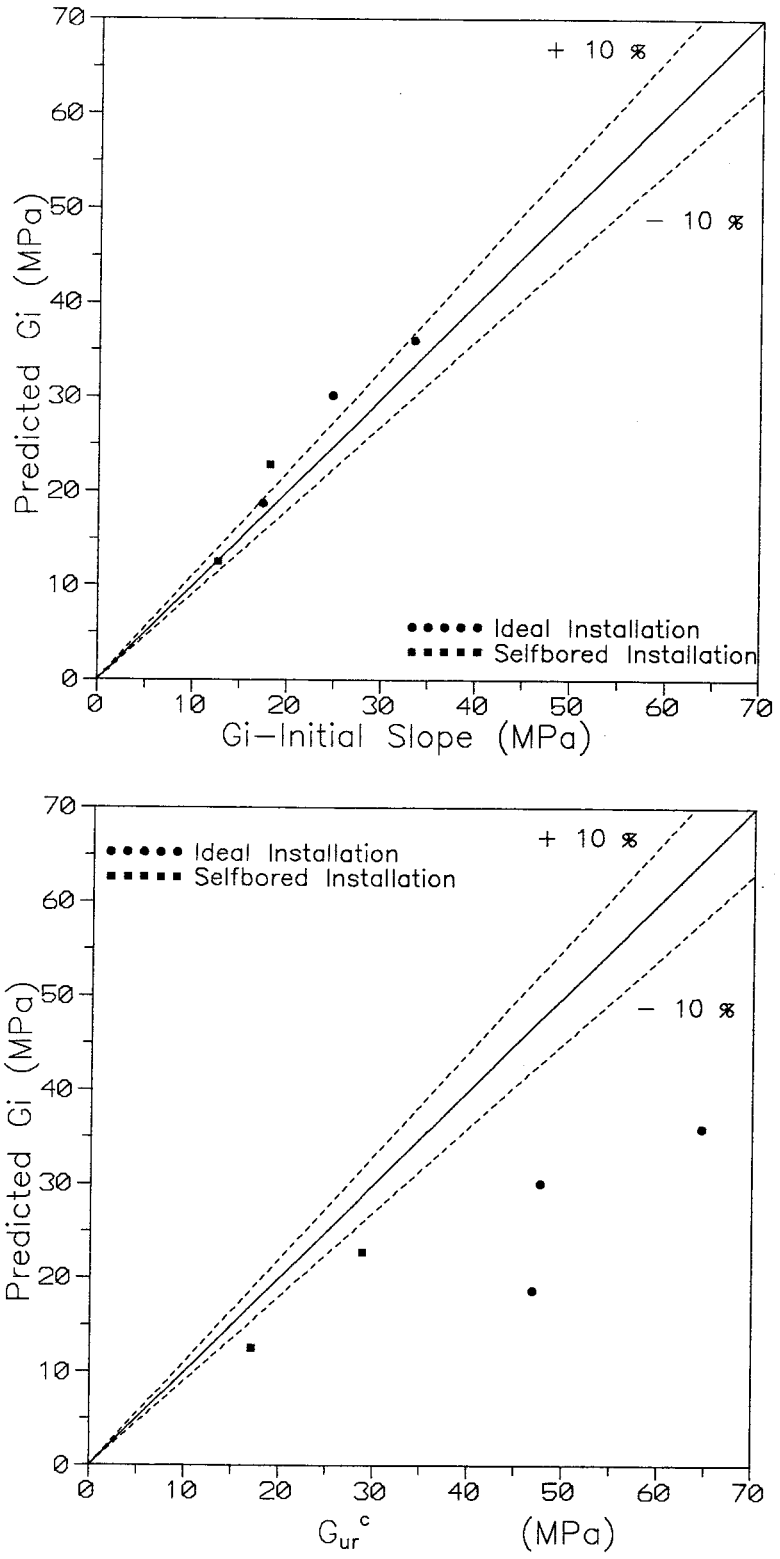

Figure 2.32: Predicted Results of the Curve Matching: Shear Modulus

The following observations can be drawn:

1. Both the predicted plane strain friction angles and the lateral stresses compare well with the reference values for each test. The average error is less than 10 %, resulting in a high accuracy for the model. Nevertheless, the predicted results are somehow underestimated. This may be caused by one (or the combined effects) of the following reasons:

- Disturbance of the chamber test: A small amount of disturbance that occurred during the sand pluviation or pressuremeter selfboring can impose a disturbed shape in the testing curve, affecting the match.

- Boundary effects: Given the findings of the last subsection the model was not corrected to account for boundary effects in the testing curve. However, it may be possible that such effects are still present to a small extent on the chamber results.

- Simplifications built in the cavity expansion model: Although most of the main features of the shearing behavior of the sand were accomplished by the new model, it still idealizes the medium based on a simplistic stress strain relationship.

- Natural variability and sensitivity of the analysis: As commented before, the natural variability of the solution is an inherent characteristic of the fitting interpretation methodology. This variability can be decreased with an increase of the quality of the testing curve, or the establishment of constraints between the input variables in slightly disturbed or disturbed data.

- Accuracy of the "reference" triaxial values: Dispersion of the results and experimental errors involved with the testing methodologies adopted to derive the "reference" soil parameters have to be acknowledged. Moreover, laboratory testing that does not impose the same conditions as those that prevail during the pressuremeter expansion also constitute a source of discrepancy for the comparisons. Bellotti et al, 1987 carried out conventional rather than plane strain triaxial tests to derive their friction angles. The "reference" values were defined after the application of the empirical relationship of Lade and Lee, 1976. Although this relationship is based on a large database it is still subject to the criticisms present with the use of empirical equations to convert experimental variables.

2. The predicted Gi is bounded by both the modulus defined by the initial slope of the experimental curve and by the unload reload (stress level corrected) modulus. The predicted Gi tends to be closer,

however, to the former variable. The reason for overestimation in relation to the stiffness measured by the initial slope of the testing curve is the same as the one put forward for Fahey's tests on subsection 2.5.1. The reason for underestimation in relation to Gur^c may be related to the different strain amplitudes that are related to each of these moduli. The important aspect is the fact that the magnitude of the predicted Gi compares extremely well with the G_0 values related by Bellotti et al, 1987 in Table 2.5. As noted in subsection 2.3.4 the pressuremeter modulus Gi reflects the soil response at a shear strain amplitude in the range of 10^{-1} %, whereas the modulus G_0 reflects the response at a shear strain level below 10^{-3} %. Assuming the reduction curve proposed by Idriss, 1990 to be universally applied for all granular soils, with the strain level differences above it shall be expected to have a Gi with a magnitude of 30 to 50 % the value of G_0 (see Figure 2.17). Using all the predicted Gi's and the respective G_0's of Table 2.5 an average modulus ratio of 24 % is obtained for Gi/G_0. The slight difference for the magnitude expected based on the curve of Idriss, 1990 can be accounted by factors such as soil cross anisotropy (Gi and G_0 are moduli related to different shearing directions) as well as difference in the tested sands.

In conclusion, the proposed methodology of interpretation has the capability to simulate reasonably well the pressuremeter loading curve when the new cavity expansion model is adopted. Provided that the sand has a dilatant behavior during shear, the new interpretation approach leads to accurate predictions of friction angle, lateral stress and shear modulus with either ideal installation (undisturbed) or selfbored (slightly disturbed) pressuremeter tests. In spite of the encouraging results of this section it shall be emphasized that more tests still need to be interpreted to confirm the reliability of the proposed interpretation methodology. This is principally the case of sands that have different characteristics than those related here for Ticino and Leighton Buzzard sands, or sands that behave in a different manner during shear.

Factors like the strain range of curve match and the sensitivity of the new model to changes in the input parameters have to be considered for the prediction of reliable results with the curve fitting technique. The following section addresses the problem of the interpretation of field curves, in which the above variables may play a more dominant role.

2.6 PARTICULAR ASPECTS OF THE FITTING TECHNIQUE IN SANDS

2.6.1 Strain Range of Curve Match

For undisturbed or disturbed data the strain range of curve match between field and model curves may be of importance. In order to investigate this aspect SBPM tests carried out by the writer will be interpreted and discussed herein. The SBPM tests were obtained with an extensive field testing programme in one of the UBC research sites near the city of Vancouver, in which the UBC SBPM was used. The details of the testing programme as well as the characteristics of the adopted granular site are explored in the next chapters.

2.6.1.1 High Quality Testing Curves

Typical SBPM tests are expanded to (cavity) circumferential strains in the range of 10 %. Under the traditional interpretation methodology only the last loading points obtained within this testing range are used to define the slope in the log-log graph, hence the friction angle. This is so because it is argued that the initial stages of expansion can be considerably affected by the disturbance generated prior to the test. Following this same reasoning, it may be also argued that if the approach followed by FDPM tests is adopted for the SBPM, with a testing stage carried out to a considerably high cavity strain, then it will be possible to predict truly undisturbed soil parameters from the interpretation of the latest stages of the experimental data.

In order to assess this hypothesis a series of curve fitting interpretations was carried out here. With this purpose a high quality field curve expanded to a circumferential strain around 20 % was adopted for the interpretation analyses. The fitting ranges chosen for the match of both experimental and idealized (model) curves varied from 0 to 5 %, 5 to 10 %, 10 to 15 % and above 15 %.

The interpretation analysis was conducted with the new cavity expansion model, following the interpretation methodology advocated in section 2.4. The adopted values of ϕ_{cv} and ν were respectively 34° and 0.25, since these values were experimentally obtained in drained triaxial tests with undisturbed samples of this site (see Appendix C). The stiffness adopted in the new cavity expansion model (to incorporate elastic strains in the plastic zone) refers to the value of Gur measured during the unload reload stage of the field test. The chosen test came from the testing sounding SBP09, at a depth of 5.3 m in the UBC research

site. It is a high quality testing curve based on the visual quality assessment criteria put forward by Robertson, 1982. This testing curve is shown in the top plot of Figure 2.33.

Figure 2.33 also shows the curve fit results at each of the chosen (cavity) strain ranges. The top plot presents the match between both field and idealized model curves, whereas the bottom plot shows the predicted parameters for each matching case. For this high quality curve the following comments apply:

1. The predicted soil parameters are not unique and depend on the range of match adopted during fitting. Nevertheless, for curve matches between 0 to 5 % or 5 to 10 % the same idealized curve suffices to represent the measured experimental data. The same set of predicted soil parameters are obtained in this range. For curve matches above ≈ 10 % it is not possible to obtain a unique set of predicted parameters. The higher is the range adopted for match (above ≈ 10 %), the higher are the differences between the predicted set of parameters and the parameters obtained with the match of the initial part of the experimental curve.

2. The predicted parameters from the curve match between 0 and 10 % ($\phi = 43°$, $\sigma_h = 33$ kPa and Gi = 11 MPa) are consistent with the expected values for this site. A deeper insight into the predicted sand parameters at this research site is given in Chapter 4 with the aid of reference laboratory test results and additional curve fitting analyses. The quality of curve match in this range is excellent, which suggests that the simple model developed herein could "capture" the essential shearing behavior of this particular sand in situ.

3. The predicted soil parameters for the curve match above ≈ 10 % do not seem to be realistic. The predicted effective lateral stresses appear to be extremely overestimated (consider, for instance, that the effective vertical stress at this depth is around 60 kPa). The predicted friction angles appear to be extremely underestimated. This is so because friction values below the constant volume angle ϕ_{cv} are predicted, suggesting a contractive behavior during shear rather than dilatant. A fully contractive behavior was not observed in the triaxial laboratory tests with the undisturbed samples, as commented in the Appendix C.

The findings above suggest that for high quality SBPM testing curves meaningful parameters from the fitting technique can be solely obtained if the match is carried out with the initial loading points of the

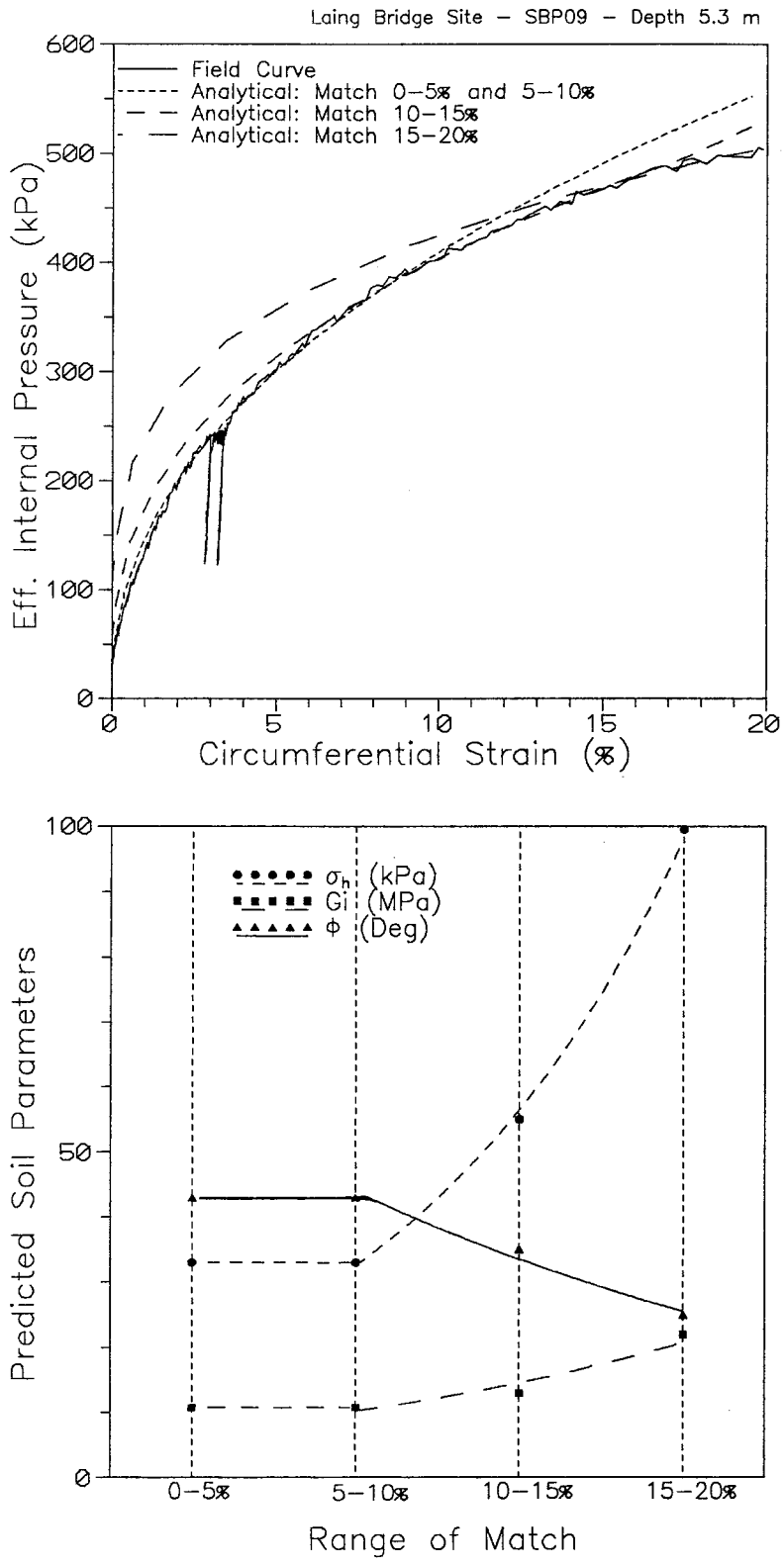

Figure 2.33: Influence of Range of Fitting on Results: Undisturbed Test
(a) Curve Fitting at Distinct Ranges, (b) Variation of Parameters

testing curve, between 0 to ≈ 10 % (cavity strain). This finding is directly in opposition to the common belief that only the latest stages of the testing curve are useful for the interpretation analysis. Perhaps the information experimentally measured for cavity strains above ≈ 10 % is influenced by external factors that are not considered in the new cavity expansion model. Two possible factors are prone to hamper the interpretation analysis at the high strain levels of the SBPM test:

1. End Effects.

In the section 2.5 it was observed that simple plane strain solutions can be used to interpret undisturbed or slightly disturbed tests, provided that expansion is carried out to low (cavity) circumferential strains (below ≈ 10 %) and the SBPM has a slenderness ratio above 6. For expansions above this strain the size of the plastic zone starts to become very large, and the expansion deviates from the expansion of a cylinder.

Figure 2.34 was prepared to compare the size of the plastic zone developed at the latest stages of expansion. Using the results of the curve fit between 0 to 10 % it was possible to predict the development of the elasto-plastic boundary throughout the testing stage, more specifically during a cavity strain of 10 % and 20 %.

The UBC SBPM has an expanding section only 6 diameters (12 radii) long and so, as illustrated in this figure, it is unlikely that a plane strain solution will be applicable in the latest stages of expansion. At these stages a compromise between the cylindrical and the spherical cavity expansion theory would have to be developed (see the shape of the plastic zone in this figure) for the interpretation analysis.

2. Strain Softening of the Sand.

The typical shear behavior of the sand at a constant confining pressure was discussed by Vaid et al, 1980. Over a considerable range of strain, both initially loose and dense samples undergo volume expansion, and at very large shear strains tend to approach an ultimate strength and critical void ratio. This ultimate state is commonly referred to the critical state of the sand (Atkinson and Bransby, 1978), at which the sand shears with no change in stress or specific volume.

Medium dense to dense sands present an initial small contractive section during shear, which is followed by a dilative behavior up to the critical state. The void ratio gradually increases to the critical

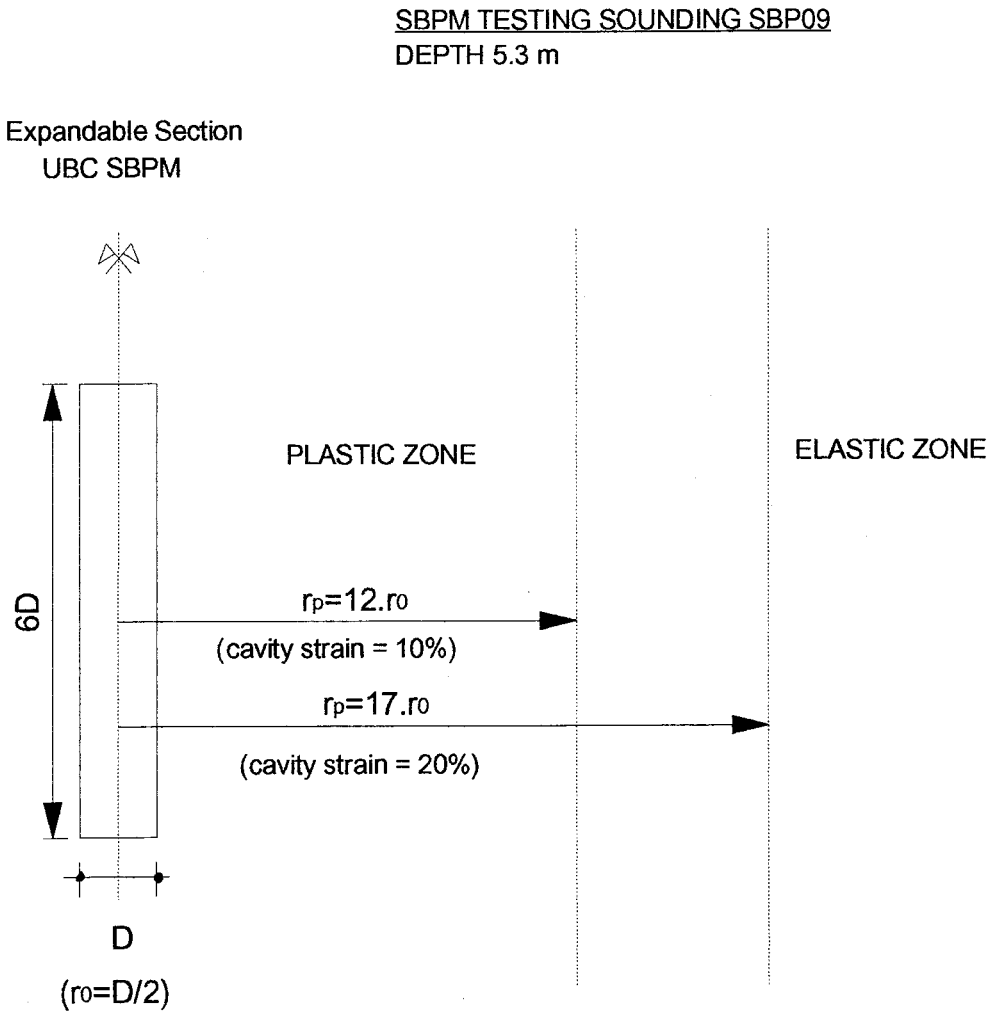

Figure 2.34: Schematic of Plastic Zones Developed at Cavity Strains of 10 and 20 %

value and the mobilized angle of friction gradually decreases from the peak value, corresponding to the maximum dilation rate, to the lower bound value, corresponding to the critical state (null dilation rate).

The above features were noticed by Lee and Seed, 1967 with drained triaxial tests in Sacramento River sand. Based on the results of these authors and the comments of Vaid et al, 1980 it is possible to visualize the typical (experimental) stress strain curve of medium dense to dense sands. This typical curve is shown in Figure 2.35. A similar stress-strain curves were obtained by Vaid et al, 1980 with drained simple shear tests in medium dense to dense Ottawa sand. The brittleness of these latter curves was, however, reduced. Figure 2.35 also shows the elasto-plastic representation idealized by the new model developed in this thesis. Note that the elasto-plastic model does not consider the strain softening effect observed in the laboratory, but rather assumes the sand is dilating at the peak rate at all the stages of expansion.

In the latest stages of the test the expansion takes place with the imposition of very high levels of shear stress and strain in the sand surrounding the cavity. Based on the experimental sand behavior related above, it may be possible to speculate that in the latest stages of expansion an annulus of sand at critical state conditions will be developed between the cavity wall and the elasto plastic boundary.

In this case the expansion process can be understood as the expansion of a two-layered system, composed of an inner layer shearing at constant volume conditions encompassed by an outer (plastic) layer where dilative volume change takes place. The response of this critical state annulus of sand has a dominant effect on the measured testing response at the latest stages of expansion. As schematically shown in Figure 2.36 the pressuremeter curve deflects from the undisturbed model response, following a path close to the response defined by the critical state annulus. Therefore, in an opposite fashion to that observed for the initial stages of expansion, both experimental and model curves continuously deviate for testing strains above $\approx$ 10 % (this is noticed in Figure 2.33 when comparing the field and the idealized curve matched between 0 to 10 %). If reliable parameters are sought with the curve fitting in the latest stages of expansion, then the cavity expansion model has to be modified to account for the strain softening of the sand. Failure to do so results in the prediction of unrealistically high σ_h's and low ϕ's, such as those presented in Figure 2.33.

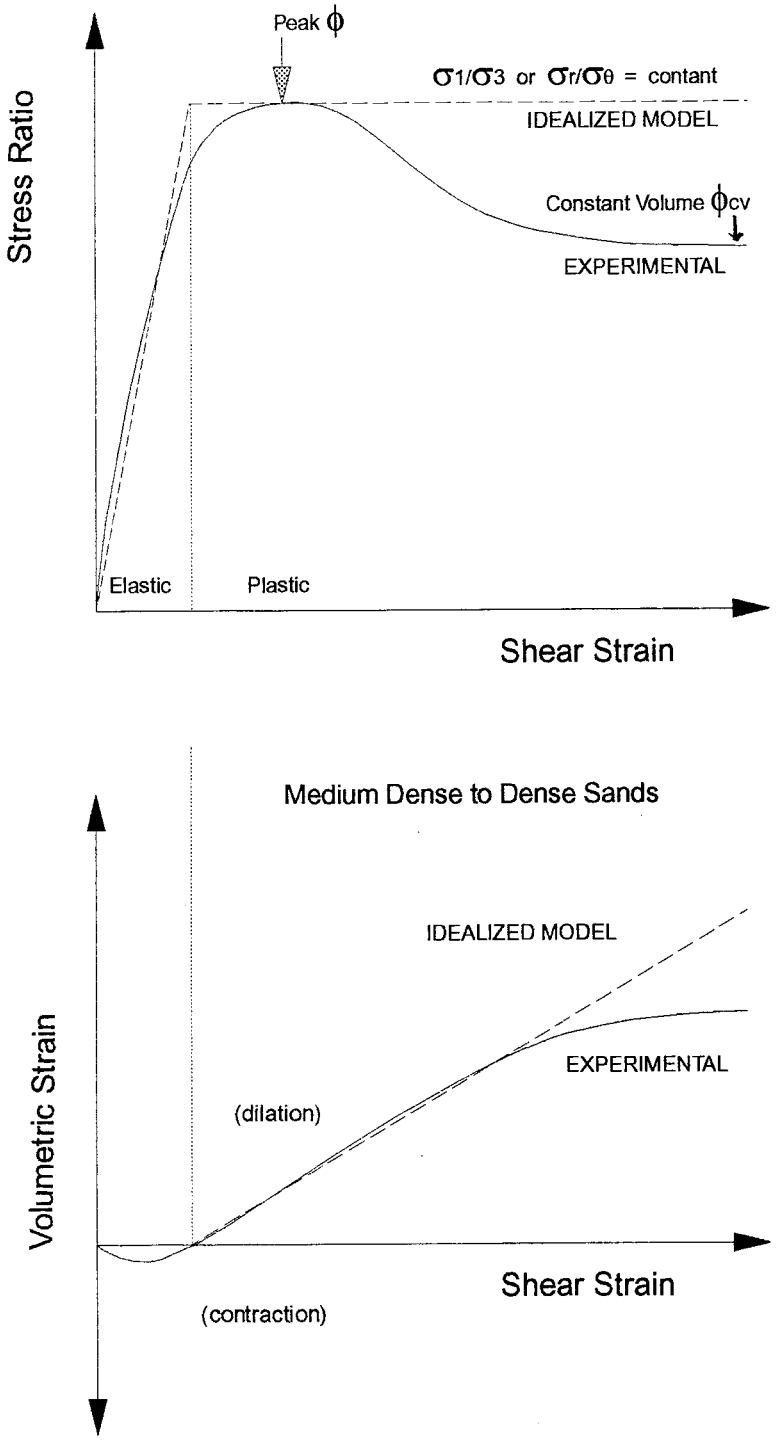

Figure 2.35: Idealized and Typical Experimental Stress Strain Curves of Sand During Shear

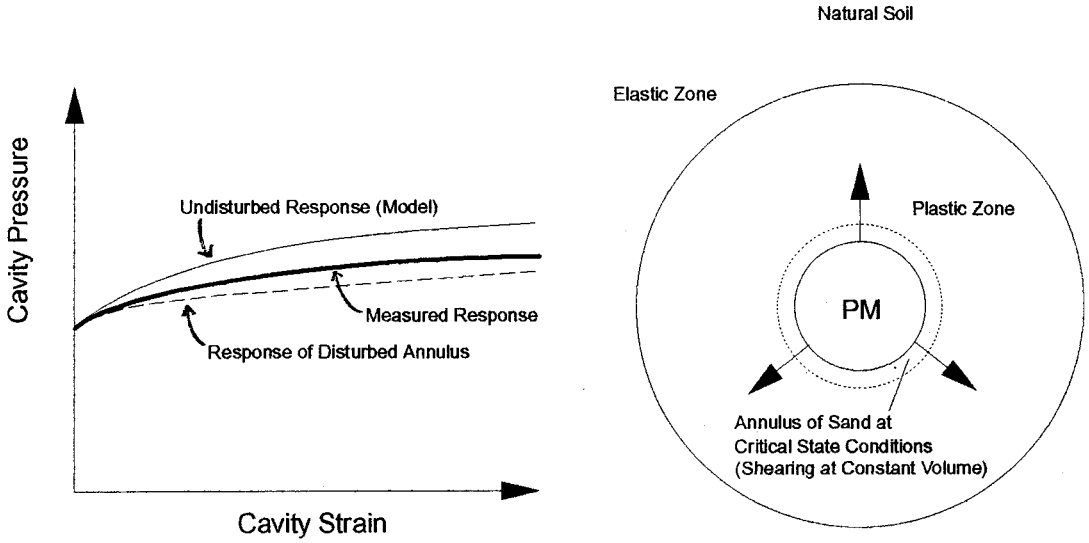

FINAL STAGES OF EXPANSION: ~10 % and Above

(End Effects Not Considered)

Figure 2.36: Effect of Continuous Shearing on Measured SBPM Response

In order to further investigate the above speculation, another analysis with the testing curve of Figure 2.33 was carried out. The (plane strain) finite difference numerical methodology proposed by Manassero, 1989 (see subsection 2.2.5) was chosen to be applied, since it is capable of predicting the variation of stress ratio and volumetric strain with the mobilized shear strain in any element of sand surrounding the expanding cavity. The numerical analysis was carried out with a Quickbasic program written specifically for this purpose. It is assumed (for the purpose of the numerical analysis) that end effects did not exist in the latest stages of the expansion test. The following steps were taken:

- The soil surrounding the cavity was subdivided into 1100 elements of thickness 0.1 mm. The output in terms of volumetric strain, stress ratio, shear strain and cavity (circumferential) strain was specified for only a few elements located at distinct radii around the cavity, as depicted in Figure 2.37. With this output it was possible to infer the behavior of the plastic zone throughout the expansion process.

- The finite difference technique of Manassero, 1989 was interactively applied for each of the 1100 elements. For each pair of cavity σ_r and ε_θ it was possible to define the values of σ_θ and ε_r at the wall (element 1) applying Manassero's equations. Using the differential equations of stresses and strains for an expanding cavity the values of σ_r and ε_θ at the adjacent soil element were then obtained. Applying again Manassero's equations in this new element it was possible to obtain another set of σ_θ and ε_r. This process continued up to the last soil element (1100), when another pair of experimentally measured σ_r and ε_θ was selected at the wall and the interaction with all the elements restarted.

- Simultaneous to the derivation of σ_r, σ_θ, ε_θ and ε_r, the values of stress ratio, volumetric strain and shear strain were also computed at each element during all the stages of the test. The program was written in such a manner that if for a particular soil element the mobilized stress ratio becomes lower than the constant volume principal stress ratio (defined by K_{cv}, or $(1+\sin\phi_{cv})/(1-\sin\phi_{cv})$), then the stress ratio is set as constant and equal to K_{cv} for all the subsequent interactions. Moreover, a null dilation rate ($d\varepsilon_v/d\gamma = 0$) is also imposed in this same element for all the subsequent interactions.

- Once the whole testing curve was analyzed and the values of σ_r, σ_θ, ε_θ and ε_r were known for each of the 1100 elements at all stages of expansion, the program wrote an ASCII file containing the stress-strain relationships for the chosen soil elements.

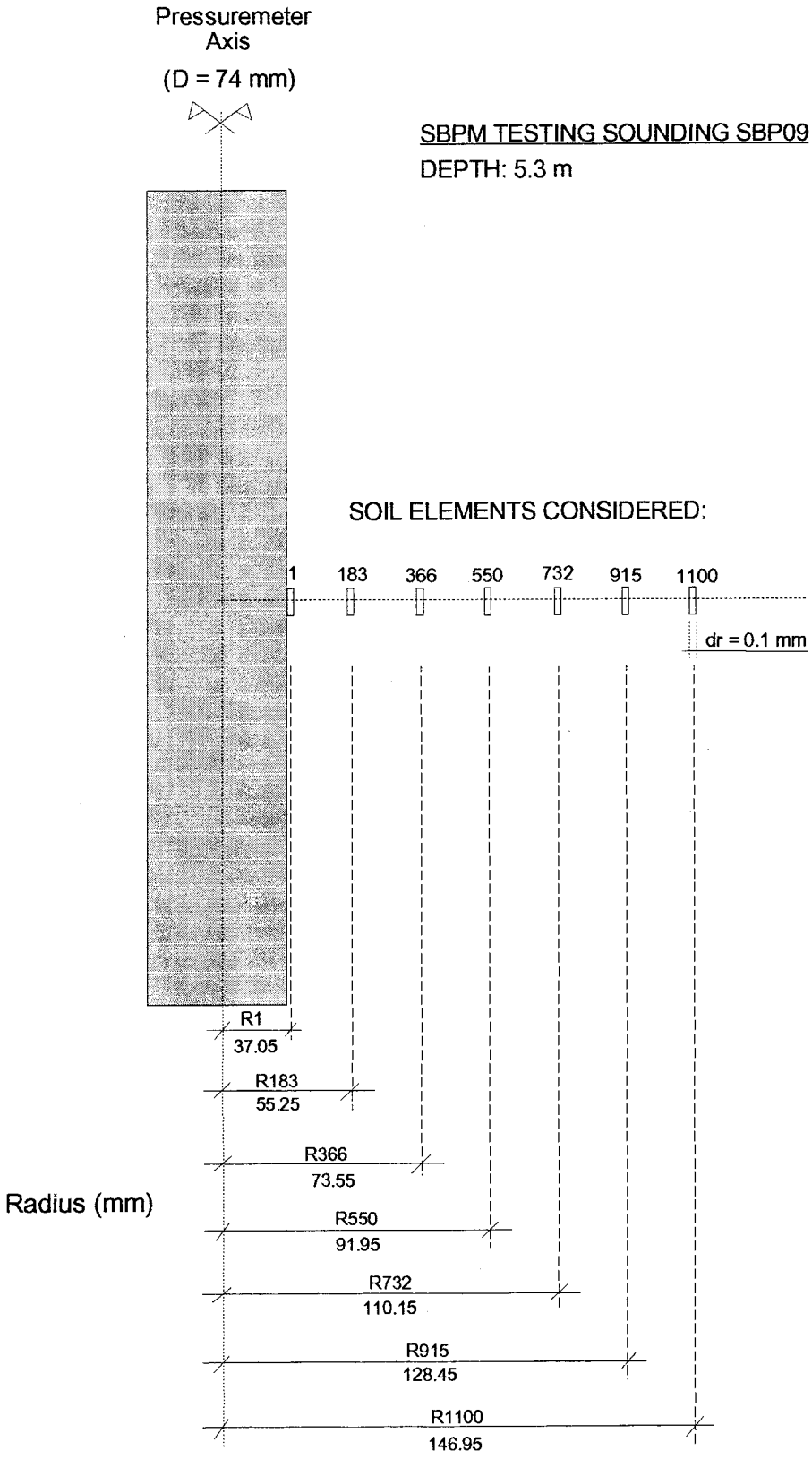

Figure 2.37: Soil Elements Around the Probe Chosen for the Numerical Analysis Following Manassero, 1989

Figure 2.38(a) presents the (idealized) variations of volumetric strain against cavity circumferential strain for each of the elements selected. It shall be noticed that the critical state condition is mobilized at the soil element when the curve reaches a horizontal level, characteristic of $d\varepsilon_v = 0$. The results of this figure indicate that, indeed, critical conditions are successively reached in each of the soil elements around the cavity. The analyses indicate that the critical condition was achieved at the cavity wall for an circumferential strain around 5 %. The annulus of soil at critical conditions expanded to a radius of 55.2 mm (element 183) for a cavity strain around 7.5 %, and continued expanding afterwards. This annulus expanded up to a radius above 91.9 mm (element 550), or $\approx 2.5\ r_0$, at the final expansion stage of this particular test.

Figure 2.38(b) was prepared in order to compare the size of the annulus of sand in critical state conditions in relation to the size of the plastic zone. Using the idealized model curve, fitted between 5 to 10 % of this same experimental curve, it was possible to predict the development of the elasto-plastic boundary throughout the testing stage. This information, together with the results of Figure 2.38(a), allowed the estimation of the zone of material around the cavity under either dilative shearing (plastic zone) or critical (constant volume) conditions. These zones are plotted in this figure against the circumferential strains measured during the test. It can be noticed that the volume of soil under constant volume conditions gradually increased in relation to the respective volume of soil under dilative (plastic) conditions. For instance, when the cavity strain was 10 % the critical state layer was equivalent to 7.7 % of the size of the plastic zone. This percentage increased to 11 % when the cavity strain reached 17 %.

In conclusion, for sands the cavity expansion process shall not be carried out to cavity strains beyond $\approx$ 10 %, where high gradients of shear stress and strain are imposed in the surrounding soil. These high gradients of stress and strain may induce the formation of an annulus of sand at critical (constant volume) conditions. This annulus grows simultaneously with the plastic zone, and at a faster rate. This phenomenon may partially explain the poor results for curve matches in the latest stages of the test, as the new cavity expansion model is developed based on the cavity expansion at a constant (peak) dilation rate. End effects are also prone to happen at the latest stages of expansion, hampering the usage of plane strain solutions for the interpretation of the SBPM curve.

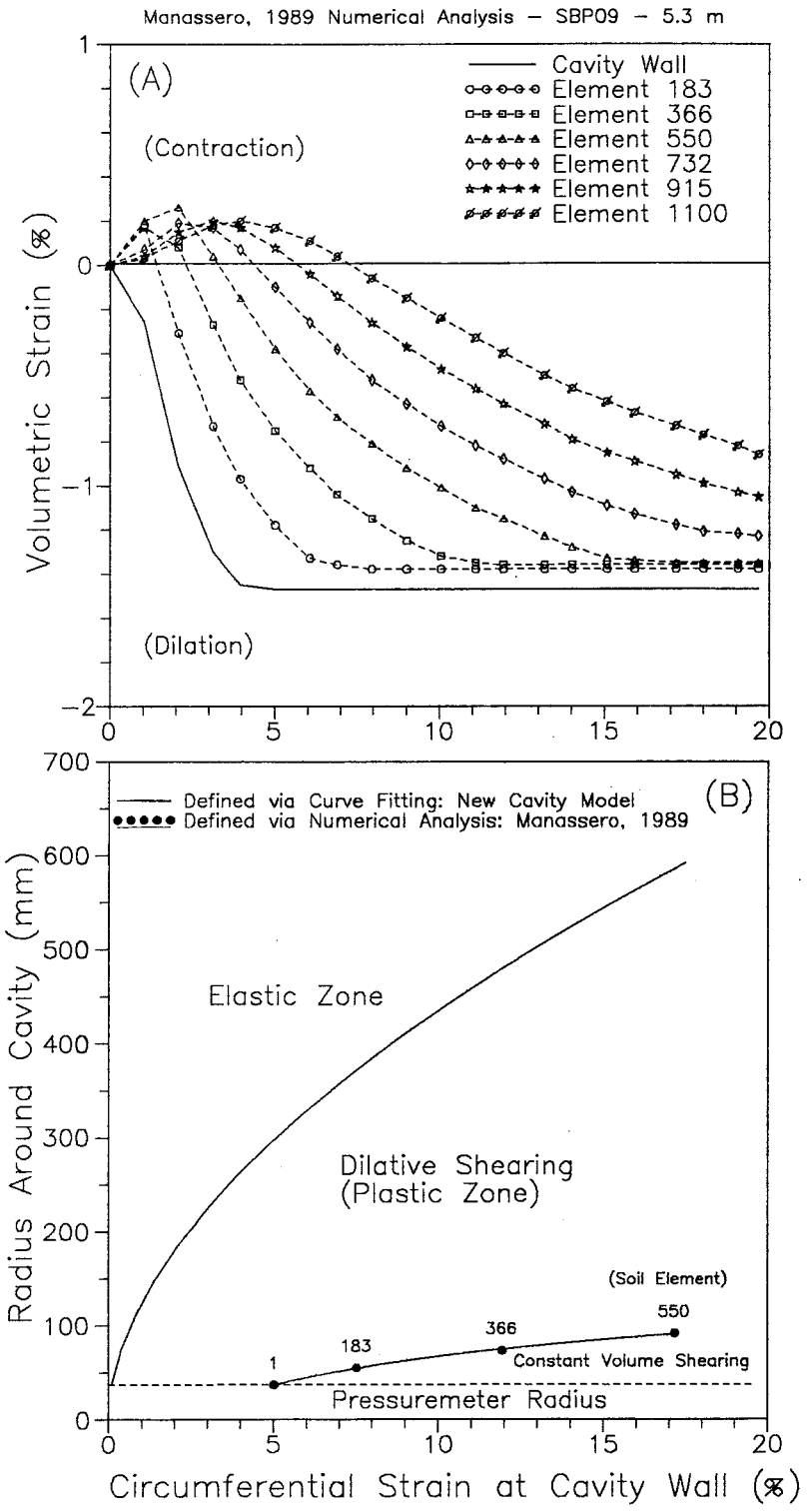

Figure 2.38: Results of Numerical Analysis for Test SBP09: 5.3m. (a) Volumetric Strain against Cavity Strain for Soil Elements, (b) Relation between Plastic and Critical State Zones Developed around the Probe

On the other hand, the example presented herein demonstrates that high quality SBPM tests in (medium dense to dense) sands can be reasonably well analyzed with the experimental information contained between 0 to around 10 % cavity strain.

2.6.1.2 Disturbed Testing Curves

Disturbance affects the shape of the testing curve, and consequently shall also influence the final set of predicted soil parameters.

In order to assess the likely influence of disturbance on the predicted parameters another series of curve fitting interpretations was carried out here. For this purpose a disturbed field curve was selected. The disturbed characteristics of the chosen curve are assessed based on the following evidence:

1. The shape of the curve does not follow the "high quality standards" put forward by Robertson, 1982 with his visual quality assessment criteria. This is circumstantial evidence of the disturbed characteristics of this field curve.

2. The chosen curve came from the testing sounding SBP19, at a depth of 5.3 m in the research site. This particular sounding consisted of 2 insertion trials at the same borehole. The first trial was carried out up to 5.7 m at a high penetration rate, resulting in the plugging of the cutting shoe to an extent of 70 % of its sectional area. This invariably disturbed the surrounding sand up to ≈ 6 m deep. This is strong evidence of the disturbed characteristics of this particular field curve.

As in the last subsection, the interpretation analysis was conducted with the new cavity expansion model following the interpretation methodology advocated in section 2.4. The same values of ϕ_{cv}, ν as well as Gur were adopted. However, a higher number of fitting ranges were selected for the interpretation analyses. The fitting ranges chosen for the match of both experimental and model curves varied from 0 to 3 %, 3 to 6 %, 4 to 7 %, 5 to 8 %, 6 to 9 %, 7 to 10 % and 9 to 10 %. Given the findings of the last subsection, the interpretation analysis was carried out up to a cavity strain of ≈ 10 %.

Figure 2.39 shows the chosen field curve and the obtained results. The top plot presents the match between both field and idealized model curves. For clarity, only 3 model curves are shown. The bottom plot shows the predicted parameters for each matching case.

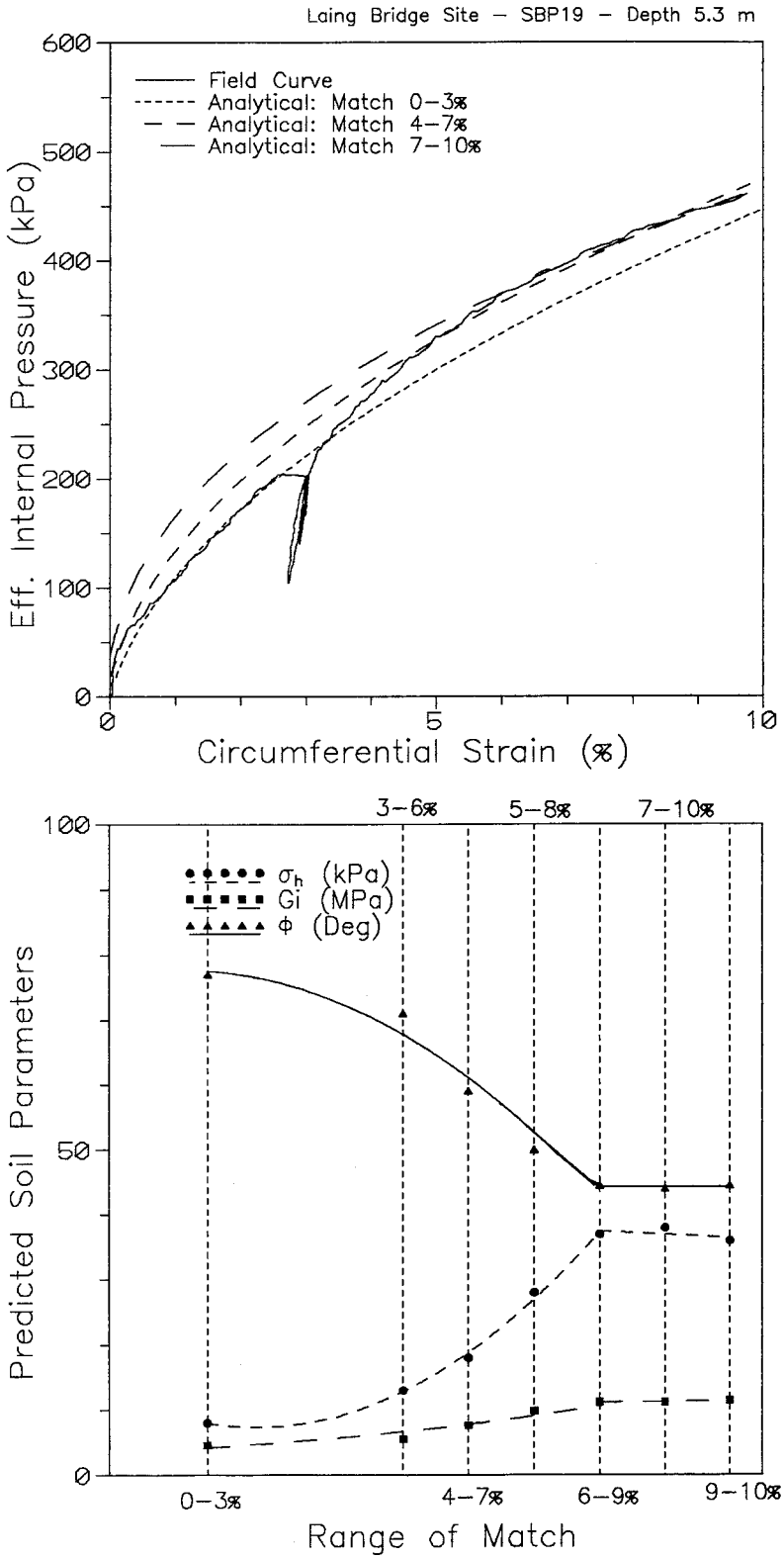

Figure 2.39: Influence of Range of Fitting on Results: Disturbed Test
(a) Curve Fitting at Distinct Ranges, (b) Variation of Parameters

For this disturbed testing curve the following comments apply:

1. The quality of curve match is excellent in either the initial or in the latest stages of the field curve. This does not mean that the predicted soil parameters (for each of the fitting cases) are equally reliable.

2. As for the high quality testing curves the parameters obtained are not unique, and depend on the range of match. Nevertheless, for each of the predicted parameters, the variation with the range of curve match "levels off" for matches at the latest stages of the test (close to 10 %). For curve matches in the initial ranges of the test, from 0 to ≈ 5 % it is not possible to obtain a unique set of predicted parameters.

3. The predicted parameters for curve matches between ≈ 5 % and 10 % (average $\phi = 44.2°$, $\sigma_h = 37$ kPa and Gi = 11.3 MPa) agree well with the parameters obtained with the fitting interpretation of the initial stages of the undisturbed curve (notice that both curves are related to the same testing depth).

4. The predicted soil parameters for the curve match in the initial stages of the field test do not seem to be realistic. This observation was also given with the results of the analysis carried out in the latest stages (beyond 10 %) of the undisturbed curve. With the disturbed curve, however, it appears that overestimated friction angles (above 50°) and underestimated effective lateral stresses (below 20 kPa) were predicted.

The findings above suggest that for disturbed SBPM testing curves meaningful parameters from the fitting technique can be solely obtained if the match is carried out with the latest stages (above ≈ 5 % and below 10 %) of the field curve. This is caused by the fact that disturbance affects the initial shape of the testing curve, reducing its "roundness". At the latest stages of this same curve, below a cavity strain of approximately 10 %, the effects of disturbance are decreased. For cavity strains beyond ≈ 10 % the effects of disturbance on the testing curve may be even erased, but other factors start to dominate (as noted in the last subsection) hampering the fitting interpretation analysis.

The effects of disturbance on the field testing curve are visualized in Figure 2.40. When disturbance is generated during the selfboring process an annulus of disturbed and loose soil is formed around the probe. The diameter of this annulus is unknown and will depend on the degree of disturbance generated prior to the testing stage. The response of this annulus of soil, schematically shown in Figure 2.40(a), influences the measured response of the test. The expansion process can be also understood as the cavity expansion in a two-layered system, one looser close to the SBPM shaft and another denser around this first

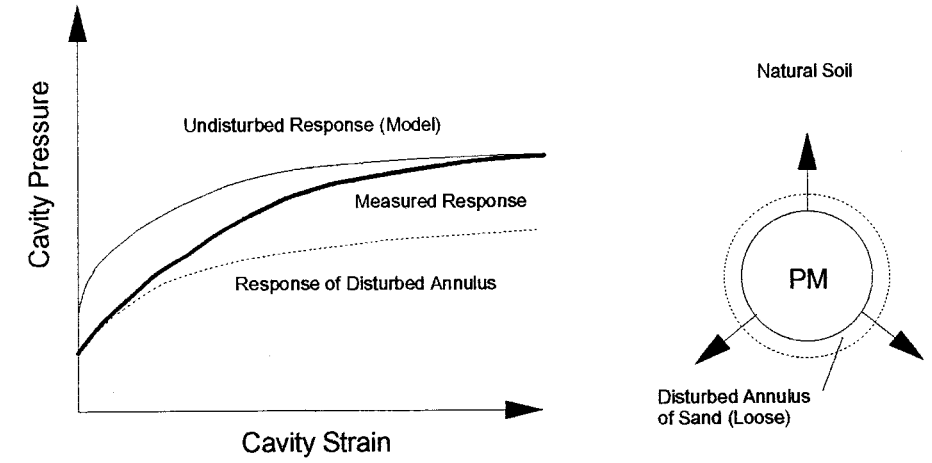

(A) INITIAL STAGES OF EXPANSION: 0 to ~ 5 %

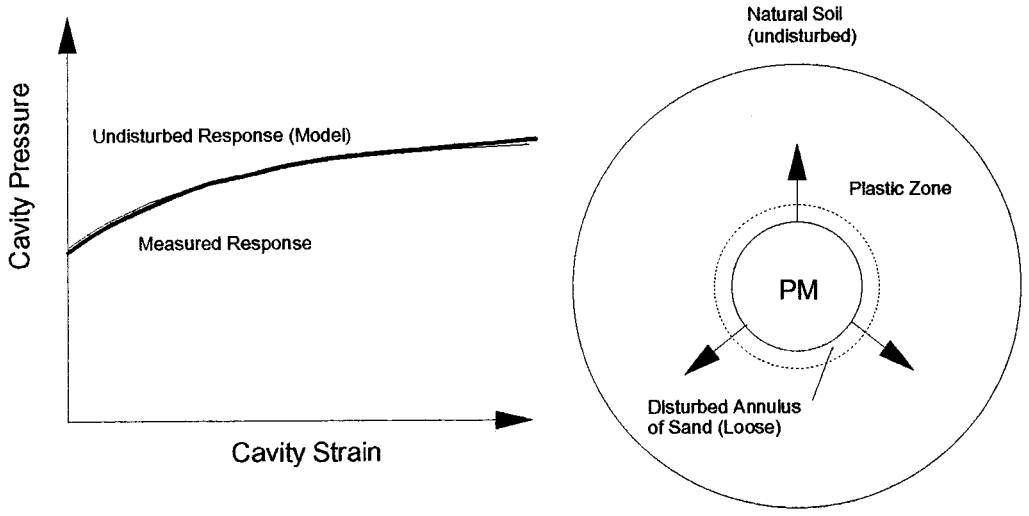

(B) FINAL STAGES OF EXPANSION: ~5 to ~10 %

Figure 2.40: Effect of Disturbance on Measured SBPM Response

layer. The SBPM testing curve will initially follow the path defined by the looser (disturbed) annulus of sand, therefore reducing its initial smooth "roundness". As the plastic zone grows in the latest stages of expansion (beyond ≈ 5 %), the effects of the disturbed annulus on the measured response are continuously decreased. This is schematically shown in Figure 2.40(b), and results from the fact that a larger zone of undisturbed soil starts to be encompassed by the expanding plastic zone. The measured cavity response at the latest stages of expansion predominantly reflects the shearing response of this undisturbed zone of soil.

In conclusion, the interpretation methodology advocated in this thesis allows the prediction of reliable soil parameters in either undisturbed or disturbed data. This represents an advance in relation to the traditional interpretation methodologies, that could only be applied in high quality SBPM curves. Nevertheless, the reliability of the predicted soil parameters may be expected to be directly proportional to the quality of the testing curve. For high quality or slightly disturbed testing curves the reliability of the predicted parameters is high. For disturbed curves the reliability of the parameters is somehow reduced. Table 2.6 presents the probable reliability of the predicted parameters from testing curves with different degrees of disturbance. The recommended fitting ranges for these curves are also given. As a general rule, for either undisturbed or disturbed data the curve fitting shall be carried out in the latest stages of expansion (between ≈ 5 % to ≈ 10 %).

Table 2.6 is solely valid for SBPM testing curves in sands that are analyzed in accordance with the interpretation methodology of this thesis. In order to efficiently use this table, knowledge of the quality of the testing curve is required. A subjective (visual) disturbance assessment, like the one proposed by Robertson, 1982, does not allow the clear distinction between "slightly" disturbed, disturbed or "highly" disturbed testing curves. Therefore, a numerical disturbance quantification is presented in Chapter 3 and discussed in the light of several field testing examples.

2.6.2 Sensitivity Analysis

The sensitivity of the new cavity expansion or the Carter et al, 1986 models to changes in the input variables also dictates the reliability that one can place in each of the individual (predicted) soil parameters. The basic answers sought in this subsection are related to questions of the type:

1. How does the fitting curve vary with the change of each of the input variables?

2. Based on (1) what can we infer in regard to the accuracy of each of these variables?

QUALITY OF TESTING CURVE	DEGREE OF DISTURBANCE	RECOMMENDED FITTING RANGE	RELIABILITY OF PREDICTED PARAMETERS
Undisturbed or Slightly Disturbed	Low	0 to ≈ 10 %	High
Disturbed	Medium	≈ 5 % to ≈ 10 %	High to Medium
Highly Disturbed	High	Close to 10 %	Medium to Low (?)

Table 2.6: Recommended Fitting Range of SBPM Tests in Sands

3. What is the influence of the estimation of either ϕ_{cv} or ν for the curve matching?

In order to assess the sensitivity of the model to changes in the input parameters a parametric analysis was carried out. This analysis took into consideration the variation of ± 10 % of each of the input parameters while keeping the remaining variables constant. The basic values selected to be varied were those derived from the fitting interpretation of the high quality SBPM test of Figure 2.33. This specific testing curve is presented again in Figure 2.41, together with the interpreted ("optimum") values and the idealized model curve from the Carter et al, 1986 model. The optimum values were assessed with the interpretation methodology advocated in this thesis.

Figure 2.42(a), (b) and (c) present the idealized model curves obtained after a variation of ± 10 % in each of the basic soil parameters ϕ, Gi and σ_h, while keeping the others with the respective values presented in Figure 2.41. For each curve the same values of ϕ_{cv} and ν, respectively of 34° and 0.25, were used. It is noticed in Figure 2.42 that small variations in the value of ϕ can influence the model curve to a larger extent than the same variation produced by changes in either Gi or σ_h. This implies that for this cavity expansion model (or the new model) ϕ is the less sensitive parameter for changes that eventually take place in the model curve during the fitting process, meaning that ϕ is the parameter in which prediction a higher degree of confidence can be placed. Both the σ_h and Gi have similar sensitivities to possible changes in the model curve, suggesting that for these variables the same amount of confidence shall be placed. Since the variability of Gi and σ_h for changes in the model curve during the match is higher than the variability of ϕ, it can be concluded that the accuracy of the prediction of the former variables is lower than the accuracy of the prediction of ϕ. Nevertheless, the accuracy of any of the predicted soil parameters is still high, as demonstrated in section 2.5.

Suppose now that during the match one of the input variables is mistakenly adopted. This could lead to erroneous conclusions in regard to the remaining of the coupled set of variables if a good fit is obtained. In order to simulate this situation, another parametric analysis was carried out. In this case each of the basic soil parameters of Carter et al, 1986 model (1st variable, either ϕ, σ_h or Gi) was varied by a known percentage of the "optimum" value of Figure 2.41, while keeping the 2nd variable constant (equal to the "optimum" value) and letting the 3rd variable to vary in order to produce the best curve match with the

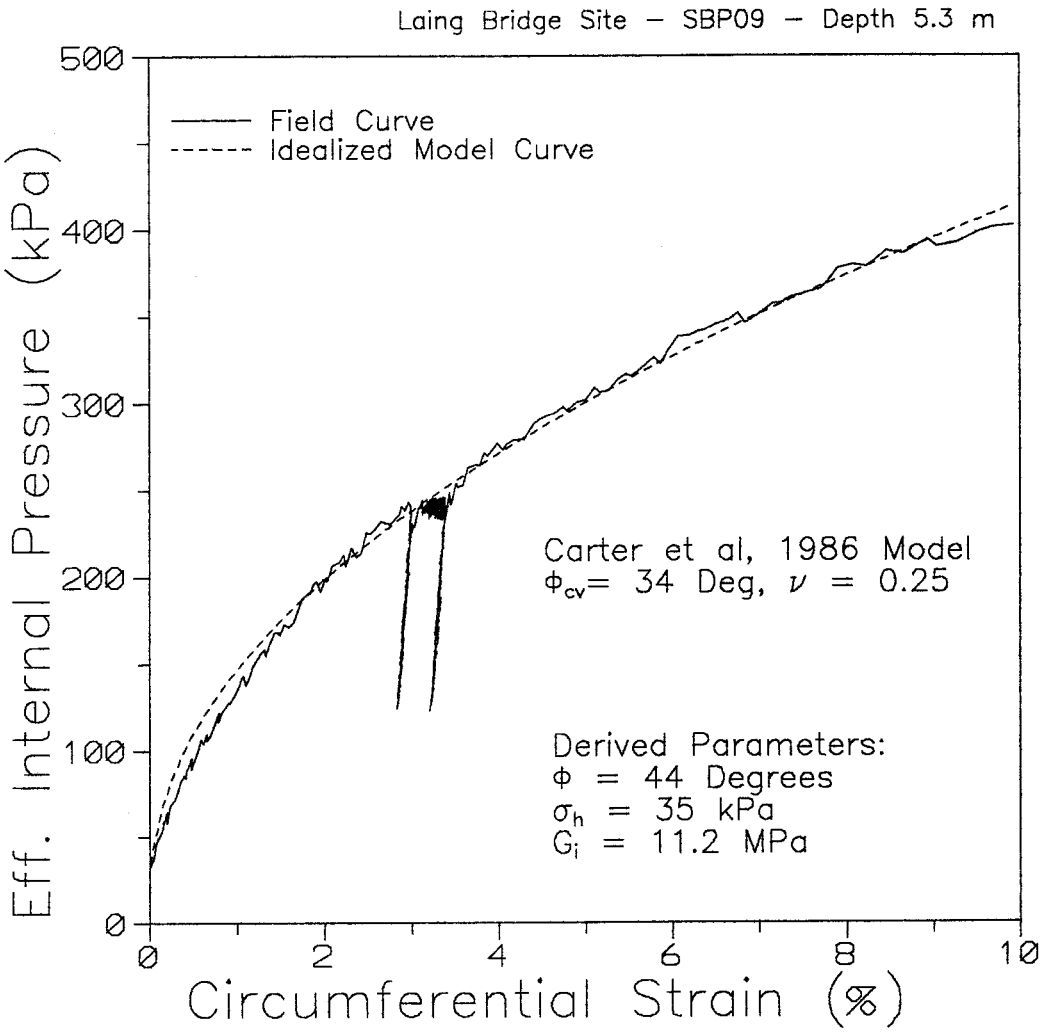

Figure 2.41: Curve Fitting of Test SBP09 (5.3 m) with Carter et al, 1986 Model

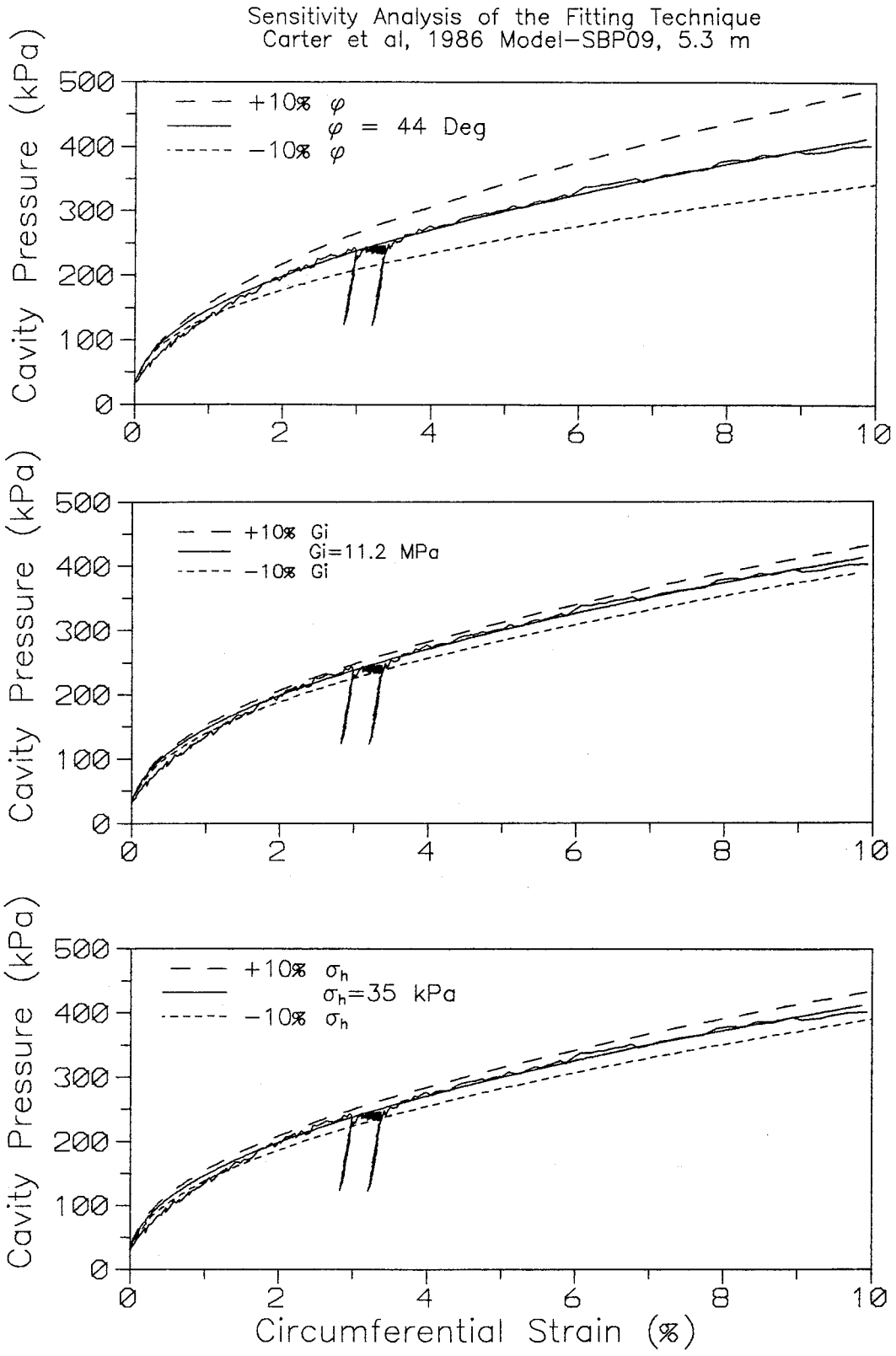

Figure 2.42: Sensitivity Analysis of the Curve Fitting: (a) Friction Angle, (b) Shear Modulus (c) Lateral Stress

experimental data of this same figure. Table 2.7 indicates the respective percentage of increase or decrease of the 3rd variable when the 1st variable is incorrectly assessed 20 % below or above the "optimum" value.

The following observations can be given with this table:

1. The percentage of variation of ϕ to the "optimum" value is lower than 8 % when an error of $\pm$ 20 % in either Gi or σ_h happens. Moreover, when ϕ is varied within $\pm$ 20 % of the "optimum" value a extremely high (and similar) variation on either Gi or σ_h is required to allow the fitting with the experimental curve. This is due to the differential sensitivities of ϕ, σ_h and Gi to the variations in the model curve. However, the quality of the curve match with an over or underestimated ϕ is poor, being easily noticed during the visual fitting procedure. The findings of this item suggest that the match in the final slope of the experimental curve is extremely dominated by ϕ, implying that if a high quality testing curve is adopted during the match then a highly accurate (plane strain) ϕ is to be predicted.

2. The percentage of variation of σ_h due to an error in Gi (while keeping ϕ constant) is similar to the percentage of variation of Gi given by an error in σ_h. This implies that, if ϕ is properly assessed during the match, similar error (if one exists) is to be expected in respect to both Gi and σ_h, i.e., if for instance Gi is overestimated by 20 % similar magnitude of underestimation shall be expected for σ_h. However, since in the proposed interpretation methodology the constraint between Gi, G_0 (or Gur) and ϕ can be adopted during the curve match (Equations 2.81 or 2.82), it turns out that if ϕ is properly assessed, then Gi will also be properly assessed. Consequently, given the observations of this item, σ_h will be well established too.

Either for Carter et al, 1986 or the new cavity expansion model the knowledge of the constant volume friction angle (ϕ_{cv}) is required. As experimentally demonstrated by Negussey et al, 1984 the constant volume friction angle represents a constant material property, dependent on the sand mineralogy and independent of particle size, confining pressure and density. It can be obtained with laboratory triaxial tests with undisturbed or reconstituted samples of the site, as done in this thesis and presented in Appendix C. In the absence of that, the table proposed by Robertson and Hughes, 1986 or the simple dry heap method of Cornforth, 1973 with washed samples retrieved in the site can be adopted. Based on the experience of the writer this latter approach leads to a ϕ_{cv} as close as 1 to 2° of the value defined by the laboratory tests.

PARAMETER VARIED TO A KNOWN PERCENTAGE (1st Variable)		PARAMETER NOT VARIED EQUAL TO OPTIMUM VALUE (2nd Variable)		PARAMETER VARIED TO ACCOMPLISH BEST CURVE MATCH (3rd Variable)	
VARIABLE	VALUE	VARIABLE	VALUE	VARIABLE	VALUE
σ_h - 20 %	28 kPa	ϕ	44°	Gi	14 MPa (+ 25 %)*
σ_h	35 kPa	ϕ	44°		8.9 MPa (- 20 %)*
σ_h + 20 %	42 kPa	ϕ	44°	Gi	
σ_h - 20 %	28 kPa	Gi	11.2 MPa	ϕ	47° (+ 6.8 %)*
σ_h	35 kPa	Gi	11.2 MPa		41° (- 6.8 %)*
σ_h + 20 %	42 kPa	Gi	11.2 MPa	ϕ	
Gi - 20 %	9.0 MPa	σ_h	35 kPa	ϕ	47.5° (+ 7.9 %)*
Gi	11.2 MPa	σ_h	35 kPa		42° (- 4.5 %)*
Gi + 20 %	13.4 MPa	σ_h	35 kPa	ϕ	
Gi - 20 %	9.0 MPa	ϕ	44°	σ_h	43 kPa (+22 %)*
Gi	11.2 MPa	ϕ	44°		30 kPa (- 14 %)*
Gi + 20 %	13.4 MPa	ϕ	44°	σ_h	
ϕ - 20 %	35.2°	Gi	11.2 MPa	σ_h	61 kPa (+ 74 %)*1
ϕ	44°	Gi	11.2 MPa		20 kPa (- 42 %)*1
ϕ + 20 %	52.8°	Gi	11.2 MPa	σ_h	
ϕ - 20 %	35.2°	σ_h	35 kPa	Gi	30 MPa (+ 167 %)*1
ϕ	44°	σ_h	35 kPa		7.0 MPa (- 37 %)*1
ϕ + 20 %	52.8°	σ_h	35 kPa	Gi	

* Variation in relation to the optimum value of this variable
1-Poor Curve Match

Table 2.7: Sensitivity of Fitting Results for Increase or Decrease in one of the Input Parameters

As speculated by Ferreira, 1992, the associated error in the interpreted soil parameters is generally small when the value of ϕ_{cv} is assumed during the curve fitting. This author additionally suggests that, in the absence of laboratory data, an average value of 35° for ϕ_{cv} shall be adopted. In order to assess this speculation and hence evaluate the sensitivity of the model to changes in either the value of ϕ_{cv} or ν, another parametric (curve fitting) analysis was carried out with the same experimental curve presented in Figure 2.41. In this analysis the values of ϕ_{cv} and ν were allowed to respectively vary as much as $\pm$ 10 % and $\pm$ 20 % of the "optimum" values related in this same figure. For each case a new set of predicted soil parameters was obtained by the fitting interpretation and compared to the "optimum" set derived with the "optimum" values of 34° and 0.25, experimentally defined for ϕ_{cv} and ν.

Table 2.8(a) and (b) indicate the respective variation in each of the predicted soil parameters given by the variation of either ϕ_{cv} or ν. As demonstrated by the last row of each of the tables the average variation of the basic soil parameters was well below 10 %, suggesting that the model curve is almost insensitive to variations in either ϕ_{cv} or ν. The reduced sensitivity of Gi in comparison to the sensitivity of σ_h comes from the use of Equation 2.81 during the curve match. Gi is not allowed to vary independently to variations in ϕ. Since ϕ is the least sensitive variable of the model it turns out that the sensitivity of Gi to changes in either ϕ_{cv} or ν is also reduced. Nevertheless, the average variation of σ_h for this example was in the range of $\pm$ 6 % of the "optimum" value. This places a high degree of confidence on the speculations of Ferreira, 1992, suggesting that in the absence of laboratory baselines for ϕ_{cv} or ν "educated guesses" for these parameters can be made.

2.7 SUMMARY AND CONCLUSIONS

This chapter emphasized the analytical interpretation of selfboring pressuremeter testing curves in sands. Emphasis was placed on the development of a new approach to analyze the data and derive reliable predictions of the basic soil parameters, namely the friction angle, the lateral stress and the shear modulus.

A comprehensive review of the existing cavity expansion models to simulate the pressuremeter expansion in sands was presented. A new cavity expansion model that extends the rheological equations put forward by Hughes et al, 1977 was devised to be used under the framework of a new interpretation methodology. This new methodology relies on a curve fitting technique to match both experimental and

ϕ_{cv} (Deg)	VARIATION (%)	PREDICTED SOIL PARAMETERS		
		σ_h (kPa)	Gi (MPa)	ϕ (Deg)
30.6	-10	33	11.1	43.7
34	0	35	11.2	44
37.4	+10	37	11.5	44.5
Average Variation:		± 6 %	± 2 %	± 1 %

Observation: $\nu = 0.25$ during the curve fitting

(A) Variation of Predicted Results for Variation of Constant Volume Friction Angle

ν	VARIATION (%)	PREDICTED SOIL PARAMETERS		
		σ_h (kPa)	Gi (MPa)	ϕ (Deg)
0.20	-20	37	11.2	44
0.25	0	35	11.2	44
0.30	+20	33	11.2	44
Average Variation:		± 6 %	± 0 %	± 0 %

Observation: $\phi_{cv} = 34°$ during the curve fitting

(B) Variation of Predicted Results for Variation of Poisson Coefficient

Table 2.8: Sensitivity of Fitting Results for (a) Constant Volume Friction Angle, (b) Poisson Coefficient

idealized curves, thus defining a "coupled" set of basic soil parameters. These parameters are linked to each other by the constitutive model and can vary in accordance to some factors discussed in this chapter.

The reliability of the Hughes et al, 1977, the Carter et al, 1986 as well as the new cavity expansion models was assessed with the use of a limited, but well established, calibration chamber database. The major aspects that can potentially influence the new interpretation methodology were addressed and discussed in the light of several analyses performed. These aspects are related to the possible influence of end effects over the final results, the sensitivity of the analytical curve to changes in the input variables, the variability of the solution for changes in either ϕ_{cv} or ν, and the influence of the strain range of curve match for the reliable prediction of the parameters.

The main findings of this chapter can be given by:

• The interpretation methodologies currently available for the analysis in sands lead to unreliable predictions of the basic soil parameters in disturbed SBPM data. These methodologies are extremely sensitive to small amounts of disturbance in the testing curve, and should be solely applied to high quality testing curves. The current interpretation approaches predict "uncoupled" soil parameters that respond differentially to the disturbance of the test and are related to distinct stress-strain idealizations.

• Simplistic cavity expansion models can be used to simulate the complex behavior that takes place in the sand surrounding an expanding cavity, provided that realistic assumptions regarding the stress-strain and volume change of the sand are incorporated in the rheological equations. Models that idealize the stress-strain response of the sand with an elastic perfectly plastic representation, encompass the shear volume coupling characteristic of the sand with a simple linear volumetric strain relationship, consider the elastic component of strain given by the increase in the average normal stress around the cavity, and do not extensively rely on input parameters from laboratory tests, are recommended for the SBPM interpretation. The new cavity expansion model developed in this thesis has all the above mentioned features and solves the cavity expansion problem in a step by step manner for each position of the elasto-plastic boundary. Contrary to Carter et al, 1986 model, the new model adopts different shear moduli in both the plastic and the elastic zones. Nevertheless both models give similar results for Poisson's coefficients in the range of 0.2, suggesting that either one or another model can be efficiently used in the pressuremeter interpretation analysis in sands.

• The new interpretation methodology advocated in this thesis is simple to apply and can be easily incorporated in any personal computer. When this new methodology is used in conjunction with the new cavity expansion model it has the capability to simulate reasonably well the pressuremeter loading curve of controlled chamber tests. Reliable results with an accuracy within 10 % of the reference values were obtained for either undisturbed or disturbed data. It shall be emphasized, however, that several factors are prone to happen during and before the interpretation process, leading to an increase or decrease of the reported accuracy. Factors like the disturbance of the test, the simplifications of the model and the strain range of curve match do play an important role for the final reliability of the derived parameters.

• Both the new and the Carter et al, 1986 cavity expansion models have the ability to reasonably simulate the stress-strain-volume change behavior of medium dense to dense sands during shear. The parameters predicted with the use of these models are extremely reliable if high quality SBPM testing curves are analyzed. The reliability of the parameters with the interpretation of slightly disturbed or disturbed curves is somehow reduced. The Hughes et al, 1977 model leads to conservative estimates of the strength and the stiffness of the sand. This latter conclusion was also obtained by Yu, 1993.

• Cylindrical cavity expansion theory can be adopted for the interpretation of SBPM tests that are carried out to low cavity strains, below $\approx$ 10 %. This is valid for SBPM probes with slenderness ratios above 6. Plane strain solutions can also be adopted, provided that the pressuremeter is expanded in an unrestrained medium where boundary effects do not exist (and the aforementioned conditions apply).

• The friction angle is the least sensitive and most reliable parameter obtained by the curve fitting analysis. Given the fact that the curve match is extremely dominated by the friction angle it is unlikely that a ϕ that differs more than 10 % of the "optimum" value can be obtained with a high quality testing curve. The error built into either Gi or σ_h will be of similar magnitude, and close to the error built in ϕ if the link provided by Equation 2.81 or 2.82 between this latter variable and Gi and G_0 (or Gur) is adopted during the curve fitting process.

• The final error in the predicted results given by the estimation of the constant volume friction angle or the Poisson's coefficient is negligible if an "educated guess" of these variables (between $\pm$ 10 or 20 % of the "real" unknown values) is given.

• The strain range of match adopted between idealized and experimental curves during the fitting process has a fundamental weight for the accuracy of the final results. For undisturbed tests reliable predictions of the soil parameters can be solely obtained with curve matches between cavity strains of 0 to ≈ 10 %. Beyond this strain level the new cavity expansion model can not be used anymore, as the sand surrounding the cavity may start to shear under critical conditions and the cavity expansion deviates from the idealized cylindrical form. For disturbed tests reasonably reliable results can be obtained by matching both field and idealized model curves in the latest stages of the test, between cavity strains of ≈ 5 % to ≈ 10 %. The initial stages of the disturbed tests are considerably affected to render a reliable prediction of the sand parameters. As a general rule, however, it is concluded that for either undisturbed or disturbed data the curve fitting shall be carried out in the latter stages of expansion, between cavity strains of ≈ 5 % to ≈ 10 %. For undisturbed tests, the idealized model curve obtained in this manner will also suffice to represent the experimental behavior in the initial stages of expansion. For highly disturbed tests the curve match shall be solely accomplished with the latest loading points of the field curve (strain ranges very close to ≈ 10 %).

• Using a hyperbolic model to establish a link between the predicted pressuremeter modulus and the unload reload shear modulus of the pressuremeter test (or the low strain maximum shear modulus of the sand) it is possible to optimize the fitting process of slightly disturbed or disturbed data. The link between these variables helps the establishment of the initial value of Gi, as well as its magnitude in the course of the fitting process. The hyperbolic model additionally serves to establish the idealized shear stress-shear strain monotonic "elastic" curve of the sand, when used together with the final curve fitting parameters. This curve allows the prediction of the stiffness ratio of the sand (G/G_0) for each level of induced shear strain. This adds a new dimension to the pressuremeter predicted modulus, turning it relevant to any engineering application where the average level of working strains differs from those imposed by the pressuremeter test.

The interpretation methodology proposed in this thesis is easy to understand and simple to apply. Although simple, the new cavity expansion model can "capture" the most significant aspects of the complex pressuremeter expansion in medium dense to dense sands. The combined use of the new interpretation methodology with the new model leads to the derivation of reliable and significant predictions

of the basic soil parameters from either undisturbed or disturbed data. Nevertheless, it is recommended that only high quality testing curves are used in the new interpretation analysis. This is so because the variability of the curve fitting results is decreased and an easier match can be accomplished.

In this regard the following chapter demonstrates how to enhance the quality of the testing curve, discussing the distinct variables that shall be considered for the optimization of the insertion procedure of the SBPM designed in the University of British Columbia (UBC).

CHAPTER 3.0 INSERTION AND TESTING PROCEDURE FOR THE UBC SBPM

3.1 INTRODUCTION

In this chapter emphasis is placed on the field determination of the UBC SBPM insertion and testing procedure, with attention to the variables that affect the quality of the test. This chapter introduces the new disturbance quantification criteria proposed in this thesis and discusses on the several variables that were gradually changed to enhance the quality of the pressuremeter testing data. With an understanding of the influence of each of these variables the recommended insertion procedure for the UBC SBPM is given.

The conclusions of this chapter concentrate on what has been learned throughout the field testing programme to carry out selfboring pressuremeter tests in which disturbance is minimized.

3.2 FIELD TESTING PROGRAMME

The field testing programme proposed for this thesis required the use of a well known research site, where the soil characteristics were well documented. From the standard sites of the In Situ Testing Group at UBC, a site called "Laing Bridge South" or "Laing Bridge" was selected. It is ideal not only because of its proximity to UBC but also because it has been extensively studied in the past (Sully, 1991 and Howie, 1991). The Laing Bridge site is located in the Fraser Delta, near the city of Vancouver and at the International Airport. The geological characteristics of this delta and geotechnical details of the research site will be presented in the next chapter and only briefly discussed here.

The Fraser Delta is characterized by the presence of sediments deposited in the Quaternary age via alluvial process. The deposition process took place after the last glaciation under a variable sea level and high energy environment. The stratigraphy of the Laing Bridge site is basically comprised of a 2 to 3 m thin surface layer of sandy silt underlain by a stratum of fine to medium sand of 15 to 20 m in thickness which, in turn, is underlain by a thick layer of normally consolidated clayey silt to silty clay. This last layer extends down to the Pleistocene till. The sand deposits of the Fraser Delta were not ice loaded.

The testing programme targeted the 5 to 15 m depth range of this site, where the sand presents a uniformly graded condition. At this depth interval the relative density (Dr) is extremely variable due to the variability of the depositional conditions. In general the Dr increases from 40 to 60 % based on the

piezocone interpreted results. Silt content is low in this range, below 5 %, and the sand is basically composed of medium to fine grain particles with a subangular to subrounded shape.

The field testing programme consisted of 130 SBPM tests, 26 full displacement (FDPM) tests and other in situ tests. These latter additional in situ tests served to characterize the geotechnical features of the site close to the pressuremeter soundings. They consisted of piezocone tests (CPT) with pore pressure sensors at different locations (face, behind the tip and behind the friction sleeve), the standard penetration test (SPT) with energy measurement, and downhole seismic piezocone tests (SCPT). The seismic cone tests furnished this thesis with the evaluation of the (low strain) maximum shear modulus of the sand via downhole shear wave measurements. Both disturbed and "undisturbed" samples (170 mm x 50 mm) were obtained in the sand. These samples were retrieved with a stationary piston sampler denominated ST1 from Rocktest Inc. The samples were used in triaxial tests, in order to obtain the peak friction angles of this sand as well as the values of ϕ_{cv} and ν required by some of the cavity expansion models. The results of these tests are given in Appendix C.

Figure 3.1 and Table 3.1 present the location, the reference names and the general information of the in situ testing programme at the Laing Bridge site. At each test sounding a unique reference name (like SBP01) is given, although in this sounding several pressuremeter tests were carried out at different depths in the profile. As can be seen by Table 3.1, several soundings were performed throughout the experimental stage of this thesis. This is because each of the test soundings had a particular purpose. In each sounding a unique combination of equipment, testing procedure and insertion characteristics was adopted, as detailed in Table 3.2. It shall be noted that the testing depths represent the values measured from surface to the middle section of the expandable portion of the UBC SBPM.

The initial tests from FDP01 to SBP05 were performed to familiarize the writer with both the data acquisition system and the testing / insertion possibilities of this highly advanced probe. They also served to evaluate and modify the recently developed UBC SBPM data acquisition system. The subsequent tests, from SBP06 to SBP19, served to gradually improve both the design and field insertion procedures adopted for the UBC SBPM. This allowed the development of a customized insertion procedure, enhancing considerably the final quality of the derived testing curves. A new methodology was established to assess

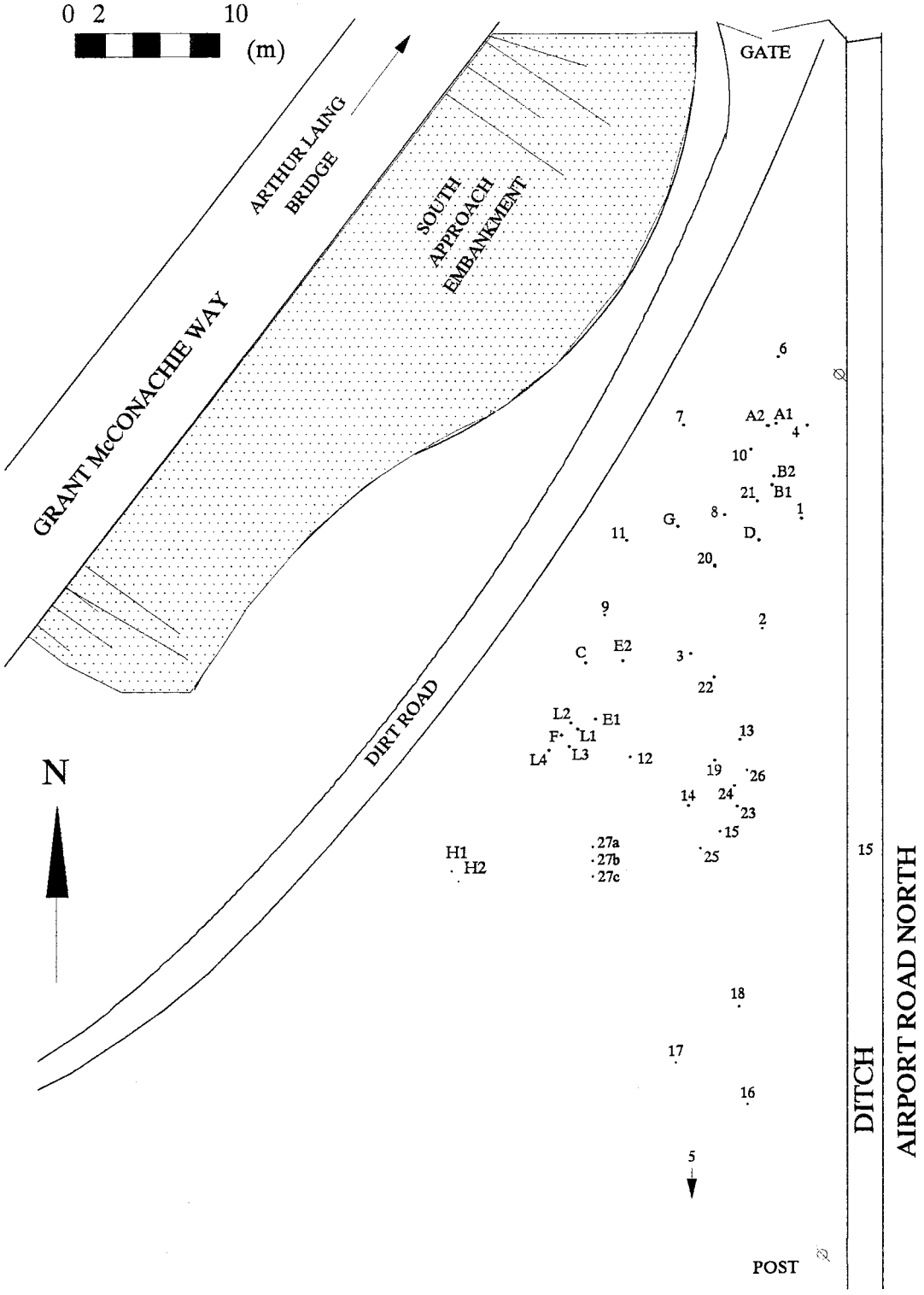

Figure 3.1: Location of In Situ Tests at Laing Bridge Site

SYMBOL	REFERENCE	DATE	TYPE OF IN SITU TEST
1	FDP01	5-1-91	Full Displacement Pressuremeter
2	FDP02	5-17-91	Full Displacement Pressuremeter
3	FDP03	6-1-91	Full Displacement Pressuremeter
4	SBP01	7-17-91	Selfboring Pressuremeter
5	SBP02	8-1-91	Selfboring Pressuremeter
6	SBP03	8-27-91	Selfboring Pressuremeter
7	SBP04	8-30-91	Selfboring Pressuremeter
8	SBP05	10-3-91	Selfboring Pressuremeter
9	SBP06	10-24-91	Selfboring Pressuremeter
10	SBP07	2-5-92	Selfboring Pressuremeter
11	SBP08	2-20-92	Selfboring Pressuremeter
12	SBP09	3-31-92	Selfboring Pressuremeter
13	SBP10	4-8-92	Selfboring Pressuremeter
14	SBP11	4-23-92	Selfboring Pressuremeter
15	SBP12	5-12-92	Selfboring Pressuremeter
16	SBP13	6-9-92	Selfboring Pressuremeter
17	SBP14	6-30-92	Selfboring Pressuremeter
18	SBP15	7-9-92	Selfboring Pressuremeter
19	SBP16	9-24-92	Selfboring Pressuremeter
20	SBP17	10-30-92	Selfboring Pressuremeter
21	SBP18	11-25-92	Selfboring Pressuremeter
22	SBP19	11-30-92	Selfboring Pressuremeter
23	SBP20	4-16-93	Selfboring Pressuremeter
24	SBP21	5-21-93	Selfboring Pressuremeter
25	SBP22	5-27-93	Selfboring Pressuremeter
26	SBP23	6-3-93	Selfboring Pressuremeter
27a,27b and 27c	FDP04, 05, 06	6-16-93	Full Displacement Pressuremeter

PRESSUREMETER TESTS

A1,A2	SC01,SC02	8-21-91	Downhole Seismic Cone-UBC#7
A1,B2	C02,C03	9-12-91	Piezocone Test-HOG#3-PPbhFS
C	DMT01	9-19-91	Marchetti Dilatometer Test
D	C04	9-26-91	Piezocone Test-HOG#3-PPFace
E1,E2	FV01,SPT01	10-10-91	Field Vane and SPT with Energy Measurement
F	SC03	10-17-91	Downhole Seismic Cone-UBC#9-PPFace
G	C05	11-13-91	Piezocone Test-UBC#9-PPface, PPbhFS
H1,H2	C06,C07	9-18-92	Piezocone Test-HOG#3, UBC#9-PPFace, PPbhFS and PPbhTip

OTHER IN SITU TESTS

OBSERVATIONS:
Piezocone (CPT): Sectional Area = 10 cm^2, Diameter (D) = 35.6 mm. Details in Campanella and Robertson, 1981
Pore Pressure Filter: Polypropylene, with thickness of 5 mm
Pore Pressure Measurements:
PPFace (U1) = Pore pressure sensor located at the face of the piezocone, at a L/D = 0.4
PPbhTip (U2) = Pore pressure sensor located behind the tip of the piezocone, at a L/D = 0.9
PPbhFS (U3) = Pore pressure sensor located behind the friction sleeve, at a L/D = 4.9
Downhole Seismic Cone (SCPT): Sectional Area = 10 cm^2, Diameter (D) = 35.6 mm. Details in Campanella et al, 1986

L1 to L4	ST1	March 93	Soil Sampling with ST1 Sampler

SOIL SAMPLING

Table 3.1: Testing Programme at the Laing Bridge Site

TEST SOUNDING	MAXIMUM DEPTH (m)	LANTERN	SETTING[1]	NOZZLE	TESTING DEPTHS (m)	RATE OF INFLATION (kPa/s)	SHOE[2] PLUGGING (%)
FDP01-1MA91	5.3	1	-	-	-	-	-
FDP02-17MA91	6.3	2	-	-	2,3,5	3.9	-
FDP03-1JN91	4.4	2	-	-	2,3,4	3.8	-
SBP01-17JL91	12.4	3	CJ 50mm	A	-	-	-
SBP02-1AG91	10.4	3	CJ 35mm	A	-	-	-
SBP03-27AG91	10.9	3	CJ 30mm	A	2.3,3.3,4.3,5.3,6.3	1.1	50
SBP04-30AG91	14.5	3	CJ 30mm	A	-	-	-
SBP05-3OT91	10.6	3	CJ 20mm	B	2,3,4,5	2.8,3.5,2.8,2.8	50
SBP06-24OT91	15.4	3	CJ 20mm	B	3,4,5	3.3	50
SBP07-5FB92	7.9	4	CJ 20mm	B	6.4	9.6	75
SBP08-20FB92	14.3	7	CJ 20mm	C	5.2,7.1,8.6,11.5,14	9.6	50
SBP09-31MR92	7.6	8	CJ 10mm	C	5.3,7.3	2.5	0
SBP10-8AP92	10	8	CJ 10mm	C	4.5,5.5,6.5,7.5,8.5	2.5,5.0,9.7,9.7,9.7	50
SBP11-23AP92	12.9	9	CJ 10mm	C	5.0,6.3,7.4,8.4,9.4,10.4,11.5,12.5	9.7	75
SBP12-12MA92	16.5	9	CJ 10mm	C	4.4,5.4,7.4,9.4,10.4,11.5,12.5,13.5,15.5	3.4	25
SBP13-9JN92	16.5	9	CJ 0mm	C	4.4,5.4,6.4,7.4,8.4,9.5,10.5 .... 13.5	9.3,5.0.....5.0,9.3	25
SBP14-30JN92	9.8	9	SH	-	4.4,5.4,6.4,7.4,8.4	3.4	0
SBP15-9JL92	7.5	9	SH	-	4.4,5.4	3.4	0
SBP16-24ST92	15.3	10-OLR	CJ -5mm	C	4.3,5.3,6.3,7.3,8.3,9.3,10.3 .... 15.3	1.8	50
SBP17-30OT92	12.7	10-OLR	CJ -5mm	C*	1.9,2.9,4.9,5.9,6.9,7.9 .... 11.9,12.7	3.4	0
SBP18-25NV92	7.3	10-TOLR	CJ -5mm	C*	4.3,5.3,6.3,7.3	3.4	0
SBP19-30NV92	13.3	10-TOLR	CJ -5mm	C*	4.3,5.3,6.3,7.3,8.3,9.3,10.3 .... 13.3	3.4	70 / 0**
SBP20-16AP93	5.2	7	CJ 10mm	C*	4.2,5.2	3.4	50
SBP21-21MA93	13.4	7	CJ 10mm	C*	4.2,5.2,6.2,7.2,8.2,9.2,10.2,11.2 ... 13.2	3.4	75
SBP22-27MA93	13	9	CJ 30mm	C*	4.3,5.3,6.3,7.3,8.3,9.3,10.3,11.3,12.3	3.4	25
SBP23-3JN93	14.7	7	CJ 20mm	C*	4.3,5.3,6.3,7.3,8.3,9.3,10.3,11.3 ... 14.3	3.4	25
FDP04	7.3	7	-	-	1.3,2.3,3.3,4.3,5.3,6.3,7.3	7.0	-
FDP05 - 16JN93	7.3	7	-	-	1.3,2.3,3.3,4.3,5.3,6.3,7.3	2.4	-
FDP06	6.3	7	-	-	1.3,2.3,3.3,4.3,5.3,6.3	0.5	-

* Nozzle C with 4 steel vanes to stop the jetting rod to bend at the dense sand layer

** 70% plugging in the 1st trial (tests at 4.3,5.3 m). No plugging in the 2nd trial in the same borehole.

1- Distance from the edge of the cutting shoe to the tip of the jetting nozzle

2- Sectional area covered by plug material over the total sectional area of the cutting shoe

OLR = Oversized Lantern Retainer,TOLR = Tapered Oversized Lantern Retainer

CJ = Central Jetting System, SH = Shower Head System

Table 3.2: Characteristic of the Pressuremeter Tests Performed at the Site

the influence of the jetting or equipment related variables in order to optimize the insertion procedure. This optimization took in consideration the following key experimental variables:

1. Different steel lanterns.
2. Plugging of the cutting shoe.
3. Different jetting rod positions.
4. Different jetting systems.
5. Dimensional differences along shaft.

Testing soundings SBP20 to 23 were carried out to complement the database gathered to study the influence of the steel lantern on the unload reload shear modulus Gur. Full displacement pressuremeter tests were performed from FDP04 to 06 to assess the effects of variation of the rate of inflation on the derived testing curve.

3.3 UBC SBPM EQUIPMENT CHARACTERISTICS

During the last 13 years the department of Civil Engineering at the University of British Columbia has been involved in research and development with the pressuremeter. In the early stages of this research emphasis was placed on the full displacement pressuremeter test (Brown, 1985, O' Neil, 1985, Campanella and Robertson, 1986, Hers, 1989 and Howie, 1991). The research work carried out with the full displacement pressuremeter was performed with a pressuremeter probe that was an adaptation of the selfboring pressuremeter operated and developed by Dr. Hughes. The focus of the past research has been mainly directed towards the equipment design and the testing methodologies of FDPM with a view to developing a cone-pressuremeter. A broad range of soil types have been used for this purpose using all the available UBC research sites in the Fraser Delta.

With the build up of experience with the FDPM the research objectives of the In Situ Testing Group at UBC have shifted toward selfboring to obtain soil values for correlation to cone data. Early developments evaluated the selfboring installation, membrane protection and the development of a full automated data processing / instrumentation system. This led to the construction of the UBC selfboring pressuremeter in 1988 for Sully's research (Sully, 1991).

The equipment used for the tests of this thesis is a second UBC SBPM probe described by Campanella et al, 1990, with additional modifications in the instrumentation system and the mechanical design. These

modifications led to a highly automated pressuremeter system, capable of full control of the expansion test and simultaneous measurement of several external variables during the insertion, testing and dissipation stages of the probe operation. A full description of the UBC SBPM system is presented in the Appendix A. This includes the detailed description of the UBC testing, pumping and pushing units.

With the development of the UBC FDPM, and later the UBC SBPM, a comprehensive study of the types of steel "Chinese" lanterns (external shield) to protect the pressuremeter was initiated. This section presents the main findings with respect to the use of such steel lanterns in the UBC SBPM.

3.3.1 Steel Lantern Characteristics

In order to mitigate damage to the rubber membrane used in the expandable section of the pressuremeter, given the high frictional forces generated during the selfboring process, a stainless steel lantern is required. It is in general made of flexible and curved steel strips that are longitudinally mounted and riveted or spot-welded together at the ends.

Depending on the design of the lantern the steel strips can be:

1. Overlapped and riveted together with a degree of overlap sufficient to reduce the existing gaps, thus decreasing the soil ingress during the lantern deflation.

2. Composed of butted strips bonded to a secondary rubber membrane, in order to avoid overlapping and soil ingress.

Depending on the disposition and dimensions of the overlapping strips, and position and concentration of welds along the longitudinal strips, different designs can be achieved. These differences in the designs lead to differences in the lantern "membrane resistance" and system "compliance" corrections required to reduce the raw pressuremeter data (see calibration results in Appendix B).

Butted steel strip lantern is the current standard protective sheath adopted by Cambridge In Situ, Ltd. for the English Camkometer. This lantern (defined here as "Camkometer" lantern) was reported by Fahey et al, 1988, and has the great advantage of preventing soil to ingress in between the strips. This added advantage, however, introduces a more sophisticated and difficult to manufacture design. It is consequently much more expensive than the overlapped and welded steel lantern.

Past research with the FDPM (O' Neil, 1985, Brown, 1985) has indicated that depending on the lantern and membrane characteristics distinct corrections must be placed over the measured pressuremeter

results. Commercially available overlapping steel strip lanterns protecting rigid urethane membranes have shown to produce both high and rate dependent membrane resistance corrections. This led to the development and construction of a UBC lantern and membrane system for the UBC pressuremeter in weak soils. A simple rubber membrane and overlapping steel strip lantern are extremely attractive, given the less expensive and quicker ways of replacing the lantern in case of accident in the field. Another reason to proceed with the development of the UBC steel lanterns was related to the maximum circumferential strains that were desired during the pressuremeter expansion. In the early stages of the UBC FDPM (O' Neil, 1985, Brown, 1985) development, emphasis was placed in the expansion of the test up to a circumferential strain of 20 % in order to overcome the disturbance effects generated during insertion. Since the standard Camkometer lantern is designed to achieve a maximum strain of approximately 10 % (Hughes, 1991 personal communication), it did not satisfy the testing requirements of that time. The UBC steel lanterns, on the other hand, could be designed to fulfill this requirement.

Depending of the lantern design, the steel strips can be either clamped at both sides or screwed (or riveted) to a lantern retainer. The steel strips can have distinct dimensions and curvature, and can be grouped together by spot welding in order to increase the resistance of the lantern and its capability to withstand soil intrusion. The individual strips used in the steel lanterns of this research are commercially available 316 stainless steel strips manufactured by Rocktest Inc. for their pressuremeter. These strips have an approximate thickness of 0.3 mm and can be obtained in distinct widths and lengths. The curvature of the individual strips used was lower than the curvature of the UBC SBPM probe. The strips were secured in place by the clamping action of both bottom and upper lantern retainer rings.

Unlike the UBC steel lanterns, the Camkometer lantern accounts for the effects of soil ingress by the adoption of an inner membrane bonded to the steel strip. With the use of 18 flat and narrow strips (12 mm), it is possible to have a final lantern extremely well adjusted to the body of the pressuremeter. The Camkometer lantern is screwed at both ends to steel rings. These steel rings have the freedom to move longitudinally (as the membrane expands) by modifying the original lantern rings to be fully floating.

Figure 3.2 presents the layout of the designs of the UBC steel lanterns, plus the layout of the Camkometer lantern. This figure is complemented by Table 3.3, were the general characteristics of each of the lanterns are presented. The main points of interest are:

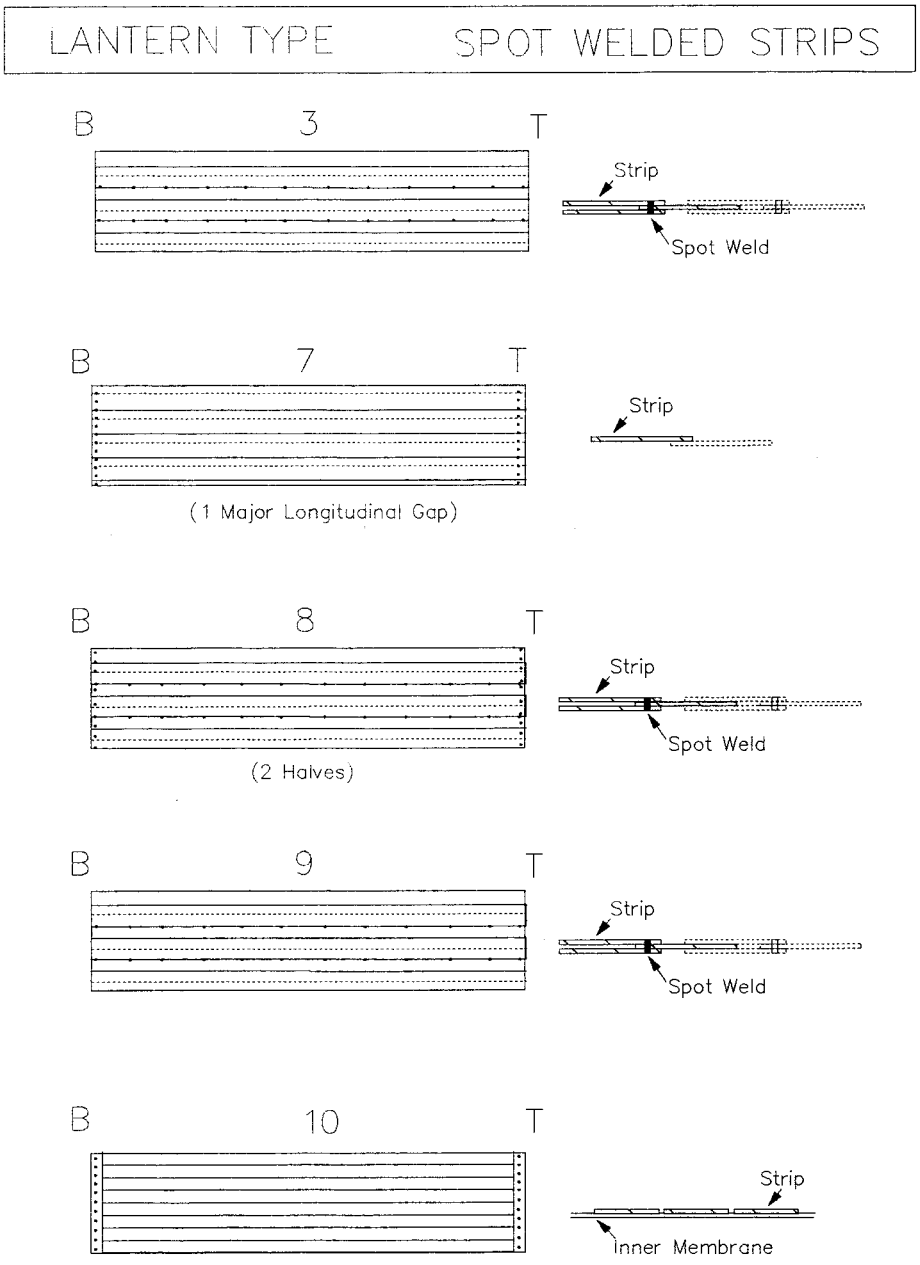

CONVENTIONS:

·	Spot Weld
——— or ·····	Steel Strip Junction or Gap
B	Bottom of Lantern
T	Top of Lantern

OBS:
The bottom of the lantern is near the cutting shoe
Drawings not to scale

Figure 3.2: Steel Lanterns Adopted in the UBC SBPM

LANTERN	STEEL STRIPS (mm)		CHARACTERISTICS OF STRIPS
	LENGTH	WIDTH	
1	540	16	Welded at both bottom and top to a collar 1 row of strips overlapped. Movement in between strips
2	450	16	Welded at bottom to a lantern retainer 3 rows of strips welded together
3	470	24.5	3 rows of strips welded together Movement in between welded group of strips
4	500	24.5	Welded at bottom and top by 2 lines of rivets 2 rows of strips welded together Movement at both major longitudinal gaps
5	470	24.5	Welded at bottom and top by 2 lines of rivets 3 rows of strips welded together
6	480	24.5	Same as lantern 5, with 3 sections instead of 2 halves
7	480	24.5	Welded at both bottom and top 1 row of strips overlapped Movement in between strips
8	470	24.5	Welded at both bottom and top by 1 line of weld spots 3 rows of strips welded together Movement at both major longitudinal gaps
9	480	17.5	3 rows of strips welded together Movement in between welded group of strips
10	545	10	Camkometer type lantern 18 flat steel strips bounded to an inner rubber membrane No overlapping and extremely high flexibility Fully floating lantern retainers

Table 3.3: General Characteristics of the Lanterns Used

1. Lanterns 1 and 2 (not shown) were the original lanterns adopted in the initial design of the UBC FDPM. They have not been used in the present research.

2. Lantern 3 has a similar steel strip configuration to Lantern 2, but has a wider strip which is clamped at both top and bottom by the lantern retainers.

3. Lanterns 4 to 6 were soon discarded for any future use with the UBC SBPM. Lantern 4 proved to be extremely weak for usage in sands, as it was easily destroyed in SBP07. The calibration tests of lanterns 5 to 6 indicated problems of differential expansion along the radius.

4. Lantern 7 has a similar design to Lantern 1, but it is shorter in length and has wider strips. It is riveted at both bottom and top sections and has a major longitudinal gap for assemblage purposes.

5. Lantern 8 has the same design as lantern 3 with 1 row of spot-welds at both bottom and top sections. It constitutes 2 halves that move independently. It has a much higher density of spot-welds than lantern 3.

6. Lantern 9 has exactly the same design as lantern 3, but it adopts a shorter width steel strip.

7. Lantern 10 is the standard Camkometer lantern.

In this thesis a study of the UBC SBPM lanterns was carried out with the analysis of results of several field tests in which specific lanterns (see Table 3.2) were tried out. The influence of the different lanterns on the unload reload shear modulus Gur of the SBPM was investigated, as shown next.

3.3.2 Effects of the Lanterns on Gur

Since Gur is much less affected by disturbance (Jamiolkowski et al, 1985) than any other pressuremeter variable, it was possible to study the isolated effect of the lantern with results from different test soundings (each sounding had a different imposed disturbance, as will be shown later). All the Gur moduli compared here were corrected for compliance effects, as recommended by Fahey and Jewell, 1990 and described in Appendix B.

Generally, Gur will decrease non linearly with increasing stress reduction of the unload loop, or increasing cavity strain amplitude ($d\varepsilon_\theta$) mobilized during unloading. The pressuremeter Gur modulus is also affected by the average plane strain effective stress mobilized at the plastic zone, increasing with an increase in the effective pressure at the cavity wall at the beginning of the unloading stage (P_{cu}).

In order to isolate strain effects in the tests performed herein it was decided to compare only modulus values from loops with similar strain amplitudes. Additional care was taken to not exceed the maximum unloading pressure for each loop (as recommended by Wroth, 1982), thus avoiding reverse plastic failure. In this thesis loops with a degree of pressure unload (dP_u / P_{cu}) of 40 % were used for the comparison. This led to loop cavity strain amplitudes between 0.1 and 0.3 %.

Since the Gur is also pressure dependent only the loops with a P_{cu} close to 360 kPa have been used in the comparison. This value was chosen on the basis of the pressure that was customarily reached at the cavity wall at the beginning of the holding phases before unload. For the testing program with lanterns 3 to 9 the holding phase started with a ε_θ around 2 % whereas for lantern 10 it started at $\approx$ 3 %, in accordance with the "command files" created (see Appendix A).

A holding phase was adopted before the unload reload loop to reduce the creep influence over the measured Gur. A minimum hold time of 8 min. was adopted to yield a final target creep value of 0.01 %/min prior to unloading.

It was decided to directly compare the slope of the loops, i.e. the uncorrected for in situ stress level Gur. The pressuremeter Gur modulus was also compared to the profile of (low strain) maximum shear modulus G_0 at the Laing Bridge site, as determined by the downhole seismic cone. The G_0 modulus is equivalent to a shear strain amplitude of 10^{-4} % with an equivalent mean effective stress equal to the original in situ stresses. Since strain and stress differences of G_0 and Gur will tend to give different moduli for the same depth tested the Gur/G_0 ratio is of interest.

The results of Hughes and Robertson, 1984 for SBPM and FDPM tests in the McDonald's Farm site, Vancouver, indicated ratios of Gur/G_0 from 0.5 to 1.05. These tests were carried out with loops with strain amplitudes in the range of 0.2 to 0.3 % and P_{cu} below 600 kPa. The G_0 was obtained from downhole seismic cone tests. Bellotti et al, 1987 obtained Gur/G_0 ratios from 0.2 to 0.7 for calibration chamber tests with Ticino sand at relative densities of 40 to 80 %. The unload reload loops had an average $d\varepsilon_\theta$ of 0.1 % and P_{cu} below 800 kPa. The G_0's were obtained by resonant column tests on identically prepared specimens. Bruzzi et al, 1986 obtained Gur/G_0 between 0.5 and 0.7 in Po River site, Italy (Borehole 4017), for pressuremeter loops with an average 0.08 % $d\varepsilon_\theta$ and P_{cu} below 740 kPa. The G_0 was measured by cross hole seismic tests.

Thus, the available literature on this subject indicates that for sands with similar densities as Laing Bridge, and pressuremeter tests with P_{cu} and $d\varepsilon_\theta$ in the range of those adopted here, a Gur/G_0 ratio from 0.5 to 1 (closer to 1) is to be expected.

Figure 3.3 presents the Gur results for different testing soundings, in accordance with the field testing program presented before. All steel lanterns, except the no. 10 (Camkometer lantern), gave Gur/G_0 ratios well in excess of 1 suggesting the existence of a mechanical stiffness built into these lanterns. The Camkometer lantern gave Gur/G_0 ratios between 0.5 to 0.9 in agreement with the above published values, valid for loops with similar characteristics as those carried out in this research.

The high values of the measured Gur/G_0 can be directly related to overlapping of strips, i.e., the greater the overlap length (or area) the higher is the Gur/G_0. Because of the lateral stress a frictional resistance is developed at all overlaps and with sand ingress this friction can be further increased. The higher the friction, the stiffer the membrane will be since a relatively high internal pressure increase or decrease is needed to initiate strain. Therefore, only lantern no. 10 (Camkometer lantern), which has no overlapping can be expected to give accurate measurements of Gur without a friction-stiffness component.

This subsection discussed the influence of the adoption of the steel lanterns in the UBC SBPM. The overlap lantern friction had influence on the unload reload Gur modulus. This friction added to the effect generated by the compliance of the lanterns. The friction effect was responsible for very high Gur values for all steel lanterns. The UBC steel lanterns are generally not suitable for modulus evaluation via unload reload loops, unless the friction effect is somehow incorporated in the compliance calibrations of these lanterns. The Camkometer lantern (no. 10) gives reliable Gur measurements as there is no friction effect added to the compliance of this lantern. Therefore, the Camkometer lantern is the one recommended here for usage with the UBC SBPM under optimum insertion procedures.

3.3.3 Method of Installation

It should be noted that in the UBC SBPM system selfboring is achieved by jetting rather than by cutting the soil (as used in traditional SBPM systems). The jetting in sand was introduced by Hughes et al, 1984, and uses high velocity jets of mud to break the granular soil during insertion. Jetting was basically devised to simplify the design of the selfboring equipment as well as to speed-up insertion and

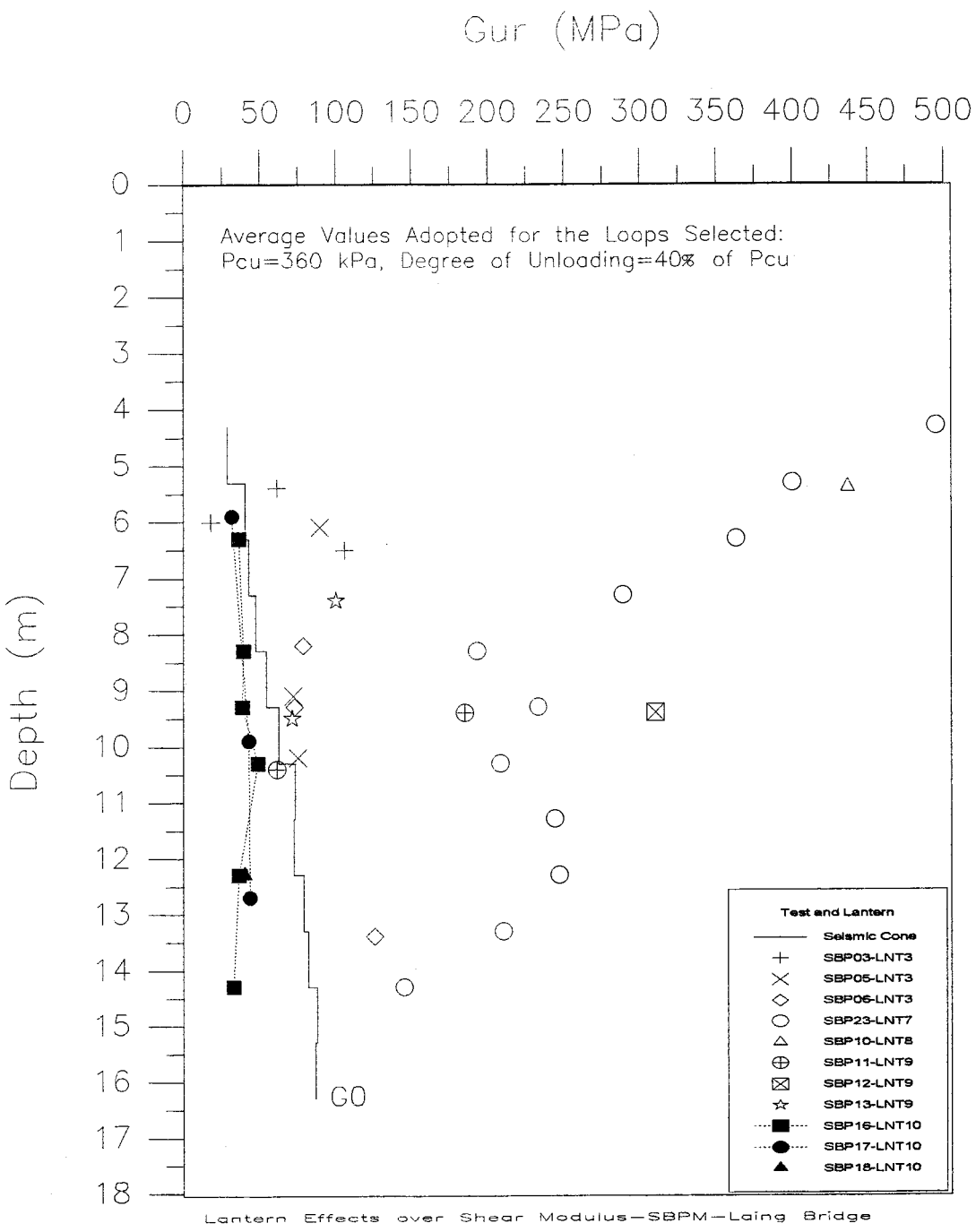

Figure 3.3: Lantern Effects on Gur

improve production. This is particularly important in offshore environments. Although it was conceived almost 10 years ago, jetting still represents a new concept of inserting a SBPM in the ground.

The basic modification of the jetting system in relation to the traditional system is the substitution of the cutter bit by a roller bit (stiff clays) or a jetting nozzle (soft clays and sands) (Clough et al, 1990). The holes in the jetting nozzle constrict the fluid flow, increasing considerably the jet velocity. These jets are generally directed upwards in the direction of the surface, so that washboring in front of the shoe does not happen. The mud shall be pumped at sufficiently high pressure to break the soil during the jetting (or selfboring) process, and, as in the traditional system, a trial and error procedure is required to optimize the insertion variables in a new environment.

Since one of the objectives of this chapter is the definition of the UBC SBPM insertion procedure, i.e., the optimum combination of drilling variables that speeds the insertion and minimizes disturbance, the knowledge of the previous experience gathered by other researchers in this respect is of interest. This experience is reviewed next.

3.4 REVIEW OF INSERTION PROCEDURES

The installation of the selfboring pressuremeter greatly affects the quality and reliability of the derived parameters. The key to the insertion process is to balance the removal of soil in front and inside the cutting shoe with the speed of advancement and other drilling variables, like mud pressure and velocity. The optimum insertion should not considerably alter the stress regime nor the density of the surrounding soil.

3.4.1 Key Insertion Parameters in Clays

Most of the existing experience is related to selfboring in clays (Denby, 1978, Benoit, 1983, Atwood, 1990, Findlay, 1991 and others). With the "traditional" rotating cutter system the parameters that are generally controlled are those that relate to the equipment design (dimensional tolerances, position, rotation and type of cutter bit), to the rig characteristics (pushing force), to the drilling equipment (fluid flow and pressure) as well as the rate of advance.

The pushing force and mud pressure are in general controlled by the driller in charge of the selfboring operation. If the rate of flow return suddenly decreases and the pressure increases it may be possible that the shoe got plugged. In sands the possibility of shoe plugging is less likely to occur than in clays (with

exception to dense to very dense sands) and a sudden increase of flow pressure may be indicative of another effect, most probably the increase of the density of the selfbored sand.

Insertion should be ideally carried out at a constant rate, which requires varying the pushing force to suit the variable soil conditions. The rate of penetration depends on the type of soil selfbored and the characteristics of the cutting or jetting systems. As a starting point Ghionna et al, 1981 suggested a value not greater than 120 cm/min (in clays) to minimize soil disturbance.

The position of the chopping bit is important in the sense as it can influence the stress regime of the surrounding soil. If the cutter is set too far behind the cutting shoe then an increase of the level of stresses in the surrounding soil can occur, whereas if the cutter is set too close to the cutting shoe a reduction of the level of stresses occurs.

Another important aspect is the diameter of the shoe, lantern and overall equipment in relation to the selfbored borehole. Discrepancies in diameter can arise due to equipment imperfections, differential rubber membrane thickness or improper shoe sizes. Law and Eden, 1980 demonstrated that an oversized cutting shoe (or any other section of the SBPM) creates a gap between the borehole and the pressuremeter probe, causing stress relief. An undersized cutting shoe imposes a certain load to the surrounding soil prior to the pressuremeter test.

The jetting system advocated by Hughes et al, 1984 for the SBPM insertion suffers from the same optimization needs as the "traditional" cutting system. The only difference is the fact that the action produced by the rotation of the cutter is replaced by the action of the high velocity jets from each orifice of the jetting nozzle. A comprehensive study program carried out in the University of New Hampshire (Atwood, 1990) with "traditional" and jetting systems demonstrated that the key optimization parameters for jetting in clays are the same as those (related above) of the "traditional" system. The optimum drilling time of the jetting system has been shown to be at least of three times faster than equivalent drilling times of the "traditional" system. The water flows were, however, five times higher than those of the "traditional" system.

3.4.2 Key Insertion Parameters in Sands

In sands the key insertion parameters are the same as those related above for clays, for both "traditional" and jetting systems. This is supported by the experience related by different researchers for SBPM insertion in sands, as presented in Table 3.4.

For the "traditional" system typical penetration rates vary from 1.3 to 4.0 cm/min. The cutter rotation can vary from 40 to 400 rpm, and can be located as far as 5 cm behind the shoe. A non unique combination of drilling variables appears to exist for selfboring in different sites. This is also the case of the few documented jetting insertions (Hughes, 1984 and Howie, 1991). For the jetting system typical penetration rates vary from 24 to 220 cm/min, with mud flows as high as 78 l/min. The jetting nozzle (center of orifices) is in general located between 1 to 2.5 cm behind the cutting shoe. Similar to the case of clays, both the penetration rates and the mud flows adopted for the jetting system are considerably higher than those required by the "traditional" system.

The large variation related for each of the key insertion parameters of Table 3.4 reflects the variable soil conditions (density, stress level, etc.) encountered by each of the authors during the selfboring process. It is concluded, therefore, that the insertion of the SBPM has to be optimized in each new granular deposit. The values related in Table 3.4 serve as a starting point for the establishment of the optimum combination of the drilling variables.

In sands, however, the frictional forces that develop between the soil and instrument can be very high. According to Fahey and Randolph, 1984 the optimization of the insertion procedure in sands is more critical than in the case of clays, as the derived parameters (via traditional methods) are extremely sensitive to the high frictional forces developed in the soil-probe interface, as well as the disturbance generated by improper drilling variables.

In summary, the above review shows that several variables have to be considered in the field optimization of the SBPM insertion. Granular deposits are more prone to disturbance during the selfboring process than deposits composed of fine particles. This is caused by the fact that high frictional forces develop in the soil-probe interface during selfboring in sands, and by the lack of cohesive bonding between the granular particles. For clays there is a relatively large amount of experience to influence the

TEST LOCATION	D_{50} (mm)	Dr (%)	C / N[1] POSITION (cm)	MUD[2] FLOW (l/min)	CUTTER TYPE	RATE OF ADVANCE (cm/min)	REFERENCE
Pacifica Site, USA Lightly Cemented Sand English Camkometer	NA	NA	0.6	4300 (air)	Spade Type	0.5-1.3	Bachus, 1983
Po River Valley, Italy Slightly Aged Medium Dense Sand, OCR = 1 to 2 English Camkometer	0.2-0.4	NA	1.5-4.7	10-16	Helical Type	2.0-3.5	Bruzzi et al, 1986
Norwegian Dense Granular Deposits English Camkometer	NA	NA	3.0-5.0	NA	Spade Type	3.0	Lacasse et al, 1990
McDonald's Farm, Canada Loose to Dense Sand Hughes Pressuremeter	0.1-0.6	40-60	NA	NA	Spade Type	2.0-4.0	Robertson, 1982

TRADITIONAL SYSTEM

McDonald's Farm, Canada Loose to Dense Sand Hughes Pressuremeter	0.1-0.6	40-60	1.0-2.5	20-43	Jetting Nozzle	42-220	Hughes, 1984
Lulu Island, Canada Medium Dense Sand Hughes Pressuremeter	0.13 to 0.17	50-60	2.0	54-78	Jetting Nozzle	24-90	Howie, 1991

JETTING SYSTEM

1-Rotating cutter (traditional system) or jetting nozzle (jetting system)
2-Mixture of water and bentonite mud

Table 3.4: Successful SBPM Drilling Variables in Sand

establishment of guidelines with respect to the optimum drilling variables. Less experience exists for insertion in sands, principally with the jetting system. For any of the cases a trial and error procedure has to be established at each new site to properly define the optimum combination of drilling variables.

The main effect of disturbance on the testing curve is the change of its shape in relation to the "undisturbed" shape. Since the "undisturbed" shape is unknown, it becomes difficult to access the degree of disturbance present in the curve due to the improper insertion process. If the numerical degree of disturbance is known after each field trial with the SBPM it becomes easier to readjust the drilling variables towards the "optimum" general combination. Several testing results originating from different field trials can be then successively assessed to indicate which combination of drilling variables minimizes the disturbance of the testing curve. In order to do that a procedure to numerically quantify the disturbance of the testing curve must exist. This procedure is introduced next.

3.5 NUMERICAL QUANTIFICATION OF DISTURBANCE

The major benefit from an optimization routine carried out in the field is the faster selection of the optimum drilling variables, which depends on the subjective opinion of the pressuremeter operator in regard to defining the "undisturbed" testing curve. As a basis for what can be defined as "undisturbed", it is common to use the accumulated experience reported in literature. This experience indicates that high quality curves in both sands and clays are invariably characterized by a continuous and smooth curvilinear shape throughout the strain range of the test.

Denby, 1978 and Benoit, 1983 observed that disturbance in pressuremeter tests in clays tends to "flatten out" the initial stage of the pressure expansion curve, leading to an almost linear shape. Disturbance can be present in the pressuremeter curve in different amounts, and hence different disturbed shapes will exist. Wroth, 1984 noticed that highly disturbed tests on sand can be easily determined by the visual inspection of any pressuremeter operator. In this extreme case there is no dispute whether the curve is "undisturbed" or just "slightly" disturbed.

Robertson, 1982 noted that there is no generally recognized criterion for the assessment of the quality of SBPM testing curves. In general a subjective approach by the visual inspection of the testing curve is used. Based on his experience with the SBPM Robertson, 1982 tried to compile the basic requirements that would serve as a guide for the selection of "undisturbed" testing curves. These requirements are:

1. No inflection point near the beginning of the curve.

2. All arms move in a consistent manner leading to lift offs that are close together in strain.

3. The pore pressure measured before the test is close to the hydrostatic value.

However, these requirements are broad and undoubtedly different pressuremeter operators will still have a different approach to classify the disturbance of the pressuremeter curve. The major drawback of the visual inspection routine is the lack of a recognized "undisturbed" reference curve. General statements as those above can lead to different conclusions, because of each pressuremeter operator's concept of what shall be the smoothness and roundness of the "undisturbed" curve.

Findlay, 1991 presented a methodology to overcome the pitfalls above and numerically quantify the disturbance of pressuremeter tests in clays. He compared the shape of pressuremeter curves, obtained from tests with various degrees of disturbance, to an empirical coefficient that was related to the initial slope of the testing curve. This coefficient was related to the slope developed within 1 to 5% cavity strain, since the findings of Benoit, 1983 and Denby, 1978 demonstrated that disturbance is mainly concentrated in the initial stage of the test. Findlay, 1991 defined typical disturbance values for "undisturbed" SBPM and (disturbed) push-in pressuremeter tests, in order to guide future expected coefficients in each case. The major drawback, however, was the fact that the obtained range of coefficients was site specific, and therefore typical undisturbed values for one particular clay deposit couldn't be used at a different site. This drawback removes the universality of Findlay's suggested approach, and may not lead to a much better criteria than the one previously used for clays and sands based on a visual inspection of the curve.

On the other hand, with the concepts stated by Findlay, 1991 and the fitting technique advocated in the previous chapter, one can formulate a disturbance criteria that could be universally applicable. With a fitting technique the reference "undisturbed" curve is known, since it is defined by the idealized model curve. It should be noted that this curve will differ for each site and depth in accordance with the fitted soil parameters (σ_h, Gi, ϕ). The higher the disturbance the higher will be the influence in the initial stage of the field curve, and hence the greater the deviation from the idealized ("undisturbed") model curve. If this initial deviation, or differential area as presented in Figure 3.4 can be numerically quantified, than it should be possible to quantify the disturbance of the test. Similar to the empirical coefficient of Findlay, a

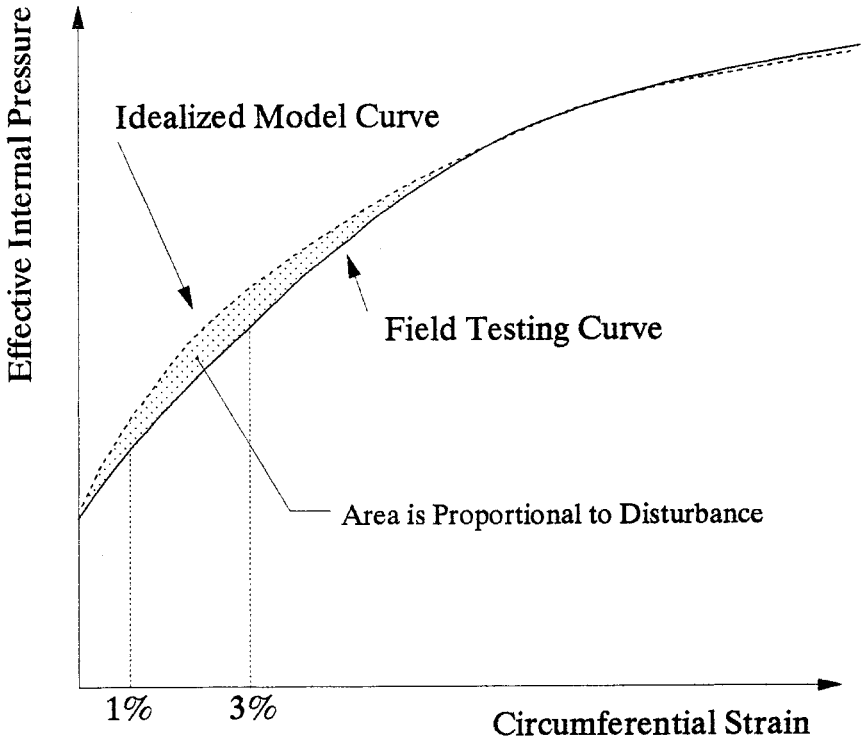

Figure 3.4: Disturbance Evaluation of SBPM Testing Curve

numerical coefficient of disturbance (CD) was devised for this research, which measures the average deviation at 1 and 3 % circumferential strain for a testing curve. This range is based on the experience of the writer and literature findings regarding the zone most affected by disturbance. It is proposed that the new CD parameter is defined by the following equation:

$$CD = \left(\left| \frac{Pci\,(1\%) - Pc\,(1\%)}{Pci\,(1\%)} \right| + \left| \frac{Pc\,i(3\%) - Pc\,(3\%)}{Pc\,i(3\%)} \right| \right) x \frac{1}{2} \times 100 \quad (\%) \qquad (3.1)$$

where:

Pci is the idealized cavity pressure by the model at the circumferential strain given;

Pc is the equivalent testing cavity pressure at similar strain.

The CD value varies from 0 % (fully undisturbed) to 100 % (highly disturbed) for SBPM tests in which, in general, the idealized model curve stays above the field curve. Since CD is defined as a normalized ratio it can be used with any of the existing cavity expansion models discussed on Chapter 2. The use of a stress ratio, rather than a direct measurement of an area provides an analogous yet simpler evaluation of CD in the field and thus leads to a faster derivation. With a computer and the QuickBasic program mentioned in the last chapter, the CD can be easily obtained with the direct evaluation of the fitted curve on the screen of the computer.

It can be noted that CD is not an independent variable, but rather a variable that depends on the strain range of curve matching. As a general rule, it is recommended that the curve fitting is performed between ≈ 5 to ≈ 10 % circumferential strain for either undisturbed or disturbed data. Once the model curve is matched a value of CD can be devised. It is suggested here that for CD's below 10 % the field curve can be considered of high quality ("low" disturbance). For CD's from 10 to 30 % the field curve is of good to medium quality ("medium" disturbance). For CD's higher than 30 % the quality of the field curve is low ("high" disturbance). As presented in Table 2.6 the reliability of the predicted parameter is expected to be proportional to the quality of the curve, hence the numerical value of the coefficient of disturbance. For CD's lower than 10 % the reliability of the derived parameters is high. The reliability of "medium" quality

field curves may still be high, although reduced to some extent. The reliability of field curves with CD's above 30 % is probably low.

An initial assessment of the usefulness of the numerical quantification of disturbance is given in Figure 3.5. This figure presents the calculated CD of one of the testing soundings (SBP13) in which shoe plugging occurred to an extent of 25 % of the cross-sectional area of the cutting shoe. In the same plot is shown the plane strain ϕ by both the traditional log-log approach of Hughes et al, 1977, and the curve fitting methodology discussed in the last chapter (with Hughes et al, 1977 model). It can be seen that disturbance is not homogeneous throughout the profile, but it varies with the characteristics of the soil tested and insertion difficulties. The data suggests that all the ϕ determinations by the log-log plot were considerably influenced by the initial disturbance of the test, except at 8.4 and 10.5 m for which the CD was only 2-4 % and the log-log ϕ agreed with the curve fitted ϕ. The data also indicates that the curve fitting technique is less disturbance sensitive than the traditional log-log interpretation approach, as the variability of the curve fitted ϕ's is low. This finding substantiates the comments above regarding the reliability of soil parameters predicted with slightly disturbed ("medium" disturbance, 10 % < CD < 30 %) curves, and the usefulness of the CD coefficient.

3.6 INSERTION PROCEDURE FOR THE UBC SBPM

A mud flow and penetration rate that was close to the literature "optimum" values of Table 3.4 was adopted. For this research an average mud flow of 20 l/min (5 to 6 gpm) was adopted during insertion. This allowed an average penetration rate of 50 cm/min (0.8 cm/s) throughout the testing depths up to the 10 Tonne capacity of the pushing rig. Since the pushing and pumping units shared the same source of hydraulic power from the research truck (see Appendix A), after the attainment of the operational capacity of the rig "extra" hydraulic power had to be obtained at the expense of the pumping power of the system. In general, in the densest layers of the site (below 8 to 9 m depth) the rig capacity was reached. Figure 3.6 presents a typical output of the "sounding" file of the pressuremeter. It demonstrates that beyond this depth there was a slight decrease in the flow rate employed, followed by a variation of the penetration rate around the mean value of 50 cm/min. This variation was not excessively high and all the testing soundings used in the comparisons of this thesis suffered from similar problems.

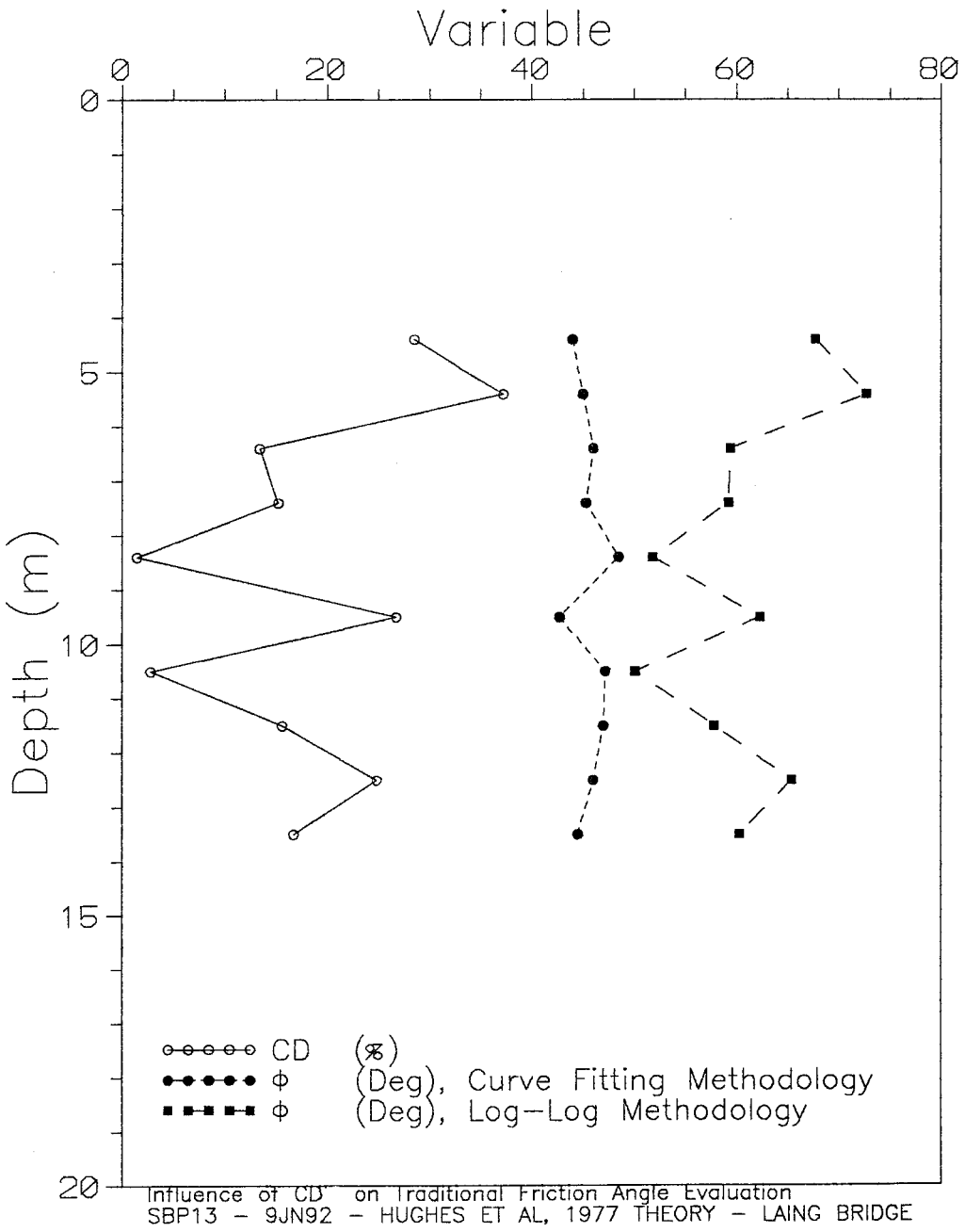

Figure 3.5: Practical Numerical Assessment of Disturbance

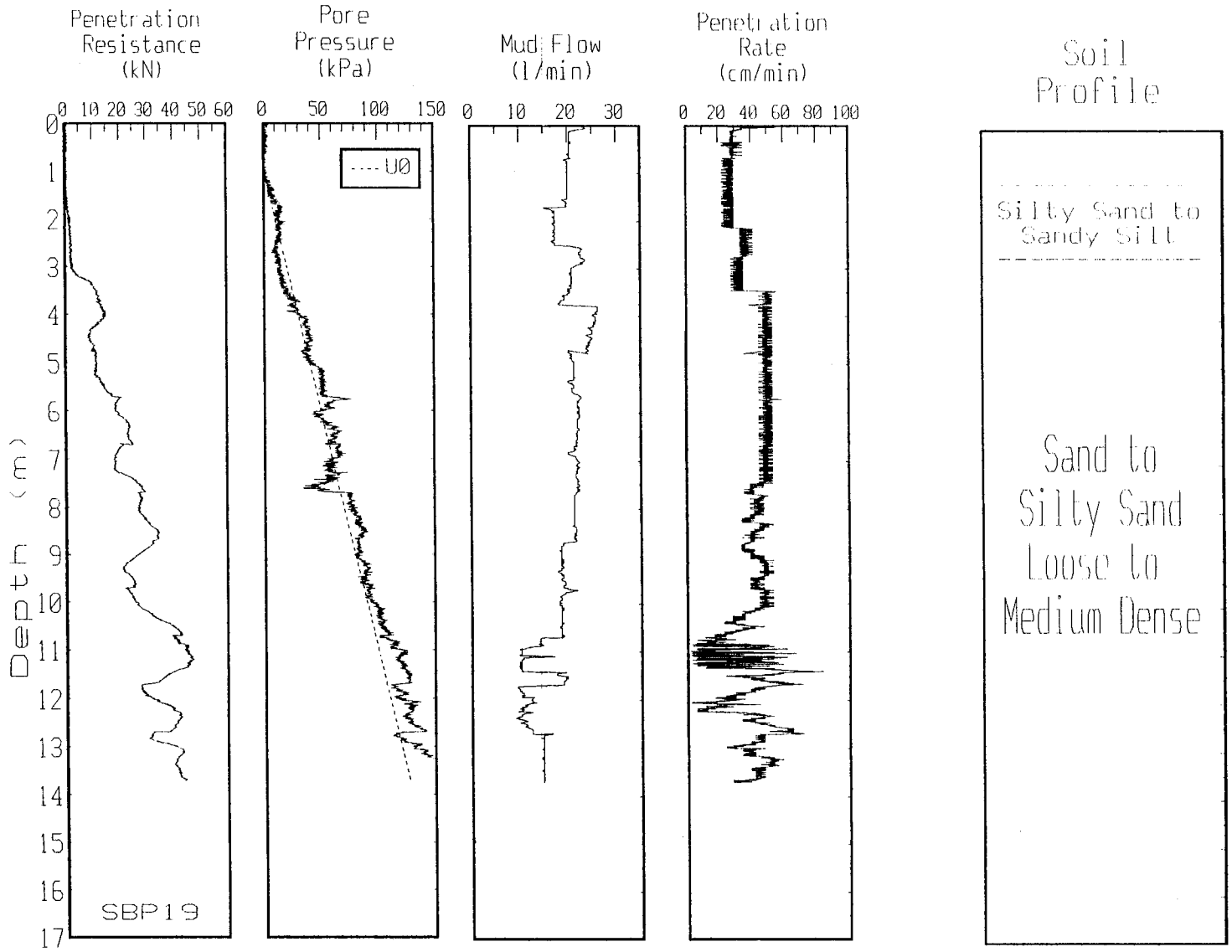

Figure 3.6: Typical Variables Obtained with the Sounding File of the UBC SBPM

Sounding results like the ones of this figure were used in conjunction with the field characteristics of the test (shoe plugging, equipment characteristics, settings, etc.), and the CD defined above to draw conclusions regarding the insertion quality. This quality controls the amount of disturbance that is imposed in the pressuremeter testing curve.

Based on the experience of the writer throughout the experimental testing stage, the insertion quality is a function of the characteristics of the SBPM probe (type of jetting system and dimensional tolerances), the drilling variables (position of the jetting rod, mud flow and pressure, rate of advance) and the unexpected occurrences in the field (as the plugging of the cutting shoe). The influence of each of these variables upon the disturbance generated during selfboring will be assessed in the following subsections. This aids in the development of the best (insertion) procedure to reduce the likelihood of disturbance in the UBC SBPM results. The best insertion procedure at the Laing Bridge site is the one that leads to testing curves in which the CD parameter is below 10 %.

3.6.1 Shoe Plugging

The existence of two layers with differing soil characteristics (see Figure 3.6) in Laing Bridge site would require different jetting variables during insertion, i.e. distinct jetting flow velocities would be needed to selfbore the surficial silty sand to sandy silt material and the underlying clean sand strata with minimum disturbance. This was not possible because the UBC SBPM pumping unit was not capable of producing the high flows for "optimum" insertion in fine-grained soils (see Clough and Denby, 1980, Lacasse and Lunne, 1982 and Atwood, 1990). As such, partial plugging of the shoe with the surficial fine-grained material was invariably observed in many of the SBPM soundings. This section addresses the likely effect of partial plugging during selfboring, and how the insertion procedure can be varied to deal with this problem.

The total plugging of the shoe can, as a first approximation, be visualized as the penetration of a full displacement in situ device into the soil. Full displacement pressuremeters (or piezocones) have a solid cone apex of 60° in front and in the position of the cutting shoe.

The penetration of a piezocone in a granular medium is a very complex phenomenon and difficult to analytically model. When the tip of the cone passes through an element of sand, very high stresses are developed, which is followed by a substantial unloading of stresses as the cone proceeds further and the soil

element passes the shoulder of the cone. Moreover, experimental results of Chong, 1988 indicate that loose and dense sands tend to dilate after the insertion of a piezocone.

Hughes and Robertson, 1985 have qualitatively discussed the effects of the cone passage in sands and presented arguments regarding the possible stress history of the elements of soil after the cone passage. As the cone approaches any element of soil the stress path of this element will move towards the failure line of the material, and then will follow it. Effective radial stresses as high as several orders of magnitude greater than the original lateral stress can be hypothesized at this stage. The stress path will follow the failure line, pushing the yield surface until the soil element passes through the shoulder of the cone. At this stage the stress path follows an unloading path below the yield surface, and reverse failure (with the circumferential stress as the major principal stress) is likely to occur. All the elements of soil will follow a similar stress path, but elements that are located at a greater distance from the probe shaft will be stressed to a lower extent. An annulus of soil with high residual stresses will exist beyond the soil elements close to the shaft, probably due to arching effects. Based on speculations of Withers et al, 1989 a zone of intense shearing and discontinuities may also exist between the probe shaft and the end of the induced plastic zone.

Therefore, it can be expected that extremely complex stress, density and strain histories will be imposed in the soil in the event of total (presumably extending to partial) plugging of the cutting shoe. The disturbance mechanism in the SBPM is further complicated by the fact that plugging will not occur evenly around the shoe surface, and therefore the disturbance effects will not be evenly distributed in the soil around the equipment.

Shoe plugging effects were considered in the comparison of two test soundings, 5 m apart (SBP11 and SBP12) in which the plug in the field, estimated by visual inspection of the shoe after withdrawal of the probe, varied from 25 to 75 % of the total cross-sectional area of the cutting shoe. Similar equipment and jetting variables (rate of penetration and flow) were adopted for these two tests. Typical averaged (of the 6 strain arms of the UBC SBPM) testing curves are compared in Figure 3.7 for one testing depth. It can be noted that the larger the plug the larger will be the lift off stress (indicating high residual stresses set up at the soil-probe interface), as well as the CD parameter. The post lift off stage of the curve will reflect the overall loose condition of the soil surrounding the SBPM, after the passage of the partially plugged SBPM.

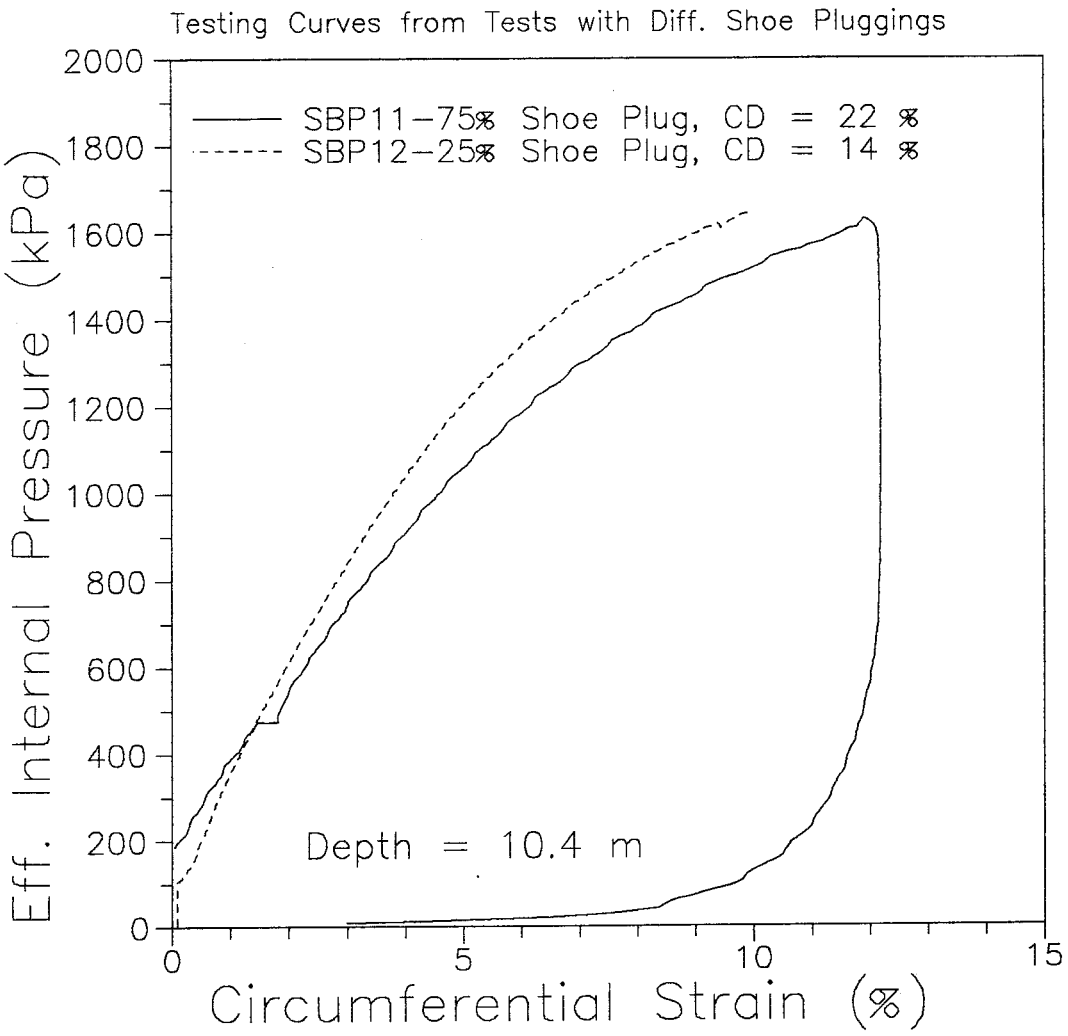

Figure 3.7: Typical Comparison of Curves from Tests with Different Shoe Pluggings

The influence of plugging in the original soil conditions can be also "picked up" by the total (tip plus friction in the lantern) load measured by the load cell of the UBC SBPM. The results of Figure 3.8 suggest that there is an increase of the penetration resistance with the increase of the percentage of shoe plug. As well, there is a correspondence between the increase in CD with the increase of penetration resistance.

This subsection discussed the effect of shoe plugging on the results. It is suggested that the higher is the percentage of shoe plugging, the higher will be the load imposed by the cutting shoe in the virgin ground during selfboring and hence disturbance (or CD). To reduce plugging of the shoe the following procedures were found to be effective:

1. Since the plugged soil was always lightly plastic and fine, the insertion procedure in that material was changed to a slower rate of penetration ($\approx$ 25 cm/min) and sometimes a higher pumping rate ($\approx$ 30 l/min) (more close to values obtained by Atwood, 1990 and others in clay). The slower rate can be noted in the sounding profile of Figure 3.6.

2. It was found necessary to prebore through the surface 1 to 3 m with a large dummy cone or with a push-in casing to by-pass the fines responsible for plugging.

3. The jetting rod position was gradually optimized, as will be discussed next.

3.6.2 Jetting Rod Position

The jetting rod position and the mechanical design of the nozzle are important variables that have to be optimized for the SBPM insertion process. They are used in conjunction with the specified mud flow and penetration rate to reduce the amount of tip load in virgin ground during selfboring, which in turn reduces the likelihood of soil plugging.

Wroth, 1982, observed that the amount of disturbance that can be generated in the soil is strongly related to the position of the cutter bit in traditional SBPM systems. If the cutter or the jetting nozzle (assuming that similar disturbance effects would operate in both selfboring systems) is placed too far behind the edge of the cutting shoe then a temporary plug is formed inside the shoe. In contrast, if the cutter or jetting nozzle is placed too close to the edge of the cutting shoe then washboring or stress relief may occur ahead of the shoe. A balance will exist between these 2 extreme positions and may be obtained in a trial and error field optimization, as commented previously.

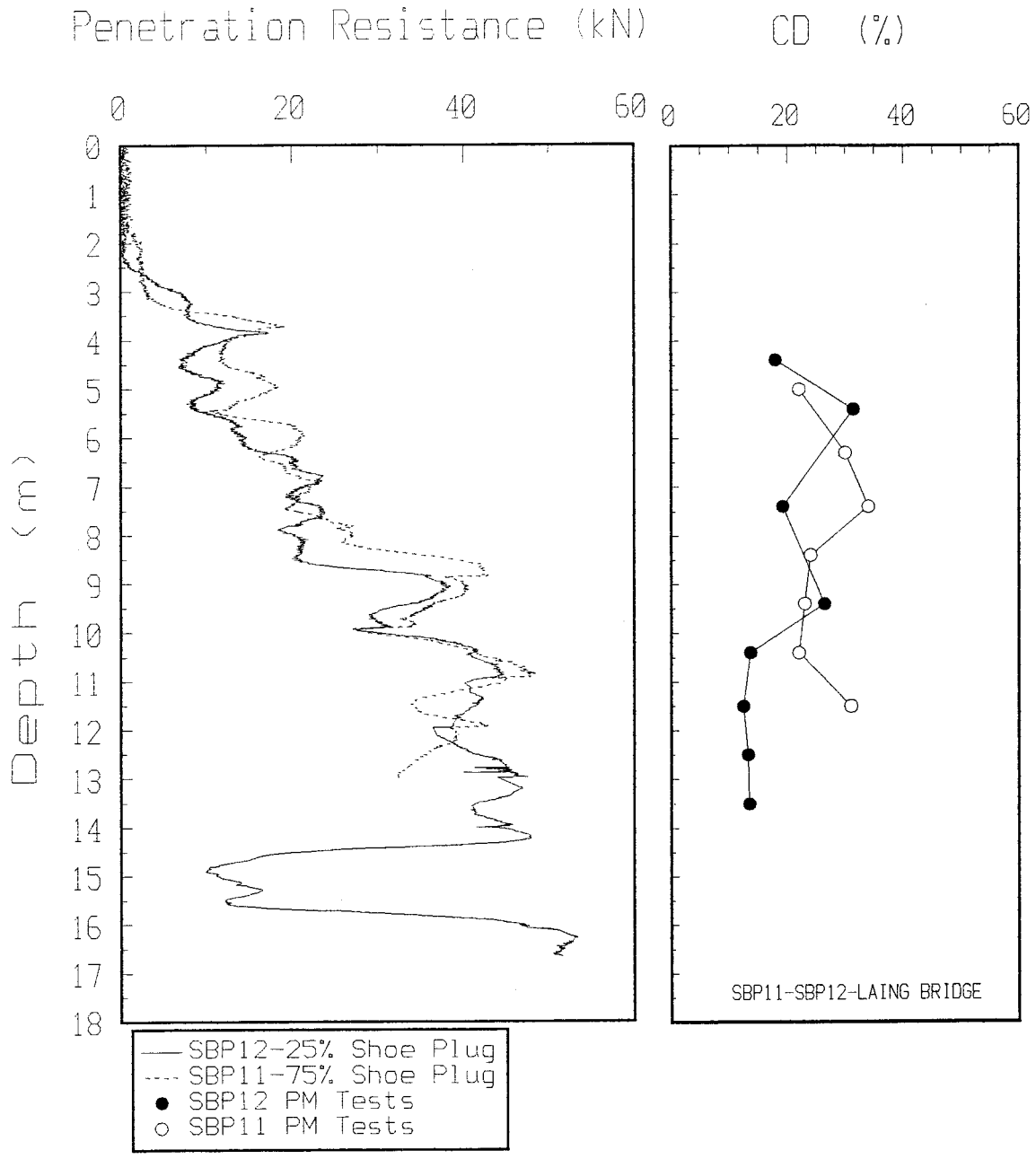

Figure 3.8: Relationship Between Disturbance and Penetration Resistance

In this thesis the optimum setting of the jetting rod (or nozzle) of the central jetting system was refined by the gradual optimization of the insertion routine, in order to reduce the amount of disturbance to a target CD of 10 %. Since one of the major problems during selfboring at the Laing Bridge site was the plugging of the cutting shoe, the optimum rod position assisted in the reduction of this occurrence.

Table 3.5 and Figure 3.9 present the trial and error process to optimize the rod position and the design of the jetting nozzle. The optimum rod position was achieved simultaneously with the process of definition of the insertion procedure for the UBC SBPM. Throughout this process, the gradual improvement of the number and diameter of the orifices of the jetting nozzles, and the gradual decrease of the jetting nozzle distance in relation to the edge of the cutting shoe helped to reduce the likelihood of shoe plugging. Optimum shoe plugging percentages of 0 % were obtained only after SBP17, as observed in Table 3.5. The optimum jetting rod position was obtained with the nozzle tip located at -5 mm (tip outside the shoe) in relation to the cutting shoe. This leads to a distance of 18.4 mm between the centerline of the orifices of the jetting nozzle and the edge of the cutting shoe. This value is in between the values reported by Hughes, 1984 and Howie, 1991 in Table 3.4.

Figure 3.9 demonstrates that with the gradual optimization of the jetting rod position there was a considerable reduction of the amount of disturbance generated during selfboring. The quality of the testing curves increased from SBP01 to SBP19, such that in testing soundings SBP18 and 19 the majority of the curves presented "low" disturbance characteristics based on the CD parameter. The most relevant aspects of the comparison presented in Figure 3.9 are given by:

1. The testing soundings considered herein are the ones in which the central jetting system for selfboring was used. The shower head system (both systems are presented in Appendix A), adopted in SBP14 and 15, effectively eliminated plugging yet still yielded pressuremeter curves with "medium" disturbance characteristics due to overcoring during insertion.

2. All the testing soundings of this figure presented a variable effect of disturbance along depth. Most of the peaks of disturbance tend to be aligned at similar depths for all testing soundings. One example is between depths 9 to 9.5 m. In this range the highest CD of SBP19 is obtained. A careful inspection of the sounding results of this testing sounding, expressed in Figure 3.6, reveals that at this depth the measured

TEST SOUNDING	ROD POSITION[1] (mm)	NOZZLE TYPE	SHOE PLUGGING[2] (%)
SBP01	50	A	NA
SBP02	35	A	NA
SBP03	30	A	50
SBP04	30	A	NA
SBP05	20	B	50
SBP06	20	B	50
SBP07	20	B	75
SBP08	20	C	50
SBP09	10	C	0
SBP10	10	C	50
SBP11	10	C	75
SBP12	10	C	25
SBP13	0	C	25
SBP14	SH	--	0
SBP15	SH	--	0
SBP16	-5	C*	50
SBP17	-5	C*	0
SBP18	-5	C*	0
SBP19	-5	C*	0

OBSERVATIONS:

SH = Shower Head Jetting System, NA = Not Available
1-Distance from the edge of the cutting shoe to the tip of the jetting nozzle. Central jetting system
2-Sectional area covered by plug material over the total sectional area of the cutting shoe

NOZZLE TYPE:

A= 8 holes of 3.55 mm (diameter) @ 21.3 mm from nozzle tip
B=3 holes of 5.7 mm (diameter) @ 20.6 mm from nozzle tip
C=4 holes of 4.0 mm (diameter) @ 23.4 mm from nozzle tip
C* = Nozzle C with 4 steel vanes to reduce bending of the jetting rod during insertion

Table 3.5: Establishment of the Optimum Jetting Rod and Nozzle Type

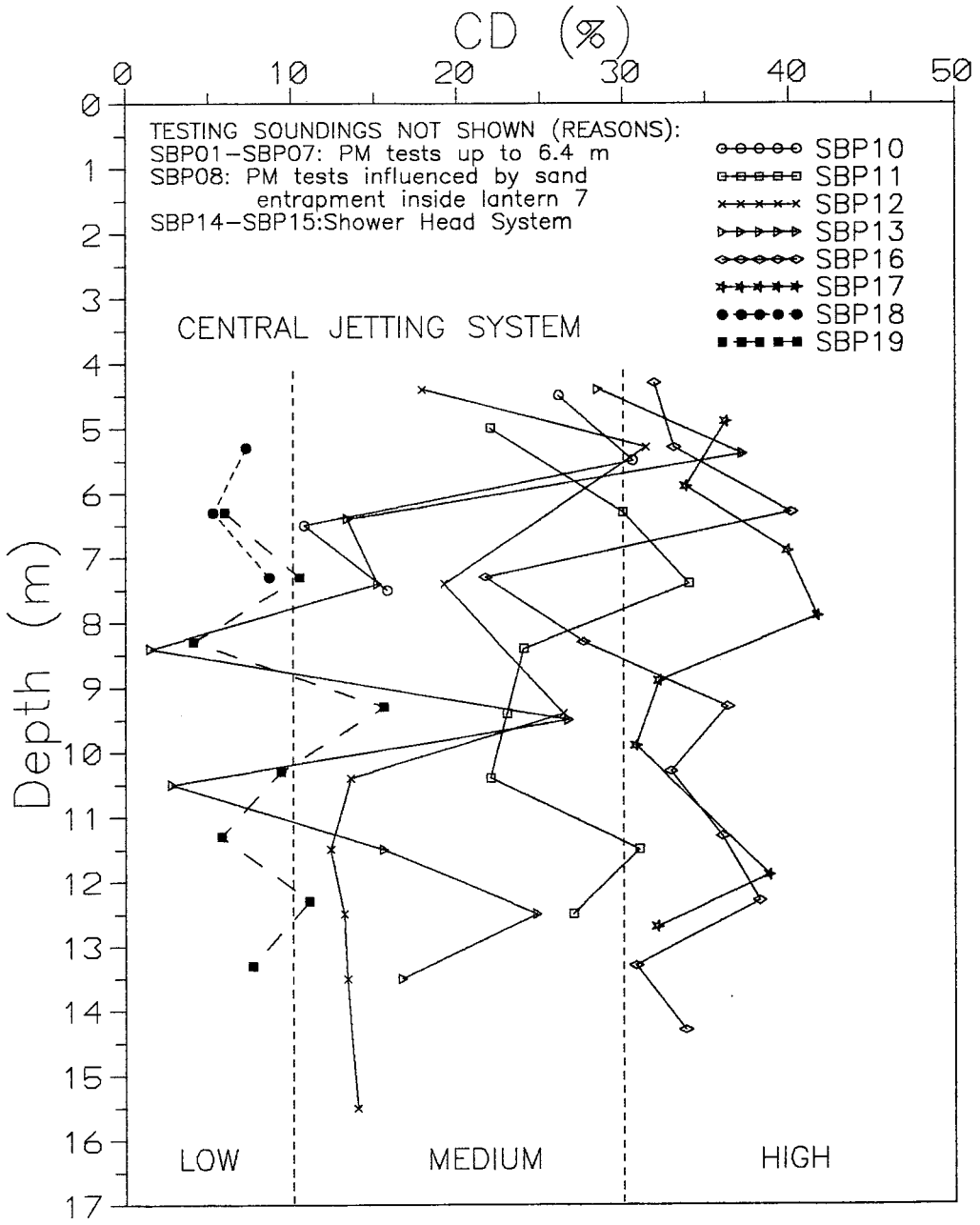

Figure 3.9: Comparison of Coefficient of Disturbance for Different Testing Soundings

penetration resistance presented a trough. This was most probably caused by the presence of a loose sand layer at that depth. Thus, it may be speculated that the CD variability with depth is caused by the adoption of a single combination of jetting variables along a randomly variable stratigraphic profile. The looser the layer being selfbored, the higher will be the disturbance. The review presented in section 3.4 indicates that it is difficult to specify a unique "optimum" combination of all jetting variables because of density, strength and general variability of the soil conditions of most natural deposits with depth.

This subsection emphasized the importance of the numerical assessment of disturbance to properly evaluate the best combination of the jetting variables in the optimization process of the insertion procedure. The CD parameter, together with all the sounding measurements of the UBC SBPM system, allows a better understanding of the disturbance process and the probable influence of some of the key variables in this context.

The next subsection will briefly focus on the results obtained with another jetting system, which was tried out in the test soundings SBP14 and 15.

3.6.3 Jetting System

An alternative design for the jetting system was devised by Campanella et al, 1990 in sands and J. Benoit (stated in Findlay, 1991) in clays. In both cases a "shower head" (SH) system was designed. This system jets the fluid through radial orifices at the inner wall of the cutting shoe. The center jetting rod is removed and the jets are directed upwards to the center of the shoe. It has the attractive feature of allowing jetting in deposits with particles of slightly higher diameter than those that are usually selfbored by the traditional central jetting system (CJ). Also, the SH system is very effective at eliminating blockage. On the other hand the position of the jets can not be easily adjusted, and the SBPM requires a newly manufactured cutting head each time a new jet location is tried.

Since its initial conception by Campanella et al, 1990, no conclusive opinion regarding the usefulness of this system was developed. Therefore, two test soundings (SBP14 and 15) were carried out with the new shower head system. In both soundings similar field problems were noticed. as summarized below:

1. During the initial stages of the selfboring process there was a large amount of sand flushed out of the borehole with the returning mud. This amount was much higher than the "typical" amount observed by the writer in the nearby SBP13 (CJ system) borehole or any other testing sounding with the CJ system. It

was also noticed that the SH was totally clean after withdrawal of the probe from the ground. Both observations may indicate that overcoring occurred with this system.

2. Continuous pumping at a very low rate (≈ 1.9 l/min or 0.5 gpm) during pressuremeter expansion tests was started from SBP12 to reduce plugging of the orifices of the jetting nozzle. With the shower head it was difficult to keep the mud level at the surface constant (the mud level shall be kept greater than the water level to help prevent borehole collapse), whereas with the CJ system the above rate proved sufficient to keep the mud level constant. With the SH a high average pumping rate of 3.5 times the previous cited value was required. This also suggests that the mud was being lost in front of the cutting shoe (due to overcoring), and therefore it was not returning back to the surface.

The consequence of overcoring is the opening of a large void space in the zone surrounding the pressuremeter shaft. This space will eventually be filled by loose sand once the selfboring process is terminated and the soil around the probe starts to settle. Therefore, underestimation of the soil parameters may occur with the interpretation of the pressuremeter curves using this jetting system.

In conclusion, more research is still needed with this new and promising jetting system. The present design and procedures (mud flow and rate of advance, as specified before) cause overcoring in front of the shoe during selfboring, which is accompanied by a general "loosening" of the soil surrounding the SBPM. For the current research SH development was abandoned after SBP15 because of the need for redesign and technician support, and emphasis was placed in the development of the insertion procedure with the CJ system. It is believed, however, that with a modified design and a SBPM insertion with less flow and at a faster advance rate it would be possible to overcome the overcoring problem. For instance, in clays Findlay, 1991 demonstrated that the shower head can be as reliable as the traditional central jetting system.

3.6.4 Dimensional Differences Along Shaft

The use of the Camkometer lantern (no. 10) introduced a possible source of disturbance generation. Since this lantern was not originally designed for the UBC SBPM unit, an adaptation of the clamping system had to be devised. This adaptation led to the design of oversized floating rings (lantern retainers) at the ends, to hold the lantern. The objective of the present subsection is to discuss this modification and its likely influence on the pressuremeter testing curve.

For this study four testing soundings were performed with the oversized lantern retainer. They were SBP16, 17, 18 and 19. SBP16 and 17 were carried out with an oversized lantern retainer that had a large diameter difference with respect to the diameter of the lantern (1.5 mm) and a lesser difference to the diameter of the cutting shoe (0.5 mm). In SBP18 and 19 a new lantern retainer was tried, in order to reduce the dimensional differences in relation to the remaining parts of the pressuremeter unit. In this case a tapered retainer, with diameter varying from 74 mm at the shoe connection (same diameter as the shoe) to 74.5 mm at the lantern connection was devised. A lesser diameter difference of 0.5 mm with respect to the diameter of the lantern was obtained at the top of the retainer, because two rubber membranes were used beneath the Camkometer lantern. Figure 3.10(a) presents the configuration of the base of the pressuremeter unit in both conditions (SBP16, 17 and SBP18, 19).

The dimensional tolerances along the shaft of the pressuremeter can be of extreme importance in the process of soil disturbance. Fahey and Randolph, 1984 carried out SBPM tests in a granular deposit in which oversized and undersized cutting shoes were used. In the oversized case stress relief occurred at the cavity wall, and a certain amount of strain was required to bring the cavity pressure to the original ground stress. In the case of the undersized shoe there was a combined effect of increase in lateral stress and friction (during insertion) in the cavity wall. This led to final residual cavity stresses that were again below the original ground stresses. Such disturbance mechanisms hampered not only the derivation of σ_h by the lift off visual technique, but also the derivation of all other soil variables using the traditional interpretation methods.

Similarly, the dimensional differences of SBP16 to 19 imposed disturbance in the surrounding soil during SBPM insertion. When the oversized lantern retainer of SBP16 and 17 was used a small loading and subsequent unloading of the soil in the vicinity of the pressuremeter shaft took place. This was caused by the initial outward soil displacement of 0.67 % of the diameter of the shoe, and the final inward displacement of 2.0 % of this same diameter.

In Figure 3.10(b) the idealized change of lateral stress coefficient (defined in terms of effective stress ratio K) for various soil elements close to the shaft is schematically shown. Initially the soil is in an undisturbed state, represented by a coefficient of lateral stress equal to K_0. With optimum SBPM insertion

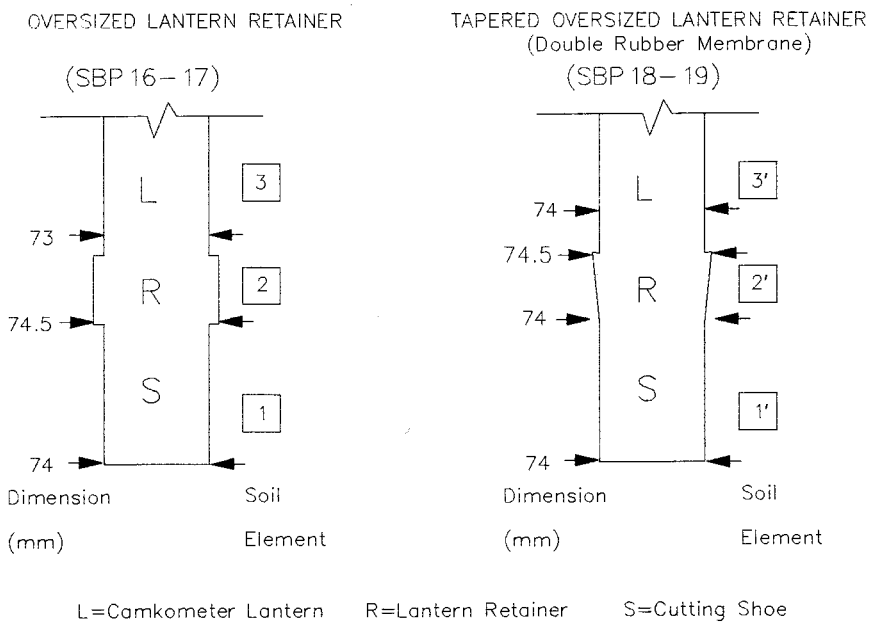

(A) DIMENSION OF OVERSIZED LANTERN RETAINER

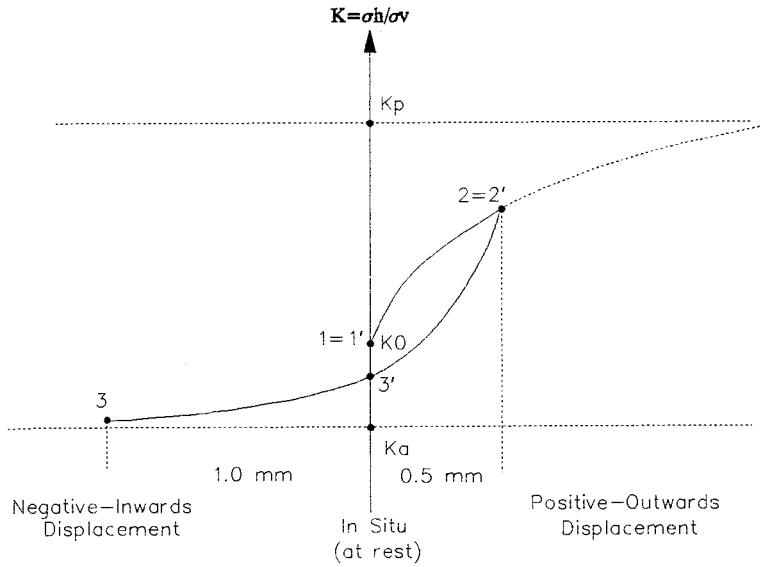

(B) IDEALIZED CHANGE OF LATERAL STRESS COEFF. K IN THE VICINITY OF THE PROBE

Figure 3.10: Characteristics and Effects Caused by the Oversized Lantern Retainer Rings

conditions, this is the stress state of the soil element 1. With outwards soil movement there is an increase of σ_h. Since the vertical stress does not change, there is a residual increase in the coefficient of lateral stress. As the pressuremeter moves down there is a high inwards soil movement close to the lantern surface. This is accompanied by a large decrease of σ_h and a large decrease in the coefficient of lateral stress K. At this stage the stress path of soil element 3 moves towards the active failure condition.

In the case of SBP18 and 19 a similar loading and unloading mechanism is imposed in the surrounding soil. In this case, however, there is a gradual outwards displacement of the material up to 0.67 % of the shoe diameter, followed by a final inward soil displacement of similar magnitude. In Figure 3.10(b) the idealized variation of K in this condition is shown. It is hypothesized that soil elements 1' and 2' behaved in a somewhat similar fashion to 1 and 2. At the onset of unloading the stress path of element 3' moves in the direction of the active failure condition, and the lateral stress coefficient decreases to a value close to, but not equal to, the initial K_0 value. Although this simplified representation is instructive it is further complicated by the friction that is developed along the pressuremeter shaft.

The extent of the above disturbance effects surrounding the pressuremeter will depend on the sensitivity of the material to the loading-unloading generated. This sensitivity will be a function of the initial density and confining characteristics at each depth. In Figure 3.11 the effects of dimensional differences are shown for a typical set of tests. In this figure, the calculation of CD coefficient for SBP17 and 19 were very different. The CD of 6 % suggests almost no disturbance for SBP19 with tapered lantern retainers, while SBP17 had a CD of 40 % with unacceptable disturbance due to large diameter changes. This same conclusion can be seen for all depths in the profile of Figure 3.9 where CD vs. depth is shown for SBP17 and 19. Thus, the idealized concept shown in Figure 3.10 is validated for SBP17, whereas in the case of SBP19 the disturbance at the soil-probe interface was considerably low to affect the overall shape of the testing curve.

This subsection presented the likely disturbance effects caused by the variation of the tolerances in the dimensions of the pressuremeter unit. Enlarged lantern retainers are required for clamping purposes with the Camkometer lantern (no. 10). In the UBC SBPM the taper design and the small increase in diameter of only ≈ 0.7 % has essentially no effect on disturbance, as high quality testing curves (CD's below 10 %)

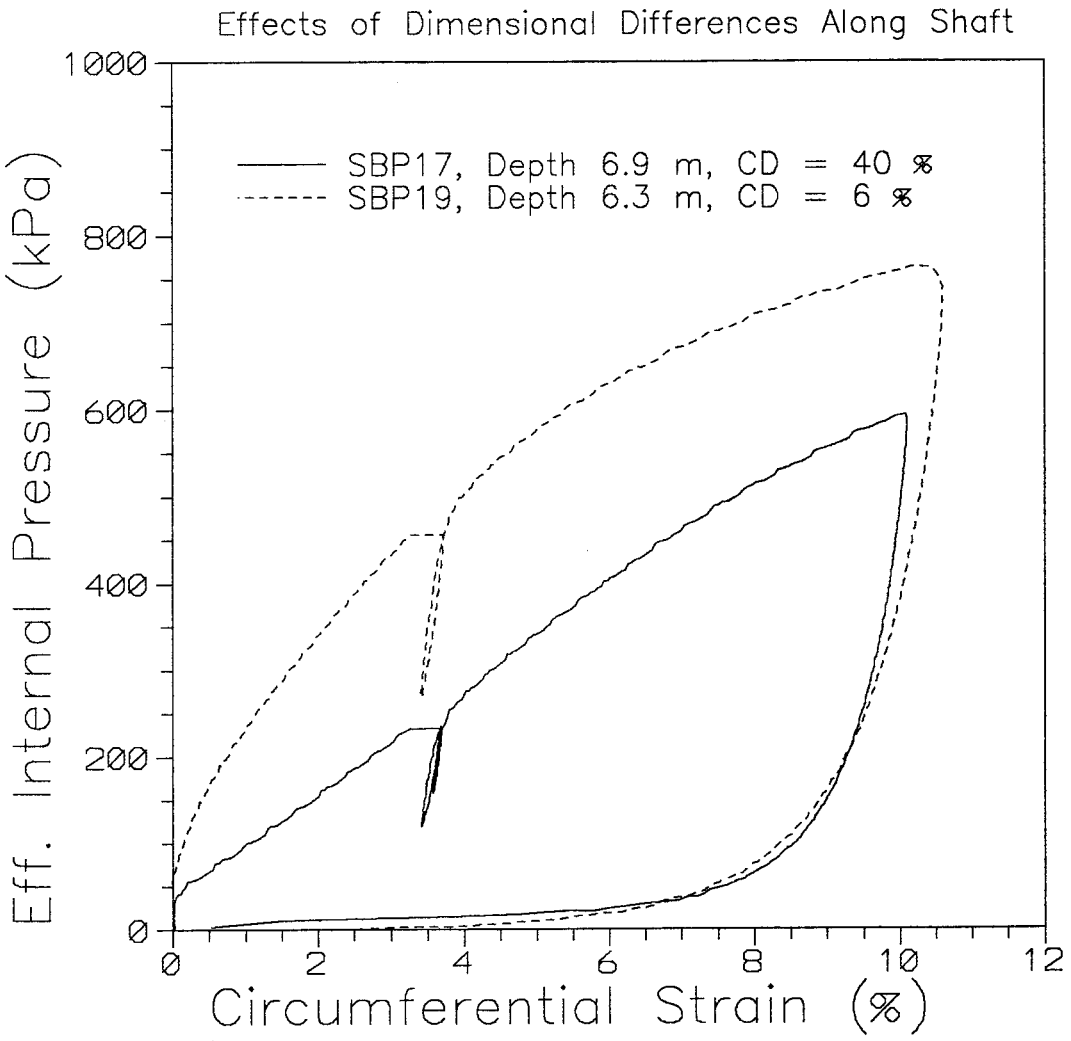

Figure 3.11: Effects of Dimensional Differences Along Shaft

were obtained in SBP18 and 19. Additionally there is an important advantage from the oversized lantern retainer since the lateral stress is slightly reduced, thus decreasing the shaft friction during insertion which reduces the required pushing force (hence penetration resistance) and possible soil disturbance.

3.6.5 Recommended UBC SBPM Insertion Procedure

The insertion procedure developed for the UBC SBPM takes into consideration all the possible variables that could cause disturbance on the testing curve. Optimization of the procedure was obtained during several field trials, in which the disturbance caused by the key variables was assessed and gradually minimized. The preceding subsections discussed the likely effects of such variables in the generation of disturbance. This subsection presents the recommended insertion procedure for the UBC SBPM.

Based on what has been learned throughout all the test soundings, the following combination of equipment characteristics and insertion variables are recommended for the UBC SBPM:

1. Equipment Characteristics:

- Camkometer lantern (lantern 10) with 2 inner (Gooch or Alliance) rubber membranes of 1 mm thickness each.
- Central jetting system with nozzle C.
- Tapered (0.5 mm) oversized lantern retainer rings.

2. Insertion Variables:

- Average mud flow rate of 20 l/min (5-6 gpm).
- Average penetration rate of 25 cm/min in sandy silts and 50 cm/min in sands.
- Jetting rod at -5 mm (centerline of orifices 18.4 mm behind the edge of cutting shoe).

3. Important Details:

- The surficial grass shall be removed prior to the "dummy" cone insertion. This avoids plugging of the orifices of the nozzle with grass inside the borehole.
- Preboring of surface soil or pushing of a large diameter "dummy" cone and casing up to 3 m is recommended to reduce the likelihood of shoe plugging.
- Slow pump of mud during the test at 1.9 l/min (0.5 gpm) to avoid plugging of the jetting nozzle.
- At the end of each pressuremeter test the mud shall be pumped at a rate of 29 l/min, for $\approx$ 30 s. This allows all the sand particles in suspension inside the borehole to be flushed out.

- 1 full expansion pressuremeter test at each depth (1 m min. depth interval) is recommended.
- Electronics/air cable shall be taped to the BW rod in a "spiral" manner, each 50 cm. A 3M cloth duct tape (48 mm wide) is recommended.

Insertion carried out in a consistent manner will allow a considerable improvement in the quality of the pressuremeter curves derived from the UBC SBPM system, when used in granular sites of the Fraser Delta.

3.7 TESTING PROCEDURE

The testing procedure describes the manner in which the pressuremeter pressure expansion is carried out in the field to allow the subsequent interpretation analysis of all the desired soil parameters. It was shown in the last chapter that the fitting technique requires a testing curve expanded to a circumferential strain of 10 %, with at least one unload reload loop. The recommended procedure will follow this basic requirement. It is important to determine, however, the influence of the variation of the rate of inflation on the derived testing curve (and pore pressure development), in order to obtain a practical value for the expansion rate of the UBC SBPM. The practical hold time prior to the unload reload loops is also discussed in this section.

3.7.1 Rate of Inflation

All the pressuremeter tests carried out for this thesis were done in stress controlled conditions, since this is the manner in which the UBC SBPM system is currently designed to operate.

In order to investigate the influence of different expansion rates in the pressuremeter data a testing programme with 3 profiles of FDPM tests 1 m apart at the site was planned, as presented in Table 3.2 for FDP04, 05 and 06. The rates of inflation adopted in each testing profile respectively varied from 0.5 to 7.0 kPa/s, which encompass most of the rates previously adopted for the other soundings. Pressuremeter testing curves were compared at the same depth level from 4.3 to 6.3 m, in the clean sand layer. Results for deeper depths were not compared as FDPM refusal occurred around 8 m in all testing profiles.

The repeatability of the soil stratigraphic conditions at the 3 FDPM soundings was checked by comparing the penetration resistances measured at the load cell of the pressuremeter. Similar to the cone bearing resistance Q_t of conventional cones, this penetration resistance reflects the initial density and confining conditions of the soil. For FDP04, 05 and 06 an average difference of 2.5 kN (5 % of full scale resistance) was noticed, thus indicating similar initial soil conditions at each FDPM profile.

The testing results for the 4.3 m depth, presented in Figures 3.12 and 3.13, are similar of the obtained at the other depths. The following comments can be made:

1. The excess pore pressures are essentially null for all the rates employed. The desired drained soil behavior during expansion was therefore obtained for the rates adopted.

2. Good agreement is noted between the shapes of the pressuremeter curves under distinct rates of inflation .

It seems, therefore, that for the rates adopted similar stress-strain curves were obtained. This conclusion agrees with the experimental observations of Jackson et al, 1980, that noticed in uniaxial compression tests in sands that the loading rate has a relatively minor effect on the stress-strain response for loading times greater than 1 millisecond.

Since a compromise between a low rate to always allow a fully drained expansion and a fast rate for a quick test is desired, an intermediate expansion rate is recommended for the UBC SBPM. As the best testing results of SBP18 and 19 were obtained with a rate of inflation of 3.4 kPa/s, the recommended rate will be in the range of 3 to 4 kPa/s.

3.7.2 Holding Time Prior to Unload Reload Loops

Creep will influence the unload reload loops of the test. It was observed by Hughes, 1982 and Howie, 1991 that unloading in a stress controlled manner without dissipation of the creep strains will lead to unload reload loops with an initial rounded shape. A similar effect was observed by Whittle et al, 1992 for loops in clays. This occurs because at the start of the unload a high creep rate exists. The higher the initial creep rate and amount of pressure unload, the larger will be the initial roundness of the loop.

Creep strains developed during this process will accumulate with the strains caused by the elastic shearing of the surrounding material, causing an error in the derived Gur modulus. Murthy, 1992 observed that creep tends to decrease the unload reload modulus Gur. By performing several consecutive unload reload loops he noticed that the soil modulus increased with the number of loops, and stabilized after a particular amount of strain accumulation. On the other hand the creep rate decreased from loop to loop,

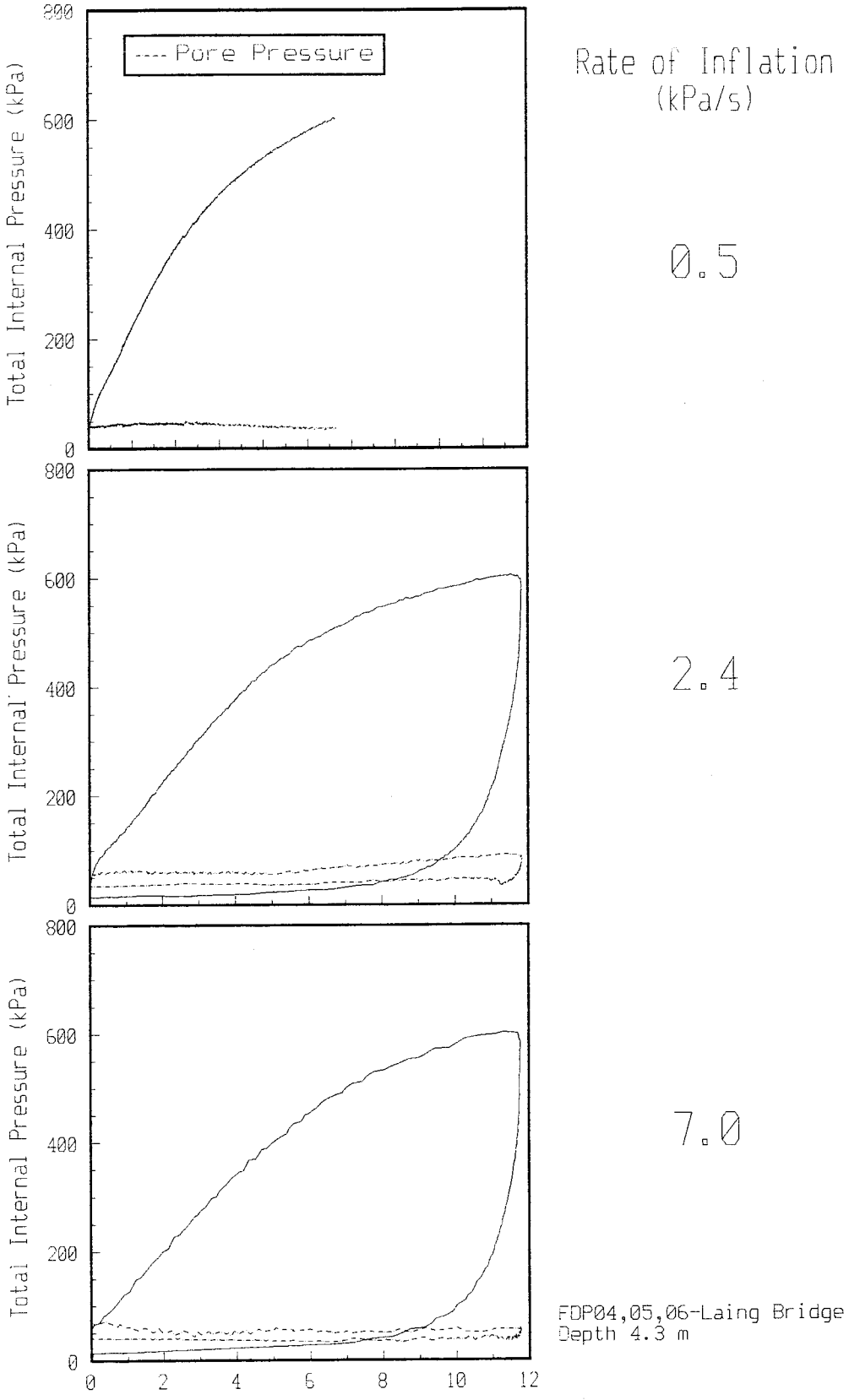

Figure 3.12: Influence of Rate of Inflation on Pore Pressure Development

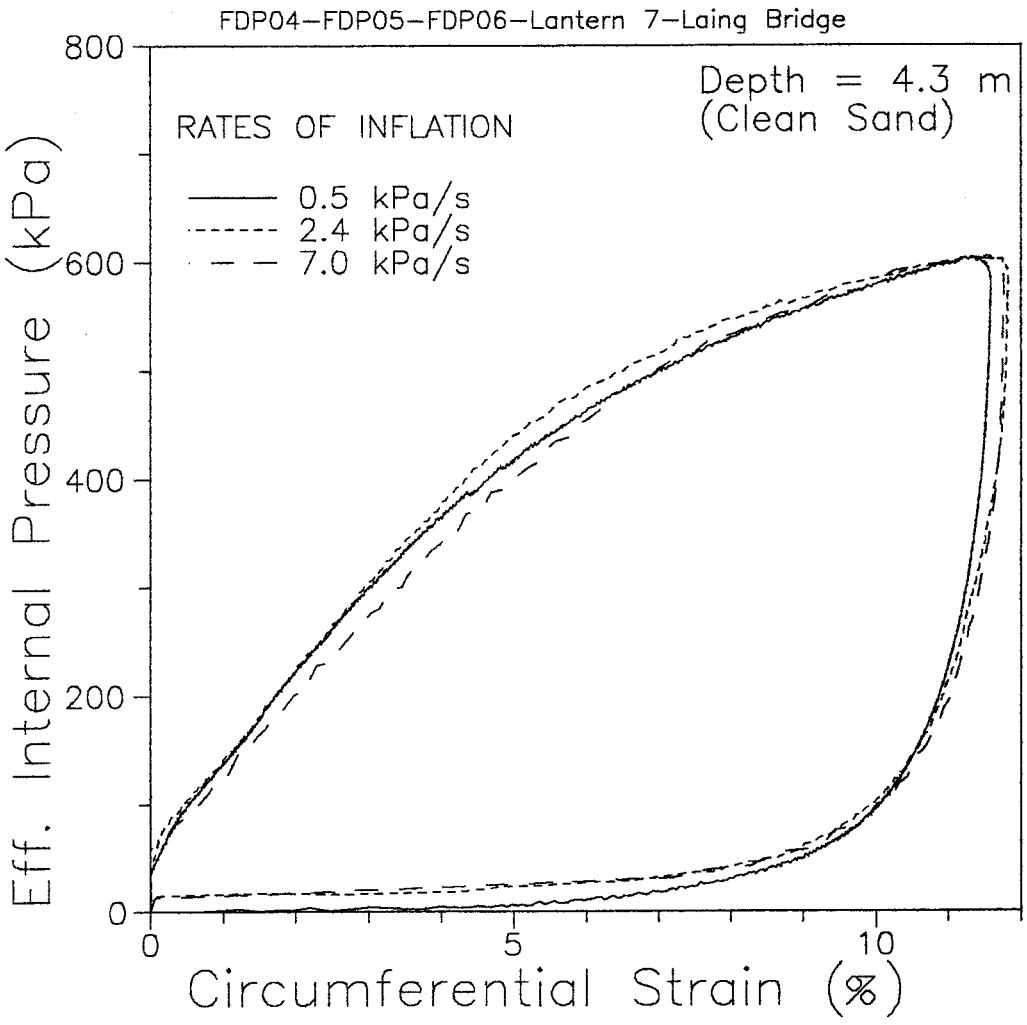

Figure 3.13: Influence of Rate of Inflation on Testing Curve

reaching a value below 0.01%/min for the loop in which the Gur stabilized. Howie, 1991 concluded that pressure holding phases have to be adopted prior to unload reload loops if the modulus is to be measured in sands. He suggested that a final creep rate of 0.1 %/min should happen in the end of this holding phase.

Based on the above considerations it is suggested that the holding phases have to be designed to yield a maximum creep rate of 0.01%/min before the start of the unloading stage. In this research an average 8 min. holding time was chosen prior to the loops, because it is fast enough for practical applications of the pressuremeter. This time has proven to yield creep rates in the range of 0.001 %/min prior to the loop stage.

The influence of the above proposed rate on the measured Gur modulus is demonstrated for one of the test sounding of this research. It will be assumed here that creep takes place only during the unloading stage of the loop, that the creep rate during this stage is constant and equal to the value at the end of the holding phase, and that creep strains can be simply calculated by the multiplication of the unloading time versus this constant creep rate. Table 3.6 presents the basic information and creep strain estimation of the loops of tests in the sounding SBP17. These loops were carried out with a degree of pressure unloading (dP_u / P_{cu}) of 40 % at the recommended rate of 3.4 kPa/s. The "uncorrected" modulus in column G is the standard value obtained after the compliance correction. The "corrected" modulus in column J is calculated with a "creep free" unloading strain (column I), based on the assumptions above. This very simplified example illustrates that for final creep rates below the target value (see column D) the average underestimation of the measured Gur will be in the range of 3 %. Using this same data it is simple to demonstrate that, if the final creep rates of column D were in the range of 0.1 %/min (recommended by Howie, 1991), the final underestimation of Gur would be as high as $\approx$ 30 %.

Based on the above findings a recommended testing procedure is proposed for the UBC SBPM.

3.7.3 Recommended UBC SBPM Testing Procedure

The recommended procedure follows the basic characteristics illustrated in Figure 3.14. The following comments apply:

1. Inflation should be carried out in stress controlled manner with a rate between 3 to 4 kPa/s throughout the loading and unloading stages of the test.

A	B	C	D	E	F	G	H	I	J	K
Depth (m)	Pcu (kPa)	$\varepsilon_{\theta h}$[1] (%)	Final Creep[2] Rate (%/min)	Unload Time[3] (min)	$d\varepsilon_\theta$[4] (%)	Gur[5] (MPa)	Creep Strain[6] x 10^{-3} (%/min)	$d\varepsilon_c$[7] (%)	Gur-c[8] (MPa)	Error[9] (%)
4.9	229	3.40	0.006	0.618	0.223	27.51	3.708	0.219	28.14	2.2
5.9	291	3.45	0.013	0.755	0.257	31.59	9.815	0.247	33.20	4.8
6.9	232	3.50	0.009	0.659	0.264	26.56	5.931	0.263	26.68	0.4
7.9	277	3.80	0.007	0.727	0.337	23.00	5.089	0.331	23.49	2.0
8.9	294	2.90	0.005	0.809	0.324	26.79	4.045	0.319	27.30	1.8
9.9	407	2.45	0.006	0.975	0.277	42.61	5.850	0.271	43.81	2.7
11.9	333	3.00	0.010	0.908	0.317	31.62	9.080	0.307	32.89	3.8
12.7	449	2.60	0.010	0.989	0.291	43.27	9.890	0.281	45.24	4.3
			Average = 0.008 %/min							Average = 2.7± 1.4 % (± 1 std. dev.)

1-Cavity strain at the start of the 8 min. holding phase
2-Creep rate at the end of holding phase and start of unloading
3-Time elapsed from upper unloading point to lowest unloading point of the loop
4-Cavity strain mobilized during unload-Includes creep strain
5-Defined as 0.5 $dP_u/d\varepsilon_\theta$ - contains creep strain and is compliance corrected
6-Circ. creep strain = unload time versus final creep rate
7-Corrected cavity strain mobilized during unload-without creep strain, compliance corrected
8-Defined as 0.5 $dP_u/d\varepsilon_\theta$ - does not contain creep strain and is compliance corrected
9-Defined as [(Gur-c - Gur) / Gur-c] x 100 (%)

SBP17-Rate of inflation and deflation = 3.4 kPa/s
Loops with average dP_u/P_{cu} of 40 % and holding phases of 8 min.

Table 3.6: Influence of Creep Strain on Unload Reload Modulus

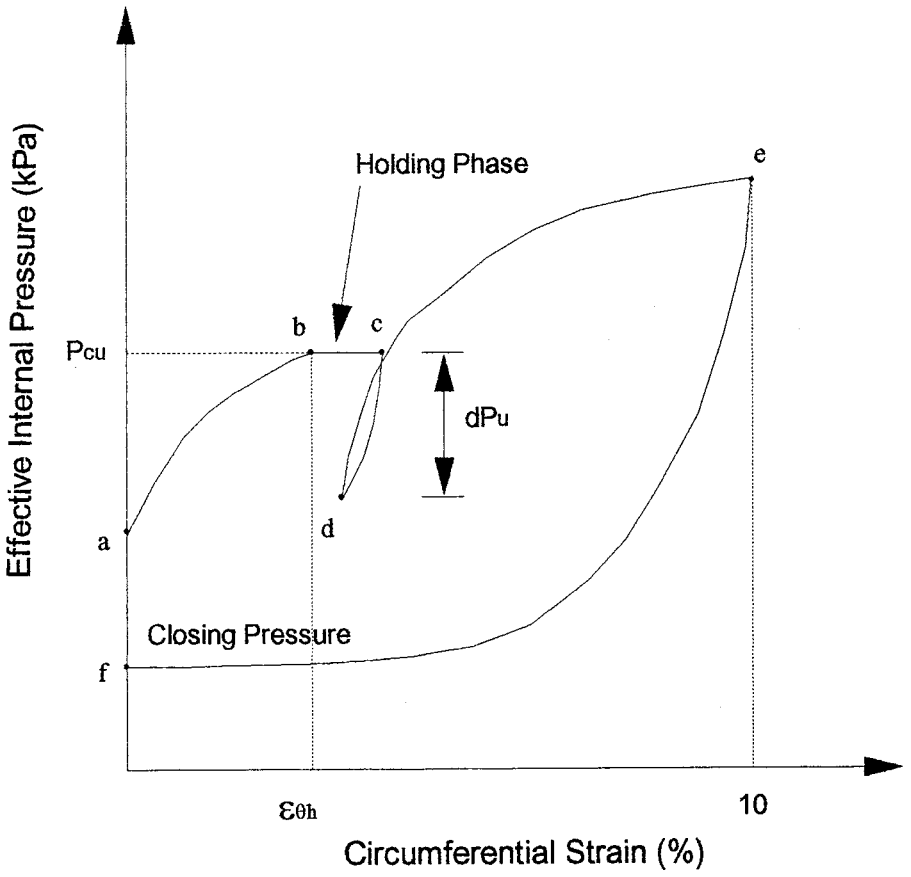

Loop Characteristics

Holding Phase (b-c) of 8 to 10 min.

$\varepsilon_{\theta h}$ = 2 to 3 %

P_{cu} = variable in accordance with testing depth

dP_u/P_{cu} = 40 %

Figure 3.14: Proposed Testing Procedure for Selfboring Pressuremeter Tests

2. At a circumferential strain between 2 and 3 % the pressure should be held constant to allow dissipation of the creep strain rate to a value below 0.01 %/min. A minimum holding time of 8 min. is recommended.

3. An unload reload loop should be carried out. To ensure a well defined loop with enough data points the degree of pressure unloading (dP_u / P_{cu}) should be around 40 %.

4. The probe should be finally expanded to a maximum circumferential strain of 10 %, followed by a final unloading in order to allow the determination of the closing pressure.

The above recommended procedure was used in the test soundings SBP18 and 19.

3.8 SUMMARY AND CONCLUSIONS

In this chapter emphasis was placed on the field determination of the insertion procedure for the UBC SBPM. Optimization of the key insertion variables led to the reduction of the disturbance imposed in the testing curve. The identification and discussion of likely disturbance effects caused by each of the insertion variables was presented. This helped to define the best insertion conditions that are recommended in the UBC SBPM insertion procedure. The aim of this procedure is to minimize disturbance during insertion.

It is important to minimize or (if possible) eliminate all the possible sources of disturbance on the pressuremeter curve. Disturbance leads to a pronounced reduction of the initial roundness of the shape of the pressuremeter testing curve. Disturbance generated during selfboring is a complex combination of the influence of variables related to the jetting parameters adopted during insertion, to the equipment used, to random field occurrences (such as shoe plugging), as well as to secondary unknown factors (vibration, non verticality, etc.).

Using the new interpretation methodology proposed in the last chapter a coefficient of disturbance CD was developed. This allowed the numerical quantification of the disturbance present in the pressuremeter curves of this thesis, thus removing the subjectiveness that existed so far in the assessment of the quality of such curves. Typical ranges of expected CD values, corresponding to different degrees of curve quality, were proposed. According to the experience of the writer, with CD's lower than 10 % it is possible to obtain high quality SBPM curves in sands. The CD parameter has been shown to properly identify the degradation of the quality of the pressuremeter curve caused partial shoe plugging, improper jetting rod positions and dimensional tolerances.

The optimization of the insertion procedure of the UBC SBPM took into consideration the minimization of the CD parameter. A constant mud flow of 20 l/min and penetration rate of 50 cm/min were adopted during these field trials. The main findings were:

- Disturbance is not evenly generated along depth. The looser the layer the more likely it is to be disturbed. It appears, therefore, that distinct combinations of jetting variables are necessary to selfbore a natural deposit. If a single combination is adopted, as in the present study, it may be expected that a residual low disturbance will be imposed in some layers.

- Partial plugging of the shoe invariably occurred in most of the SBPM tests of this research. This was caused by the presence of a surficial silty sand to sandy silt layer in the Laing Bridge soil profile. Partial plugging imposes a complex stress, density and stress history in the soil surrounding the probe. It leads to a large increase in both CD and pressuremeter penetration resistance. Plugging can be reduced or even avoided by the insertion of a large dummy cone down to 3 m depth prior to selfboring, and by the decrease in the rate of SBPM penetration in the fine and silty soils.

- Tip loading, and partial plugging with the surficial fine-grained material, were also related to the position of the jetting rod in relation to the cutting shoe. The optimum position of the rod was obtained using a trial and error procedure, in which the shoe plugging occurrence and the CD parameter were used to assess the quality of the insertion. The optimum position was obtained in SBP18 when a CD lower than 10 % was achieved. This took place with a simultaneous improvement of the design characteristics of the probe. A continuous mud flow at a low rate of 1.9 l/min (0.5 gpm) is required during the SBPM test in order to prevent the plugging of the orifices of this nozzle.

- A shower head jetting system proved to be unacceptable in its present design, since it leads to overcoring in front of the shoe. A redesign of this system should provide a very effective jetting alternative.

- Inter-strip friction due to overlapping of the strips of the steel lanterns imposed constraints on the use of these lanterns in the UBC SBPM. Only the Camkometer lantern is recommended for the UBC probe, since this lantern gave the most consistent Gur values.

- The details of the equipment design and tolerances have a significant impact on the final results. Disturbance effects are generated when SBPM tests are carried out with dimensional differences along the shaft (as is usually the case). The initial design adopted for the oversized lantern retainers led to a

substantial disturbance over the entire pressuremeter curve. With the modification of this initial design to reduce dimensional differences to less than 0.7 % (using tapered sections to gradually adjust dimensions) the disturbance effect was essentially removed from the testing curve when using the Camkometer lantern.

With an understanding of the influence of the key insertion variables the recommended UBC SBPM insertion procedure was proposed. This procedure was tried in testing soundings SBP18 and 19, leading to pressuremeter testing curves with a disturbance coefficient CD below 10 % for most of the testing depths.

Once insertion related factors are understood and the likely disturbance minimized, standardization of the test procedure is possible and recommended. Past experience with pressuremeter tests in sands indicate that rate effects may be of importance for the derivation of the Gur modulus. Pressure holding phases of 8 min. were designed to reduce the creep rates to values below a target 0.01 %/min prior to the loop stage. A simplified analysis indicates that the Gur derived in this manner will be underestimated to an average extent less than 3 %, at least for loops with a degree of pressure unloading of 40 %. Using FDPM testing results from the Laing Bridge site it was noted that for expansion rates within 0.5 to 7 kPa/s a fully drained testing curve is obtained. No influence of the above variation of expansion rates on the stress-strain testing curve was found. Based on these findings a recommended UBC SBPM testing procedure was proposed.

Standardization of the procedures adopted during insertion and testing of the SBPM in sands is essential for the derivation of repeatable results. The procedures suggested in this chapter will not only standardize the operation of this tool, but will also lead to high quality pressuremeter testing curves. These curves will be used in the next chapter to demonstrate the methodology of interpretation of the basic soil parameters, using the sand at the Laing Bridge site.

CHAPTER 4.0 TEST RESULTS AT THE UBC SITE AT LAING BRIDGE

4.1 INTRODUCTION

This chapter demonstrates the application of the proposed interpretation methodology presented in Chapter 2 on high quality field testing data. The tests were run in accordance with the recommendations put forward in Chapter 3 concerning the insertion procedure for the UBC SBPM system. The field data was gathered in an extensive field testing programme carried out by the writer at the Laing Bridge site. The detailed geological and geotechnical characteristics of this particular site are presented herein.

The predicted soil parameters from the SBPM testing curves are compared to values obtained from laboratory as well as other in situ tests, allowing a brief discussion on the significance and reliability of these parameters.

4.2 GENERAL CHARACTERISTICS OF THE LAING BRIDGE SITE

4.2.1 Geology

The Fraser River Delta is located at the western edge of the British Columbia Mainland, on the west coast of Canada. This delta comprises a triangular area bounded on the west by the Strait of Georgia, on the north by the north arm of the Fraser River, and on the south and southeast by the Cascade Mountains. The lowlands of this delta consist of flat-topped hills and plateaus which are separated by wide valleys (Clague et al, 1983). The Fraser Delta is occupied and subdivided by the Fraser River, as shown in Figure 4.1(a). The Fraser Delta serves as a model for a high energy, sand rich, estuarine system, as it has been mainly built up by sand dominated river transport during spring and summer (Milliman, 1980). Given the complexities of the depositional process as shifting of the distributary channels, eustatic water level fluctuations, etc., the sediments of this delta exhibit pronounced lateral and vertical variations in texture. The deposits of this delta are of the Quaternary age, with thickness that can vary up to 300 m.

According to Blunden, 1975, the development of the Fraser Delta started 11000 years ago. This age corresponds to the end of the last glaciation period of this area, when the ice retreat started to occur. The weight of ice depressed the land to an extent so that its level became lower than the existing sea level. A submarine delta was then formed and ideal conditions for the accumulation of sediments were generated.

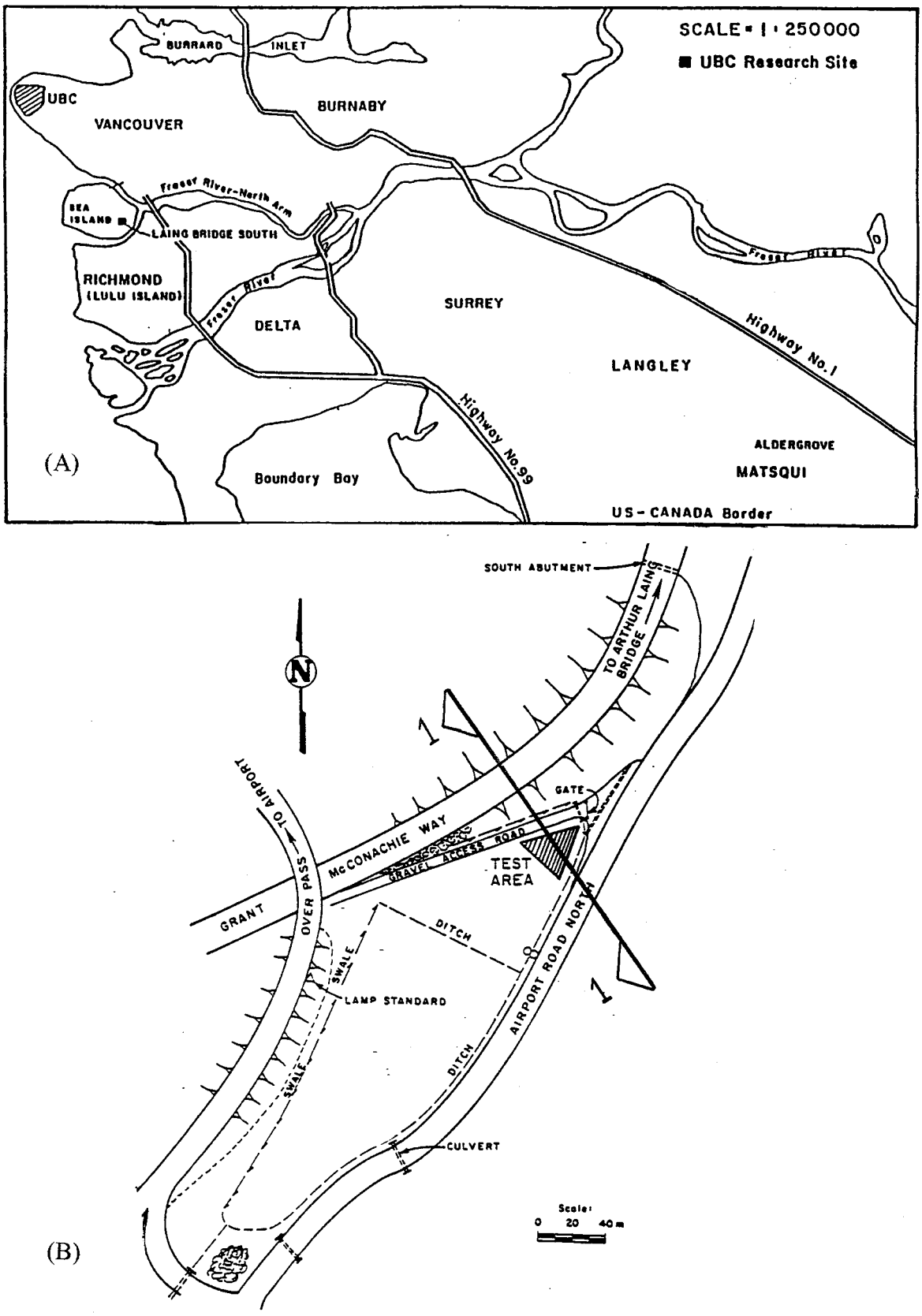

Figure 4.1: (a) Laing Bridge Site Location, (b) Test Area in this Site (Modified after Sully, 1991)

Underlying the Delta there is Tertiary bedrock overlain by Pleistocene deposits, which consist of a series of thin seams of glacial till and glacial outwash from previous glacial ages. About 11000 years ago large amounts of meltwater were funneled into the valley of the Fraser River, subjecting the area to deposition of fine sediments discharged into the sea by the Fraser River. As a result, the Fraser River floodplain rapidly prograded westward. While these events were occurring the level of the sea continued to fall relative to the land (Clague et al, 1982). This period of low sea levels during the early Holocene stage was followed by a marine transgression caused by an 11 m rise in the sea level. This relatively rapid sea level rise continued until 5000 to 5500 years ago. During this period coarser sediments were deposited over the finer grained clays and silts already submerged in the submarine delta. The deposition of these granular sediments took place under a dynamically high and variable energy environment. Westward progradation of the Fraser Delta continued at a slow rate after 5000 years ago, due to low fluctuations of the sea level. During this period organic sedimentation commenced over nearly the entire eastern portion of the delta.

The Fraser Delta continues to prograde westwards, although in a pattern of sedimentation which is slower than those from the past. The present rate of increase of the Fraser Delta varies from 2.5 to 8.5 m per year, depending on the depth of water and tide effects. The maximum tidal range is almost 5 m at the mouth of the river, close to the Laing Bridge site, decreasing both landward and with increasing river flow (Ages and Woollard, 1976). The present geological profile of the Fraser Delta is shown in Figure 4.2.

Since the Fraser Delta deposits were formed only after the last glaciation they have not been mechanically overconsolidated by ice load. Thus, based on geological evidence they are normally consolidated. On the other hand post glacial events may have taken place. Extensive rework by channel migration (Monahan et al, 1992), and seismic liquefaction (Clague et al, 1992) have undoubtedly affected the original characteristics of these deposits.

4.2.2 Location and Features

The Laing Bridge site is located in an area of Sea Island close to Grant McConachie Way, the Arthur Laing Bridge and the Vancouver International Airport. As shown in Figure 4.1(a) Sea Island lies between the north and middle arms of the Fraser River.

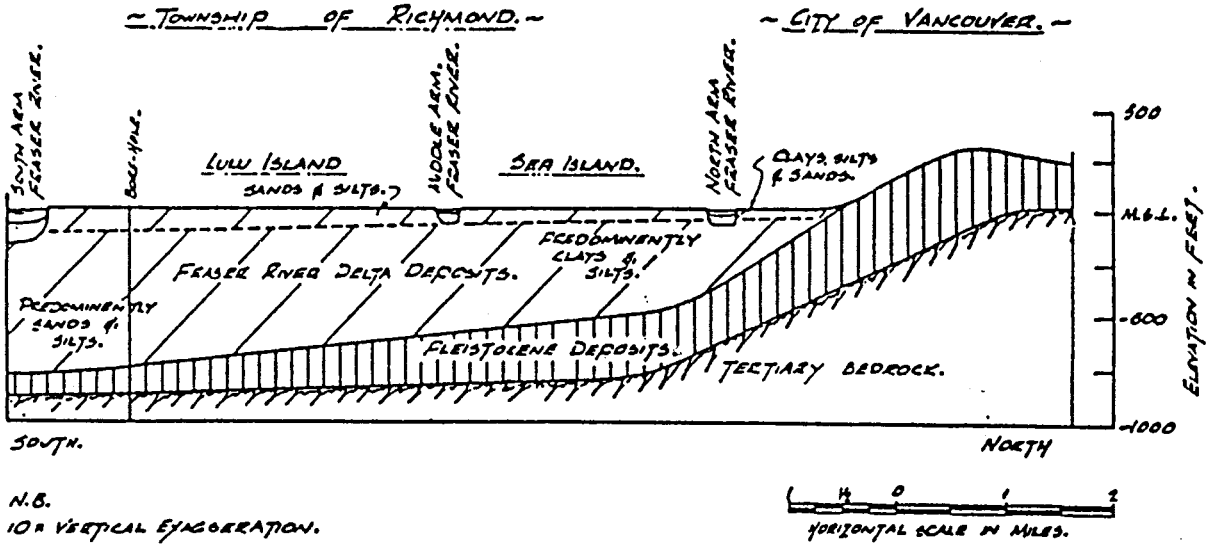

Figure 4.2: Geological Cross Section of the Fraser Delta (after Blunden, 1975)

The test area in Laing Bridge site is presented in Figure 4.1(b). The topography is fairly flat with a slope of about 1% north eastwards. The site is grassed and is surrounded by a series of ditches and swales. The average groundwater level is about 0.5 to 2.5 m below ground surface, varying in accordance with the tidal regime of the nearby Fraser River. The site is bounded on the north by the South Approach embankment, constructed in 1970 to connect the airport to downtown Vancouver (Bertok, 1987). It is bounded on the south by a major drainage ditch. The field test programme was performed in a triangular area constrained by the major ditch and an existing gravel road (see Figure 4.1(b)). Along the side of this area the South Approach embankment has a variable height of 0 to 4 m.

Fill was placed on the site during the construction of the South Approach embankment and the McConachie overpass. This fill has a thickness of 1 to 1.5 m and overlays the original Fraser Delta sediments at this location.

4.2.3 Stratigraphy

Based on the results of the in situ testing programme carried out by the writer, the general site characteristics summarized by Bertok, 1987, and a field survey of the site, the geotechnical and topographical profile of section 1-1 from Figure 4.1(b) can be established. It is presented in Figure 4.3.

The stratigraphic profile consists of 1.0 to 1.5 m of sandy fill, underlain by a sandy silt layer 1.5 to 2.0 m thick. Below this layer there is a fine sand stratum with thickness varying from 15 to 20 m. The fine sand is underlain by a clayey silt to silty clay layer that extends down to the Pleistocene till deposits.

A better insight into the stratigraphic variations along the profile can be obtained with the testing results of a logging tool like the piezocone (CPTU). Figure 4.4 presents a typical CPTU profile at the site, obtained from piezocone sounding (C06) with the pore pressure sensor located behind the tip. The close to zero differential pore pressures throughout the initial 20 meters of the profile is indicative of a drained penetration condition, typical of sands. This can be also seen by the close agreement of penetration pore pressure (measured behind the tip, U_2) with the hydrostatic pore pressure (U_0) of the groundwater.

The negative pore pressure values in the surficial sandy silt layer indicates a slightly overconsolidation effect, as demonstrated by Robertson and Campanella, 1989 at other sites on the Fraser Delta. The overconsolidation of this layer was probably caused by desiccation. The clayey silt to silty clay below

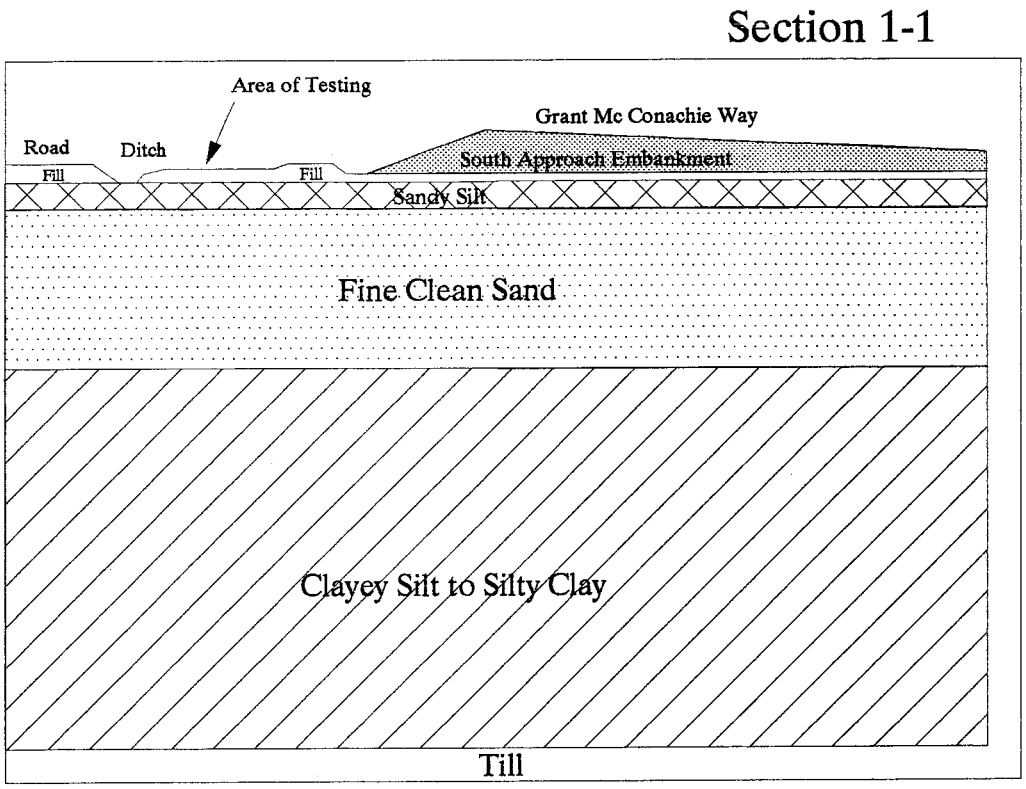

Figure 4.3: Section 1-1 of Laing Bridge Site

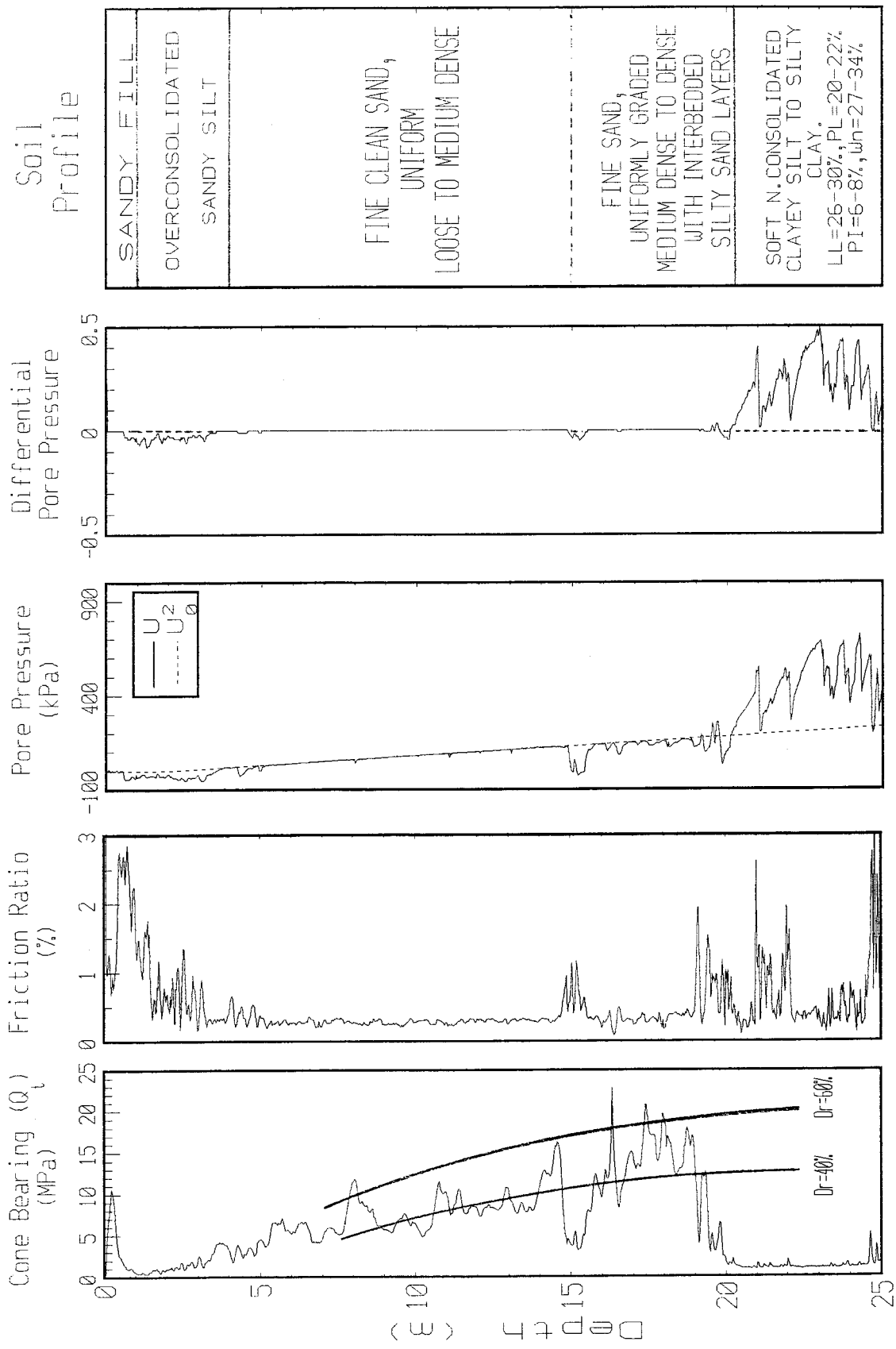

Figure 4.4: Typical Piezocone Profile in Laing Bridge Site

20 m of depth is normally consolidated based on consolidation tests (Bertok, 1987 and Le Clair, 1988) and interpretation of piezocone data. The almost constant values of friction ratio for depths of 5 to 15 m indicates a fairly uniform and clean sand. Between approximately 15 m to 20 m a transition layer of sand interbedded with fine lenses of silty material exists. This is readily seen by the high variation of the friction ratios and dynamic pore pressures measured by the CPTU. As noted in the last chapter the UBC SBPM tests were carried out in the uniform sand between 5 and 15 m of the profile.

However, the sand of this deposit has a notably high variation in density, as can be seen by the variability of the cone bearing resistances Q_t in Figure 4.4. This is caused by the variation of the environmental and energy associated conditions during the sand deposition, as noted before. Based on the Baldi et al, 1982 empirical relationship for relative density (Dr) determinations, valid for a medium compressible unaged quartz sand, this sand deposit can be depicted as having loose (40 %) to dense (60 %) characteristics within 5 to 15 m of depth. This density generally increases with depth.

4.2.4 Maximum Shear Modulus

The results of downhole seismic piezocone (SCPT) tests were used to measure the (low strain) maximum shear modulus profile of this sand deposit. The seismic modulus of the SCPT (G_0) is measured at a strain amplitude of approximately 10^{-4} % and below (Campanella et al, 1986). Figure 4.5 presents the results of tests SC01 and SC02, performed 1.3 m apart in the field. The downhole shear wave velocity was calculated using the cross correlation digital signal processing analysis presented in Campanella and Stewart, 1990. This wave was generated by a swinging hammer hit on each side of the pads of the UBC research vehicle. G_0 was derived with the use of the measured shear wave velocities, the density of the sand (from laboratory tests of Bertok, 1987) and the following equation (White, 1965):

$$G_0 = \rho V_s^2 \tag{4.1}$$

where ρ is the soil density and V_s is the shear wave velocity.

As expected, the stiffness obtained by both SCPT testing profiles show a trend of variation similar to the piezocone bearing results of Figure 4.4. As noted by Houlsby and Hitchman, 1988, Schnaid and Houlsby, 1991 and others, the cone bearing reflects the density and mean stress level of the sand prior to the CPT insertion. Laboratory testing results published in the literature demonstrate that the shear wave

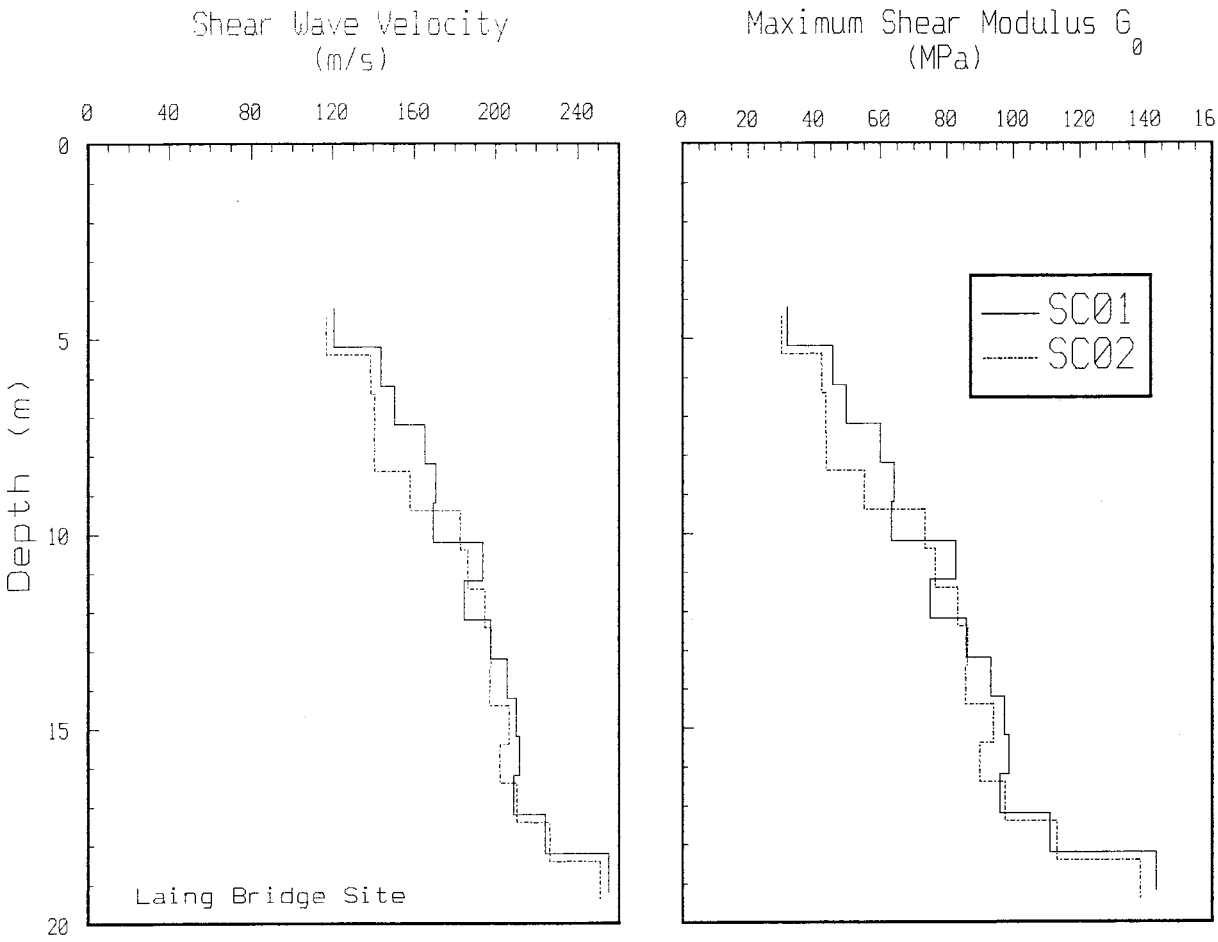

Figure 4.5: Profiles of Shear Wave Velocity and Maximum Shear Modulus

velocity in sands is affected by the same variables. G_0 is very dependent on the void ratio of the sand (Hardin and Drnevich, 1972), on the stress levels that respectively act in the directions of shear wave propagation and particle movement (Roesler, 1979) as well as on the ratio of such stress components (Yu and Richart, 1984). Hence, G_0 reflects the maximum stiffness of the sand under the in situ mean effective stress ($(\sigma_v + \sigma_h)/2$) and density regimes.

The average of both G_0 evaluations of Figure 4.5 was used in the interpretation of the pressuremeter data of the Laing Bridge site.

4.2.5 Laboratory Testing Results

A laboratory testing programme was carried out with all the "undisturbed" and disturbed samples retrieved from the site. It was directed towards the determination of the basic characteristics of the sand, including its classification. It also had the objective of evaluating the typical shearing behavior of the sand, and of obtaining the peak friction angle ϕ at distinct depths.

4.2.5.1 Soil Strength

The peak friction angles and the stress-strain behavior of the sand were experimentally obtained with isotropically consolidated drained triaxial (CID) tests, using reconstituted and undisturbed samples from the ST1 sampler. A total of 7 CID undisturbed and 9 reconstituted triaxial tests were performed under distinct densities and stress level conditions, as detailed in Appendix C. A value of 34° and 0.25 was respectively obtained for ϕ_{cv} (constant volume friction angle) and ν (Poisson's ratio) from the triaxial tests. These values were used in the interpretation of the pressuremeter data of the Laing Bridge site.

4.2.5.2 Soil Classification

Soil classification, grain size analysis and Atterberg Limits were obtained with the disturbed samples retrieved inside the split spoon sampler (ASTM D1586 and D1587). This sampler was employed simultaneously with the standard penetration test (SPT01) performed at each 1.5 m of the Laing Bridge profile. A total of 16 sieve analyses and 2 Atterberg limit tests were performed.

The sand retrieved by the ST1 sampler also allowed minimum and maximum void ratio determinations, as well as the performance of two specific gravity tests. A visual petrographic analysis and one X Ray Powder Diffractometer test were kindly performed by Dr. Lee Grout of the UBC Geological Sciences department.

The sieve analyses indicate that the granular deposit at Laing Bridge is a uniform sand with a small amount of silt content, classified as SP to SP-SM using the Unified Classification of the soils. The X ray results show that the main mineral of this granular deposit is quartz (67.3 %), followed by feldspar (14 %), anhydrite (14.7 %), chlorite (3.5 %) and miscellaneous (0.5 %). The quartz grains can be classified as subangular to subrounded in shape, with a sphericity of 0.77 in accordance with the chart of Rittenhouse, 1943. The gradation of the material is extremely uniform. The sand between 5 to 15 m is basically composed of medium (average of 68 ± 8 % passing sieve #30) to fine (average of 17 ± 7 % passing sieve #60) grain particles, with an average D_{10} of 0.14 ± 0.02 mm and D_{50} of 0.31 ± 0.05 mm. The surficial sandy silt contains a high amount of silt, varying from 60 % at 2 m deep to 2.6 % at 4.7 m. The average fines content between 5 to 15 m in depth is below 5 %. Laboratory tests of Bertok, 1987 indicated a water content in this same sand varying between 20 to 30 %, with an average unit weight of 19.6 kN/m^3.

Minimum and maximum void ratio determinations of the granular samples retrieved from 5 to 15 m of the profile were carried out in accordance to the ASTM D2049-69. The minimum and maximum void ratios were respectively 0.51 and 0.84. The average calculated specific gravity of the sand was 2.67 in accordance with the testing procedures suggested by Lambe, 1951. This value was used in conjunction with the minimum and maximum void ratios to define the initial and after consolidation relative densities of all the samples tested in the triaxial cell.

4.3 INTERPRETATION OF UBC SBPM DATA

4.3.1 Testing Curves

The UBC SBPM measures the pressure versus displacement (or strain, with the use of Equation 2.2) response at six distinct directions along the horizontal plane. These directions are given by 0, 60, 120, 180, 240 and 300 degrees, respectively related to arms 1 to 6 around the center of the UBC probe. Arm 1 (at 0 degrees) was in general directed towards the magnetic north at the Laing Bridge site.

Therefore, with the UBC SBPM it is possible to obtain an array of pressure expansion (testing) curves at the same depth. A typical example is presented in Figure 4.6 for the depth 8.3 m of SBP19. Using this data it is possible to obtain a set of sand parameters (ϕ, σ_h, Gi) related to each of the distinct expansion directions of the probe. Moreover, using the displacement measured in each of the strain arms at given

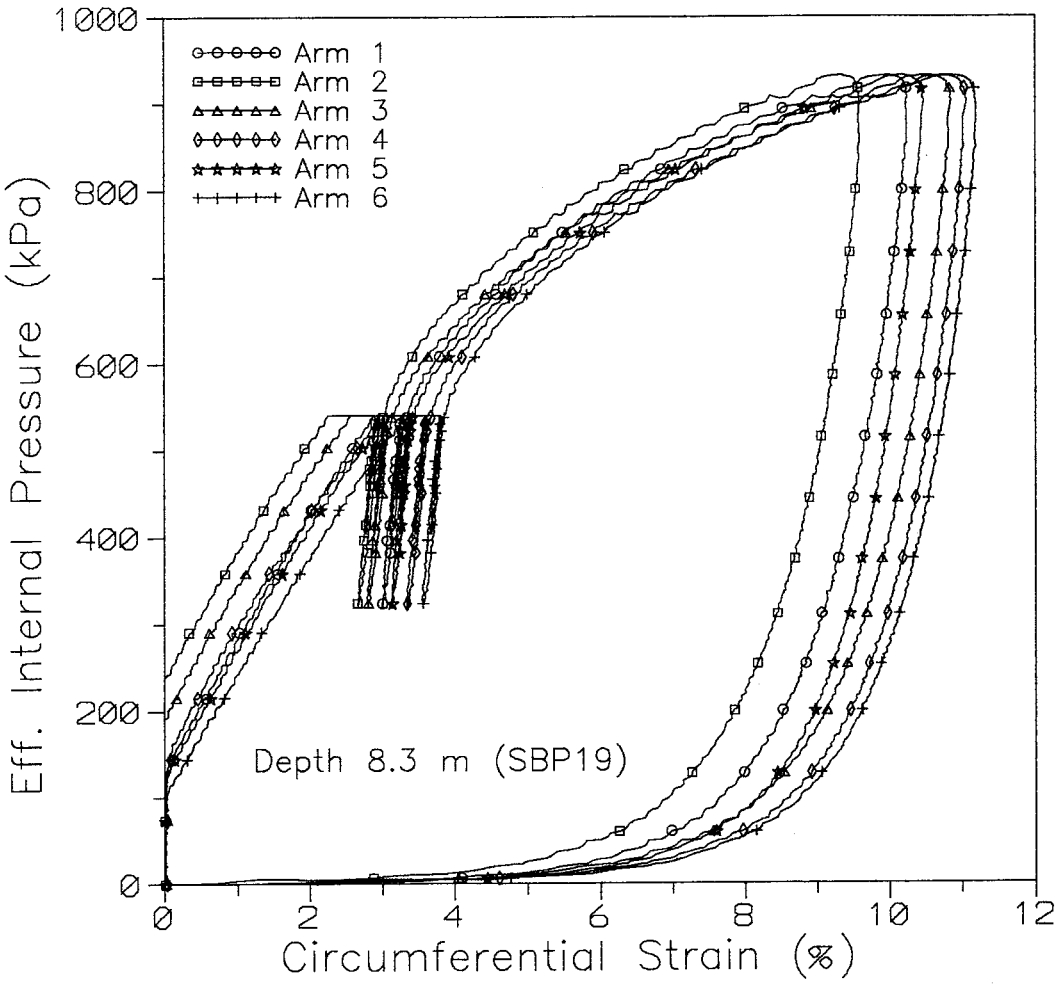

Figure 4.6: Typical Pressure Expansion Curves Measured by the UBC SBPM at Laing Bridge Site

levels of internal pressure it is possible to track the expansion of the cavity wall. Figure 4.7 presents the displacements measured in each of the arms during the testing expansion of Figure 4.6. For this particular example the UBC SBPM tended to expand to a slightly lesser extent in the direction of the strain arms 1, 2 and 3, than in the opposite direction (arms 4, 5 and 6). Perhaps the noted displacement differences are related to the influence of each of the following variables:

1. Soil anisotropy: Soil anisotropy (fabric and lateral stress) along the horizontal plane is reflected by a differential behavior of the strain arms, hence the measured pressure expansion curve.

2. Differential disturbance: It is unlikely that the (low) disturbance generated during the "optimum" insertion of the UBC probe will be evenly distributed along the horizontal direction. It is possible that stress relief (or increase) is differentially imposed around the cavity. Note, for instance, the variability of lift off stresses measured by the testing curves of Figure 4.6.

3. Translation of the center of the SBPM: If the soil is isotropic, and undisturbed, then the non concentric circles of Figure 4.7 represent the (displacement) response of a SBPM test with a constantly moving axial center.

It appears, therefore, that the average pressure expansion curve, rather than each individual curve, is more appropriate in the curve fitting interpretation analysis. The averaging of the output of the strain arms of the SBPM helps in the compensation of errors due to the differential disturbance imposed in the horizontal plane during insertion. It also dilutes the anisotropic soil response along the horizontal testing plane and assumes the soil is isotropic, which looks like a good assumption for this soil since the measured displacements give a cylindrical response in Figure 4.7. The greater the number of strain arms, the better will be the averaged response of the surrounding soil.

Therefore, only the average testing curve at each depth was used to estimate the sand parameters of the Laing Bridge site. This approach for SBPM test data interpretation is commonly done in practice. In commercial probes, like the one owed by Cambridge In Situ (Camkometer probe), the average output of the (three) strain measuring sensors is used in the interpretation process. The Menard pressuremeter adopts the volume change of the expanding cavity to infer the average radial displacement of the cavity wall.

The average testing curves adopted herein were obtained with the field testing programme carried out by the writer, as described in the last chapter. The best quality curves from both test soundings SBP18 and

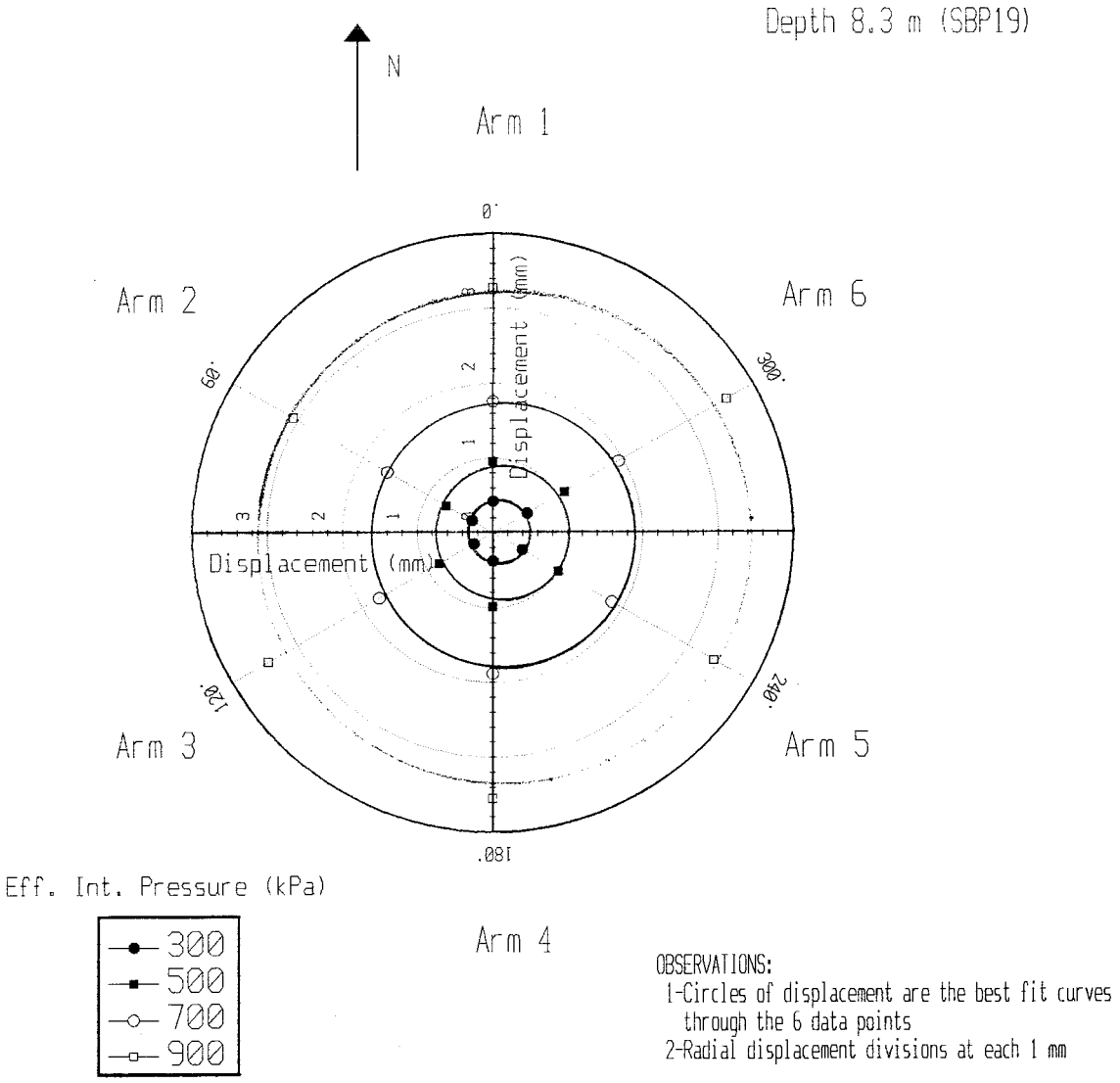

Figure 4.7: Typical Displacements Measured during the Expansion Stage of the UBC SBPM

SBP19 were selected for this purpose, since the "optimum" insertion procedure was adopted for these soundings.

4.3.2 Curve Fitting Interpretation

The most representative curves for this site are those for depths 5.3 m (SBP18), 6.3 m, 8.3 m, 10.3 m, and 13.3 m (SBP19), for which the CD was below 10 %. In each of the pressuremeter tests an unload reload loop was carried out. This furnished the new cavity expansion model with the shear modulus Gur, required to define the elastic strains in the plastic zone surrounding the cavity.

The methodology of interpretation of these curves followed recommendations put forward in Chapter 2, with the use of the new cavity expansion model. Plots showing the comparison between the measured experimental data and the curves fitted manually are presented in Figures 4.8 to 4.10, for each of the SBPM tests chosen. In general the curve fits are reasonably good, giving confidence in the derived basic soil parameters. Discrepancies found between the curves are due to a small amount of disturbance generated during insertion of the UBC SBPM, as noted in Chapter 3 for SBP18 and 19.

The final set of curve fitting parameters is shown in Table 4.1, together with the triaxial peak friction angles, the seismic low strain G_0 values and the unload reload moduli of the pressuremeter tests. The disturbance coefficients defined after match are also shown. As expected they are low, but not null.

In order to comment on the consistency of the derived set of parameters for the granular deposit of Laing Bridge site, a comparison was made between the predicted parameters and the reference values. A similar approach was followed before in Chapter 2 with the chamber data, in order to validate the consistency of both the new and the Carter et al, 1986 cavity expansion models. The comparison between predicted (SBPM test interpretation) and reference (lab., etc.) geotechnical values is discussed next.

4.3.2.1 Friction Angle

In order to have a basis of comparison for the predicted friction angles, the results of the laboratory triaxial tests were used. The comparison of pressuremeter and triaxial friction angles is widely used in practice (Robertson and Hughes, 1986, Bellotti et al, 1987, East et al, 1988, Manassero, 1989 and Newman et al, 1991), since triaxial tests are faster and easier to perform than other laboratory devices. Besides, most current engineering designs still rely on strength parameters derived from the triaxial test.

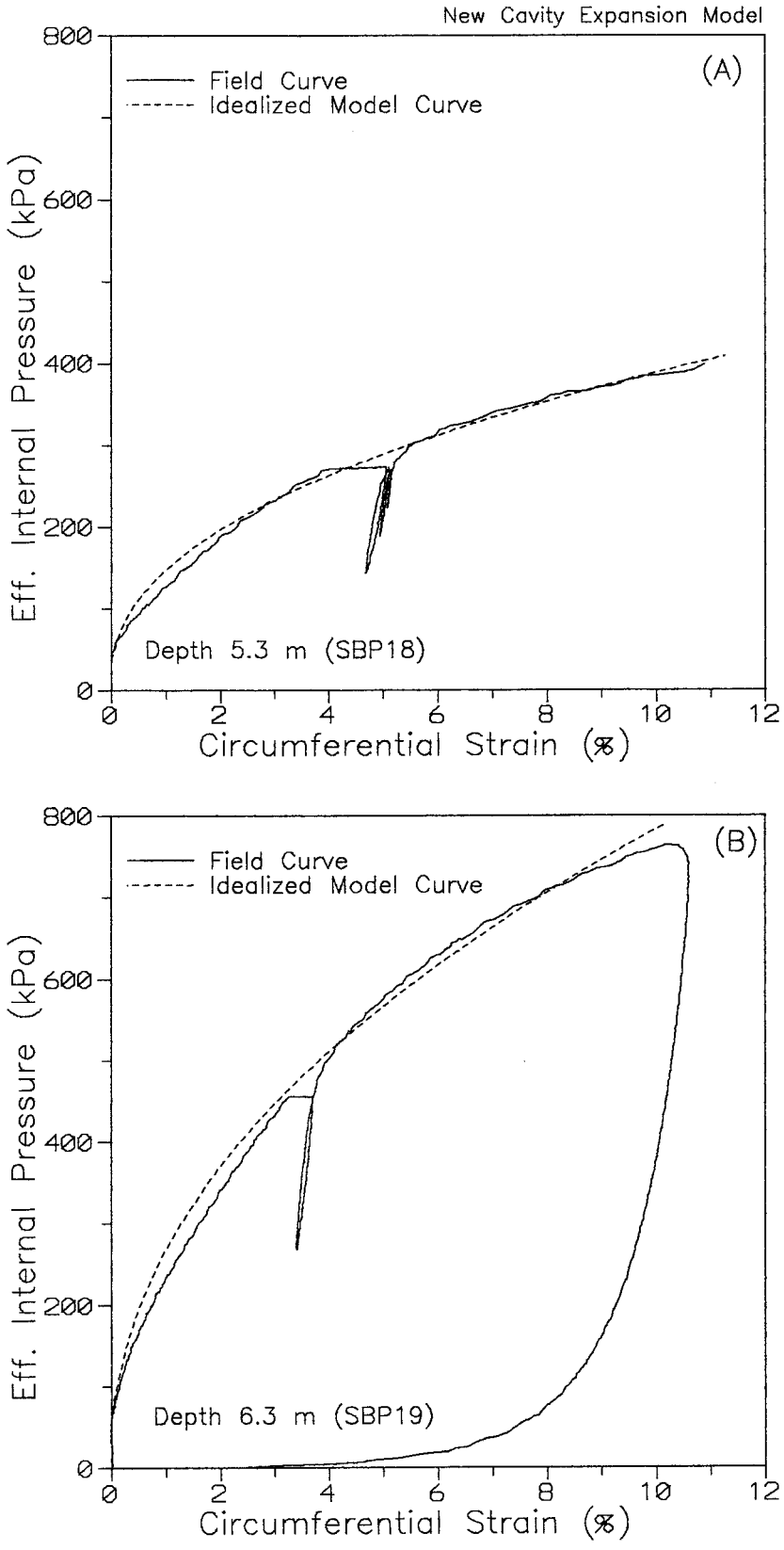

Figure 4.8: Final Curve Matching with Field Data: (a) Depth 5.3 m, (b) Depth 6.3 m

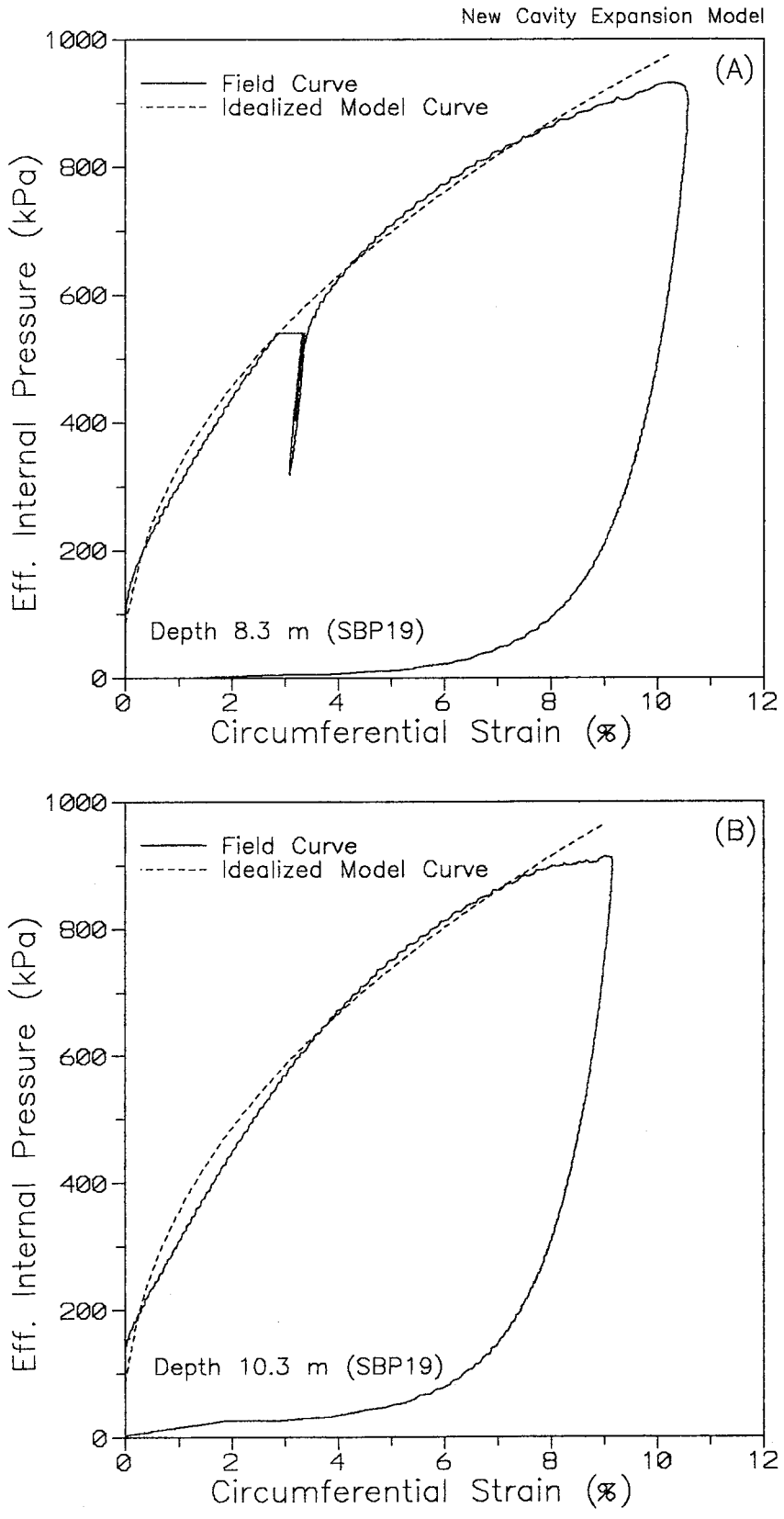

Figure 4.9: Final Curve Matching with Field Data: (a) Depth 8.3 m, (b) Depth 10.3 m

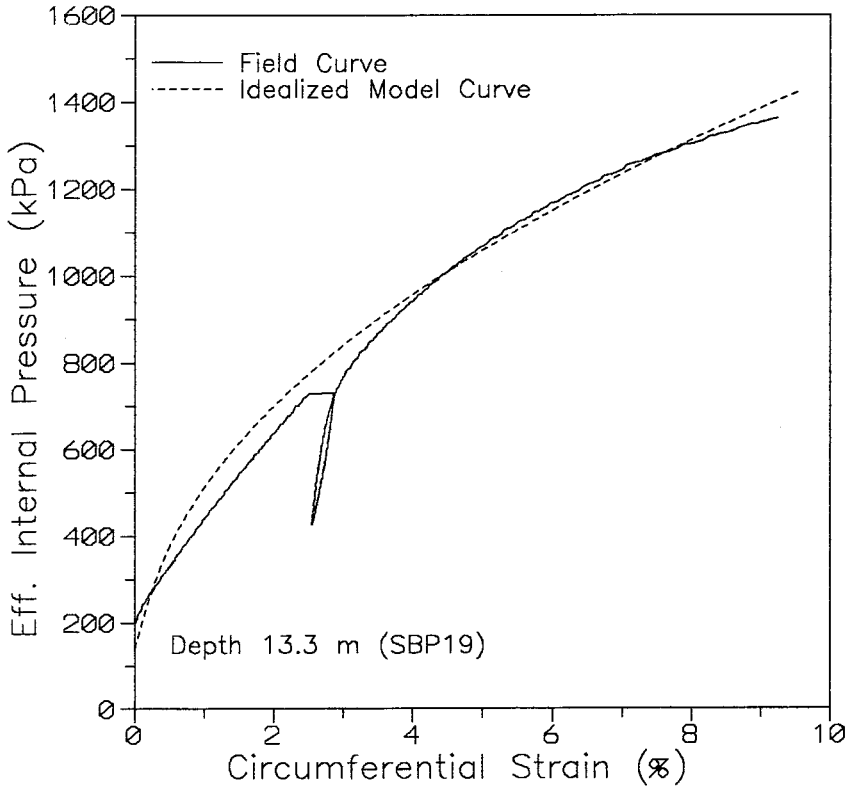

Figure 4.10: Final Curve Matching with Field Data: Depth 13.3 m

DEPTH [1] (m)	σ_v [2] (kPa)	Gur[3] (MPa)	Gur^C [4] (MPa)	G_0 [5] (MPa)	ϕ_{TRX} [6] (Deg)	ϕ^{PS}_{TRX} [7] (Deg)	CURVE FITTING RESULTS				
							ϕ (Deg)	σ_h (kPa)	Gi (MPa)	K (σ_h/σ_v)	CD (%)
5.3	63	16.9	11.1	40.2	38.7	41.5	43.5	37	11.0	0.6	7.3
6.3	73	30.6	20.7	42.6	39.1	41.6	48.5	70	14.4	0.9	6.0
8.3	93	37.9	26.2	54.4	40.5*	43.7*	48.5	85	18.3	0.9	4.1
10.3	113	NA	NA	72.9	38.2*	40.3*	46	86	22.2	0.7	9.4
13.3	143	47.2	34.8	81.9	39.1	41.6	48.5	140	27.6	0.9	7.7

Observation: * Value interpolated from experimental data, NA = Not available.
ϕ_{cv} = 34° and ν = 0.25 during curve fitting

1-Distance from ground surface to the centre of the expandable section of the pressuremeter
2-Effective vertical stress considering the (hydrostatic) ground water level during the day of the field test
3-From the unload reload loops performed during the expansion stage: Degree of pressure unload = 40 %
4-Corrected for stress level via Bellotti et al, 1989 equations with soil parameters from the fitting analysis
5-Low strain modulus from downhole seismic cone tests (SC01 and SC02)
6-Results of the triaxial testing programme with "undisturbed" samples at similar testing depths
7-Converted plane strain friction angles derived using the Lade and Lee, 1976 empirical correlation

Table 4.1: Curve Fitting Results in Laing Bridge Site

The triaxial peak friction angles adopted here were obtained with the "undisturbed" samples of the ST1 sampler (details in Appendix C). The drained friction angles of the triaxial test (ϕ_{TRX}) were further converted into "plane strain" (ϕ^{PS}_{TRX}) angles by using the empirical relationship proposed by Lade and Lee, 1976. This relationship is largely used when comparing friction angles of triaxial and pressuremeter devices (used by all the authors cited above), and provides an initial estimate of the plane strain ϕ in the absence of other tests.

The comparison between plane strain friction angles predicted by the pressuremeter and axially symmetric triaxial values is presented on the top plot of Figure 4.11. It is noted that the pressuremeter angles are, on average, 8° above the peak triaxial values. These differences are accounted by two factors:

1. The (pressuremeter) plane strain friction angles shall be indeed higher than the (triaxial) axially symmetric values:

The lengthy review presented by Lee, 1970 and Ladd et al, 1977 on this subject indicate that the plane strain friction angle can be as high as 6 to 8° degrees greater than the ϕ_{TRX}, depending on the initial porosity of the sample. The greatest difference is associated with dense sands at low confining pressures (which appears to be the present case), and the smaller differences are associated with either loose sands at all confining pressures or dense sands at sufficiently high confining pressures to prevent dilation to occur.

2. The stress paths imposed in the virgin sand by both triaxial compression and plane strain pressuremeter tests are different. This topic is discussed in the next comparison.

The bottom plot of Figure 4.11 illustrates the comparison between predicted friction angles and "converted" plane strain values (ϕ^{PS}_{TRX}) from the triaxial test. It can be noticed that the predicted pressuremeter angles are still higher than the "reference" values, although the overestimation is slightly above 10 %. Several combined reasons can be used to explain the differences, as follows:

1. Simplifications built into the new cavity expansion model:

Although it "captures" the essential behavior of medium dense to dense sands during shear, it still idealizes the medium with a linearly elastic perfectly plastic representation.

2. Differences in the modes of deformation (and stress paths) imposed by triaxial and pressuremeter testing devices:

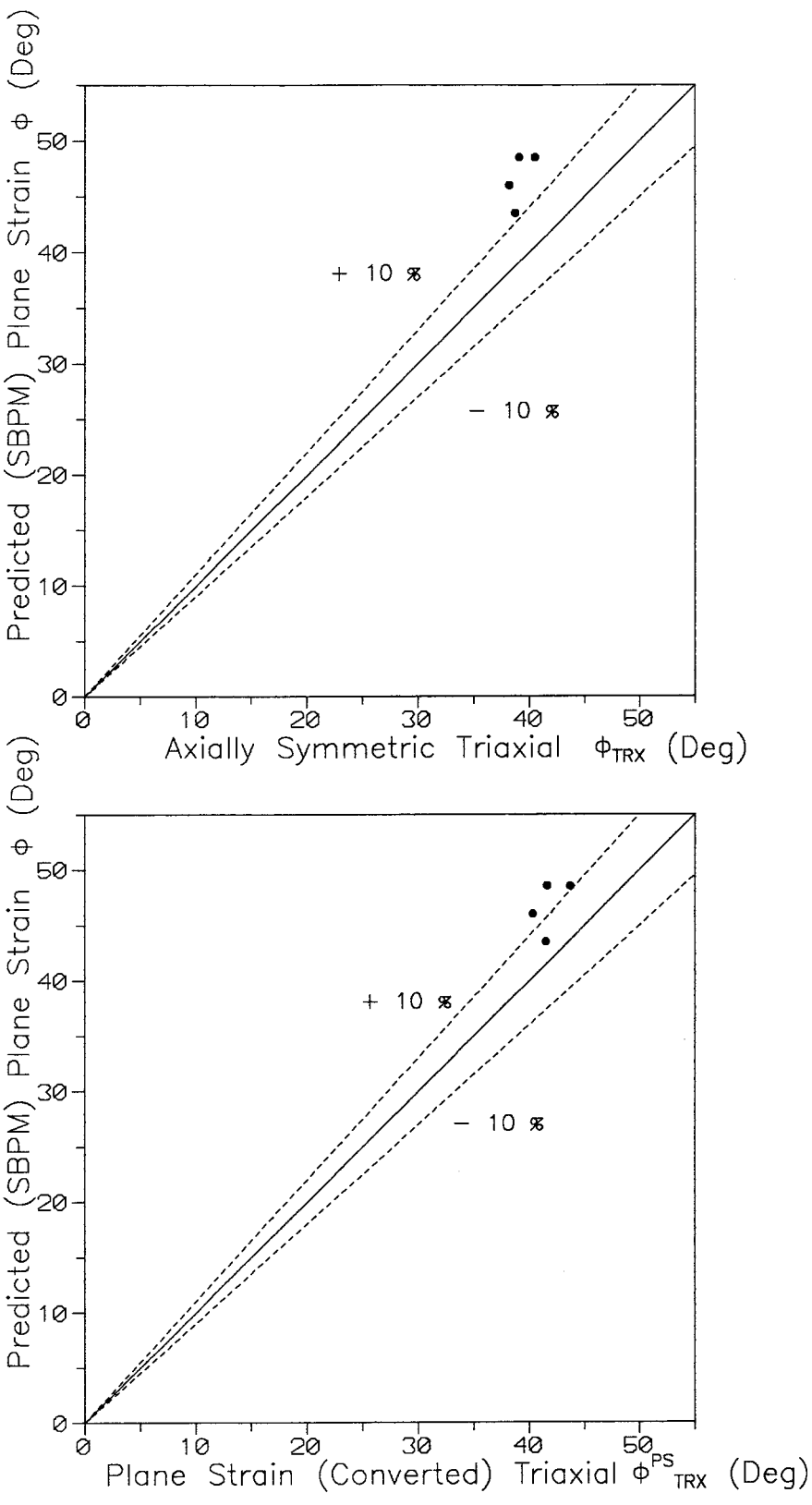

Figure 4.11: Comparison of Curve Fitting Results: Friction Angles

Wood and Wroth, 1977 observed that the mode of shear deformation imposed by pressuremeter tests corresponds to the deformation which could be imposed in a plane strain triaxial compression test with the sample in the horizontal position (the plane where σ_v acts in the field would be the laboratory σ_2 plane). This differential mode of deformation imposes differences in the mechanical properties measured during shear, as the mobilized stress ratio and the secant deformation modulus. This is due to the fact that natural granular deposits are composed of anisotropically assembled particles (cross anisotropic fabric), as demonstrated by Oda, 1972.

3. Failure mechanism of pressuremeter tests in sands:

Fahey, 1986 noticed in X Ray radiographs of the chamber tests with Leighton Buzzard sand that no evidence of the development of shear bands could be seen, even for cavity strains greater than 30 %. He speculated that the pressuremeter is an almost perfect "pure shear" plane strain test, and the predicted parameters are indeed higher than those experimentally measured in testing devices that allow the development of planes of rupture (or progressive failure).

The points discussed above suggest that the predicted friction angles of the pressuremeter test are indeed consistent with the geotechnical characteristics of the deposit (density, confining stress, mineralogy, etc.). The consistency of the results is directly related to the quality of the testing curves, as well the capacity of the model to "capture" the essential shearing behavior of this sand. Indeed, the Laing Bridge sand exhibited a highly dilatant behavior when sheared in the triaxial cell (see Appendix C), which conforms with the basic premise of the new cavity expansion model.

Friction angles predicted by the pressuremeter are higher than those obtained by other testing devices, since the pressuremeter angles refer to a special shearing mechanism (under plane strain conditions) that can be solely simulated in the laboratory by cubic or plane strain triaxial tests.

4.3.2.2 Coefficient of Earth Pressure at Rest

Table 4.1 presents the interpreted values of the coefficient of earth pressure at rest (K assumed as K_0) for the granular deposit of Laing Bridge site. A range of K varying from 0.6 to 0.9 was obtained, reflecting the natural variability of the sand strata with depth (see for instance the profile of Q_t expressed in Figure 4.4). According to Schmertmann, 1985 in only very few cases in nature are we likely to encounter

sands laid down in a manner as to result in an uniform lateral stress (or any other basic soil parameter) throughout the vertical profile.

However, the predicted values of K from the proposed methodology are higher than the "expected" K_0 values of a normally consolidated uncemented (NC) sand. This can be better visualized with the K results expressed in Table 4.2, calculated after using well established empirical relationships and the axially symmetric friction angles obtained by the triaxial tests. It can be noticed in this table that the predicted SBPM K's are higher than the normally consolidated K_0 values calculated with Jáky, 1944 equation. Assuming that K_0 is uniquely related to overconsolidation ratio (OCR) and soil strength during one dimensional unloading, the equation proposed by Schmidt, 1966 can be also used to predict overconsolidated K_0 values. This exercise suggests that the predicted SBPM K's for Laing Bridge site are equivalent to those obtained in mechanically overconsolidated granular samples subjected to OCR's in the range of 2 to 4. Based on geological evidence, the deposits of the Fraser Delta did not suffer from any kind of mechanical preloading. Hence, other site related phenomena must have happened to yield the high lateral stresses predicted by the SBPM test interpretation. The high values of K_0 in this site can be associated to one or the combined effect of the following factors:

1. Depositional characteristics of the Fraser Delta sediments:

According to Monahan et al, 1993 the sands in this delta have been deposited under a high energy environment. Migration of the main channel of the Fraser River also took place extensively during the past. This migration has been recorded, at least, over a 100 year period of time (Milliman, 1980, Clague et al, 1983), leading to reworking of the entire subaerial topset sands of the Fraser Delta (Monahan et al, 1992). The erosion and filling processes associated with this channel migration, allied with the high energy of deposition of the granular particles, could have imposed an over consolidated characteristic to this sand. It could also "lock in" high lateral stresses in the granular deposit.

2. Increase of K_0 with time:

According to Sully, 1991 the K_0 in normally consolidated soils increases with time due to post depositional history. As the soil is deposited the K values approach the NC K_0 profile given by the empirical equation of Jáky, 1944. As the soil becomes progressively buried the lateral strain condition is

DEPTH (m)	ϕ_{TRX} (Deg)	PREDICTED COEFFICIENTS OF EARTH PRESSURE K_0			
		OCR = 1	OCR = 2	OCR = 3	OCR = 4
4	42.3	0.32	0.52	0.68	0.83
5	38.7	0.37	0.58	0.74	0.89
6	39.1	0.36	0.57	0.74	0.89
7	43.5	0.31	0.50	0.66	0.81
9	37.6	0.38	0.60	0.76	0.91
11	38.8	0.37	0.58	0.74	0.89
14	39.1	0.36	0.57	0.74	0.89
Equations Used:		Jáky, 1944	Schmidt, 1966		

Determination of K_0:

1-By Jáky, 1944 empirical equation for normally consolidated soil:

$$K_o = 1\text{-}\sin \phi_{TRX}$$

2-By Schmidt, 1966 empirical equation for overconsolidated soil:

$$K_0(OC) = (1\text{-}\sin \phi_{TRX}).OCR^{\omega} \text{ where } \omega = \sin \phi_{TRX}$$

Table 4.2: Assessment of Coefficient of Earth Pressure by Empirical Formulae

modified and stress redistribution as a result of anisotropic hardening occurs, so that K_0 increases above the NC K_0 profile. The results presented by Graham and Jefferies, 1986 from several different hydraulic fills concur with the idea of K increasing with time. The analysis carried out by these authors on high quality SBPM data indicates K values that are typically two to three times higher than the K_0 predictions of Jáky's equation. Since the fills were placed hydraulically, without compaction and preloading, they are, by definition, "normally consolidated". These authors concluded that the horizontal in situ stresses in granular deposits can be "much greater than most of us would have expected".

3. Influence of past earthquakes in the Fraser Delta:

Clague et al, 1992 presented conclusive evidence for seismic liquefaction and cyclic shearing of the granular sediments of five sites close to the Vancouver metropolitan area. According to Robertson, 1982 this past seismic activity was responsible for the generation of high "locked in" horizontal stresses in the sand of a site close to Laing Bridge, leading to K_0 values that were almost double the NC K_0 values predicted by the Jáky, 1944 equation. Indeed cyclic shearing affects the lateral stress of the sand. Youd and Craven, 1975 studied the variation of the lateral stress coefficient of dry Ottawa sand when subjected to a cyclic shear loading history in the simple shear apparatus. They concluded that during repeated shear straining the coefficient of lateral stress increases with both shear strain amplitude and the number of cycles. Therefore, prehistoric earthquakes in the Fraser Delta could have imposed a lateral stress regime in the sand above the expected NC K_0 profile of Jáky's equation.

Minor factors that could preload the sand in this site would be the stockpiling of earth material for the construction of the South Approach embankment, and the ground water level fluctuations (as much as 2.5 m (Bertok, 1987)) due to the tidal influence of the nearby Fraser River.

Conclusively it can be said that the measurement of lateral stresses in sands is a difficult task, and no reliable in situ methodology exists so far for that purpose. The interpretation of SBPM high quality testing results based on the methodology advocated in this thesis constitute an initial step in this direction. It must be emphasized, however, that more experience is still required to validate the applicability of the predicted lateral stresses. The high accuracy obtained by the proposed methodology in relation to the prediction of the lateral stresses of the chamber tests (in Chapter 2) suggests that the values of K_0 established for the Laing Bridge site are consistent. It is the writer's opinion that K_0's at the Laing Bridge site are indeed high,

caused by several of the combined effects of the possible overconsolidation and lateral stress increase mechanisms speculated above.

4.3.2.3 Shear Modulus

The predicted initial shear moduli from the SBPM (Gi's) were compared with other in situ shear moduli. The unload reload modulus Gur, its stress level corrected value Gur^c and the seismic low strain modulus G_0 were adopted as a basis of comparison to Gi. As commented in Chapter 2 the SBPM Gi represents an index for the sand stiffness in the "elastic" zone surrounding the probe. Go was determined with seismic cone tests, as discussed before, whereas the pressuremeter Gur was obtained in accordance to the testing procedure recommended in Chapter 3. The stress level correction proposed by Bellotti et al, 1989 was adopted to convert the Gur modulus to Gur^c. This latter modulus is related to the original average normal effective stress of the sand.

The comparison between Gi and the pressuremeter unload reload moduli is presented in Figure 4.12. The top plot of this same figure shows the comparison between Gi and Gur, whereas the bottom plot shows the comparison between Gi and Gur^c. For the particular characteristics of the unload reload loops carried out in this thesis (degree of cavity pressure unload, cavity strain amplitude and P_{cu}), there seems to exist a reasonable constant ratio between predicted Gi's, measured Gur's and calculated Gur^c 's. In the case of Gur, the comparison of Figure 4.12 indicates that an average ratio of Gur/Gi in the range of 2 was obtained when considering all the testing depths.

The much higher value of Gur in relation to Gi comes from the fact that the deformation parameter is influenced by the stress level of the test. As commented before, the initial modulus Gi is related to the average normal effective stress σ_m of the elastic zone, hence the in situ σ_h of the deposit. The unload reload modulus Gur represents the stiffness of the sand close to the cavity wall, hence it is related to the average normal effective stress σ_{av} that existed in the plastic zone prior to the loop stage (see discussion in Chapter 2). Table 4.3 presents the estimate of both levels of stress for each of the testing depths. It is noticed in this table that the average stress level that existed in the plastic zone prior to the loop is approximately double the average stress level in the elastic zone. Given the stress level dependency of the measured modulus in sands, where higher moduli are measured for higher stress levels, it is expected that the measured Gur's will be considerably higher than the Gi's.

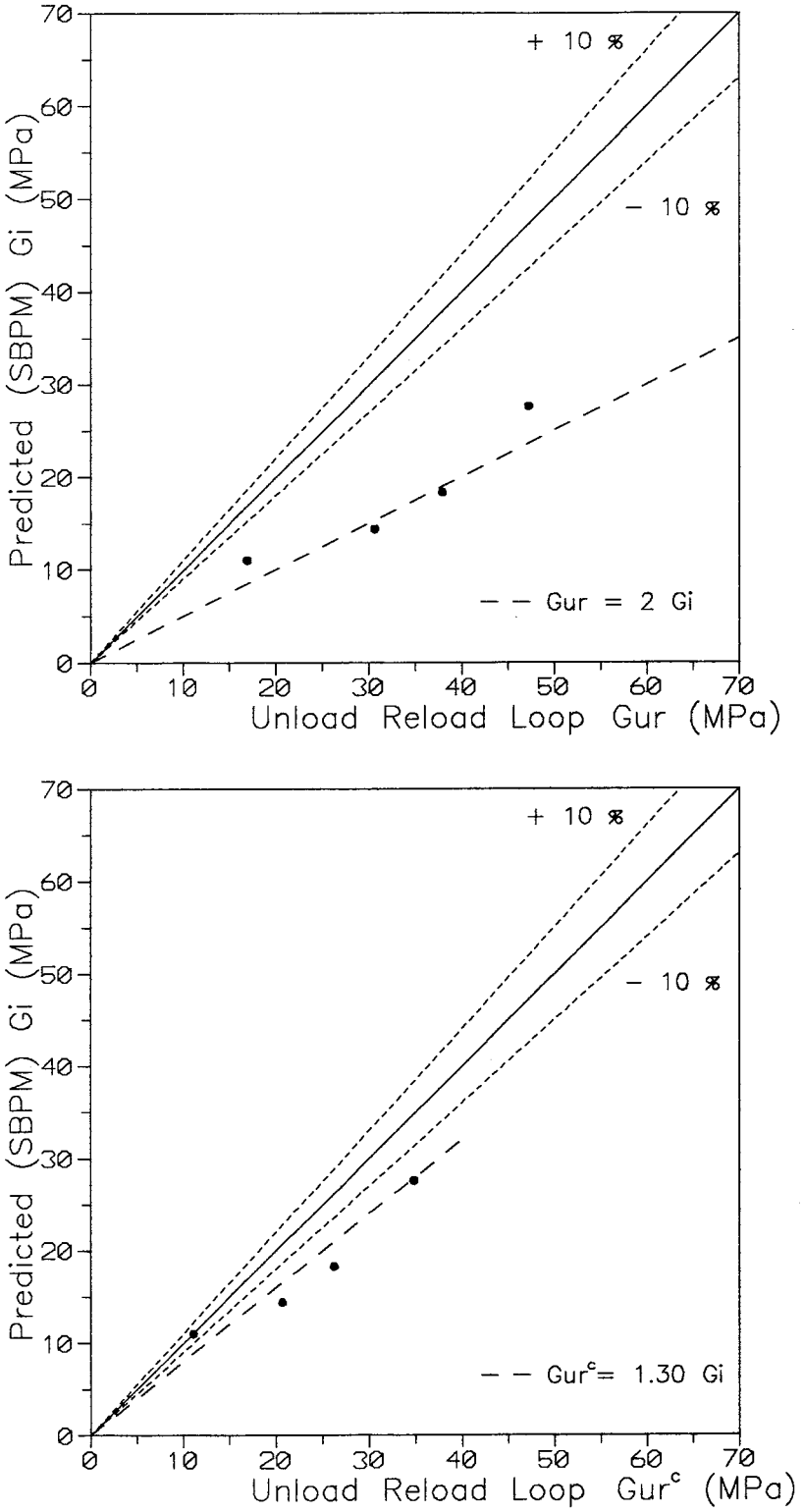

Figure 4.12: Comparison of Curve Fitting Results: Shear Modulus

TEST	DEPTH (m)	UNLOAD RELOAD LOOP (Gur, Gur^c)		CURVE FITTING (Gi)	
		γ_{av}[1] x 10^{-1} (%)	σ_{av}[2] (kPa)	γ_f[3] x 10^{-1} (%)	σ_m[4] = σ_h (kPa)
SBP18	5.3	1.9	88.2	2.3	37
SBP19	6.3	1.7	152.5	3.6	70
SBP19	8.3	1.5	177.5	3.5	85
SBP19	10.3	NA	NA	--	--
SBP19	13.3	1.7	257.4	3.8	140
	Average:	1.7 x 10^{-1} %	169 kPa	3.3 x 10^{-1} %	83 kPa

1-Average shear strain amplitude imposed by the loop cycle within the surrounding sand (Bellotti et al, 1989):

$\gamma_{av} = 0.5.\beta.\Delta\gamma_c$

where:

0.5 is a factor to produce a single amplitude of strain, as adopted by Seed and Idriss, 1970

β is a empirical reduction factor based on the chamber data of Bellotti et al, 1987

$\Delta\gamma_c$ is the shear strain amplitude of the loop cycle in the cavity wall = 2 $d\varepsilon_\theta$

2-Average normal effective stress within the plastic zone that existed prior to the loop stage (Bellotti et al, 1989):

$\sigma_{av} = \sigma_h + \alpha(P_{cu} - \sigma_h)$

where:

α is a empirical reduction factor based on the chamber data of Bellotti et al, 1987

P_{cu} is the effective internal pressure at the start of the unload reload loop

3-Calculated by Equation 2.33

4-Average normal effective stress in the horizontal plane = σ_h predicted by the curve fitting analysis

Table 4.3: Strain and Stress Levels Related to Gur and Gi

The comparison between Gur^c and Gi in Figure 4.12 indicates an average ratio of Gur^c/Gi in the range of 1.3 when all the testing depths are considered. Since both Gur^c and Gi are related to the same value of average normal effective stress they should be, in principle, the same. The discrepancy between calculated Gur^c's and predicted Gi's may be given by the differences in the amplitude of shear strain that is related to each of these moduli. Gur is related to the average shear strain amplitude γ_{av} imposed by the loop cycle in the surrounding sand, whereas Gi is assumed to be related to the limit shear strain amplitude γ_f mobilized in the elasto-plastic boundary. Using the average shear strain amplitude related to Gur^c and Gi in Table 4.3, it is possible to show in Figure 4.13 the expected values for the stiffness ratios Gur^c/G_0 and Gi/G_0. These values are respectively 0.26 and 0.17. The ratio 0.26/0.17, or 1.5, represents the expected value of Gur^c/Gi, assuming that the average attenuation curve of Idriss, 1990 is valid for this particular sand. This ratio is close to the average experimental value of 1.3 presented in Figure 4.12, providing convincing evidence that the differences between Gur^c and Gi are indeed due to strain level differences.

The comparison between Gi and the seismic modulus G_0 is presented in Figure 4.14. As noted before, the shear modulus determined from in situ downhole shear wave velocity measurements represents the stiffness of the sand at shear strain amplitudes in the range of 10^{-4} %. According to the average attenuation curve of Idriss, 1990 a ratio of Gi/G_0 equal to 0.17 was expected. The experimental results of Figure 4.14 indicate a higher average ratio than the "expected" ratio based on Idriss's curve. This may be partially related to the simplified manner at which some relevant strain amplitude is related to these moduli. Another reason may be the universality of Idriss' proposed curve. Idriss's curve may not be fully applicable to sands of different gradation or mineralogy than those used to generate his curve.

The comparisons discussed above suggest that the predicted Gi of the pressuremeter test is a reasonable representation of the response of the sand when sheared in the horizontal direction with a strain amplitude in the order of 10^{-1} %.

4.3.2.4 Modulus Reduction Curve

As commented in Chapter 2 using the information obtained by the fitting technique, together with the low strain modulus (G_0) of the sand, it is possible to predict the shear stress-strain monotonic "elastic" curve of the tested sand. For that purpose, the hyperbolic model of Kondner, 1963 was adopted,

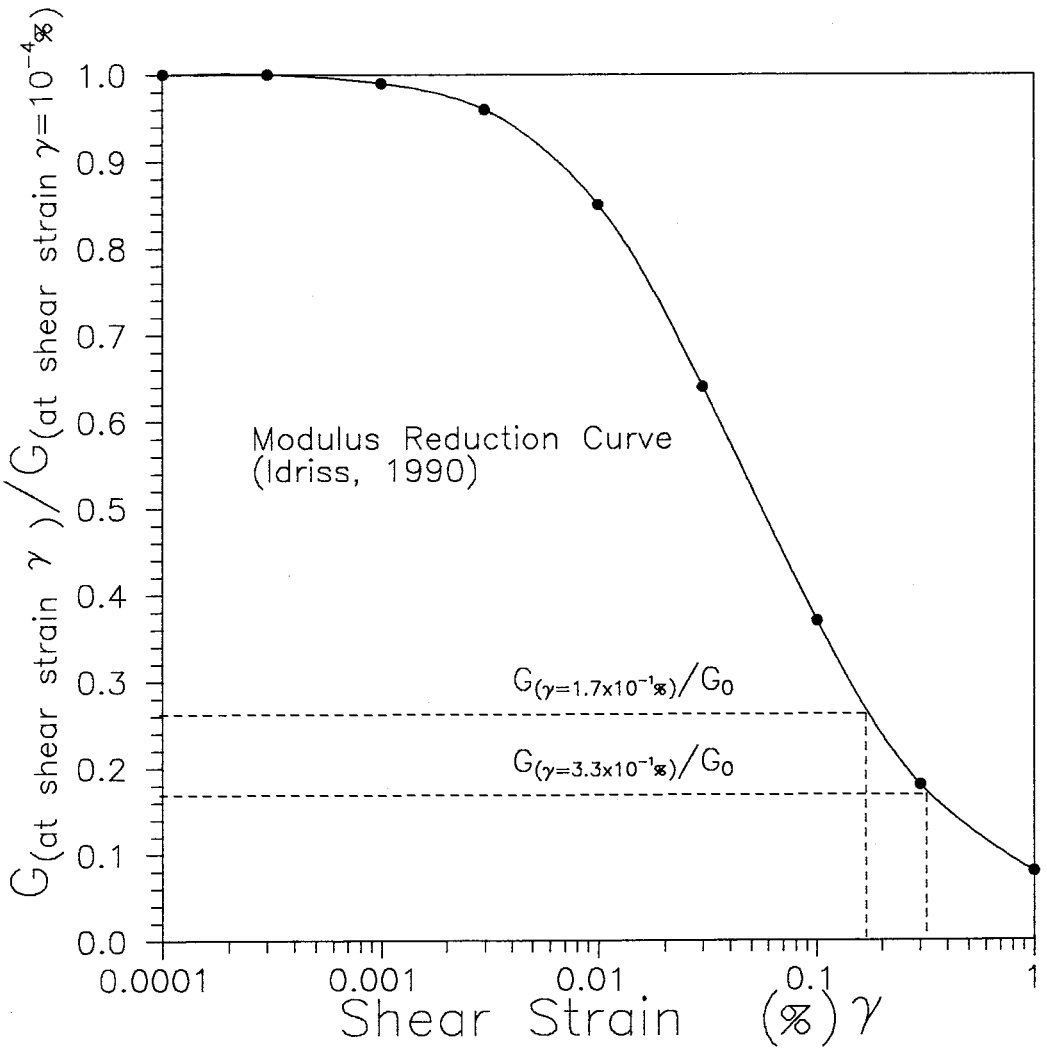

Figure 4.13: Determination of Modulus Reduction Ratio for Different Amplitudes of Shear Strain

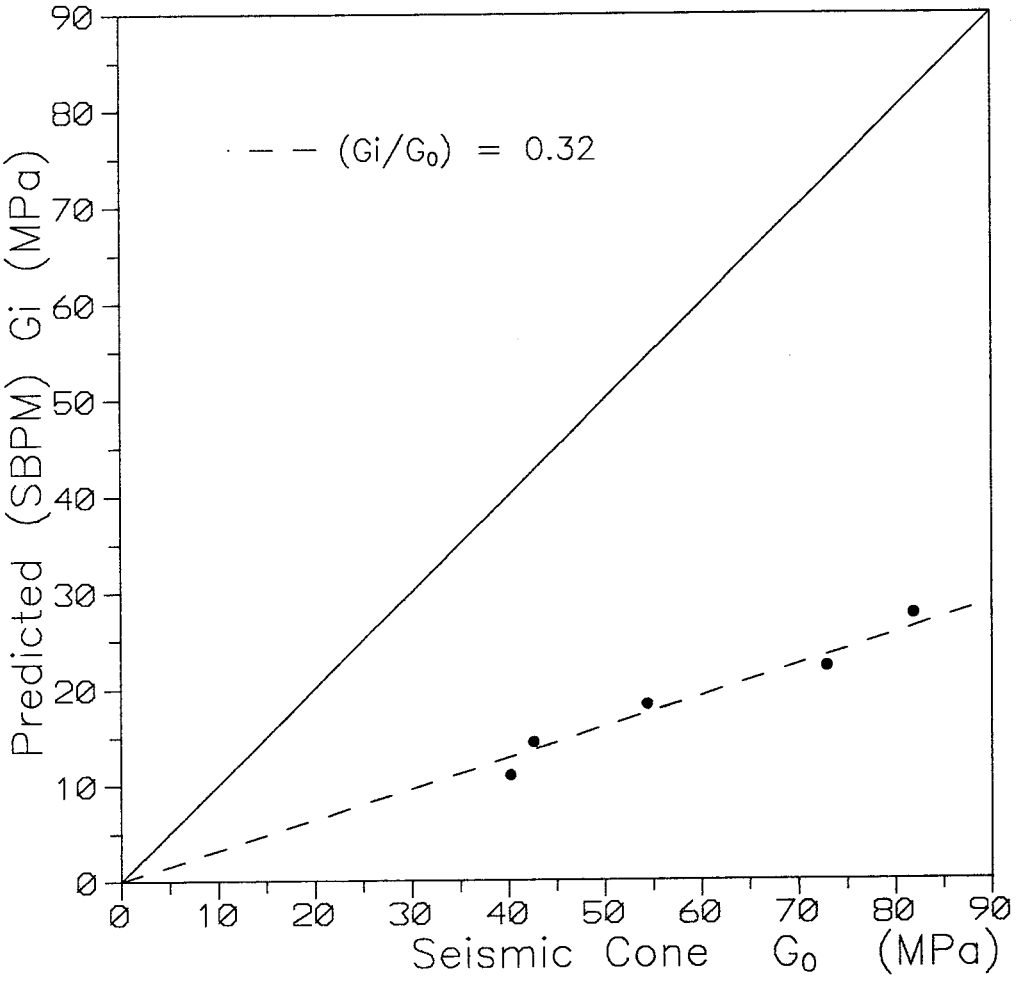

Figure 4.14: Comparison between the Predicted Gi from Curve Fitting and the Seismic Modulus G_0

allowing the development of a final hyperbolic equation (Equation 2.83) written in terms of the (fitted) basic parameters of the sand.

This subsection briefly demonstrates the use of this equation, including how to predict the secant shear modulus of the sand at a variety of shear strain levels. For that purpose it was adopted the pressuremeter curve with the lowest coefficient of disturbance. This curve is the one presented before for the depth 8.3 m, where a coefficient of disturbance of 4.1 % was obtained.

Using Equation 2.83 with the curve fitting results (ϕ, σ_h and Gi) of Table 4.1 for this depth it is possible to draw the idealized monotonic stress strain response of the tested sand, from very small strains (10^{-4} %) to large strain levels (> 1 %). This curve is presented in Figure 4.15(a), where it can be noticed:

1. The initial secant modulus of the curve, equivalent to the response at very low strain levels, leads to a shear modulus G equal to the G_0 obtained at this same depth with the seismic cone results. This was indeed expected, as the value of G_0 was used to infer the final value of Gi predicted by the fitting technique (using Equation 2.83), in accordance to the interpretation approach suggested in Chapter 2.

2. The strain level assigned to Gi in this figure is the value calculated in Table 4.3 with the fitting parameters and the Equation 2.33. This strain level represents the value above which failure starts to occur in the elasto perfectly plastic soil (γ_f). Since the hyperbolic model considers that the soil fails only at infinite strain (where $\tau = \tau_{max}$), it is possible to obtain the soil response for strain levels above γ_f.

Using the curve established in Figure 4.15(a) or Equation 2.83 it is possible to calculate the stiffness ratio of the sand (G/G_0) for each level of induced shear strain (γ), hence determine the complete curve that describes the variation of the secant shear modulus with the strain level. Figure 4.15(b) presents the stiffness ratio attenuation curve for the tested sand. This curve ideally represents the pure shear stress-strain behavior of the sand at 8.3 m depth from very low to large strains, when sheared under a average normal stress level equal to σ_h.

In Figure 4.15(b) is also shown the singular value of stiffness ratio Gur^c/G_0 as obtained with the data gathered by the unload reload loop performed during the testing stage. The agreement is good, besides of the semi-empirical approaches adopted to estimate the corrected (for stress level) Gur^c modulus and the relevant strain amplitude γ_{av}. This suggests that the idealized modulus reduction curve may indeed resemble the soil response from very small to large strain levels.

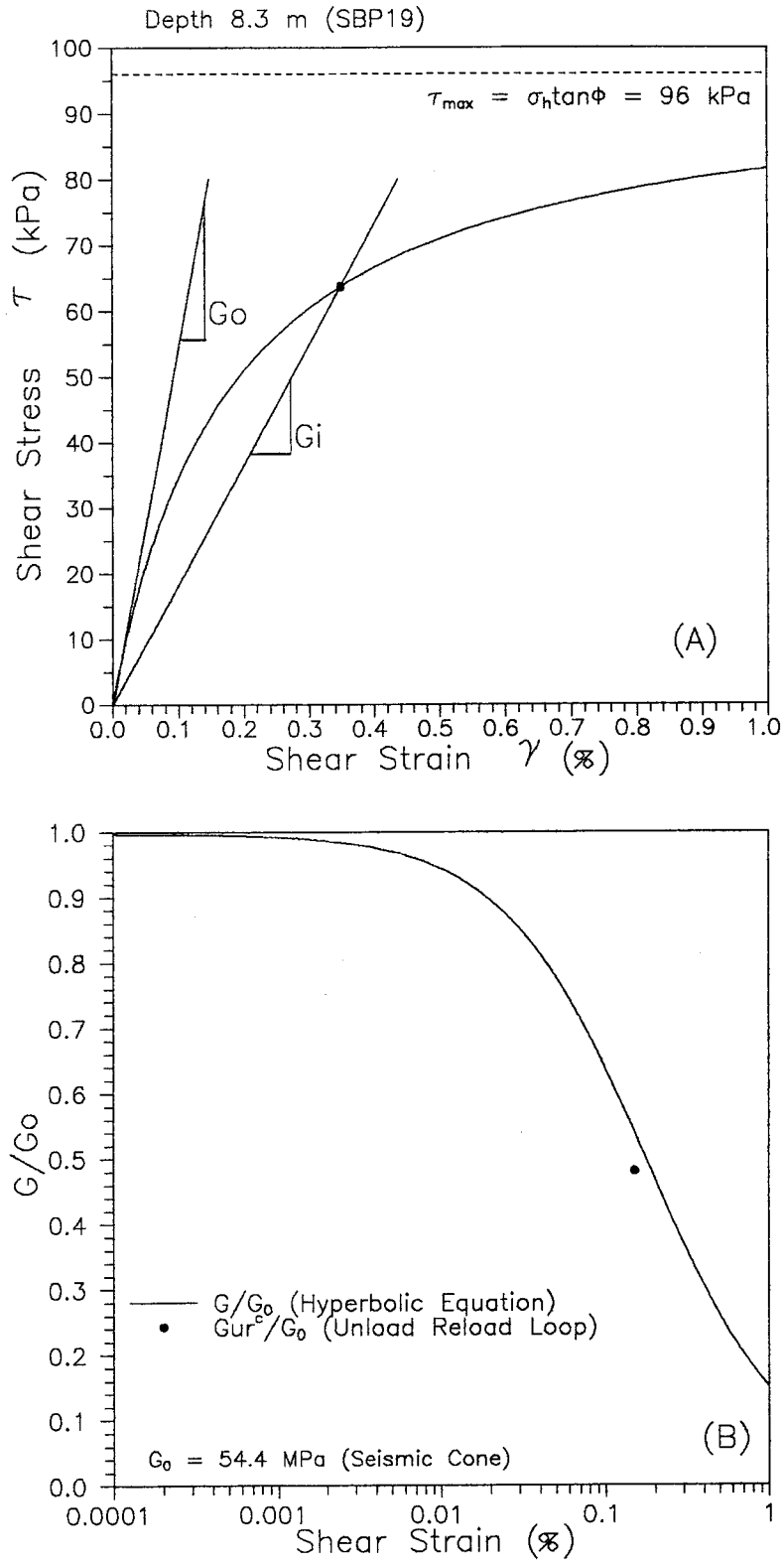

Figure 4.15: (a) Hyperbolic Stress Strain Curve for Depth 8.3 m (SBP19)
(b) Secant Shear Modulus Ratio versus Shear Strain

In conclusion, the procedure above constitutes a simple method to define the stress strain response in the elastic zone. For that the proposed procedure uses fundamental (coupled) soil parameters derived from an elasto-plastic theory into a hyperbolic model. This model is assumed to represent the soil response beyond the elasto-plastic boundary. It is emphasized that the above procedure constitutes a rational manner (with closed form solutions) to extend the elastic shear modulus of the pressuremeter to a variety of strain levels, thus allowing this modulus to be applied to any engineering problem where the design load induces a variable pattern of strains in the soil.

On the other hand, it is important to recognize that the deformation behavior of the soil is considerably affected by factors such as the consolidation history, the stress path and the stress system during shear, as demonstrated by Vaid, 1985. Vaid showed that the hyperbolic approximation of Kondner, 1963, defined with hyperbolic constants from the results of conventional triaxial tests, was not able to properly describe the undrained stress strain behavior of Haney clay under anisotropic consolidation history or other stress paths during shear. Thus, separate hyperbolic representations for each particular testing condition had to be defined. Extending such findings to the present case in sand, it is also concluded that the proposed procedure must be used with care in cases where the boundary conditions of the analyzed engineering work differs considerably from those of the pressuremeter test.

4.4 CONCLUSIONS

A methodology to interpret pressuremeter testing curves in sand was presented in Chapter 2 and used here to derive the basic soil parameters of a typical granular deposit in the Fraser Delta, at the Vancouver International Airport.

The large amount of data obtained with the field trials carried out by the writer, together with the development of a new disturbance criteria, allowed the establishment of "optimum" conditions for insertion with the UBC SBPM. The high quality testing curves adopted in this chapter are those derived under such "optimum" condition, in which disturbance was categorized and minimized.

The measured friction angles by the pressuremeter test analysis were higher than the values obtained by consolidated drained triaxial tests, most probably due to the particular shearing conditions imposed by the pressuremeter. The SBPM plane strain ϕ values of the tested sand were about 8° higher than the triaxial values and varied from 43.5 to 48.5°, reflecting the variable density and confining conditions of the

different layers of sand in the granular strata. The interpreted lateral stresses predicted by the SBPM were considerably higher than initially expected, leading to K's that varied from 0.6 to 0.9 as a result of the combined influence of several post depositional factors that took place at this site. The initial shear modulus Gi varied from 11 to 27.6 MPa, for the same reasons observed above for ϕ. Nevertheless, a good correspondence was observed between this modulus and the unload reload moduli (Gur, Gur^c), as well as the low strain modulus (G_0) from downhole shear wave velocity measurements, when stress level and strain amplitude effects are considered. It appears, therefore, that the pressuremeter modulus Gi obtained from the proposed curve fitting technique reflects the stress-strain response of the sand when sheared in the horizontal plane under a shear strain level in the order of 10^{-1} %, and average normal stress equal to σ_h.

In summary, when the proposed interpretation methodology is used on high quality testing curves obtained with the insertion and testing procedures advocated in Chapter 3, it is possible to derive a consistent set of basic soil parameters. This set is coupled by the framework of the theoretical model and represents the strength, stiffness and lateral stress of the studied sand. The predicted strength and stiffness are, however, related to the particular shearing mechanisms imposed by the pressuremeter in the surrounding soil. The set of predicted parameters may be further used in a hyperbolic model to extend the applicability of the pressuremeter modulus to a variety of strain levels. Additional validation of this latter approach may be required before it is used in design.

CHAPTER 5.0 SUMMARY AND CONCLUSIONS

5.1 SUMMARY

The emphasis of this thesis was placed on the establishment of a methodology of interpretation of selfboring pressuremeter testing results in sands. Emphasis was also placed on the standardization of both insertion and testing procedures adopted for the UBC selfboring pressuremeter, when used in granular deposits of the Fraser Delta.

Recognizing the potential value that selfboring pressuremeter testing has to predict reliable soil parameters in soils that are difficult to sample, this thesis had the following objectives:

1. Review the existing cavity expansion models developed to interpret the selfboring pressuremeter data, considering the idealized assumptions made for the models to simulate the complex process of the cavity expansion in sands.

2. Review the current interpretation methodologies applicable for predicting the basic soil parameters (ϕ, σ_h and G) from SBPM testing data in sands, discussing their possible limitations.

3. Develop a new interpretation methodology to derive the basic soil parameters of the sand, with either undisturbed or disturbed SBPM data. The new approach should lead to repeatable and reliable conclusions in the evaluation of the sand behavior in situ.

4. Evaluate the reliability of some of the existing cavity expansion models, when applied together with the new interpretation methodology to analyze SBPM testing data in sands.

5. Develop an improved cavity expansion model to be used together with the new interpretation methodology for the prediction of soil parameters from SBPM tests in sands.

6. Determine the "optimum" insertion procedure of the UBC SBPM for its use in granular deposits of the Fraser Delta. This procedure shall minimize, to a large extent, the influence of disturbance on the testing data.

7. Develop a coefficient of disturbance to serve as an index to quantify the relative quality of the insertion procedure.

The main contribution with respect to the interpretation of SBPM testing curves was the development of a new methodology of analysis. This new methodology relies on a curve fitting technique to match the

idealized model curve to experimental testing curves, and simultaneously predict the basic parameters of the sand. It was used together with a newly developed cavity expansion model. The new cavity expansion model is based on the basic principles of cavity expansion in elasto-plastic frictional materials, and extends the rheological equations of Hughes et al, 1977 to incorporate elastic strains in the expanding "plastic" zone. This model additionally differentiates between the required shear moduli of both "elastic" and "plastic" zones surrounding the probe. Initial validation of this model, as well as the new interpretation technique, was carried out with published SBPM results from calibration chamber tests. These chamber tests were carried out with different probes, installation procedures ("ideal" or selfbored), and different sands at differing conditions of density, stress history and confining pressure. The remarkably good agreement of the predictions (within 10 % of the baseline values) gives high confidence in the usage of the new interpretation methodology in SBPM testing curves in medium dense to dense sands. The proposed interpretation methodology can also be coupled to a hyperbolic model to establish the idealized shear stress-shear strain response of the tested sand. This model is useful to extend the applicability of the predicted modulus Gi to strain levels that are more relevant for the design of civil engineering works.

It has been determined that the quality of the soil parameters predicted by the proposed interpretation methodology is also dependent on factors other than the initial conditions of the sand. The quality of the testing curve (or disturbance built into this curve), the inherent sensitivity of the new cavity expansion model to changes in the input parameters, and the strain range of curve match are factors that have to be considered in the analysis of field SBPM curves. These factors were explored and discussed in detail in Chapter 2, leading to general guidelines for the interpretation of SBPM testing data in sands.

Disturbance is the major variable that reduces the quality of the testing curve, and hence, the reliability of the predicted sand parameters. In sands disturbance can be reduced to a large extent if an optimization (trial and error) routine is carried out in the field with the insertion and equipment variables. This thesis also attempted to identify the most important variables that generate soil disturbance. This was explored in detail in Chapter 3. Using the new interpretation methodology a new approach to numerically quantify the disturbance of the testing curve was created. This new disturbance criteria measures the disturbance of the curve by a "coefficient of disturbance" (CD). The CD has been found to properly reflect the degradation of the quality of the testing curve by partial plugging of the cutting shoe, improper jetting

rod positions and dimensional tolerances of the equipment. Using the CD parameter, numerical ranges for "undisturbed" (or close to), "disturbed" and "highly disturbed" testing curves were proposed. With these ranges it was possible to optimize the insertion procedure of the UBC SBPM in a particular granular deposit of the Fraser Delta. Although the conclusions were developed for the Laing Bridge site they also apply to other sites of similar sand stratigraphy.

This thesis also attempted to recommend a testing procedure for SBPM's in sands. This procedure took into consideration the findings of Chapter 2 (expansion up to 10 %, with at least 1 unload reload loop stage), the results of FDPM tests at different rates of inflation, and the assessment of the creep influence on loops with 8 min. holding phases.

Using the recommended insertion procedure it was possible to obtain high quality SBPM testing curves in the test site of the Fraser Delta. These field curves were used to further validate the proposed interpretation methodology. The predicted sand parameters were compared to soil parameters from laboratory and other in situ tests, allowing a discussion of the significance of the pressuremeter predictions. The comparisons highlighted the fact that the predicted sand strength and stiffness are related to the particular shearing mechanisms imposed by the SBPM in the surrounding medium.

Simplicity, accuracy and reliability are the essential features of the proposed methodologies of this thesis. It is believed that the information contained herein will aid pressuremeter practitioners to design safer and more economical civil engineering works.

5.2 METHODOLOGY OF INSERTION

The methodology of insertion of the SBPM is related to the procedures adopted in the field to minimize the extent of disturbance on the testing curves.

This thesis identified and discussed the major insertion and equipment variables that have to be considered during the field optimization of the SBPM insertion. The recommended UBC SBPM insertion procedure is presented in Chapter 3, and is based on the field experience gathered throughout the 23 soundings performed at the Laing Bridge site. The recommended procedure considerably enhanced the quality of the SBPM testing curves, and serves to standardize the operation of this complex device.

The main findings with respect to the selfboring process are:

1. Insertion of SBPM's with a jetting system is viable, provided that a trial and error routine is adopted in the field to establish the optimum combination of jetting variables.

2. Disturbance can be expected to be differentially generated along the selfbored profile if a constant combination of insertion variables is adopted. This is due to the differential sensitivity of the distinct sand layers to the vibration, etc. that take place during the insertion of the SBPM. Loose layers are more prone to disturbance than dense layers. There seems to be a close relationship between the density of the layer (or the pressuremeter penetration resistance) and the CD of the testing curve.

3. It is possible to reduce the amount of disturbance in the testing curve. This requires the adoption of a field optimization routine in which the CD parameter is used as a "benchmark" to guide the quality of insertion. The CD shall be minimized in the field insertion routine to values below 10 %.

The main findings with respect to the equipment adopted during the selfboring process are:

1. The current design of the UBC "shower head" jetting system requires a redesign since it leads to overcoring of the sand during SBPM insertion. This system may also prove useful if insertion is carried out at a faster rate with less mud flow.

2. Steel lanterns composed of curved strips and overlapped together should not be used to shield the SBPM, unless the strips have the same curvature as the SBPM shaft. Interstrip friction generated by the lateral stress and the accumulation of granular particles are common occurrences with the use of such lanterns. For the UBC SBPM only the Camkometer lantern (reported in Fahey et al, 1988), which has butted strips (no overlaps) and eliminates interstrip problems, is recommended.

3. The dimensional tolerances of the equipment used to assemble the SBPM have a significant impact on the final testing results. Disturbance is generated in the surrounding sand during the selfboring process when the SBPM has dimensional differences along the shaft (as is usually the case). The disturbance generated by the UBC SBPM system can be essentially removed if tapered lantern retainers, designed to reduce dimensional differences to less than 0.7 % the diameter, are adopted to hold the Camkometer lantern. Besides, for the UBC design two 1 mm thick rubber membranes are also required beneath the Camkometer lantern.

5.3 METHODOLOGY OF TESTING

Once the insertion related variables are understood and optimized it is possible to standardize the expansion (testing) routine carried out in the field.

The recommended UBC SBPM testing procedure was proposed in Chapter 3, based on the results of several pressuremeter tests at the Laing Bridge site and the findings of Chapter 2. This procedure allows the establishment of the basic soil parameters with the proposed interpretation methodology, as well it provides the new cavity expansion model with reliable input values of Gur. The main findings are:

1. The SBPM should be expanded to a maximum circumferential strain of 10 %, which is enough to yield the parameters of the sand via curve fitting technique. At least one unload reload loop stage should be carried out, after a (constant pressure) holding phase.

2. Rate of inflation in between 0.5 to 7.0 kPa/s lead to similar stress-strain testing curves in sands. They also lead to fully drained testing curves. Therefore the inflation should be carried out in stress controlled manner with a rate of inflation between 3 to 4 kPa/s. This range represents a compromise between a low rate, required to allow fully drained expansion, and a fast rate, required for a quick test. Computer controlled SBPM tests are suggested in order to ensure the repeatability and the constant rate of expansion of the test.

3. Pressure holding phases of (at least) 8 min. are effective to reduce the final creep rate to a target 0.001 %/min prior to the unload reload loop stage. A simplified analysis indicated that the Gur derived in this manner will be underestimated to an average extent of less than 3 %. This is valid for loops with a degree of pressure unload of 40 %.

5.4 METHODOLOGY OF INTERPRETATION

The methodology of interpretation is related to the procedures adopted to predict the basic soil parameters of the sand with the use of the SBPM testing curve.

The main findings in this area are:

1. The traditional methodologies currently available to interpret SBPM testing curves in sands do not lead to reasonable predictions of the basic sand parameters in disturbed SBPM test data. They can only be applied to high quality testing curves.

2. The proposed interpretation methodology, together with the new cavity expansion model, has the capability to simulate reasonably well the pressuremeter testing curve in medium dense to dense sands. Indeed, provided that the sand has a dilatant (shear induced volume increase) behavior during shear, the new approach leads to reasonably accurate predictions of the sand parameters in both undisturbed (or close to) and disturbed data.

3. The proposed interpretation methodology leads to a set of "coupled" parameters that are linked to each other by the framework of the chosen cavity expansion model. The set of parameters, rather than each individual value, can be used in a more reliable way to simulate the soil response in further design analyses.

4. Matching between the field and the idealized model curve can be either visually accomplished, or with the use of a "curve fitter" software program. The available software programs (Sigmaplot^{TM} or Kaleidagraph^{TM}) are useful for high quality testing curves, as they lead to similar results as those obtained by the visual match of the curves. On the other hand, these software programs can not be adopted for disturbed curves, as some experience related input may be required. This is because, with disturbed curves, the "strain range" of curve match has a fundamental effect on the reliability of the final predicted parameters. For these curves ($10\ \% < CD < 30\ \%$) the curve match should be accomplished between cavity strains of ≈ 5 to $\approx 10\ \%$ (to be visually defined), since disturbance will considerably affect the parameters obtained with the match in the initial stages (0 to $\approx 5\ \%$) of the testing curve. For undisturbed or slightly disturbed curves ($CD < 10\ \%$) the curve match can be accomplished between cavity strains of 0 to $\approx 10\ \%$. Beyond this strain level any of the discussed models of Chapter 2 can not be adopted, as the sand surrounding the cavity starts to shear under critical state conditions and the cavity expansion deviates from the idealized cylindrical form.

5. End effects do not appear to influence the field testing results, provided that the cavity expansion is carried out to low strains (below $\approx 10\ \%$), and the pressuremeter has a slenderness ratio (L/D) equal to (or greater than) six.

6. Both the proposed (new) and the Carter et al, 1986 models lead to similar results if the adopted Poisson's coefficient is in the range of 0.2. The Hughes et al, 1977 model tends to underestimate the strength and the stiffness of the sand, due to the lack of incorporation of elastic strains in the expanding "plastic" zone.

7. The friction angle is the least sensitive (and most reliable) parameter obtained from the curve fitting analysis. This is due to the fact that the curve match is dominated by this variable when the new (or the Carter et al, 1986) model is used. The errors in the assessment of Gi and σ_h are of similar magnitude. These errors are low (or null) if high quality testing curves are adopted, and the constraint imposed by Equation 2.81 (between the sand parameters) is adopted during the fitting process. Both the predicted strength and stiffness are intrinsically related to the particular mode of deformation imposed by the SBPM in the surrounding sand, and may be expected to differ from the parameters predicted in the same sand with other in situ or laboratory testing devices.

8. Both the Poisson's coefficient and the constant volume friction angle can be estimated in the curve fitting process. The final error of the predicted basic parameters of the sand is small (below 10 %), when "educated guesses" of ν and ϕ_{cv} are used.

5.5 FINAL REMARKS

This thesis has shown that the parameters predicted by SBPM tests in sands are affected by many factors other than the shearing behavior of the soil. These factors are related to the quality of insertion, the testing procedure and the interpretation approach. Standardization of the insertion stage of this probe constitutes an initial step to reduce the differences due to different field procedures. This standardization has been applied to the operations of a particular system (as the UBC SBPM), in order to minimize the likelihood of disturbance in the testing curve.

The new interpretation methodology provides a framework to predict consistent values of the basic sand parameters. It also furnishes the pressuremeter practitioner with a technique to numerically quantify the disturbance of the testing curve. This may prove useful in the optimization routine carried out in the field with the insertion variables. At present, the proposed methodology constitutes the most fruitful approach to analyze SBPM results in sands, although more research still needs to be devoted in this area.

5.6 SUGGESTIONS FOR FUTURE RESEARCH

Two complementary areas of research were identified with the SBPM test. One is specific to the UBC SBPM system, whereas the other can be applied to any SBPM. The first area would be the improvement of the current design of the UBC SBPM. The second area would focus on the further validation of the

proposed interpretation methodology, and its extension to sands that shear in a different manner than the sand studied here (like very loose to loose sands, cemented sands, etc.).

5.6.1 Equipment Development

• Improvement of the pumping unit, in order to make this unit operate with an independent source of hydraulic power. A high capacity pump capable of providing mud as high as 50 to 70 l/min would be recommended. This is essential for jetting in clays.

• Construction of a simulated laboratory test chamber with synthetic material, to calibrate the SBPM.

• Improvement of the data acquisition system, such that strain controlled holding phases and expansion tests would be possible.

• Improvement of the effective (pore) pressure transducer , such that it can be connected to the outer lantern rather than the inner rubber membrane.

• Improvement of the shower head jetting system. The redesign of this head and new field trials at a faster rate with less mud flow is suggested. This system may prove useful in deposits of coarse sands, where blockage of the cutting shoe may occur with the use of the central jetting system.

5.6.2 Interpretation of SBPM Data

• Validation of the proposed interpretation methodology in field tests where the soil baselines are well established. Friction angles measured in either the cuboidal or the plane strain triaxial apparatus could be used as a reference for the predicted SBPM friction angles. Shear moduli from resonant column tests with undisturbed sand samples (consolidated to the lateral stresses predicted by the SBPM for the site) would serve as a basis of reference to the predicted SBPM shear moduli.

• Verification of the capacity of the predicted SBPM soil parameters to simulate the behavior of actual engineering works. Field tests in areas where trial embankments will be constructed and monitored could be performed.

• Development of a new cavity expansion model for the interpretation of SBPM testing results in sands that: (a) present a pronounced strain softening behavior during shear; (b) contract during shear.

• Use of the SBPM data to study dilatancy of sands and apply to liquefaction analysis and trigger mechanisms.

• Use of cyclic SBPM tests to simulate and measure undrained residual strength of sands.

BIBLIOGRAPHY

ABBREVIATIONS:

CGC = Canadian Geotechnical Conference
CGJ = Canadian Geotechnical Journal
ECSMFE = European Conference on Soil Mechanics and Foundation Engineering
ESOPT = European Symposium on Penetration Testing
GTJ = Geotechnical Testing Journal
ICSMFE = International Conference of Soil Mechanics and Foundation Engineering
IJNAMG = International Journal for Numerical and Analytical Methods in Geomechanics
ISOPT = International Symposium on Penetration Testing
ISPMA = International Symposium on the Pressuremeter and Its Marine Applications
ISSRIIT = International Symposium on Soil and Rock Investigation by In Situ Testing
J-GED = Journal of the Geotechnical Engineering Division
J-SMFD = Journal of the Soil Mechanics and Foundation Division
OTC = Offshore Technology Conference
PCSMFE = Pan-American Conference of Soil Mechanics and Foundation Engineering
SCIMSP = Specialty Conference on In Situ Measurement of Soil Properties
SF = Soils and Foundations
SMS = Soil Mechanics Series
USSSRIT = Updating Subsurface Sampling of Soils and Rocks and their In-Situ Testing

Ages, A. and Woollard, A. (1976). The tides in the Fraser estuary. Pacific Marine Science Report 76-5, Canada Department of Environment.

Alpan, I. (1967). The empirical evaluation of the coefficient K_0 and K_{OR}. SF, 7, No. 1, 31-40.

Anderson, W.F. and Pyrah, I.C. (1989). Consolidation and creep effects in the PMT in clay. XII ICSMFE, Rio de Janeiro, Vol. 1, 153-156.

Andrawes, K.Z. and El-Sohby, M.A. (1973). Factors affecting coefficient of earth pressure K_0. ASCE, J-SMFD, 99, SM7, July, 527-539.

Arnold, M. (1981). An empirical evaluation of pressuremeter test data. CGJ, 18, 455-459.

Arthur, J.R.F. and Menzies, B.K. (1972). Inherent anisotropy in a sand. Geotechnique, 22, No. 1, 115-128.

Atkinson, J.H. and Bransby, P.L. (1978). The mechanics of soil-an introduction to critical state mechanics. Mc. Graw-Hill, London.

Atkinson, J.H. and Richardson, D. (1985). Elasticity and normality in soil-experimental examinations. Geotechnique, 35, No. 4, 443-449.

Atkinson, J.H. and Sallfors, G. (1991). Experimental determination of stress-strain-time characteristics in laboratory and in situ tests. X ECSMFE, Vol. 3, Firenze, 915-956.

Atwood, M.J. (1990). Investigation of jetting insertion procedures for rapidly deploying a self-boring pressuremeter in soft clays. M.Sc. Thesis, University of New Hampshire.

Bachus, R.C. (1983). An investigation of the strength deformation response of naturally occurring lightly cemented sands. Ph.D. Thesis, Department of Civil Engineering, Stanford University.

Baguelin, F. (1982). Rules of foundation design using self-boring pressuremeter test results. 1st ISPMA, Paris, 347-360.

Baguelin, F., Jézéquel, J.F. and Shields, D.H. (1978). The pressuremeter and foundation engineering. Trans Tech Publications, First Edition, Germany.

Baguelin, F., Jézéquel, J.F., Le Mee, E. and Le Méhauté, A. (1972). Expansion of cylindrical probes in cohesive soils. ASCE, J-SMFD, 98, SM11, November, 1129-1142.

Baguelin, F., Jézéquel, J.F., Lemée, E., Le Méhauté, A. (1972). Expansion of cylindrical probes in cohesive soils. ASCE, J-SMFD, 98, SM11, November, 1129-1142.

Baldi, G., Bellotti, R., Ghionna, V., Jamiolkowski, M. and Pasqualini, E. (1982). Design parameters for sands from CPT. 2nd ESOPT, Amsterdam, Vol. 2, 425-438.

Baldi, G., Bellotti, R., Ghionna, V.N., Jamiolkowski, M. and Lo Presti, D.C.F. (1989). Modulus of sands from CPT's and DMT's. XII ICSMFE, Rio de Janeiro, Vol. 1, 165-170.

Baligh, M.M. (1976). Cavity expansion in sands with curved envelopes. ASCE, J-GED, 102, GT11, November, 1131-1146.

Barden, L. and Khayatt, A. (1966). Incremental strain rate ratios and strength of sand in the triaxial test. Geotechnique, 16, No. 4, 338-357.

Been, K., Jefferies, M.G. and Hachey, J. (1991). The critical state of sands. Geotechnique 41, No. 3, 365-381.

Bellotti, R., Crippa, V., Ghionna, V.N., Jamiolkowski, M. and Robertson, P.K. (1987). Self-boring pressuremeter in pluvially deposited sands. Report to the U.S. Army, European Research Office.

Bellotti, R., Ghionna, V., Jamiolkowski, M., Robertson, P.K. and Peterson, R.W. (1989). Interpretation of moduli from self-boring pressuremeter tests in sand. Geotechnique, 39, No. 2, 269-292.

Benoit, J. (1983). Analysis of self-boring pressuremeter tests in soft clay. Ph.D. Thesis, Department of Civil Engineering, Stanford University.

Benoit, J. and Clough, G.W. (1986). Self-boring pressuremeter tests in soft clay. ASCE, J-GED, 112, No. 1, January, 60-78.

Bertok, J. (1987). Settlement of embankments and structures at Vancouver International Airport. CGJ, 24, 72-80

Bishop, A.W. (1961). Discussion on soil properties and their measurement. V ICSMFE, Vol. 3, 92-100.

Bishop, A.W. (1966). The strength of soils as engineering materials. Geotechnique, 16, 91-128.

Bishop, A.W. (1971). Shear strength parameter for undisturbed and remolded soil specimens. Proceedings of the Roscoe Memorial Symposium, Cambridge University, 3-58.

Blunden, R.H. (1975). Urban geology of Richmond, British Columbia. Adventures in Earth Science Series, 15, Canadian Geological Foundation

Bolton, M.D. (1986). The strength and dilatancy of sands. Geotechnique, 36, No. 1, 65-78.

Borsetto, M., Imperato, L., Nova, R. and Peano, A. (1983). Effects of pressuremeters of finite length in soft clay. Proceedings ISSRIIT, Paris, Vol. 2, 211-215.

Briaud, J.L. (1986). Pressuremeter and deep foundation design. 2nd ISPMA, Texas A & M, 376-405.

Brooker, E.W. and Ireland, H.O. (1965). Earth pressures at rest related to stress history. CGJ, 2, No. 1, February, 1-15.

Brown, P.T. (1985). Predicting laterally loaded pile capacity using the pressuremeter. M.Sc. Thesis, Department of Civil Engineering, University of British Columbia.

Bruzzi, D., Ghionna, V., Jamiolkowski, M., Lancellotta, R. and Manfredini, G. (1986). Self-boring pressuremeter in Po river sand. 2nd ISPMA, Texas A & M, May, 57-74.

Budhu, M. (1979). Simple shear deformation of sands. Ph.D. Thesis, University of Cambridge

Burland, J.B. (1989). Ninth Laurits Bjerrum Memorial Lecture: small is beautiful-the stiffness of soil at small strains. CGJ, 26, 499-516.

Byrne, P.M., Salgado, F.M. and Howie, J.A. (1990). Relationship between the unload shear modulus from pressuremeter tests and the maximum shear modulus for sand. 3rd ISPMA, Oxford Univ., 231-241.

Campanella, R.G. and Robertson, P.K. (1981). Applied cone research. Proceedings of the Symposium on cone penetration testing and experience, St. Louis, 343-362.

Campanella, R.G. and Robertson, P.K. (1982). State of the art in in-situ testing of soils: Developments since 1978. California Conference on USSSRIT, Santa Barbara, 245-267.

Campanella, R.G. and Robertson, P.K. (1986). Research and development of the UBC cone pressuremeter. 3rd Canadian Conference on Marine Geotechnical Engineering, Memorial University, Newfoundland.

Campanella, R.G. and Robertson, P.K. (1988). Current status of the piezocone test. ISOPT-1, Orlando, 93-116.

Campanella, R.G. and Stewart, W.P. (1990). Seismic cone analysis using digital signal processing for dynamic site characterization. 43rd CGC, Quebec.

Campanella, R.G., Gillespie, D. and Robertson, P.K. (1982). Pore pressures during cone penetration testing. 2nd ESOPT, Amsterdam, 507-512.

Campanella, R.G., Robertson, P.K. and Gillespie, D. (1986). Seismic cone penetration test. In Situ' 86, Geotechnical Special Pub. No. 6, ASCE, 116-130.

Campanella, R.G., Stewart, W.P. and Jackson, R.S. (1990). Development of the UBC self-boring pressuremeter. 3rd ISPMA, Oxford University, 65-72.

Carter, J.P., Booker, J.R. and Yeung, S.K. (1986). Cavity expansion in cohesive frictional soils. Geotechnique, 36, No. 3, 349-358.

Casagrande, A. (1936). Characteristics of cohesionless soils affecting the stability of slopes and earth fills. Journal of the Boston Society of Civil Engineers, January.

Chong, M.K. (1988). Density changes of sand on cone penetration resistance. Proc. ISOPT 1, 707-714.

Clague, J.J., Luternauer, J.L. and Hebda, R.J. (1983). Sedimentary environments and postglacial history of the Fraser Delta and lower Fraser Valley, British Columbia. Canadian Journal of Earth Sciences, 20, 1314-1326.

Clague, J.J., Naesgaard, E. and Sy, A. (1992). Liquefaction features on the Fraser delta: evidence for prehistoric earthquakes?. Canadian Journal of Earth Sciences, 29, 1734-1745.

Clarke, B.G. (1981). In situ testing of clays using the Cambridge self-boring pressuremeter. Ph.D. Thesis, Cambridge University.

Clarke, B.G. (1992). The interpretation of self-boring pressuremeter tests to produce design parameters. Proceedings of the Wroth Memorial Symposium, Oxford University, 75-88.

Clarke, B.G. and Wroth, C.P. (1985). Discussion on Effect of disturbance on parameters derived from self-boring pressuremeter tests in sand. Geotechnique, 219-222.

Clough, G.W. and Denby, G.M. (1980). Self-boring pressuremeter study of San Francisco bay mud. ASCE, J-GED, 106, GT1, January, 45-63.

Clough, G.W., Briaud, J.L. and Hughes, J.M.O. (1990). The development of pressuremeter testing. 3rd ISPMA, Oxford University, 25-45.

Cole, E.R.L. (1967). The behaviour of soils in the simple shear apparatus. Ph.D. Thesis, University of Cambridge.

Cornforth, D.H. (1964). Some experiments on the influence of strain conditions on the strength of sand. Geotechnique, 14, No. 2, June, 143-167.

Cornforth, D.H. (1973). Prediction of drained strength of sand from relative density measurements. ASTM Specialty Technical Publication 523, 281-303.

Daramola, O. (1980). Effect of consolidation age on stiffness of sand. Geotechnique, 30, 213-216.

Daramola, O. (1980a). On estimating K_0 for overconsolidated granular soils. Geotechnique, 30, 310-313.

De Souza Coutinho, A.G.F. (1988). Theories for the interpretation of pressuremeter expansion tests. Memória No. 728, LNEC, Lisbon.

De Souza Coutinho, A.G.F. (1990). Radial expansion of cylindrical cavities in sandy soils: application to pressuremeter tests. CGJ, 67, 737-748.

Denby, G.M. (1978). Self-boring pressuremeter study of the San Francisco bay mud. Ph.D. Thesis, Department of Civil Engineering, Stanford University.

Denby, G.M. and Hughes, J.M.O. (1982). Horizontal stress interpretation of pressuremeter tests. California Conference on USSSRIT, Santa Barbara, 227-244.

Dobry, R., Powell, D.J., Yokel, F.Y. and Ladd, R.S. (1980). Liquefaction potential of saturated sand-the stiffness method. Proc. 7th World Conference Earthquake Engineering, Instanbul, 3, 25-32.

Durgunoglu, H.T. and Mitchell, J.K. (1975). Static penetration resistance of soils, II-Evaluation of theory and implications for practice. Proceedings SCIMSP, Raleigh, 172-189.

East, D.R., Cincilla, W.A., Hughes, J.M.O. and Benoit, J. (1988). The use of the electric piezocone for mine tailings deposits. ISOPT-1, Orlando, 745-750.

Everard, J. (1992). In situ test methods at the Laing Bridge site. CVL 577 Final Report, Department of Civil Engineering. University of British Columbia.

Fahey, M. (1986). Expansion of a thick cylinder of sand: a laboratory simulation of the pressuremeter test. Geotechnique, 36, No. 3, 397-424.

Fahey, M. (1988). The influence of creep on in situ pore pressure dissipation tests. ISOPT-1, Orlando.

Fahey, M. (1990). Shear modulus of sand measured with the self-boring pressuremeter. Report G1010, Geomechanics Group, The University of Western Australia.

Fahey, M. (1992). Shear modulus of cohesionless soil: variation with stress and strain level. CGJ, 29, 157-161.

Fahey, M. and Carter, J.P. (1993). A finite element study of the pressuremeter test in sand using a non linear elastic plastic model. CGJ, 30, No. 2, April, 348-362.

Fahey, M. and Jewell, R. (1990). Effect of pressuremeter compliance on measurement of shear modulus. 3rd ISPMA, Oxford University, 115-124.

Fahey, M. and Randolph, M.F. (1984). Effect of disturbance on parameters derived from self-boring pressuremeter tests in sand. Geotechnique, 34, No. 1, 81-97.

Fahey, M., Jewell, R.J. and Brown, T.A. (1988). A self-boring pressuremeter system. GTJ, 11, No. 3, 187-194.

Fahey, M., Robertson, P.K. and Soliman, A.A. (1993). Towards a rational method of predicting settlements of spread footings on sand. Research Report G1086, The University of Western Australia.

Ferreira, R.S. (1992). Interpretation of pressuremeter tests using a curve fitting technique. Ph.D. Thesis, Department of Civil Engineering. University of Alberta.

Findlay, R.C. (1991). Use of the 9-arm self-boring pressuremeter to measure horizontal in situ stress, stress anisotropy, and stress-strain behavior in soft clay. Ph.D. Thesis, University of New Hampshire.

Ghionna, V., Jamiolkowski, M., Lacasse, S., Ladd, C.C., Lancellotta, R. and Lunne, T. (1983). Evaluation of selfboring pressuremeter. Proceedings of the ISSRIIT, Paris, Vol. 2, 397-402.

Gibson, R.E. and Anderson, W.F. (1961). In situ measurement of soil properties with the pressuremeter. Civil Eng. Publication Works Rev., 56, No. 658, May, 615-618.

Graham, J.P. and Jefferies, M.G. (1986). Some examples of in situ lateral stress determination in hydraulic fills using the self-boring pressuremeter. 39th CGC, Ontario, 191-199.

Green, G.E. and Bishop, A.W. (1969). A note on the drained strength of sand under generalized strain conditions. Geotechnique, 19, 144-149.

Hansen, B. (1958). Line ruptures regarded as narrow rupture zones; basic equation based on kinematic considerations. Proceedings of the Brussels Conference on Earth Pressure Problems, Vol. 1, 39-48.

Hardin, B.O. and Drnevich, V.P. (1972). Shear modulus and damping in soils: design equations and curves. ASCE, J-SMFD, 98, SM7, July, 667-691.

Hardin, B.O. and Drnevich, V.P. (1972a). Shear modulus and damping in soils: measurement and parameters effects. ASCE, J-SMFD, 98, SM6, June, 603-624.

Hedron, A.J. (1963). The behaviour of sand in one dimensional compression. Ph.D. Thesis, University of Illinois.

Hers, I. (1989). The analysis and interpretation of the cone pressuremeter in cohesive soils. M.Sc. Thesis, Department of Civil Engineering. University of British Columbia.

Hettler, A. and Vardoulakis, I. (1984). Behaviour of dry sand tested in a large triaxial apparatus. Geotechnique, 34, No. 2, 183-198.

Holtz, R.D. and Kovacs, W.D. (1981). An introduction to geotechnical engineering. Prentice-Hall, Inc.

Houlsby, G.T. and Hitchman, R. (1988). Calibration chamber tests of a cone penetrometer in sand. Geotechnique, 38, No. 1, 39-44.

Houlsby, G.T., Clarke, B.G. and Wroth, C.P. (1986). Analysis of the unloading of a pressuremeter in sand. 2nd ISPMA, Texas A & M, May, 245-262.

Howie, J.A. (1991). Factors affecting the interpretation and analysis of full-displacement pressuremeter tests in sands. Ph.D. Thesis, Department of Civil Engineering, University of British Columbia.

Hughes, J.M.O. (1973). An instrument for in situ measurement in soft clays. Ph.D. Thesis, University of Cambridge.

Hughes, J.M.O. (1982). Interpretation of pressuremeter tests for the determination of the elastic shear modulus. California Conference on USSSRIT, Santa Barbara.

Hughes, J.M.O. (1984). Pressuremeter results obtained using the Western Geosystems Inc. self-boring pressuremeter at McDonald farm. Report for the National Research Council of Canada, February.

Hughes, J.M.O. (1986). Calibration requirements. In situ test instruments: pressuremeter. Workshop on Geotechnical In Situ Testing for the Canadian Offshore, Bedford Inst. of Oceanography, Dartmouth.

Hughes, J.M.O. (1989). The pressuremeter: can useful data be obtained in granular material? Civil 577 Notes, Department of Civil Engineering, University of British Columbia.

Hughes, J.M.O. and Robertson, P.K. (1984). Full displacement pressuremeter testing in sand. SMS No. 78, Department of Civil Engineering. University of British Columbia.

Hughes, J.M.O. and Robertson, P.K. (1985). Full-displacement pressuremeter testing in sand. CGJ, 22, 298-307.

Hughes, J.M.O., Jefferies, M.G. and Morris, D.L. (1984). Self-bored pressuremeter testing in the Artic offshore. 16th OTC, OTC 4676, Houston, 255-264.

Hughes, J.M.O., Wroth, C.P. and Windle, D. (1977). Pressuremeter tests in sands. Geotechnique, 27, No. 4, 455-477.

Hunt, R.E. (1986). Geotechnical engineering techniques and practices. McGraw-Hill, New York.

Idriss, I.M. (1990). Response of soft soil sites during earthquakes. Proceedings H.B. Seed Memorial Symposium, Berkeley, 273-289.

Ishihara, K. (1982). Evaluation of soil properties for use in earthquake response analysis. International Symposium on Numerical Models in Geomechanics, Zurich.

Iwasaki, T., Tatsuoka, F. and Takagi, Y. (1978). Shear moduli of sands under cyclic torsional shear loading. SF, 18, No. 1, March, 39-56.

Jackson, J.G.J., Ehrgott, J.Q. and Rohani, B. (1980). Loading rate effects on compressibility of sand. ASCE, J-GED, Vol. 106, GT8, August, 839-852.

Jáky, J. (1944). The coefficient of earth pressure at rest. Journal for Society of Hungarian Architects and Engineers, October, 355-358. (in Hungarian).

Jamiolkowski, M., Ladd, C.C., Germaine, J.T. and Lancellotta, R. (1985). New developments in field and laboratory testing of soils. Proceedings XI ICSMFE, San Francisco, Vol. 1, 57-153.

Janbu, N. (1963). Soil compressibility as determined by oedometer and triaxial tests. 3rd ECSMFE, Wiesbaden, 2, 19-24.

Jardine, R.J., Potts, D.M., Fourie, A.B. and Burland, J.B. (1986). Studies of the influence of non linear stress-strain characteristics in soil-structure interaction. Geotechnique, 36, No. 3, 377-396.

Jefferies, M.G. (1988). Determination of horizontal geostatic stress in clay with self-bored pressuremeter. CGJ, 25, 559-573.

Jefferies, M.G., Crooks, J.H.A., Becker, D.E. and Hill, P.R. (1987). Independence of geostatic stress from overconsolidation in some Beaufort sea clays. CGJ, 24, 342-356. Plus Discussion on CGJ, 25, 624-630, 1988.

Jewell, R.J., Fahey, M. and Wroth, C.P. (1980). Laboratory studies of the pressuremeter test in sand. Geotechnique, 30, No. 4, 507-531.

Juran, I. and Mahmoodzadegan, B. (1989). Interpretation procedure for pressuremeter tests in sand. ASCE, J-GED, 115, No. 11, November, 1617-1632.

Kögler, F. (1933). Baugrundprüfung im bohrloch. Der Bauingenieur, Berlin, 19-20.

Kondner, R.L. (1963). Hyperbolic stress-strain response: cohesive soils. ASCE, J-SMFD, Vol. 89, SM1, February, 115-143

Lacasse, S. and Lunne, T. (1982). In situ horizontal stress from pressuremeter tests. 1st ISPMA, Paris, 187-207.

Lacasse, S., D'Orazio, T.B. and Bandis, C. (1990). Interpretation of self-boring and push-in pressuremeter tests. 3rd ISPMA, Oxford University, 273-285.

Ladanyi, B. (1963). Evaluation of pressuremeter tests in granular soils. 2nd PCSMFE, 1, 3-20.

Ladd, C.C., Foott, R., Ishihara, K., Schlosser, F. and Poulos, H.G. (1977). Stress-deformation and strength characteristics. State of Art Report, IX ICSMFE, Tokyo.

Lade, P.V. (1988). Effects of voids and volume changes on the behaviour of frictional materials. IJNAMG, 12, 351-370.

Lade, P.V. and Lee, K.L. (1976). Engineering properties of soils. Report UCLA-ENG-7652, University of California, School of Engineering and Applied Science.

Laier, J.E., Schmertmann, J.H. and Schaub, J.H. (1975). Effect of finite pressuremeter length in dry sand. Proceedings SCIMSP, Raleigh, 241-259.

Lambe, T.W. (1951). Soil testing for engineers. John Wiley and Sons, New York.

Lambe, T.W. and Whitman, R.V. (1979). Soil Mechanics. John Wiley & Sons, Inc.

Lambrechts, J.R. and Leonards, G.A. (1978). Effects of stress history on deformation of sand. ASCE, J-GED, 104, GT11, November, 1371-1387.

Lamé, G. (1852). Leçons sur la théorie mathématique de l'elasticité des corps solides. Bachelier, Paris, France.

Law, K.T. and Eden, W.J. (1980). Influence of cutting shoe size in self-boring pressuremeter tests in sensitive clays. CGJ, 17, 165-173.

Lee, K.L. (1970). Comparison of plane strain and triaxial tests on sand. ASCE, J-SMFD, 96, SM3, May, 901-923.

Lee, K.L. and Seed, H.B. (1967). Drained strength characteristics of sands. ASCE, J-SMFD, 93, SM6, November, 117-141.

Le Clair, D.G. (1988). Prediction of embankment performance using in situ testing. M.Sc. Thesis, Department of Civil Engineering, University of British Columbia.

Lo Presti, D. (1987). Mechanical behaviour of Ticino sand from resonant column tests. Ph.D. Thesis, Politecnico di Torino.

Mair, R.J. and Wood, D.M. (1987). Pressuremeter testing-methods and interpretation. CIRIA Report.

Manassero, M. (1989). Stress-strain relationships from drained self-boring pressuremeter tests in sands. Geotechnique, 39, No. 2, 293-307.

Marchetti, S. (1980). In situ tests by flat dilatometer. ASCE, J-GED, 106, GT3, March, 299-321.

Matsuoka, H. (1976). On the significance of the spatial mobilized plane. SF, 116, 91-100.

Mayne, P.W. and Kulhawy, F.H. (1982). K_0-OCR relationships in soil. ASCE, J-GED, 108, GT6, 851-872. and Discussions on J-GED, 109, No. 6, 1983, 859-869.

Ménard, L. (1955). Travail personnel sur le pressiomètre. Ecole Nationale des Ponts et Chaussées, Paris.

Ménard, L. (1957). Mesures in situ des propriétés physiques des sols. Annales des Ponts et Chaussées, Paris, 127, 3, 357-377.

Milliman, J.D. (1980). Sedimentation in the Fraser River and its estuary, southwestern British Columbia (Canada). Estuarine and Coastal Marine Science, 10, 609-633.

Milovic, D. (1992). Stresses and displacements for shallow foundations. Elsevier Editors.

Monahan, P.A., Luternauer, J.L. and Barrie, J.V. (1992) A delta topset "sheet" sand and modern sedimentary processes in the Fraser River delta, British Columbia. Current Research, Part A, Geological Survey of Canada, Paper 93-1A.

Murthy, R.T. (1992). Shear modulus and damping properties of sands from cyclic self-boring pressuremeter tests. M.Sc. Thesis, Department of Civil Engineering. University of British Columbia.

Negussey, D. (1984). An experimental study of the small strain response of sand. Ph.D. Thesis, Department of Civil Engineering. University of British Columbia.

Negussey, D. and Vaid, Y.P. (1990). Stress dilatancy of sand at small stress ratio states. SF, 30, No. 1, March, 155-166.

Negussey, D., Wijewickreme, W.K.D. and Vaid, Y.P. (1988). Constant-volume friction angle of granular materials. CGJ, 25, 50-55.

Newman, R.L., Chapman, T.J.P. and Simpson, B. (1991). Evaluation of pile behavior from pressuremeter tests. X ECSMFE, Firenze, Vol. 2, 501-504.

O'Neill, B. (1985). An evaluation of the full displacement pressuremeter. M.Sc. Thesis, Department of Civil Engineering. University of British Columbia.

Oda, M. (1972). Initial fabrics and their relations to mechanical properties of granular material. SF, 12, No. 1, March, 17-36.

Oda, M. (1981). Anisotropic strength of cohesionless sands. ASCE, J-GED, 107, GT9, 1219-1231.

Paikowsky, S.G. (1990). The mechanism of pile plugging in sand. Proceedings 22nd OTC, V.4, 593-604

Prapaharan, S., Chameau, J.L., Altschaeffl, A.G. and Holtz, R.D. (1990). Effect of disturbance on pressuremeter results in clays. ASCE, J-GED, Vol. 116, No. 1, 35-53.

Rittenhouse, G. (1943). A visual method of estimating two dimensional sphericity. Journal of Sedimentary Petrology, 13, No. 2, 79-81.

Robertson, P.K. (1982). In-situ testing of soil with emphasis on its application to liquefaction assessment. Ph.D. Thesis, Department of Civil Engineering. University of British Columbia.

Robertson, P.K. (1986). In situ testing and its application to foundation engineering. CGJ, 23, 573-594.

Robertson, P.K. and Campanella, R.G. (1989). Guidelines for geotechnical design using CPT and CPTU. SMS No. 120, Department of Civil Engineering. University of British Columbia.

Robertson, P.K. and Hughes, J.M.O. (1986). Determination of properties of sand from self-boring pressuremeter tests. 2nd ISPMA, Texas A & M, May, 283-302.

Roesler, S.K. (1979). Anisotropic shear modulus due to stress anisotropy. ASCE, J-GED, 105, GT7, July, 871-880.

Roscoe, K.H., Schofield, A.N. and Wroth, C.P. (1958). On the yielding of soils. Geotechnique, 8, No. 1, 22-53.

Rowe, P.W. (1962). The stress dilatancy relation for static equilibrium of an assembly of particles in contact. Proceedings of the Royal Soc. London, Series A, Vol. 269, 500-527.

Rowe, P.W. (1969). The relation between the shear strength of sands in triaxial compression, plane strain and direct shear. Geotechnique, 19, No. 1, 75-86.

Rowe, P.W. (1971). Theoretical meaning and observed values of deformation parameters for soil. Proceedings Roscoe Memorial Symposium, 143-194.

Saglamer, A. (1975). Soil parameters affecting coefficient of earth pressure at rest of cohesionless soils. Instanbul Conference on Soil Mechanics and Foundation Engineering, Vol. 1, 9-16.

Salgado, F.M. and Byrne, P.M. (1990). Finite element analysis of pressuremeter chamber tests in sand. 3rd ISPMA, Oxford University, 209-219.

Sasitharan, S. (1989). Stress path dependency of dilatancy and stress-strain response of sand. M.Sc. Thesis, Department of Civil Engineering. University of British Columbia.

Schmertmann, J. H. (1991). The mechanical aging of soils. ASCE. J-GED, Vol. 117, No. 9, 1288-1329.

Schmertmann, J.H. (1970). Static cone to compute static settlement over sand. ASCE, J-SMFD, Vol. 96, SM3, May, 1011-1043.

Schmertmann, J.H. (1975). Measurement of in situ shear strength. ASCE, Proceedings of the Specialty Conference on In Situ Measurement of Soil Properties, Vol. 2, Raleigh, 57-138.

Schmertmann, J.H. (1985). Measure and use of the insitu lateral stress. The Practice of Foundation Engineering-Osterberg Volume, Northwestern University, Department of Civil Engineering, 189-213.

Schmidt, B. (1966). Discussion of earth pressure at rest related to stress history. CGJ, 3, No. 4, 239-242.

Schnaid, F. and Houlsby, G.T. (1991). An assessment of chamber size effects in the calibration of in situ tests in sand. Geotechnique, 41, No. 3, 437-445.

Seed, H.B. and Idriss, I.M. (1970). Soil moduli and damping factors for dynamic response analyses. Report EERC 70-10, College of Engineering, University of California at Berkeley, December.

Shibuya, S., Tatsuoka, F., Teachavorasinskun, S., Park, C. and Abe, F. (1991). Elastic properties of granular materials measured in the laboratory. X ECSMFE, Firenze, 163-166.

Stroud, M.A. (1971). Sand at low stress levels in the simple shear apparatus. Ph.D. Thesis, University of Cambridge.

Sully, J.P. (1991). Measurement of in situ lateral stress during full-displacement penetration tests. Ph.D. Thesis, Department of Civil Engineering. University of British Columbia.

Suyama, K., Ohya, S., Imai, T., Matsubara, M. and Nakayama, E. (1983). Proceedings of the ISSRIIT, Paris, Vol. 2, 397-402.

Tatsuoka, F. (1976). Stress dilatancy relations of anisotropic sands in three dimensional stress conditions. SF, 16, No. 2, 1-18.

Tatsuoka, F., Iwasaki, T., Fukushima, S. and Sudo, H. (1979). Stress conditions and stress histories affecting shear modulus and damping of sand under cyclic loading. SF, 19, No. 2, 29-43.

Teachavorasinskun, S., Shibuya, S. and Tatsuoka, F. (1991). Stiffness of sands in monotonic and cyclic torsional simple shear. ASTM Publication 27, Vol. 2, Boulder, 863-878.

Terzaghi, K. and Peck, R.B. (1967). Soil mechanics in engineering practice. John Wiley and Sons, Inc.

Vaid, Y.P. (1985). Effect of consolidation history and stress path on hyperbolic stress-strain relations. CGJ, 22, 172-176.

Vaid, Y.P., Byrne, P.M. and Hughes, J.M.O. (1980). Dilation rate as a measure of liquefaction resistance of saturated granular materials. SMS No. 43, Department of Civil Engineering, UBC.

Vesíc, A.S. (1972). Expansion of cavities in infinite soil mass. ASCE, J-SMFD, 98, SM3, 265-290.

Vesíc, A.S. and Clough, G.W. (1968). Behavior of granular materials under high stresses. ASCE, J-SMFD, 94, SM3, May, 661-688.

White, J.E. (1965). Seismic waves. McGraw-Hill, Inc., New York.

Whittle, R.W., Dalton, J.C.P. and Hawkins, P.G. (1992). Shear modulus and strain excursion in the pressuremeter test. Proceedings of the Wroth Memorial Symposium, Oxford.

Windle, D. and Wroth, C.P. (1975). Electrical resistivity method for determining volume changes that occur during a pressuremeter test. Proceedings SCIMSP, Raleigh, 497-510.

Withers, N.J., Howie, J., Hughes, J.M.O. and Robertson, P.K. (1989). Performance and analysis of cone pressuremeter tests in sands. Geotechnique, 39, No. 3, 433-454.

Wong, R.K.S. and Arthur, J.R.F. (1985). Induced and inherent anisotropy in sand. Geotechnique, 35, No. 4, 471-481.

Wood, D.M. (1990). Strain-dependent moduli and pressuremeter tests. Geotechnique, 40, No. 3, 509-512.

Wood, D.M. and Wroth, C.P. (1977). Some laboratory experiments related to the results of pressuremeter tests. Geotechnique, 27, No. 2, 181-201.

Wroth, C.P. (1975). In situ measurement of initial stresses and deformation characteristics. Proceedings of the SCIMSP, Raleigh, Vol. 2, 181-230.

Wroth, C.P. (1982). British experience with the self-boring pressuremeter. Proceedings of the ISPMA, 143-164.

Wroth, C.P. (1984). The interpretation of in situ soil tests. Geotechnique, 34, No. 4, 449-489.

Wroth, C.P. and Windle, D. (1975). Analysis of the pressuremeter test allowing for volume change. Geotechnique, 25, No. 3, 598-604.

Wroth, C.P., Randolph, M.F., Houlsby, G.T. and Fahey, M. (1979). A review of the engineering properties of soils with particular reference to the shear modulus. Soil Mechanics Report No. SM048/84, Cambridge University.

Yan, L. (1986). Numerical studies of some aspects with pressuremeter tests and laterally loaded piles. M.Sc. Thesis, Department of Civil Engineering. University of British Columbia.

Youd, T.L. and Craven, T.N. (1975). Lateral stress in sands during cyclic loading. ASCE, J-GED, 101, GT2, February, 217-221.

Yu, P. and Richart, F.E. (1984). Stress ratio effects on shear modulus of dry sands. ASCE, J-GED, 110, No. 3, March, 331-345.

Yu, H.S. (1993). A new procedure for obtaining design parameters from pressuremeter tests. Australian Civil Engineering Transactions, Vol. CE34, No. 4, 353-359.

APPENDIX A DESCRIPTION OF THE UBC SBPM

A.1 INTRODUCTION

This appendix briefly presents the basic characteristics of the UBC SBPM system used in this thesis. The UBC SBPM system consists of 3 main units: the testing, the pumping and the pushing units. The testing unit consists of the data acquisition system (and related sensors) required to control the probe, the air control system required to inflate the probe, and the pressuremeter probe itself. The pumping unit is composed of the pumping equipment (and related accessories) required to flush the drilling mud during the selfboring operation. The pushing unit is a hydraulic cross-head and other accessories housed in the UBC testing vehicle.

A.2 PUSHING AND PUMPING UNITS

Selfboring of the UBC probe is achieved by the combined action of pushing and jetting. The supporting pushing and hydraulic control units are housed inside the UBC research vehicle. This in situ testing vehicle is detailed in Campanella and Robertson, 1981, and is depicted in Figure A.1(a). The research truck has 4 built in hydraulic systems that operate independently in order to give versatility to the whole pushing unit. Each of the systems is for a different task, such as the raising and leveling of the truck, the pushing and pulling of the in situ tools, or the clamping action of the steel rods. A variable volume pressure-compensated hydraulic pump is used to supply the hydraulic needs of all 4 independent systems. This hydraulic pump has an operational capacity of providing 6900 kPa (1000 psi) of pressure, which supplies the penetration head circuit (pushing rig) with a pushing capacity of 80 kN (10 tons). This corresponds approximately to the dead weight reaction of the vehicle. Thrust in the pushing rig is provided by 2 double sided cylinders connected to the chuck head of the pushing frame. The maximum stroke of the pushing frame is 121.8 cm, however during the selfboring process a stroke of 100 cm is used. This corresponds to the length of the steel BW rods used to connect the pressuremeter unit to the chuck head inside the truck.

The internal hydraulic circuit of the research truck is additionally used to supply the pumping unit of the UBC SBPM system, as represented in the layout of Figure A.1(b). Since pumping and pushing

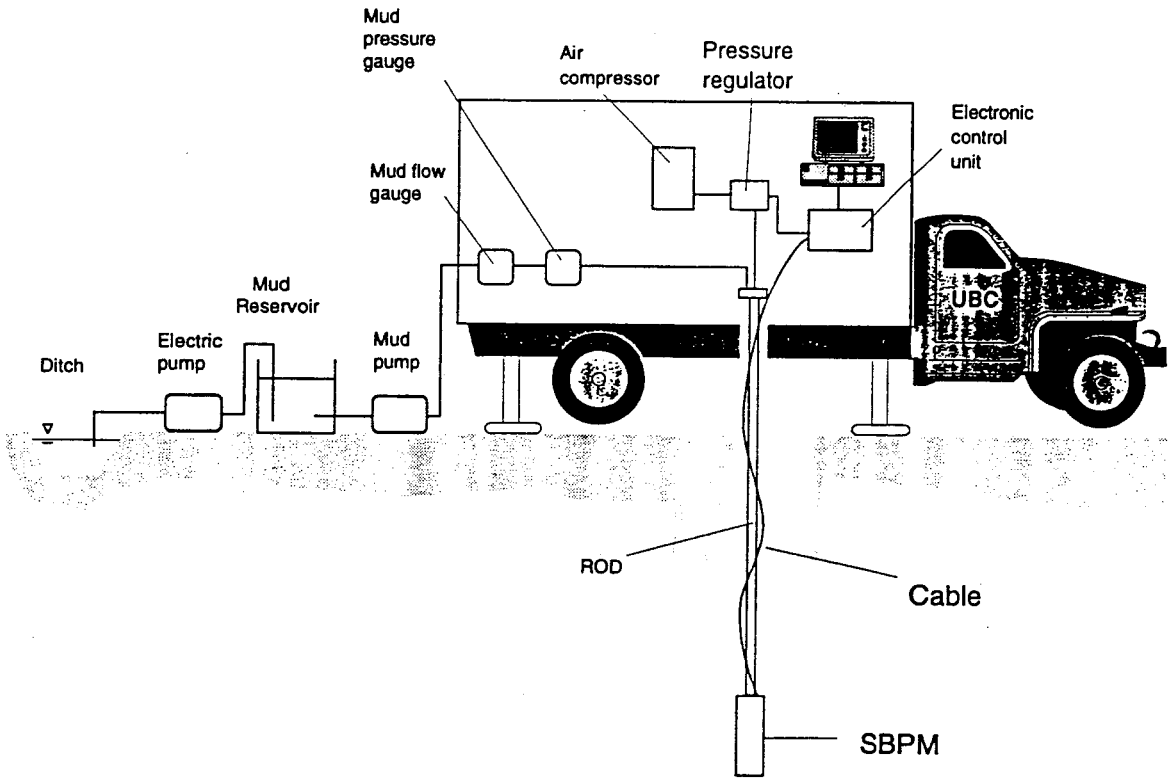

(A) LAYOUT OF SBPM DRILLING AND PUSHING EQUIPMENT

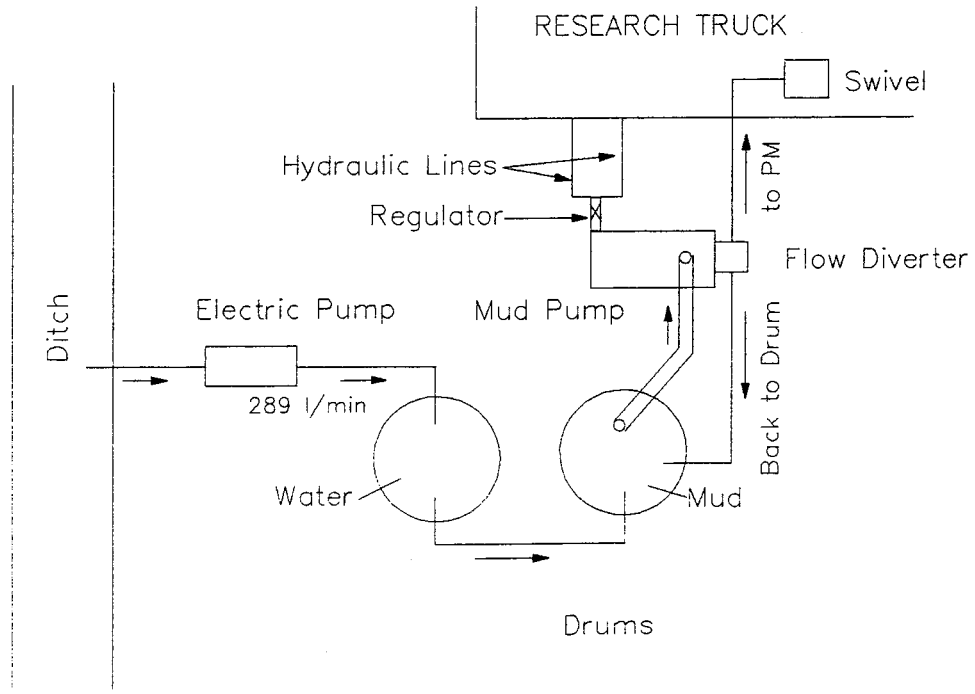

(B) LAYOUT OF HYDRAULIC AND PUMP CONTROL UNIT

Figure A.1: Pushing and Pumping Units of the UBC SBPM System

occur simultaneously during the selfboring operation, the hydraulic power available in the truck has to be shared between the pushing and pumping hydraulic units.

The connection between the truck and the outside pumping unit is done through 2 hydraulic lines. These lines feed a diaphragm type pump which is used to pump the mud during the selfboring operation. This pump is rated to provide a maximum flow of 48 l/min (12.7 gpm) under an ideal pressure condition of 3790 kPa (550 psi). A manual regulator is used to control the mud flow rate at the base of the SBPM. Water from a ditch or any other source at the site is collected through a Ponstar submersible pump to one of the 170 l (45 gallons) drums of the pumping unit. This drum serves to keep a supply of water that can be readily used in any stage of the selfboring operation.

This water is subsequently used to prepare the jetting mud, required by the selfboring operation. The water is transferred to another drum, where it is mixed with a "liquid avionic polymer" WDS-120. The WDS-120 is a drilling additive from Westcoast Drilling Supplies Ltd. that serves to improve the flow characteristics of the fluid, to prevent collapse of the selfbored hole, as well as to enable the granular minerals displaced during the selfboring operation to reach surface. A ratio of 2 glasses (200 ml each) of additive per 170 l of water was in general used in this thesis. The mixture of water and drilling additive, or jetting mud, is homogenized by diverting the flow from the mud pump back to the drum (see Figure A.1(b)) in a closed loop. This diverting process is done until a viscous and homogeneous fluid consistency is achieved.

Once the jetting mud is prepared it is forced down to the pressuremeter unit through a 1.27 mm (1/2") PVC tubing located inside the annular space of the steel BW rods. A swivel is used to adapt the BW rods to the chuck head of the pushing rig, as well to establish a link between the PVC tubings and the pumping unit. This swivel also houses a mud flow and mud pressure gauges.

A.3 TESTING UNIT

A.3.1 Data Acquisition System and Related Sensors

In a similar way as the pumping unit the pressuremeter testing unit is connected to the facilities available inside the research truck. The layout of the whole testing unit is presented in Figure A.2.

The UBC selfboring pressuremeter is equipped with 6 strain arm sensors, 2 pressure and 1

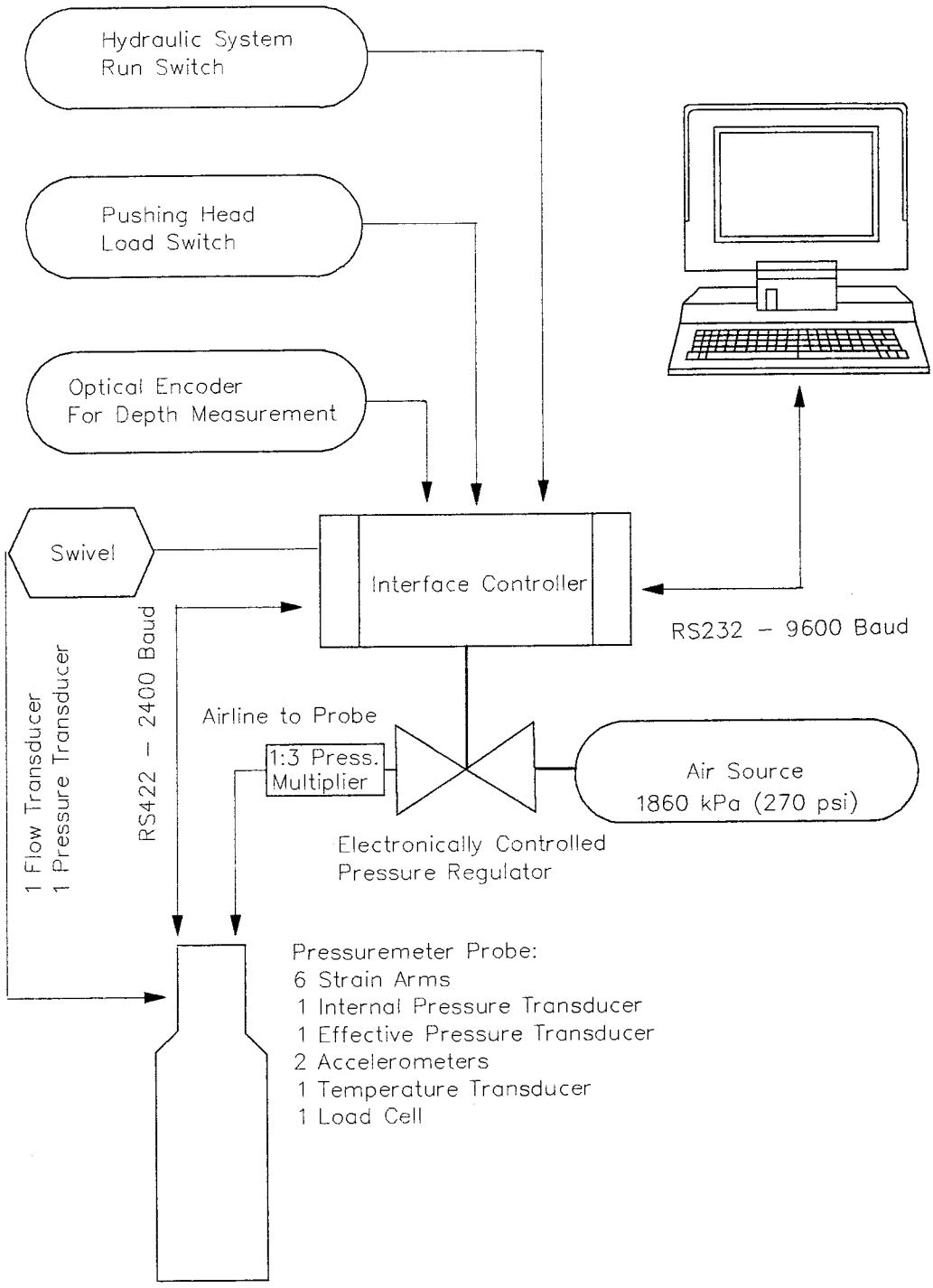

Figure A.2: Testing Unit of the UBC SBPM System

temperature transducer, 2 accelerometers and 1 load cell at the base of the cutting shoe. There are also two analog boards as well as a microcomputer board inside this probe. The function of these boards is related to amplification and conversion of the signals measured by the aforementioned sensors. Each of these sensors have an instrumentation amplifier that gets the low level signal and amplifies it up to the conversion range of the 12 bit A/D converter. The converter, a linear Technology LTC 1290, sends the digital data upwards via a high speed serial interface RS 422 to the interface controller at surface. The RS 422 serial interface is connected to a cable which is housed together with the air tube inside a 6.4 mm (outside diameter) cable that is taped to the BW rods. The air tube is used to send pressurized air downhole during the expansion of the probe and is ultimately linked, via a pressure regulator, to an air source of 1860 kPa (270 psi) inside the truck.

The interface controller contains a 12 bit D/A converter with a Motorola 68HC11 microcontroller, which is programmed to receive the raw data from downhole and convert it into ASCII format in engineering units. This ASCII data is then sent via a ribbon serial cable to a RS232 port on the IBM PC compatible 486 computer of the truck. The computer runs a data acquisition system developed at UBC to retrieve and store the pressuremeter data, as well as to set up and control the testing characteristics. The data acquisition system displays in real time all the values measured downhole, and presents a graphical display of the internal pressure versus circumferential strain of the test.

Three testing modes are accomplished during selfboring and testing, namely the "testing", "dissipation" and "sounding" modes. The data acquisition system and the interface controller "know" the present status of the test (as defined above) by the connection of two switches between the pushing rig and the interface controller. These are the "run" and the "load" switches of Figure A.2. These switches inform the controller if the swivel is being pushed or if it is in a stopped position, thus allowing the data acquisition system to change the mode of operation from "sounding" to "dissipation" modes. The variables recorded in "sounding" and "dissipation" modes are distinct and are stored in different files. The total (tip plus lateral) load, the inclination of two perpendicular planes to the probe vertical axis, the mud flow and pressure, the pore pressure, the temperature as well as the elapsed time are stored in the “sounding” file. The pore pressure dissipation, the temperature and the time elapsed in the halting stages are stored in the “dissipation” file. As commented above, these ASCII files contain the measured variables already in

engineering units. The "testing" mode is started only by manual intervention during the halted stage of the sounding. The variables recorded in this mode are the circumferential strains measured by the 6 strain arms of the probe, the internal total and pore pressures, and the time elapsed during the pressuremeter test. Similar to the other modes, these variables are recorded in a "testing" file. The baselines of each of the aforementioned sensors are also included in the files generated by the data acquisition system.

In order to keep track of the depth, principally during the "sounding" mode, an optical encoder adjusted to the hydraulic piston is connected to the interface controller. This encoder furnishes the data acquisition system with depth values of the pressuremeter probe. The depth as well as any other measured variable can be read in continuous intervals of time as low as 1 second. The frequency of reading is selected by the engineer during the selfboring operation.

The mud flow and mud pressure information is obtained through the transducers housed inside the jetting swivel. These transducers are also connected to the interface controller, as schematically shown in the layout of Figure A.2.

The interaction between the interface controller and the data acquisition system, with downhole feedback from the pressuremeter sensors, allows the knowledge of the pushing and pumping variables in the course of a selfboring operation. This knowledge helps the standardization of the pressuremeter insertion. Moreover it is also possible to fully standardize the testing variables adopted during expansion and deflation of the probe. The stress or strain levels at the commencement of the unload reload loop, the time for holding prior to the unload reload loop, the maximum stress or strain levels, and the rate of inflation, can be set up before the testing stage and controlled afterwards. The data acquisition system allows the generation of a "command" file prior to each pressuremeter test, in which the basic testing characteristics (as related above) are specified by the engineer. The interface controller uses the information of the "command" file, plus the downhole information, to control the development of the test.

A.3.2 UBC Selfboring Pressuremeter

The basic design of the UBC SBPM followed the general characteristics of the pressuremeter operated by Dr. J. M.O. Hughes. The UBC selfboring pressuremeter has an overall length of 143 cm and an external diameter of 74 mm, with an expandable section with length to diameter ratio of 6.

The UBC SBPM unit is shown in Figure A.3. The top of this figure shows the pressuremeter unit under its fully assembled condition. On the center of this figure is depicted the pressuremeter unit without the external components that shield the inner sensors and the expandable rubber membrane. This membrane encloses the strain arm heads and also supports the effective pressure transducer.

The transducer is clamped and floats on the rubber membrane during the expansion stage. This unit serves to measure the dynamic pore pressures induced in the surrounding soil. A cylindrical porous polypropylene filter 5.3 mm in diameter is encased on the top of the effective pressure transducer. The inner chamber of the transducer is saturated in the field, prior to the placement of the porous filter. The traditional UBC saturation technique (see Robertson and Campanella, 1989) with glycerin is used. The porous filter is pre-saturated in the UBC research laboratory by the application of an ultra sonic bath under vacuum. This technique led to a satisfactory sensor response during the calibration stages of the probe.

The expandable inner rubber membrane also serves to prevent water ingress into the electronic compartment inside the probe, and cause a short circuit of the boards. A compromise between a repeatable, elastic, flexible and at the same time resistant membrane had to be adopted for this expandable membrane. The urethane membrane used in the past had a good ability to withstand high differential air pressures (as high as 5000 kPa), but in addition yielded high rate dependent effects (Howie, 1991) as well as hysteretic behavior during loading and unloading in air (Hers, 1989). Given the relative low pressure range used for the tests of this thesis (up to the maximum 1750 kPa of the air control system), a low puncture resistant rubber membrane was devised as a substitute for the urethane membranes. Recent research in this area (Campanella et al, 1990, Sully, 1991) indicated that a tubing of commercially available Gooch rubber membrane of 1 mm thickness could be adopted for the UBC SBPM. The testing results of Campanella et al, 1990 and Sully, 1991 with the Gooch membrane indicated a bilinear envelope (expansion in air) with little or no hysteresis, as well as a high flexibility with very low correction for lift off stresses. This membrane was used in the tests of this thesis up to 1992, when it became difficult to find Gooch membranes for the UBC SBPM. A new rubber membrane from Alliance Rubber Company (also 1 mm in thickness) was then selected for usage in the latter tests of this thesis.

At the bottom of the pressuremeter unit two alternate jetting systems can be used for selfboring. The

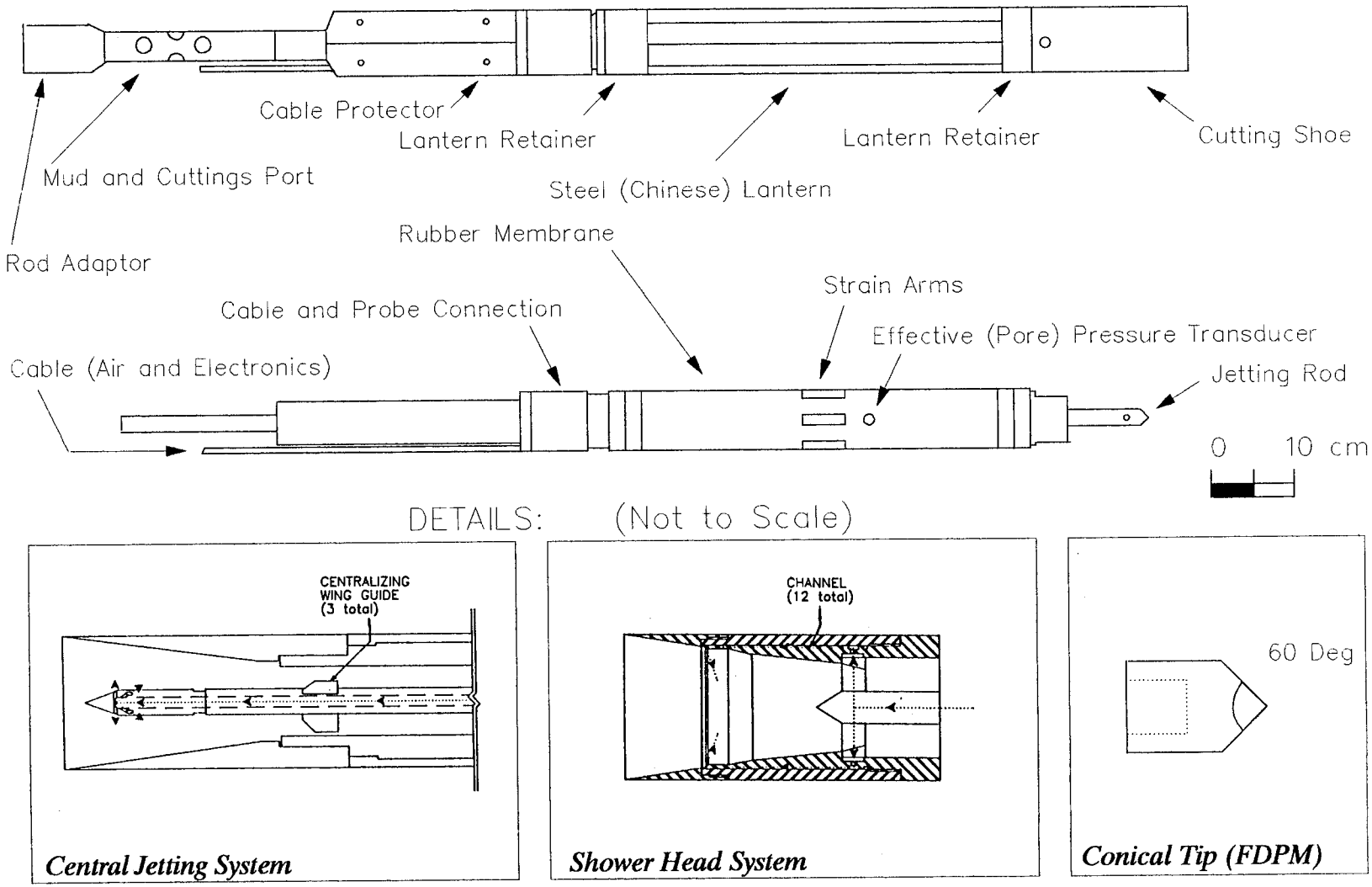

Figure A.3: UBC Selfboring Pressuremeter Sectional Assembly

initial design was made with the central jetting system, as shown in the lower left of Figure A.3. In this case the central rod is provided with 3 small vanes for stability, and a nozzle with several holes that jet the mud backwards at an angle of 45°. The main advantage of this system is that the jetting holes can be positioned at different levels inside the shoe, thus allowing a gradual optimization of the insertion procedure. In this thesis 3 nozzles were designed and used. Nozzle A had 8 holes of 3.55 mm (diameter) located at 21.3 mm from the nozzle tip. Nozzle B had 3 holes of 5.7 mm located at 20.6 mm from the nozzle tip, and nozzle C had 4 holes of 4.0 mm located at 23.4 mm from the nozzle tip. The nozzle characteristics partially followed the design given by Howie, 1991 for jetting in sands.

A shower head system has been also devised, as shown in the lower center of Figure A.3. In this system the mud passes to the outer wall and is jetted in the radial direction by a series of 12 channels (4 mm by 1.5 mm) located 40 mm from the end of the shoe. As before the direction of the jet is backwards, but at a lower inclination. The drawback of this system is that plugging can occur in the initial section of the shoe, where no jetting occurs. The internal spaces for both jetting systems limit the maximum particle size that can be washed out to 10 mm.

The UBC selfboring pressuremeter can be converted into a full displacement device with the simple replacement of the cutting shoe by a 60° conical tip. The conical tip has the same diameter as the cutting shoe, and is shown in the lower right of Figure A.3.

Six cantilever beam type strain arms, made from beryllium copper, are located 60° apart in the middle of the expandable section. Each of the arms have 4 strain gauges. Two strain gauges are mounted on each side of the beam, making up a fully active resistivity bridge. The arm is pivoted at one end and attached to a semi-spherical plexiglass dome on the other end. The plexiglass makes contact with the arm head underneath the membrane. This simple but efficient design is a consequence of previous research done by Hers, 1989. This author showed that the interaction between the membrane and the arm head can result in an apparent inwards movement prior to the lift off pressure, if the arm head is glued to the cantilever beam. The adopted arm configuration also circumvents the hysteresis problems observed with the typical design adopted for the Camkometer probe. This problem is well documented by Fahey and Jewell, 1990.

The operating range of the strain arms of the UBC SBPM is 8 mm, which represents a maximum circumferential strain of 22 %.

APPENDIX B CALIBRATION OF THE UBC SBPM

B.1 INTRODUCTION

Equipment calibration constitutes an essential part of the pressuremeter testing procedure. It is performed in order to obtain reliable and meaningful results without equipment related effects. It is also important to relate the measured signals to known engineering units. Transformation of the raw voltage signals measured at the sensors of the pressuremeter (or at the swivel) to engineering ASCII results requires a correlation between the variables. This correlation is defined by proper calibration stages performed with each of the aforementioned sensors at regular intervals of time. The calibration also warns the user of possible discontinuities, voltage drifts, non linearity, hysteresis, resolution and accuracy errors of the sensors used.

In this research a continuous calibration program with all the pressuremeter sensors was carried out at short intervals of time. In general a full calibration stage was accomplished after every other day in the field, or after some field problem (such as leakage of water into the internal probe circuitry and rupture of the air-electronics cable). This appendix briefly presents the typical calibration results obtained during the calibration stages of the UBC selfboring pressuremeter.

B.2 STRAIN ARMS

The strain arms were calibrated to furnish the relationship between the arm reading (in mm) and the corresponding electronic output (in volts). The calibration was carried out without the rubber membrane, by placing a micrometer over the head of one of the arms while keeping the others in place. The arm being calibrated was pushed into a fully retracted condition (zero strain reference) and allowed to displace outwards while measuring with the micrometer. This calibration was done at 0.05 mm increments over the initial 1 mm of total displacement, and thereafter at an increment of 0.5 mm.

Table B.1 presents the basic calibration characteristics of the strain arms. It is noticed that the accuracy of the strain arms varied from 2 to 4.1 % of the full scale output (FSO), as expected given slightly different arrangements of the resistivity bridges from arm to arm, as well as differential usage effects over the gauges. The reported percentage values lead to a generally high accuracy of measurement

SENSOR	OPERATING RANGE	ACCURACY (%FSO)	RESOLUTION	SENSITIVITY	TEMP. EFFECTS (%FSO/°C)
Strain Arms					
1	0 - 8 mm	3.973	0.006 %	-0.496 V/mm	-0.012
2	0 - 8 mm	3.862	0.006 %	-0.579 V/mm	-0.012
3	0 - 8 mm	2.971	0.006 %	-0.557 V/mm	-0.028
4	0 - 8 mm	4.169	0.006 %	-0.508 V/mm	-0.005
5	0 - 8 mm	2.404	0.006 %	-0.555 V/mm	-0.006
6	0 - 8 mm	2.000	0.006 %	-0.544 V/mm	-0.006
Internal Pressure	0 - 2976 kPa	0.53	0.70 kPa	0.00169 V/kPa	-0.064
Eff. (Pore) Pressure	0 - 1316 kPa	0.35	0.10 kPa	-0.00203 V/kPa	-0.068
Tip Load Cell	0 - 186 kN	0.361	0.040 kN	0.0259 V/kN	NA
Accelerometer					
1	0 - 20 deg	2.74	0.1 deg	0.110 V/deg	NA
2	0 - 20 deg	1.37	0.1 deg	0.113 V/deg	NA
Mud Pressure (Swivel)	0 - 3448 kPa	0.043	13.78 kPa	0.0000945 V/kPa	NA
Mud Flow (Swivel)	0 - 40 l/min	0.374	0.378 l/min	0.007308 V/l/min	NA

FSO = Full Scale Output
NA= Not Available

Table B.1: General Calibration Characteristics of the UBC SBPM Sensors

in the range of 0.1 to 0.3 mm, which closely tracks the arm movement from lift off to the full expansion of the membrane. The resolution of the arms, equal to 0.006 % (circumferential strain), did not vary from calibration to calibration. This is an intrinsic characteristic of the strain measuring system. Also due to the high value of resolution it was possible to obtain an accurate definition of the post lift off portion of the pressure expansion curves. The unload reload loops were also well delineated.

B.3 PRESSURE TRANSDUCERS

The pressure transducers of the UBC SBPM were calibrated with the use of a portable digital pressure indicator Druck DPI601.

The (total) internal pressure sensor, a subminiature flat diaphragm sensor type from Sensotec (model F, made from stainless steel), was located in an underreamed section of the pressuremeter shaft beneath the rubber membrane. It was calibrated by placing the expandable unit in a thick hollow steel tube and inflating it, with the probe connected to the interface controller and data acquisition system. Table B.1 presents the general calibration characteristics of this sensor. A high resolution of 0.7 kPa and accuracy of 0.53 % FSO were obtained. This high resolution and accuracy are important to precisely define the shape of the unload reload loops, since a large and closely spaced number of data points are required.

The effective (pore) pressure sensor of the pressuremeter, a differential diaphragm sensor type from Ashcroft (model K8, made from beryllium copper), was calibrated by placing the expandable unit of the probe in a steel chamber specially designed for this purpose. The probe was connected to the interface controller and data acquisition system, thus allowing a direct readout (in volts) of the air pressure applied inside the calibration chamber. The air pressure was applied by connecting the chamber to the air supply line of the UBC laboratory. The measured accuracy of this sensor was in the order of 0.35 % FSO as shown in Table B.1. This value leads to an average error lower than 2.5 kPa in the pressure measured, indicating that small changes in pore pressure could be sensed by the probe (the pressure measured by this sensor is transformed into pore pressure by the data acquisition system, with the use of the measured total internal pressure). The resolution of the effective pressure sensor was also high, in the range of 0.1 kPa. The calibration of this sensor with a fully saturated filter element demonstrated that the adopted saturation technique was satisfactory for a fast and precise response of the sensor.

In addition to the pressure transducers of the pressuremeter unit all other measuring sensors were calibrated in a routine basis, namely the (home made) load cell, the mud pressure and flow transducers and the 2 accelerometers at the probe shaft. Typical calibration characteristics of all these sensors are also presented in Table B.1. The measured accuracy and resolution are high enough to precisely define the insertion variables of the UBC SBPM.

B.4 MEMBRANE RESISTANCE AND LANTERN COMPLIANCE

The design of the steel lantern affects the corrections that have be applied over the experimental results. The calibration response of each of the designed steel lanterns, as well as the Camkometer lantern, is presented here. The design characteristics of these lanterns was shown in Chapter 3, with the Camkometer lantern defined as "lantern 10".

The membrane resistance is the force required to expand the membrane and the lantern in the absence of external constraints. In the field test part of the measured force (or pressure) is related to the force required to overcome the resistance offered by both the membrane and the lantern to expand. This force has to be removed from the overall value measured, in order to obtain the force applied to the soil.

Membrane resistance is conventionally measured by expanding the probe in air in its fully assembled condition. The pressure expansion curve obtained in this manner has two components, the lift off and the post lift off component. The post lift off component is strain dependent, being related to the variable resistance offered by both the membrane and the lantern during the expansion process. The experimentally obtained (post lift off) curve can be mathematically fitted by a polynomial equation. This equation provides a smooth curve that is used inside the data reduction macro to correct the raw cavity pressure.

The evaluation of the membrane resistance was done in the field with the expansion of the probe in air prior to the selfboring operation. A "command" file was created specially for this purpose. The calibration test was conducted with the expansion of the probe to a circumferential strain of 10 % at a rate of inflation of 3.4 kPa/s.

The results for each of the designed steel lanterns are shown in Figure B.1. The average of the output of each of the six strain arms is shown for each lantern. This is so because only the average calibration curve was used in the correction of the raw pressuremeter data. The expansion with the rubber membrane alone (without lantern) is also shown in this same figure.

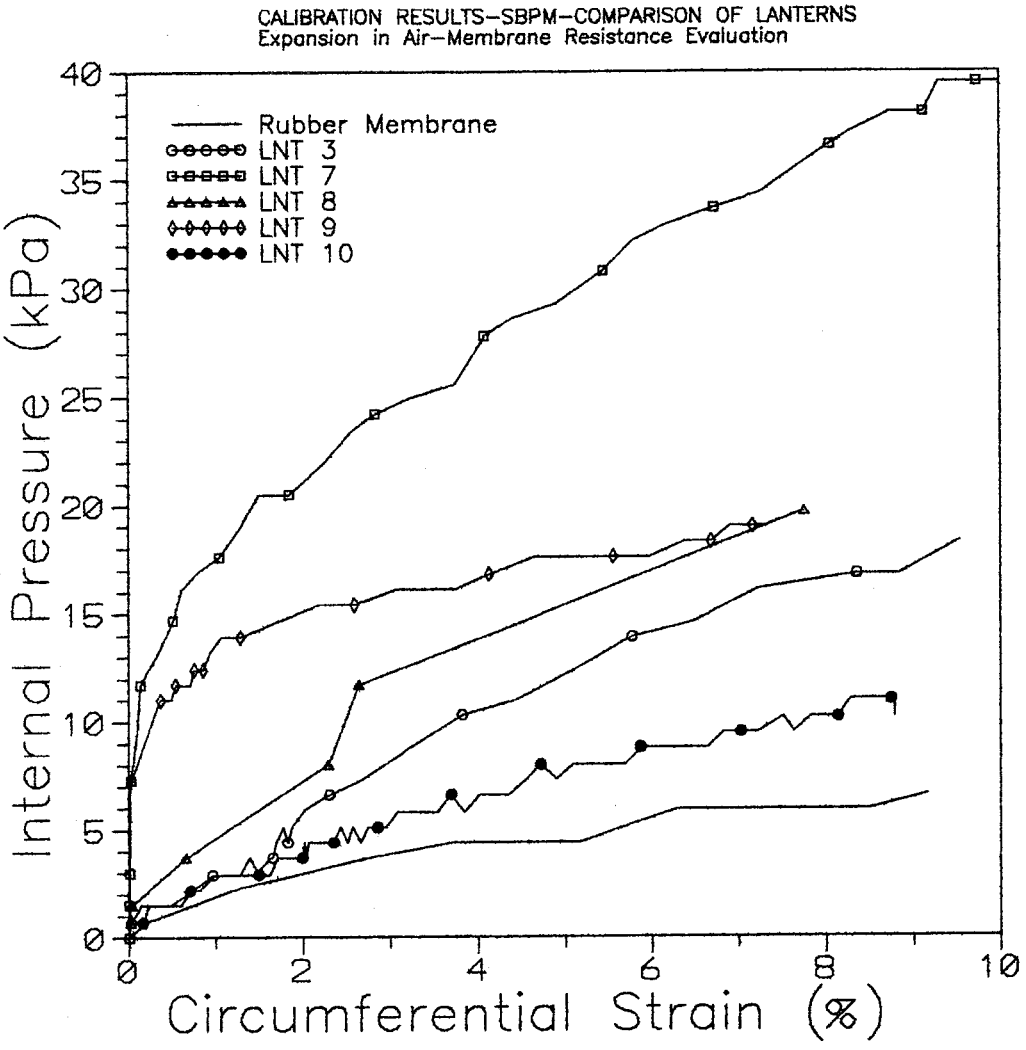

Figure B.1: Membrane Resistance from Expansion in Air

The following observations can be drawn:

1. The (post lift off) correction curve is non linear for all the steel lanterns tested, and approximately linear for the rubber membrane and the Camkometer standard lantern. The Camkometer lantern presents a low resistance to expansion because the displacement takes place on the outer rubber membrane, rather than in between the steel strips (as for the steel lanterns).

2. The use of the inner Alliance rubber membrane has proven to yield a low and linear resistance component on the total resistance to inflation. Therefore, the major component of the total resistance to inflation comes from the resistance imposed by the outer lantern.

3. The different lanterns imposed distinct lift off resistances, that varied from 0.5 to 8 kPa. This range is considerably lower than the range of (effective) lift off pressures commonly measured in the tests at the Laing Bridge site. The commonly measured lift off pressures varied from 50 to 200 kPa, depending on the depth and disturbance of the surrounding soil.

4. The different lanterns also imposed distinct post lift off resistances. The measured resistance to inflation is related to the inter-strip friction, the end clamping effects, the amount of riveting and the rigidity of the whole lantern. Although differences of more than 20 kPa can be observed from one lantern to another, in practical terms any of the lanterns can be indistinctly used. This is due to the fact that, during the field tests, a much higher range of post lift off pressures were measured. The maximum pressure measured in the field varied from $\approx$ 500 to $\approx$ 1500 kPa, respectively for tests 5 and 15 m deep in the site, whereas the maximum resistance imposed by the steel lanterns was below 40 kPa.

The compliance correction is related to the inherent volume loss of the pressuremeter tubing system, as well as the compression of the rubber membrane and the lantern. The steel lanterns are particularly prone to yield higher compliance strains than the standard Camkometer lantern, given the additional compressibility of the curved steel strips that are stacked together. Since these strips do not have the same curvature radius as the shaft of the UBC pressuremeter, they "flatten out" with the increase of the external lateral pressure.

The evaluation of the compliance strains is conventionally done with the probe inside a rigid thick walled steel tube. The probe is placed vertically and expansion is carried out at the same inflation rate as used in the field. Given the negligible displacement of the inner wall of the rigid tube (Fahey and

Jewell, 1990 measured circumferential strains in the order of 0.005 %), the measured strain is directly related to the compliance of the system (lantern plus rubber membrane). In this thesis the compliance calibration tests were carried out with a "split cylinder". This cylinder was composed of two thick steel halves, that could be screwed around the expandable section of the probe.

The compliance test results are presented in Figure B.2, where the following observations apply:

1. The compliance of the steel lanterns is predominantly caused by the lantern compression rather than the inner rubber membrane compression, or the volume expansion of the air tubing. This is noticed when comparing the compliance of the probes with and without lantern (only with the rubber membrane). A similar observation was given before in relation to the resistance to expansion in air.

2. The measured compliance curves of all the steel lanterns are non linear. These curves are also pressure dependent, as the "flattening out" of the steel strips will vary in accordance to the outside lateral (reaction) pressure applied by the split cylinder. It can be noticed that lanterns 8 and 9 presented much higher compliance strains than the remaining of the tested lanterns. The former lantern is composed of 2 halves that induce a considerably amount of strain as they move independently, whereas the latter lantern is composed by 3 rows of steel strips stacked together. This design allows a high straining of the strips. The compliance strains measured for lantern 3 are lower than the compliance strains of lantern 9 at similar internal pressures. Although both lanterns had similar designs, lantern 9 was built with steel strips of lower width (hence lower curvature radius) than the width of the strip adopted in lantern 3. This suggests that the lower is the width (or the curvature radius) of the steel strip, the higher is the "flattening out" effect.

3. The Camkometer lantern yielded a linear compliance curve. The measured stress-strain response is characteristic of the linear elastic straining of the outer rubber membrane, since this lantern is not designed with stacked steel strips. The steel strips of this lantern are bounded to the outer rubber membrane and have the same curvature radius as the probe, which suggests that these strips did not "flatten out".

4. The compliance curve of lantern 7 varied considerably in the initial 0 to 600 kPa of internal pressure of the test. It appears that this variation was caused by the readjustment of the rubber membrane and the steel strips inside the split cylinder, rather than a direct straining of the individual strips.

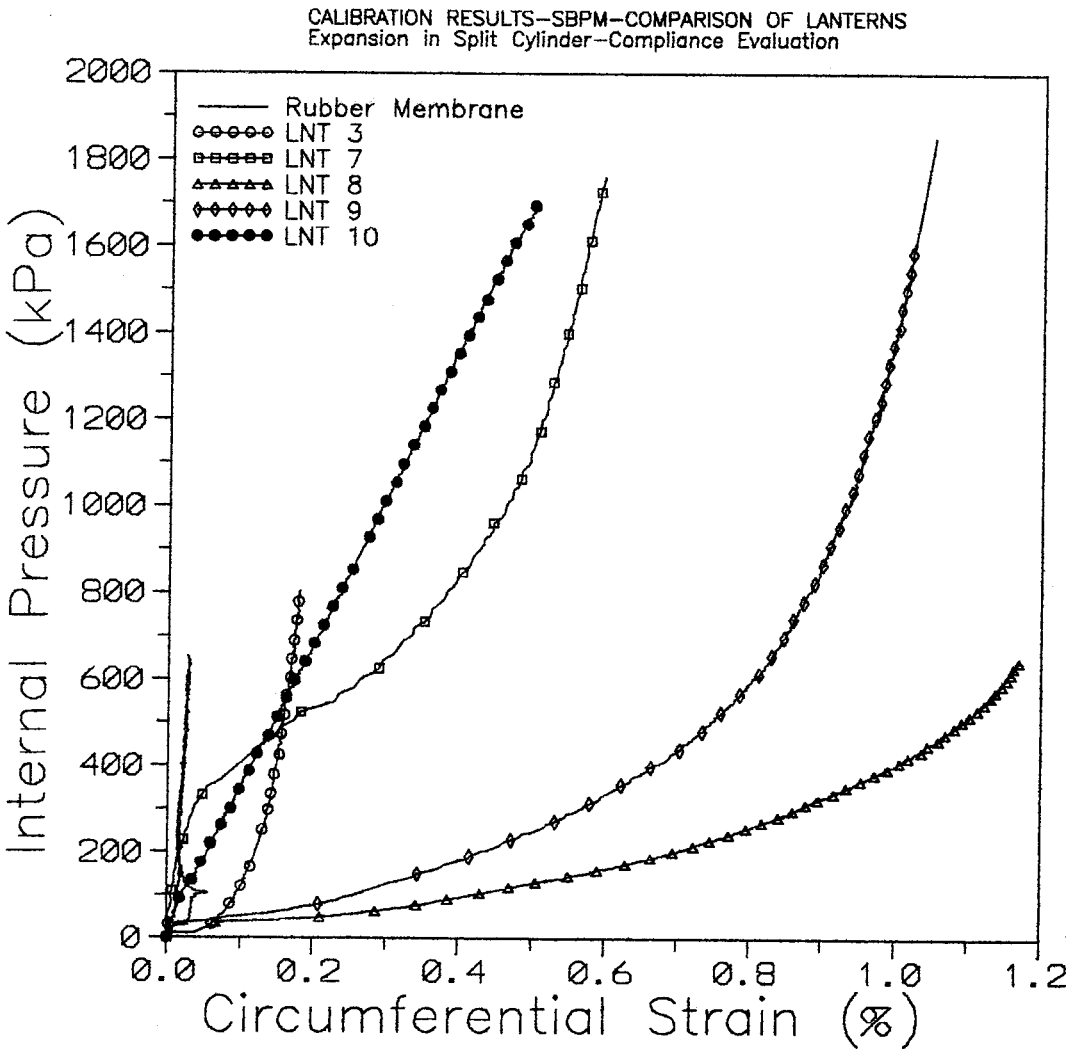

Figure B.2: Lantern Compliance from Expansion Inside Split Cylinder

The compliance calibration tests demonstrated that high corrective factors have to be applied in the raw cavity strain when the steel lanterns are used. This is principally the case of lanterns 8 and 9, where the compliance strains were as high as 1.0 %. The Camkometer lantern and the steel lanterns 3 and 7 yielded compliance strains with similar magnitude (at the same level of pressure). However, the compliance curve of the steel lanterns presented a non linear shape.

The compliance curves of Figure B.2 were also fitted by polynomial equations, in order to provide smooth correction curves for the data reduction macro (one curve per lantern type).

The data reduction macro was written for usage with any spreadsheet generated by the program Quattro Pro™ (version 1.0). This macro is composed of 2 submacros, that serve to correct the raw data for temperature and zero drift (first submacro), and membrane resistance and lantern compliance (second submacro). The submacros are linked to each other, in the sense that once the data is corrected by the first one it can be directly used into the second submacro to furnish the corrected values of strain and stress.

The process of correction of the raw data is very simple. Once the raw pressuremeter data ("testing file") is loaded into the spreadsheet the first submacro is run. The circumferential strains of each of the strain arms are corrected for the zero drift, and both the total internal and pore pressures are corrected with basis on the baseline temperature. The second submacro is then run next. The total internal pressure is subtracted from the (post lift off) membrane resistance curve. The resulting pressure is further subtracted from the pore pressure measured during the test, in order to obtain the effective internal pressure. The average circumferential strain, calculated with the strains of all the six arms, is subtracted from the compliance strain. This furnishes the soil response at the cavity wall without compliance effects.

The final corrected ASCII file contains 13 columns. The time (min), the circumferential strain of each of the six strain arms (%), the pore pressure (kPa), the effective internal pressure (kPa), the total internal pressure (kPa), the average circumferential strain (%), the strain rate (%/min) and the rate of inflation (kPa/s). The interpretation (via curve fitting technique) of the SBPM data was accomplished with the average curve of circumferential strain.

B.4.1 Compliance Correction of Unload Reload Loops

The correction to account for compliance strains has serious implications for the measured Gur modulus, and shall be not disregarded (Houlsby and Schnaid, 1992). The methodology for compliance

correction of the loops followed the recommendations presented by Fahey and Jewell, 1990. These authors suggested calibration tests inside the split cylinder with loops of the same rate of inflation and degree of unloading as those in the field.

The compliance correction of the unload reload loops of this thesis was obtained with the testing expansion inside the split cylinder. These expansions were accomplished with each of the lanterns. Unload reload loops were adopted during this calibration stage. The loops were carried out sequentially with the increase of cavity pressure, as illustrated on the top plot of Figure B.3. The apparent strains developed in each of these loops are a measure of the system compliance. The compliance of the system (rubber membrane plus lantern) is expressed as an equivalent "system shear modulus" (Gsys), defined as half the gradient of the curve of pressure versus the compliance strain.

The corrected Gur modulus is the difference of the measured modulus to the system modulus, in accordance to the following expression:

$$\frac{1}{Gur} = \frac{1}{Gmeasured} - \frac{1}{Gsys} \qquad (B.1)$$

Different lanterns yield different amounts of compliance strain during the loop stage, hence require distinct compliance corrections. The compliance correction is dependent on the internal pressure at the commencement of the unload reload loop (P_{cu}), and will be related to a particular degree of pressure unload. The bottom plot of Figure B.3 presents a typical relationship between Gsys and P_{cu} for the Camkometer lantern. This relationship is expressed by a power equation. With this power equation it is possible to evaluate the Gsys for any field loop in which the P_{cu} is known and the degree of pressure unload is 40 %. With the value of Gsys and Gmeasured it is possible to obtain the corrected value of Gur with Equation B.1.

For the other lanterns the dependence of Gsys on P_{cu} was also observed. In general, the higher was the effective pressure at the commencement of the loop the higher was the system shear modulus. This indicates that the compliance strains developed during the unload reload loop decrease (Gsys increases) with an increase of the outside pressure. The decrease of compliance strain with increase in pressure is

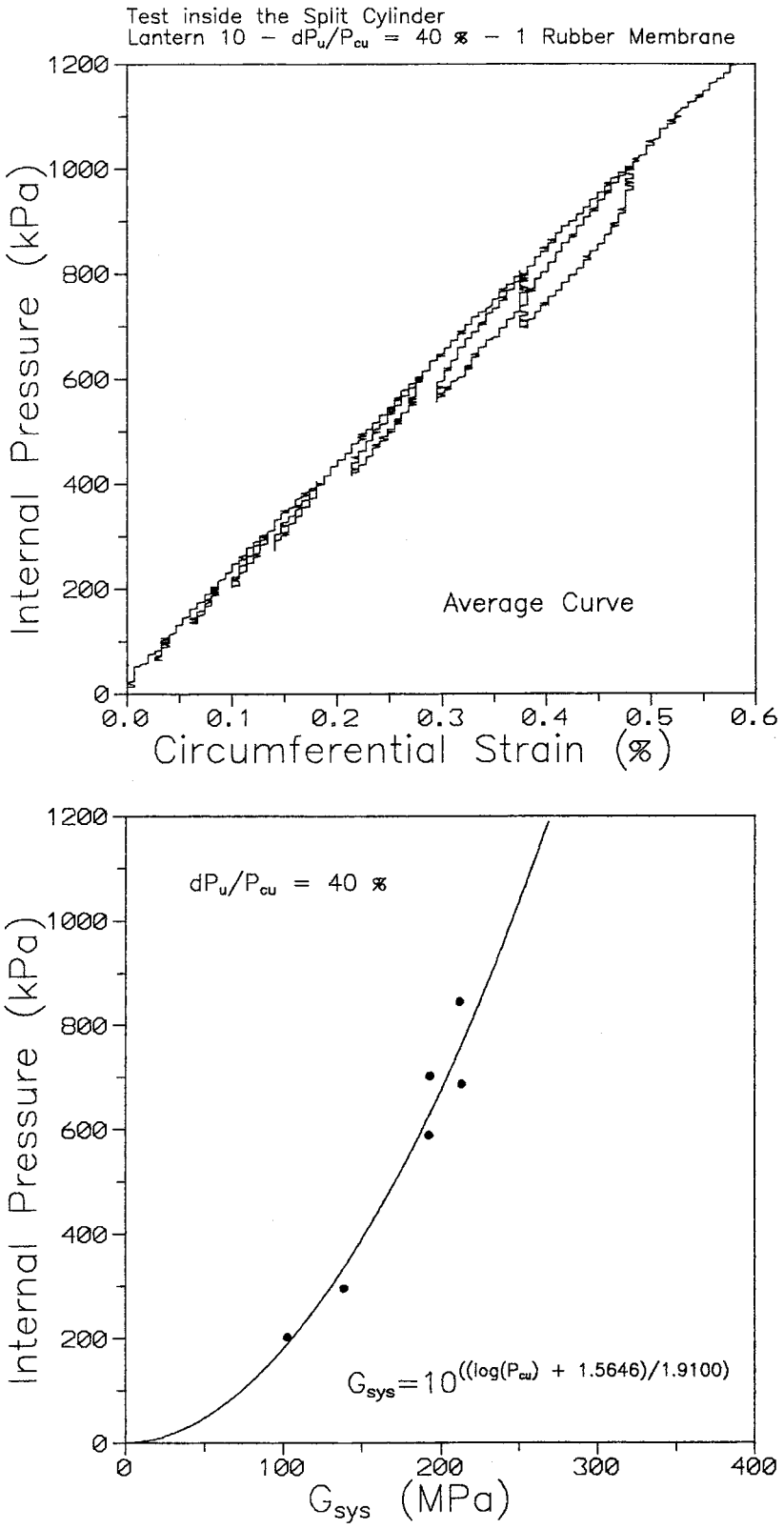

Figure B.3: Compliance Correction of Unload Reload Loops: (a) Compliance Test, (b) Determination of Gsys with Basis on Power Equation

an expected characteristic of the steel (and Camkometer) lanterns. As the outside pressure increases the membrane and the protective steel strips of the lanterns become more deformed, and hence less prone to deflect under further pressure increases.

The magnitude of the compliance correction has a fundamental influence on the shear modulus. All the Gur's presented in this thesis were corrected in accordance with the above discussed procedure.

B.5 SUMMARY

In this Appendix the general calibration characteristics of the UBC SBPM sensors were presented, together with the methodology of calibration adopted for this probe. Based on the previous discussion two main points are highlighted:

- Calibration is essential to remove any equipment related effect from the pressuremeter results, as well as to furnish the data acquisition system with proportionality constants. High accuracy and resolution of the sensors are extremely important for a precise delineation of the testing curve, principally at the stages where a high density of data points and shorter strain intervals are required.

- Membrane resistance and compliance strains are expected to occur due to the characteristics of the rubber membrane and the lanterns used. Corrective curves based on the fitting of a polynomial equation over the experimental calibration results are adopted to remove both effects from the raw testing data. Shear modulus from the unload reload loops also have to be corrected for compliance strains.

APPENDIX C RESULTS OF THE TRIAXIAL TESTS

C.1 INTRODUCTION

Isotropically consolidated triaxial tests were performed with reconstituted and "undisturbed" granular samples retrieved from 4 to 14 m in the Laing Bridge site. The triaxial testing programme was carried out to characterize the stress strain behavior of this sand, as well as to furnish the peak and constant volume friction angles.

In this thesis simple consolidated drained triaxial tests were adopted. This is due to two basic reasons: It is a fast and well established laboratory testing technique and it could reasonably well accommodate the cylindrical samples of the ST1 sampler. The reconstituted samples were formed with the remolded sand collected with this sampler.

A standard strain controlled Wyhekam Farrance triaxial frame was adopted in the triaxial tests. The basic features of the triaxial testing apparatus is presented in Figure C.1. Volume changes during the shearing and consolidation stages were monitored by a burette connected to the base of the sample. Internal back pressure and external confining pressure were monitored with the aid of a pore pressure transducer attached to the connections of the system. This transducer also enabled pore pressure measurements during the set up of the sample, saturation and shearing stages. Strains were recorded by a dial gauge located in the base of the moving frame. The precision of this gauge is 0.01 mm.

During the shearing stage records of axial load, pore pressure, volume change and axial displacement were taken at discrete time intervals. The reconstituted samples with dimensions of 35 mm x 70 mm (diameter x height) required manual readings each 20 s (up to 5 min.), 30s (up to 10 min.) and in increasing time intervals thereafter, in order to ensure a high resolution in the initial stages of shear . In this case a resolution of 0.1 % was obtained with a shearing rate of 0.2286 mm/min. A similar rate of reading intervals was adopted for the tests with the "undisturbed" samples. These samples had dimensions of 50 mm x 100 mm and were sheared at a rate of 0.0762 mm/min. The reduced shearing rate enabled a higher resolution of 0.03 % for these latter tests. On the other hand it increased the testing time to 4 hours.

A "soft" ram contact with the top cap was used in the tests with the reconstituted samples. This

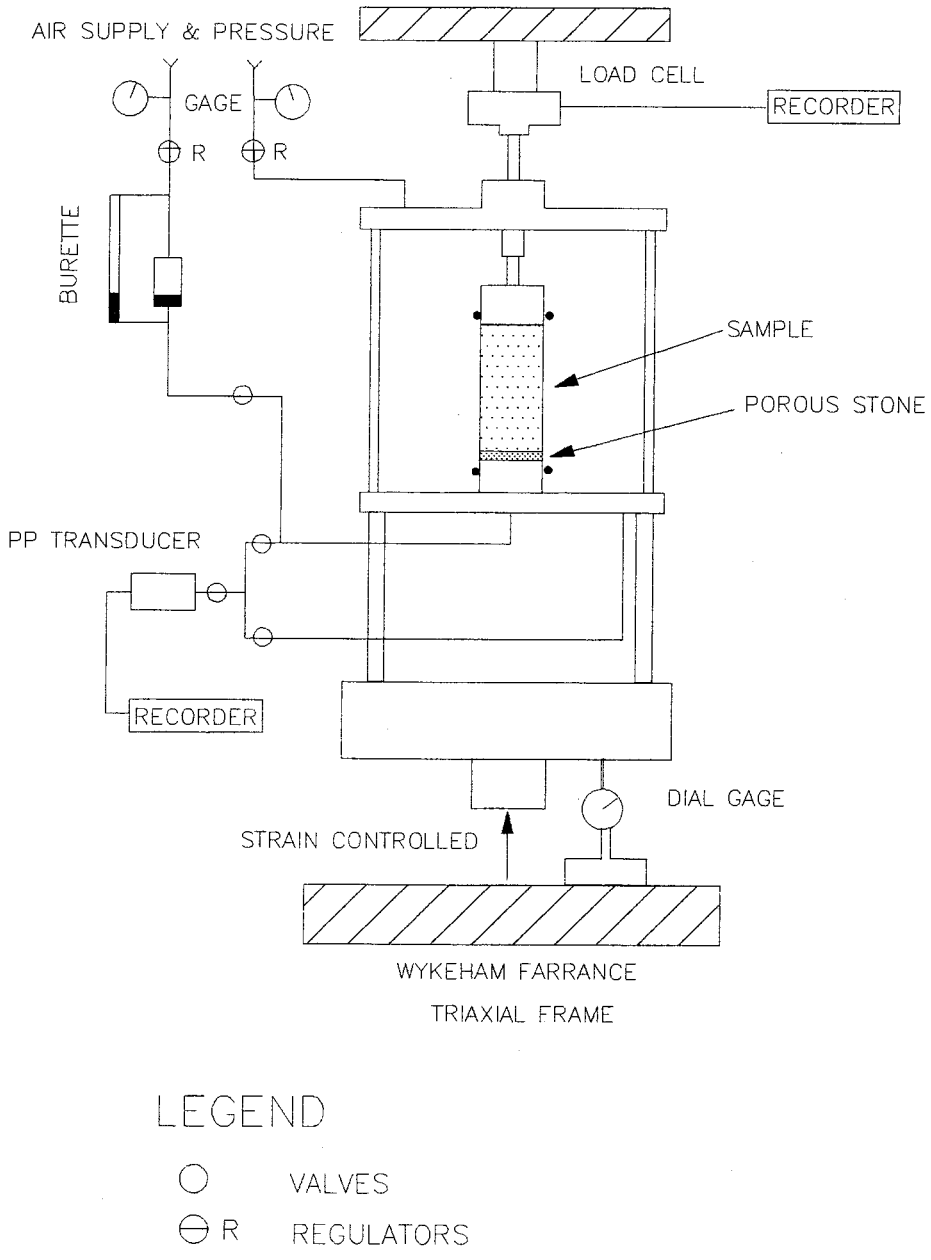

Figure C.1: Schematic of Triaxial Testing Apparatus

characteristic of the equipment has proven to accentuate the bedding errors at the initial stages of shearing. Therefore, for the subsequent tests with the "undisturbed" samples a fixed top cap and ram connection was adopted.

C.2 TESTS WITH THE RECONSTITUTED SAMPLES

The tests with the reconstituted samples were done to provide the writer with the typical stress strain behavior of the Laing Bridge sand, sheared under known density and stress regimes. It also served to provide peak friction angles under distinct sample conditions, that were used together with the angles measured by the "undisturbed" tests to define the constant volume friction angle of this sand.

The reconstituted samples were formed by using the water pluviation technique (see Negussey, 1984). This technique assures a good homogeneity of the testing specimen. With the careful control of the sample height, target relative densities were obtained. The densities chosen were 12, 24 and 45 %. Samples at each of these densities were tested under confining pressures close to those that prevail in situ, namely 50, 100 and 150 kPa. Specific details of the steps adopted in these triaxial tests can be found in the notes of the graduate course CVL 574 of the UBC Civil Engineering Department.

Typical stress strain results of the tests with the reconstituted samples are shown in Figures C.2 and C.3. The following observations apply:

1. The dilation rate, expressed by the inverse sine of the slope of the volume expansion curve (Hansen, 1958), is greatly influenced by the density of the sample and to a lesser extent by the confining pressure. It decreases with a decrease in density or with an increase in confining pressure.

2. The initial contractiveness of this sand, at all chosen densities, is followed by a dilation stage. This initial contractiveness increases with the increase in confining pressure or decrease in relative density.

3. Strain softening is apparent in most of the stress strain curves. After the peak friction angle, defined either in terms of maximum deviator stress or maximum stress ratio, there is a slightly tendency for a decrease in the dilation rate.

Based on the experimental shear behavior of Sacramento River and Ottawa sand described by Lee and Seed, 1967, the results above conform to the expected shearing behavior of loose to dense sands under low

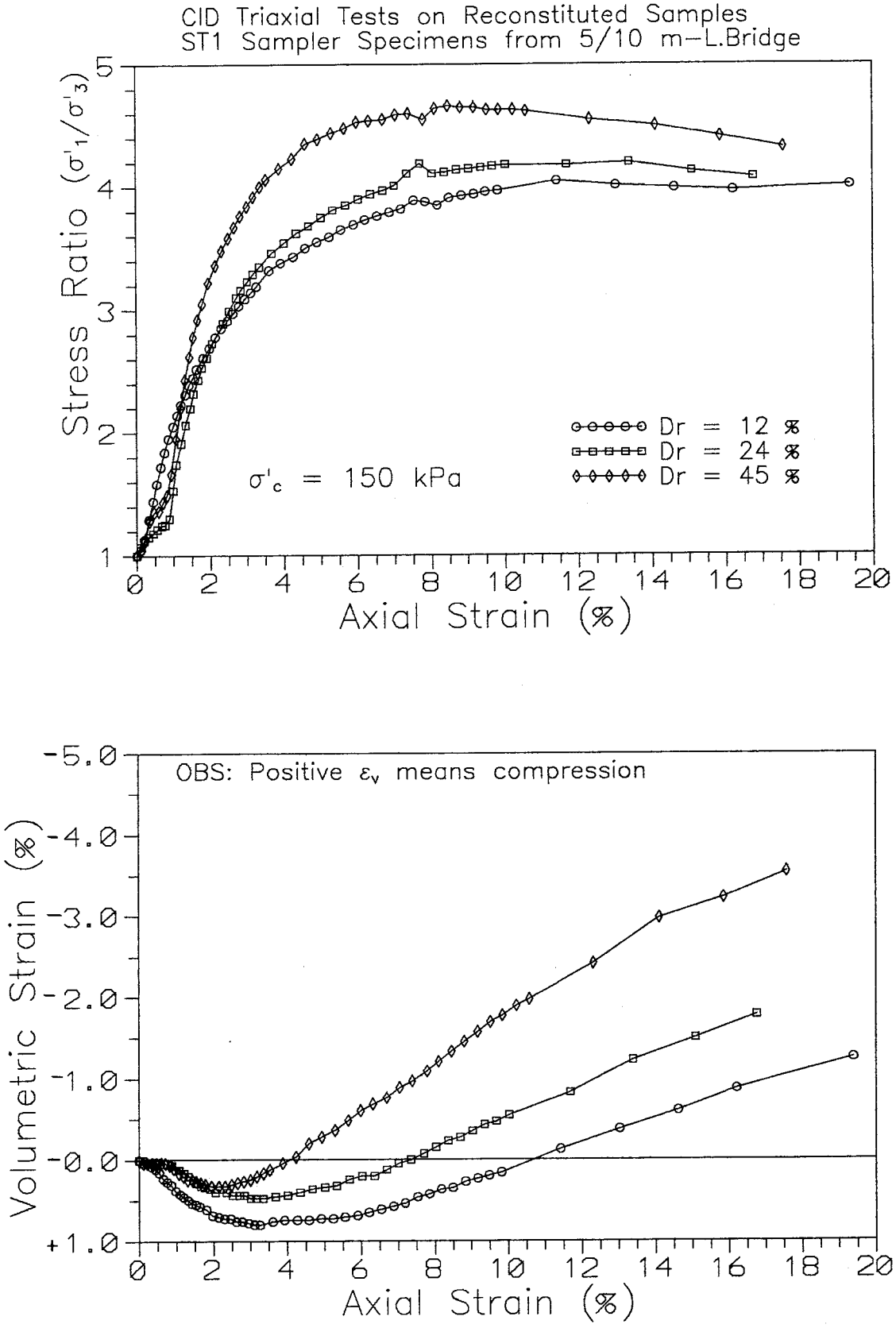

Figure C.2: Typical Stress Strain Response of the Reconstituted Samples: Constant Confining Pressure

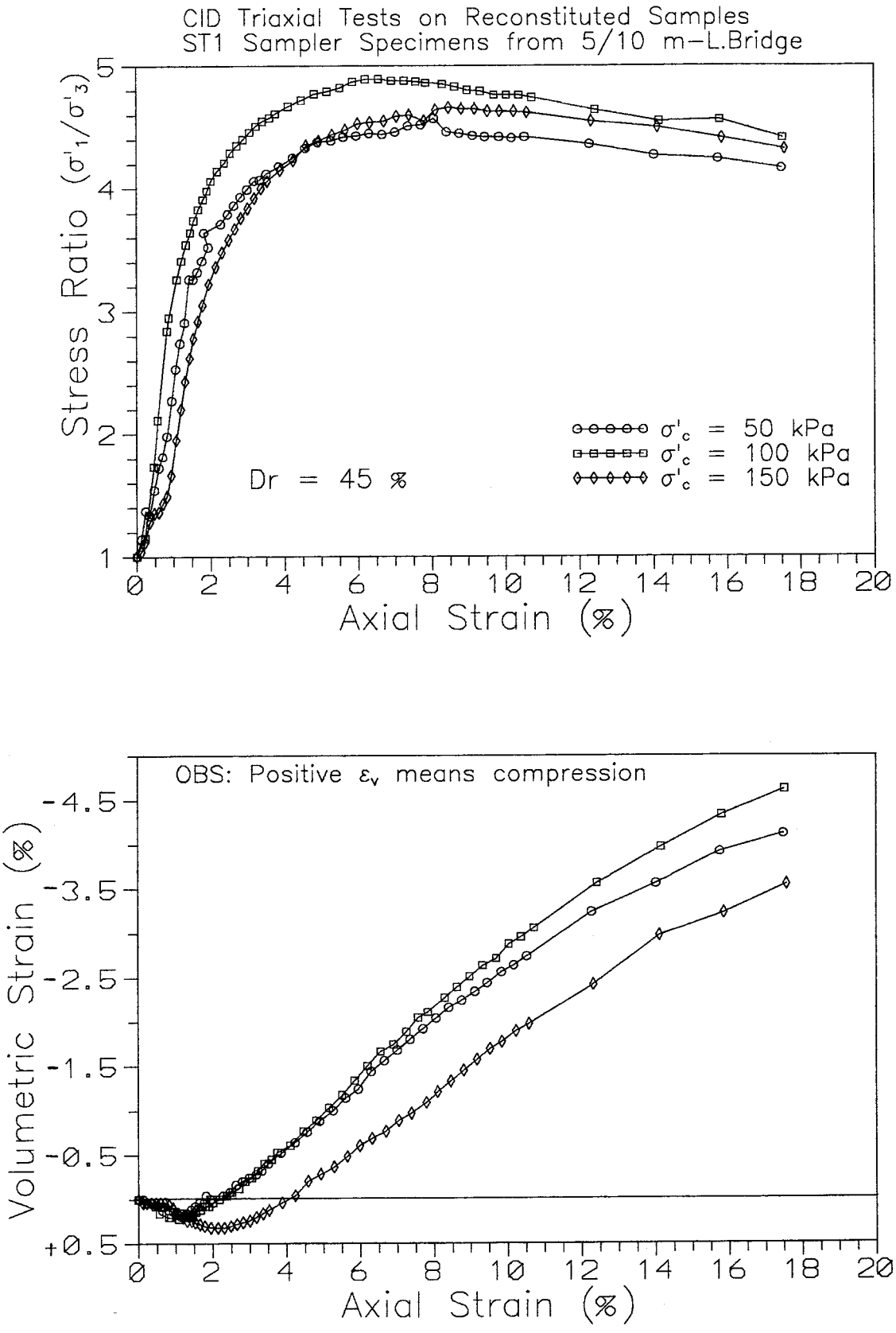

Figure C.3: Typical Stress Strain Response of the Reconstituted Samples: Constant Relative Density

to medium confining pressures. According to this author the drained shearing resistance of sands appears to be governed by three components: sliding friction, dilatancy and particle rearranging. At low pressures, dense sands dilate and exhibit a brittle type stress strain curve. Dilatancy is the major factor responsible for the significant increase in the friction angle at this level of stress. At medium pressures, the same dense sand becomes less dilative and tends to exhibit a more plastic stress strain relationship.

The granular deposit of the Laing Bridge site is characterized by loose to medium dense sand at relatively low confining pressures (vertical effective pressures varying from 50 to 150 kPa in the testing range of this thesis). Given the aforementioned results and observations it may be expected that this same sand, in situ, will shear under highly dilatant characteristics. A small initial contractive stage is expected as well as a stress strain curve with some strain softening. This is verified next with the tests in which "undisturbed" samples were employed.

C.3 TESTS WITH THE "UNDISTURBED" SAMPLES

Tests with the "undisturbed" samples were carried out to determine the peak friction angles of the Laing Bridge sand. The "undisturbed" samples are those in which a high quality of sampling was achieved in the field, and a good quality of trimming and assemblage in the triaxial cell was accomplished in the lab. It shall be noticed, however, that the retrieval percentage of the ST1 sampler was, in average, 60 %. Therefore, it may be expected that some disturbance is present in the "undisturbed" samples.

Several steps were followed from the retrieval of the "undisturbed" samples to the measurement of the peak friction angles. These steps are:

1. Storage and preparation of the sample: After the field retrieval the samples were stored in the freezer of the UBC Soil Mechanics laboratory. After 24 hours the samples were trimmed to the required dimensions by using the diamond saw machine. The top and bottom parts were smoothed with a sand paper file to allow parallelism, and hence to reduce the bedding errors. The samples were then refrozen inside the ST1 samplers and kept in the freezer until the testing day.

2. Placement of the sample on the triaxial cell: On the testing day a sample is removed from the freezer. It is left to thaw for 40 min. until it can be extruded from the ST1 sampler without destruction of the edges. The sample is placed in the triaxial cell and is covered by a 0.03 mm thick rubber membrane.

This membrane is fixed to both pedestal and top cap by rubber bands. At this stage a vacuum of 100 mm of Hg is introduced on the drainage line, enabling the final assemblage of the triaxial cell.

3. Set up of the triaxial cell and thawing of the sample: The triaxial cell is set up in the triaxial frame. A small seating load of 50 kPa is applied to the sample through the quick connection at the top part of the cell. The drainage line is released of vacuum and connected to the general deaired line of the triaxial frame. The sample is left to thaw for 4 hours with the drainage line closed.

4. Saturation stage: The saturation stage is initiated after the sample is fully thawed. Saturation is achieved by applying back pressure and cell pressure so that a net confining pressure of 10 kPa can be imposed in the sample. The saturation stage took in general 12 hours, with both drainage and cell pressure lines open. After 12 hours the drainage line is closed and the saturation level is assessed by checking the ratio $\Delta u/\Delta cell$ (known as B parameter), where Δu is the increase of the excess pore pressure in the sample generated by the change of external pressure $\Delta cell$. Typical values of B obtained for the "undisturbed" samples were above 0.95, for cell pressures greater than 210 kPa.

5. Consolidation stage: The consolidation stage is started after the sample is saturated. The initial burette reading is taken and the cell pressure is increased to the required consolidation pressure. The drainage line is opened and the sample is left to consolidate for 15 to 30 min. At this stage the sample is ready to be sheared with the in situ isotropic stress. An isotropic consolidation pressure equivalent to the effective lateral stress in the site was adopted. For the purpose of these tests, the field lateral stress was based on a K_0 of 0.65, obtained by Robertson, 1982 with SBPM tests in a nearby site.

6. Shearing stage: Once the sample is consolidated the initial values of pore pressure, external pressure, axial force, burette volume and gage displacement are taken. The chronometer is started and the test is run at the chosen shearing rate. Readings of each of the above variables are taken manually.

For the present series of triaxial tests the ram friction, uplift force, weight of the rod and thickness of the membrane were considered in the data reduction. Details of the procedures for data reduction are also found in the notes of the course CVL 574 of the UBC Civil Engineering department.

Typical results of the "undisturbed" tests are presented in Figures C.4 and C.5. It is noticed that the stress strain behavior, in terms of deviator stress and volumetric strain versus axial strain, follows the

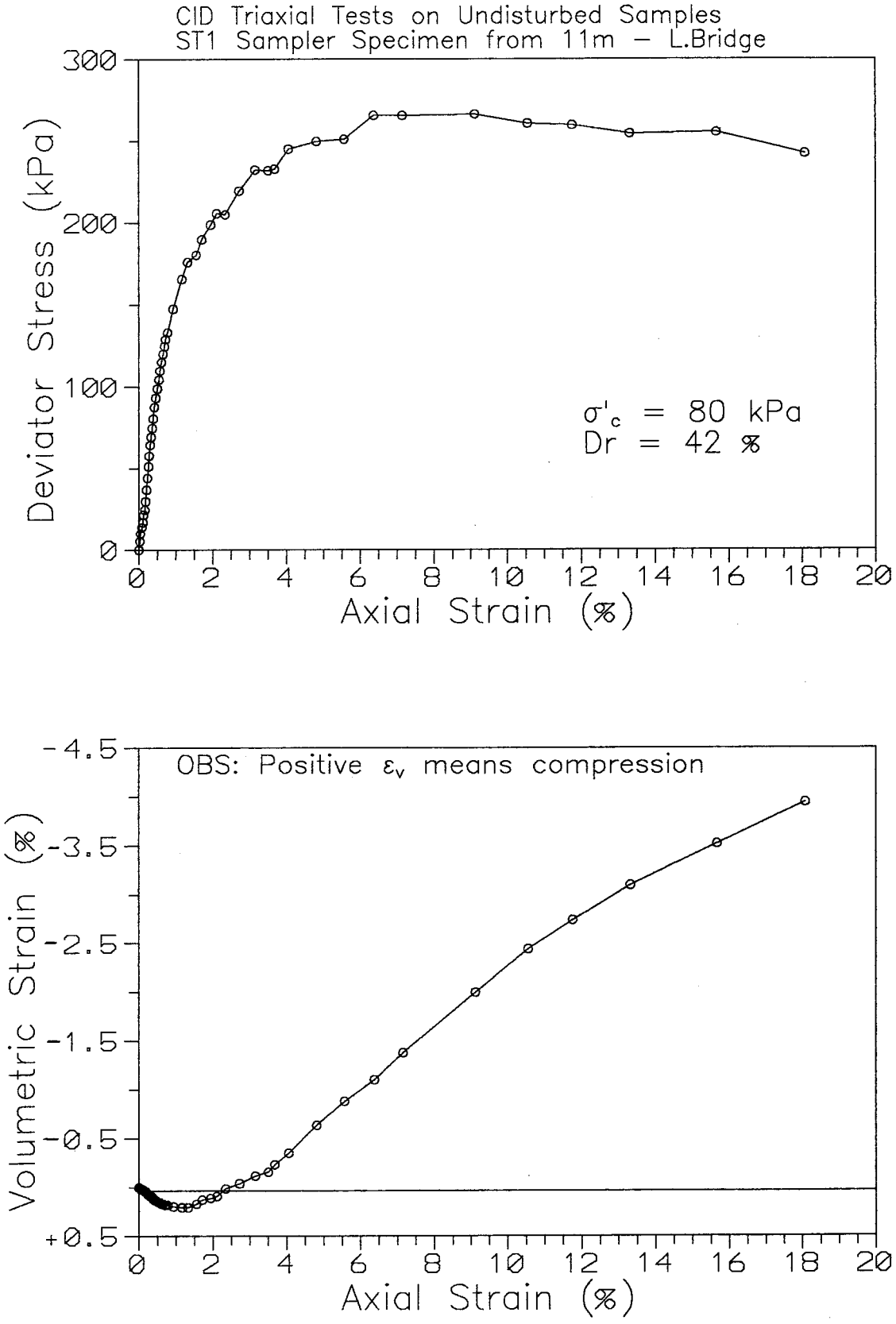

Figure C.4: Typical Stress Strain Response in the Triaxial Test: "Undisturbed" Samples

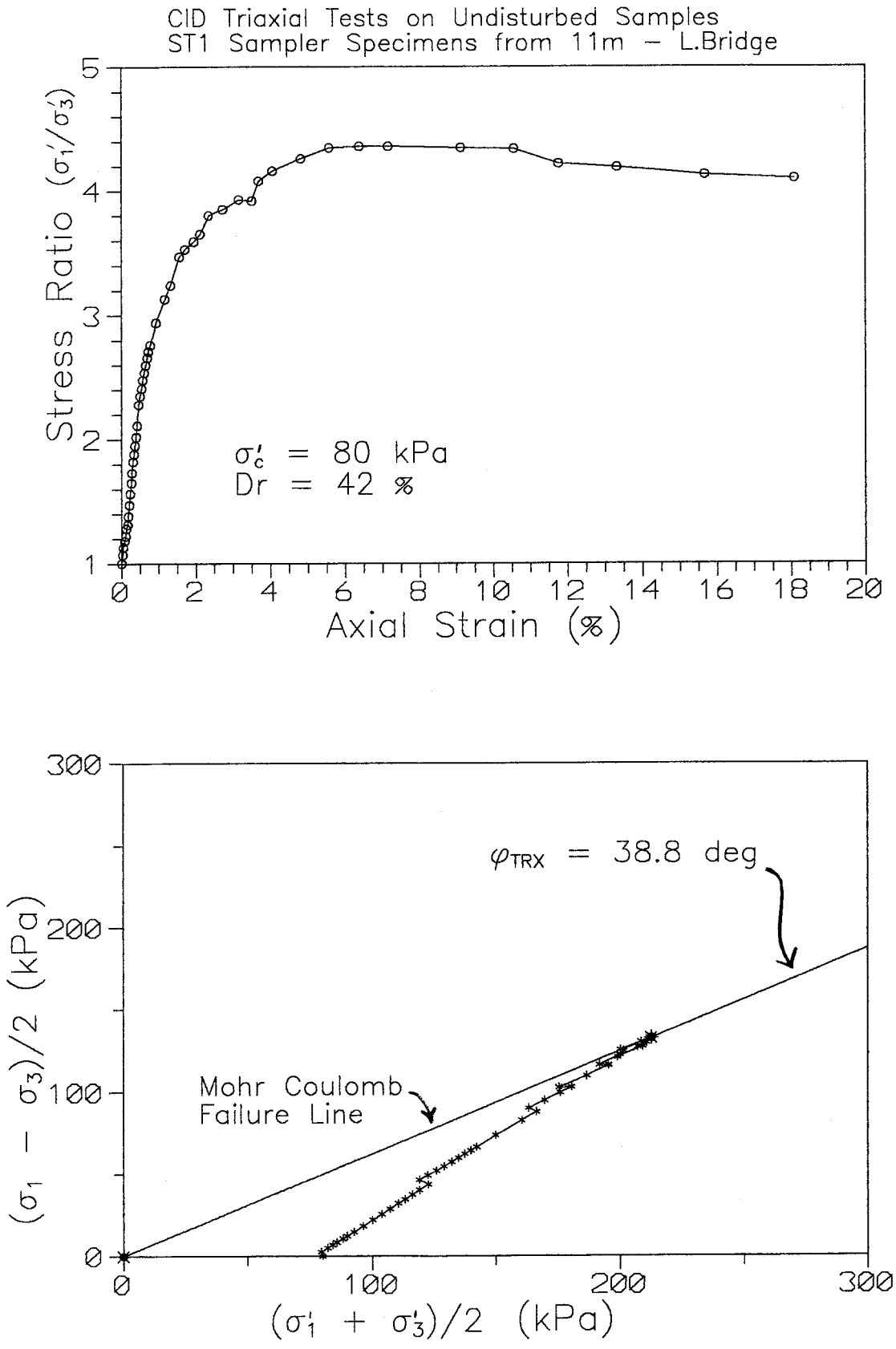

Figure C.5: Determination of the Peak Friction Angle from the Triaxial Tests: "Undisturbed" Samples

expected trend devised from the results of the reconstituted samples. A small contractive stage followed by a highly dilatant stage is observed in the curve of volumetric versus axial strain. This tendency for dilation was observed in all the tests, irrespective of the initial density of the samples. The curve of deviator stress versus axial strain presents a shape close to the curve of stress ratio versus axial strain. Indeed, in all the tests the peak deviator stress occurred at the same axial strain as the peak stress ratio. This happens due to the fully drained characteristics of these tests. A small tendency to strain softening is observed in the latter shearing stages, which indicates the continuous decrease of the friction angle (or dilation rate) with the shearing of the sample.

The peak friction angles were defined by using the maximum stress ratio failure criteria. For each test it was assumed that the Mohr Coulomb failure line passed through the origin of the Q x P' stress diagram of Lambe and Whitman, 1979 (where $P' = (\sigma'_1+\sigma'_3)/2$ and $Q = (\sigma_1-\sigma_3)/2$). This hypothesis neglects any cohesion that may exist in the granular minerals of this sand. Based on this hypothesis, the bottom plot of Figure C.5 demonstrates how the peak friction angle was calculated for the "undisturbed" samples.

Table C.1 presents the final results of the triaxial testing programme carried out with the "undisturbed" samples. Peak friction angles varying from 37.6 to 43.5° were obtained. This range of values is slightly above "typical" values published in literature for poorly graded sands at loose to medium dense conditions (see for instance tables of Holtz and Kovacs, 1981 or Hunt, 1986). Perhaps other factors not considered in the published tables are affecting the results reported in this thesis. According to Holtz and Kovacs, 1981 the peak friction angle may also be affected by grain shape, grain size distribution, mineralogy etc., that are not universally accounted for in the published tables.

Table C.1 also provides the values of Poisson's coefficient obtained with the triaxial tests. The Poisson's coefficients were computed from the volume change data of the tests, in the axial strain range of 10^{-1} %. In this strain range the stress strain behavior is almost linear and the theory of elasticity may be assumed to apply. Treating the soil as an ideally elastic isotropic material, and assuming that the volumetric strain is caused by the sum of the three major principal strains, the following equation is obtained:

TEST DEPTH (m)	σ'_C[1] (kPa)	D_r[2] (%)	ε_{af}[3] (%)	$(\sigma'_1/\sigma'_3)_{max}$[4]	ϕ_{TRX}[5] (Deg)	ν[6]	SAMPLE DENSITY[7]
4.0	35	44	5.14	5.14	42.3	0.24	Medium dense
5.0	40	43	5.86	4.34	38.7	0.28	Medium dense
6.0	45	54	4.11	4.43	39.1	0.29	Medium dense
7.0	50	72	6.25	5.43	43.5	0.35	Dense
9.0	65	20	6.53	4.14	37.6	0.22	Loose
11.0	80	42	6.38	4.36	38.8	0.30	Medium dense
14.0	100	50	10.09	4.42	39.1	0.29	Medium dense
					Average:	≈ 0.25	

1-Effective confining pressure required to bring the sample to an isotropic state of stress similar to the lateral stress in the field. The field lateral stress is based on a K_0 of 0.65, obtained by Robertson, 1982 with SBPM tests in a nearby granular site.
2-Relative density calculated from the sample volume and height. Also used here the minimum and maximum void ratios and the specific gravity value obtained in the preliminary classification tests.
3-Axial strain at the failure. Failure defined with the peak stress ratio mobilized during shear.
4-Peak stress ratio.
5-Peak (axially symmetric) friction angle.
6-Poisson's coefficient calculated with the equation $\nu = 0.5\ (1\text{-}d\varepsilon_v/d\varepsilon_a)$. The equation was used with increments of volumetric and axial strain in the strain range of 1×10^{-1} %.
7-Density classification with basis on D_r and the chart of Lade and Lee, 1976

Table C.1: Results of the Triaxial Testing Programme with "Undisturbed" Samples

$$\upsilon = \frac{1}{2}\left(1 - \frac{d\varepsilon_v}{d\varepsilon_a}\right) \qquad (C.1)$$

where: ν is the Poisson's coefficient

$d\varepsilon_v$ the increment of volumetric strain

$d\varepsilon_a$ the respective increment of axial strain.

In this equation compressive strains are positive.

The average value of ν obtained by the triaxial tests was 0.25. This value is used in some of the cavity expansion theories discussed in Chapter 2, during the interpretation of the SBPM data of the Laing Bridge site.

C.4 CONSTANT VOLUME FRICTION ANGLE

Under large shearing strain levels the void ratio of the sample tends to approach the critical void ratio of the material (Casagrande, 1936). At this stage continuous deformation occurs under no volume change, and the dilation rate is null. The friction angle measured at this stage is defined as the constant volume friction angle (ϕ_{cv}). The constant volume friction angle is an intrinsical property of the sand, and is required by all the cavity expansion models discussed in Chapter 2.

As observed by Sasitharan, 1989 and Bishop, 1971 there is a unique relationship between the peak friction angle and the maximum rate of dilatancy for a particular sand, which is independent on the stress path, density, stress levels at failure or whether extension or compression tests are performed. Indeed, the differences of peak friction angle due to differences in relative density or confining pressure of the samples can be solely explained in terms of differences of dilatancy rates. Bishop, 1971 proposed a technique to derive the constant volume friction angle with the plot of peak friction angle versus maximum dilation rate ($(d\varepsilon_v/d\varepsilon_a)_{max}$). He suggested that the extrapolation of the relationship between peak friction angle and maximum dilation rate to the axis origin (dilation rate equal to null) yields the ϕ_{cv}.

Sasitharan, 1989 adopted Bishop's technique to derive the ϕ_{cv} of Erksak sand. This author also carried out ring shear tests with this same sand. He concluded that Bishop's technique leads to values of constant volume ϕ that are reasonably close to the experimental results obtained by the ring shear tests.

Therefore, in this thesis the constant volume friction angle was obtained with the technique suggested by Bishop, 1971. Figure C.6 presents the ϕ_{cv} estimation with the use of the peak friction angles and maximum dilation rates of all the tests carried out herein. Extrapolation of the best fit line to the axis origin (where $(d\varepsilon_v/d\varepsilon_a)_{max} = 0$) leads to a constant volume friction angle of 34.5°. A value of 34° was adopted in the cavity expansion theories discussed in this thesis, during the interpretation of the SBPM data of the Laing Bridge site.

C.5 SUMMARY

A total of 16 isotropically consolidated drained triaxial tests with reconstituted and "undisturbed" samples were performed.

Triaxial tests with reconstituted samples under in situ stress conditions showed a stress strain behavior typical of loose to medium dense sands under low confining pressures. An initial contractive response followed by a non linear response behavior was observed with all the reconstituted samples. After the onset of the peak friction angle the dilation rate tended to decrease, imposing a strain softening shape on the measured stress strain curves. Similar shearing behavior was noticed with the "undisturbed" samples. The tests with the "undisturbed" samples yielded an average value of Poisson's coefficient of 0.25. The measured axially symmetric peak friction angles varied from 37.6° to 42.3°, with no apparent trend with the depth. The constant volume friction angle of the Laing Bridge sand was determined with the technique proposed by Bishop, 1971. Using all the results of the reconstituted and "undisturbed" tests, a ϕ_{cv} of 34° was obtained for this sand.

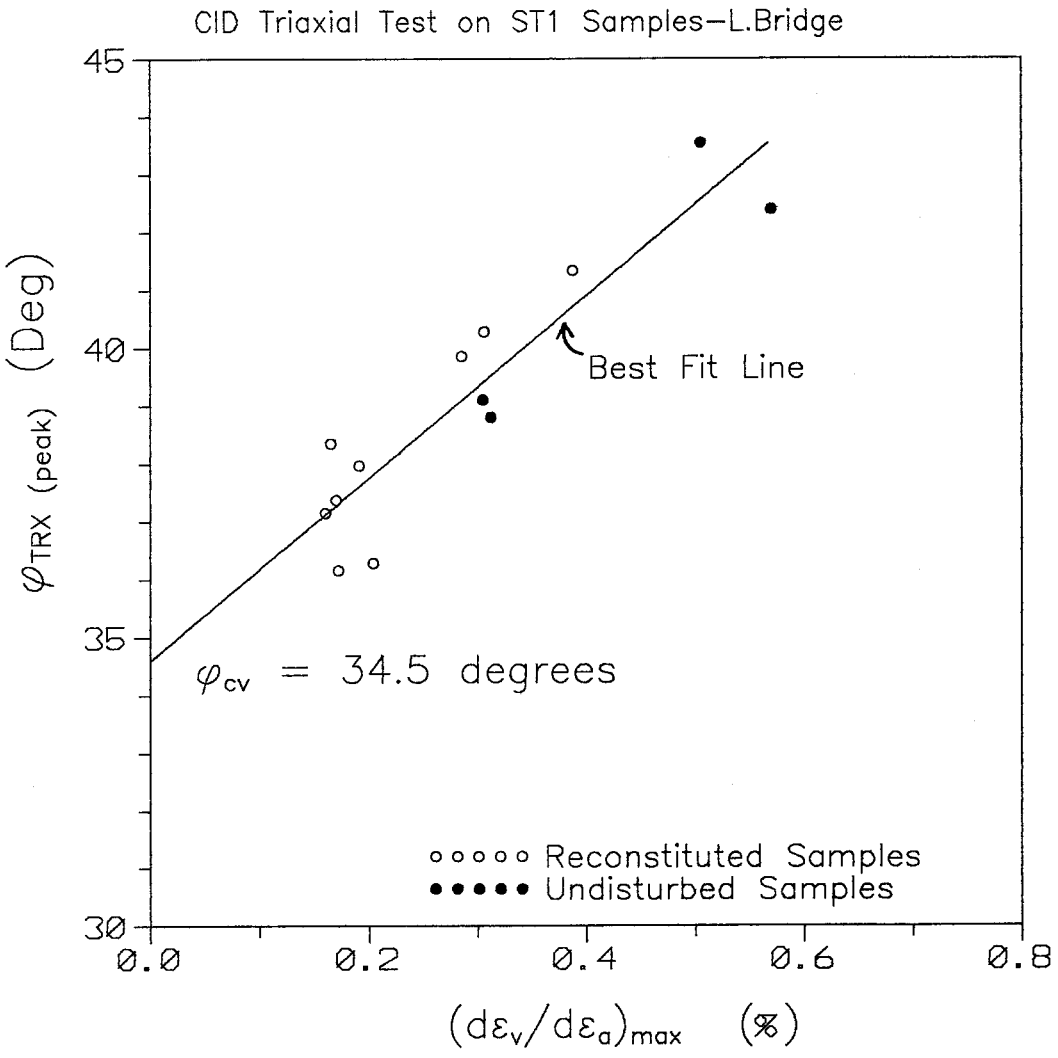

Figure C.6: Determination of the Constant Volume Friction Angle of the Laing Bridge Sand